A Study on the Dissolution of Pyrite and Its Suppression in Acidic Environments

Keiko Sasaki

(1)

A Study on the Dissolution of Pyrite and Its Suppression in Acidic Environments

A Dissertation
submitted to Hokkaido University
for Doctor (Engineering)

by

Keiko Sasaki

1997. 3.

CONTENTS

Chapter 1
Introduction

1.1 General aspects

Pyrite (iron disulfide, FeS_2) is a common sulfide mineral and occurs widely in sulfide deposits, coal seams, and marine deposits (Ishikawa, 1991). The mineral was used extensively in the early days of modern chemistry as a source of vitriol and sulfuric acid. However with the development of alternative sources and processes for the production of sulfuric acid, interest in pyrite has declined to the extent that it is frequently considered a nuisance in mining, principally because it may pose environmental hazards. Environmental damage may occur when mining sedimentary sulfide deposits with pyrite. This may occur at coal mines where the inorganic sulfur content in the coal is greater than 1% (Lowson, 1982). Pyrite also occurs in soils which have been deposited recently under anaerobic conditions.

Oxidation of pyrite produces Fe(II), Fe(III), sulfate and H^+ ions when in contact with air or other oxidants. In Japan, many mines have closed since the 1970s due to increased import of minerals and coal, and acidic mine water from these closed mines is often untreated. The pH of such water easily decreases to 1~3 in such environments. At heavy metal sulfide mines, Fe(III) species and sulfate ions form acidic and oxidizing leach-solutions which further accelerate oxidative dissolution of sulphide ores. Uncontrolled discharge of the oxidation products has caused extensive environmental damage.

The weathering of pyrite in aerobic aqueous systems is a complex biogeochemical process involving several redox reactions and microbial catalysis, as shown in **Fig. 1.1 (a)**. The oxidation of Fe(II) ions and S can be catalyzed by autotrophic bacteria, *Thiobacillus ferrooxidans* and *Thiobacillus thiooxidans* (Ingledew, 1982; Imai, 1984). Iron-oxidizing bacteria, *Thiobacillus ferrooxidans,* rapidly oxidize Fe(II) to Fe(III) ions, at 5~6 orders of magnitude faster than inorganic reactions (Lacey and Lawson, 1970). It is difficult for other bacteria to acclimatize to such environments. Pyrite is directly oxidized by Fe(III) ions, and then Fe(II) ions and sulfate are released from pyrite and elemental sulfur is also formed. This is the so-called "indirect contact mechanism" of iron-oxidizing bacteria. The released Fe(II) ions are oxidized again by *T. ferrooxidans.* Another oxidation mechanism, the "direct contact mechanism" of *T. ferrooxidans* to pyrite, has been proposed. According to this mechanism, it is necessary for the microorganisms to contact pyrite directly and dissolve it. Sulfur-oxidizing bacteria, *Thiobacillus thiooxidans*, also grow actively in these environments where they oxidize sulfur species to sulfate. Microbially mediated dissolution of pyrite occurs mainly by these two kinds of microorganism and leads to the production of acidic mine water. These

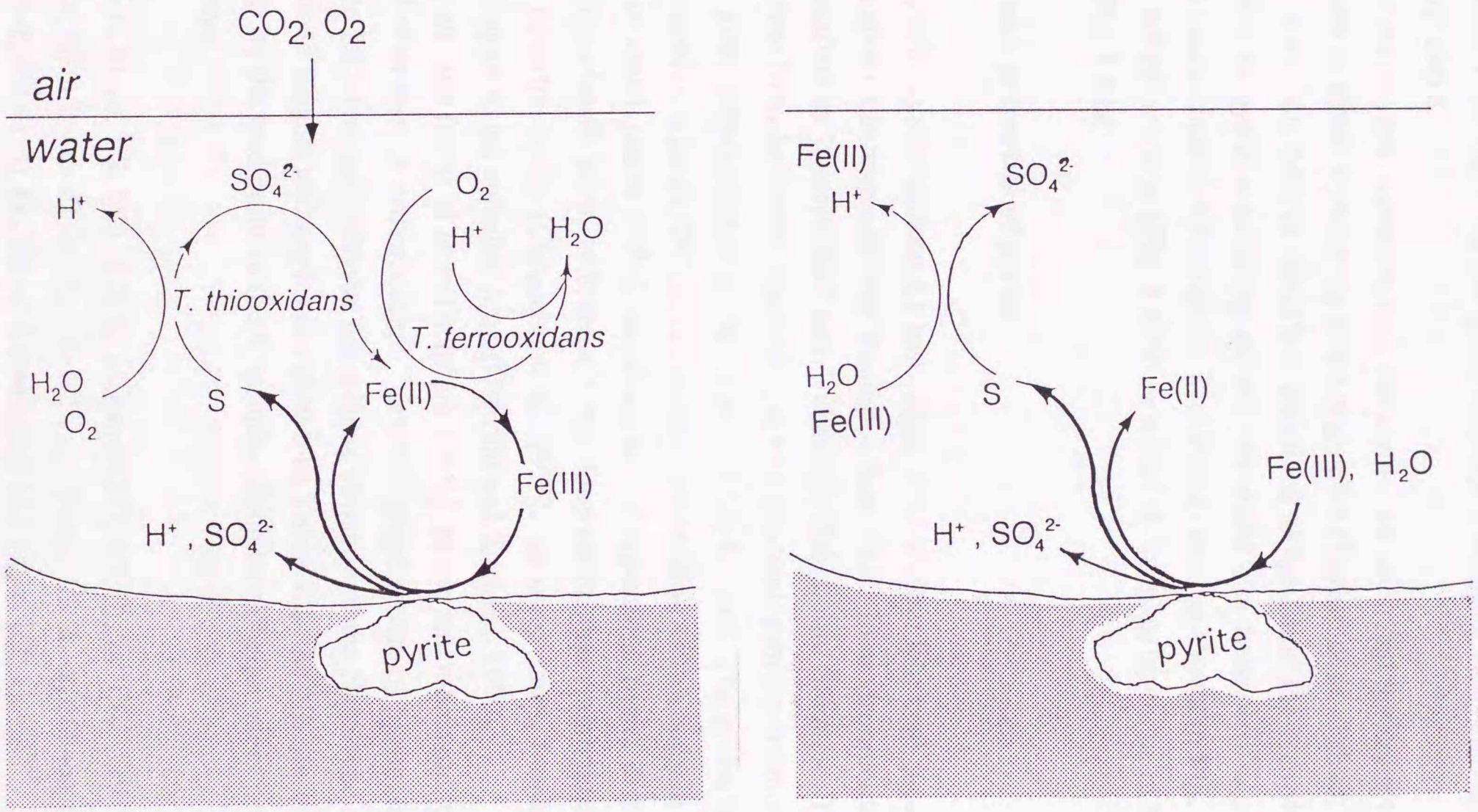

Fig. 1.1 Biogeochemical cycles of pyrite oxidation.

bacteria are detrimental to the environment described above, but they are useful as low cost catalysts in biohydrometallurgy. Here, bacterial leaching is a method to recover valuable metals (such as Cu and Zn) from low grade sulphide ores, using iron- and/or sulfur- oxidizing bacteria (Murr, 1980).

Dissolved oxygen is present near the surface of soils, and the contribution of aerobic microorganisms to pyrite weathering is not negligible (Taylor, et al., 1984a; 1984b). Deeper underground, however, there is much less dissolved oxygen, and the contribution of aerobic microorganisms to pyrite weathering is less important. In anaerobic environments pyrite dissolution is caused mainly by oxidation with Fe(III) ions, as shown in **Fig. 1.1 (b)**. We can deal with the simple reaction (**Fig. 1.1(b)**) as a part of complex reactions in the biotic system as shown in **Fig. 1.1 (a)**.

1.2 Habitat and properties of pyrite

Low grade pyritic substances associated with overburden, coal measures, and mine tailings are dispersed heterogeneously through a host rock. In environmental studies, pyrite is simply classified as "framboidal" and "euhedral" (Smith and Shumate, 1970). The term framboidal comes from the French *framboise*, and "framboidal" pyrite consists of non-crystalline pyrite having grain size diameters in the range of 0.05~1.0 μm. The grains may agglomerate to form small masses, typically 50 μm in diameter, resembling a strawberry in shape. Euhedral pyrite refers to small grains (0.5~2 μm diameter) of crystalline pyrite dispersed through a host coal. This classification is based on the observation that framboidal pyrite is more reactive than euhedral pyrite (Caruccio, et al., 1976). In some cases, framboidal pyrite is a necessary precursor to the euhedral form (Ostwald and England, 1979).

There are two forms of iron disulphide (FeS_2), pyrite and marcasite: pyrite is cubic in structure, and marcasite is orthorhombic. Crystallographic data of pyrite and marcasite are listed in **Table 1.1**. The pyrite crystal has a cubic structure of the NaCl type as shown in **Fig. 1.2**, and the bond lengths and angles are shown in **Table 1.2**: the Na site is occupied by Fe and the Cl site by the mid-point of the S_2 couple. Each atom's equivalent position in an unit cell is as follows:

Fe: (0, 0, 0), (0, 1/2, 1/2), (1/2, 0, 1/2), and (1/2, 1/2, 0);
S: (x, x, x), (1/2 +x, 1/2 -x, -x), (-x, 1/2 +x, 1/2 -x), (1/2 -x, -x, 1/2 +x), (-x, -x, -x),
(1/2 -x, 1/2 +x, x), (x, 1/2 -x, 1/2 +x), and (1/2 +x, x, 1/2 -x),

where x is known to be 0.386 (Kato, 1991).

The electrical and magnetic properties of pyrite are interrelated and defined by the 3d

valence electrons of iron and the 3p valence electrons of sulfur as in **Table 1.3**. It is accepted that Fe in pyrite is present as Fe(II). The six d electrons are paired and occupy the t_{2g} ground state, also referred to as the low-spin ground state. Consequently the Fe(II) ion in pyrite has no magnetic moment. Sulfur is present as the S_2^{2-} moiety. Ten electrons completely fill the p_σ and p_π bonding orbitals and the p_π^* antibonding orbital. Consequently S_2^{2-} also has no magnetic moment. The band gap of pyrite is reported to be 0.835~1.2 eV (e. g., Jarrett, et al., 1968). The values of resistivity and magnetic susceptibilities (χ) for pyrite are also listed in **Table 1.3**. The properties of bonds in pyrite are not simple, because of both ionicity and covalency similar to other sulfides (Sato, 1985).

Table 1.1 Physical properties of iron disulphides (Gait, 1978; Lowson, 1982)

mineral name	pyrite	marcasite
chemical name	ferrous disulfide	ferrous disulfide
composition	FeS_2	FeS_2
structure	cubic	orthorhombic
space group	Pa3	Pnnm
color	brass-yellow	bronze-yellow
density/ g cm^{-3}	5.0	4.88
Mohr hardness	6~6.5	6~6.5
m_p/℃	1171	450
cell dimensions		
a_0	5.4175	4.443
b_0		5.423
c_0		3.386

Table 1.2 Crystallographic data of pyrite (Gait, 1978; Lowson, 1982)

distance between two iron atoms on the 110 face		0.382 nm
distance between two sulfur atoms of the sulfur pair on the 111 axis		0.206 nm
distance between iron and the centre of a sulfur pair on the 001 and 110 face		0.270 nm
distance between adjacent sulfur atoms		0.226 nm
S-Fe-S bond angle	85.66°	and 94.34°
Fe-S-Fe bond angle		115.5°
S-S-Fe bond angle		102.4°

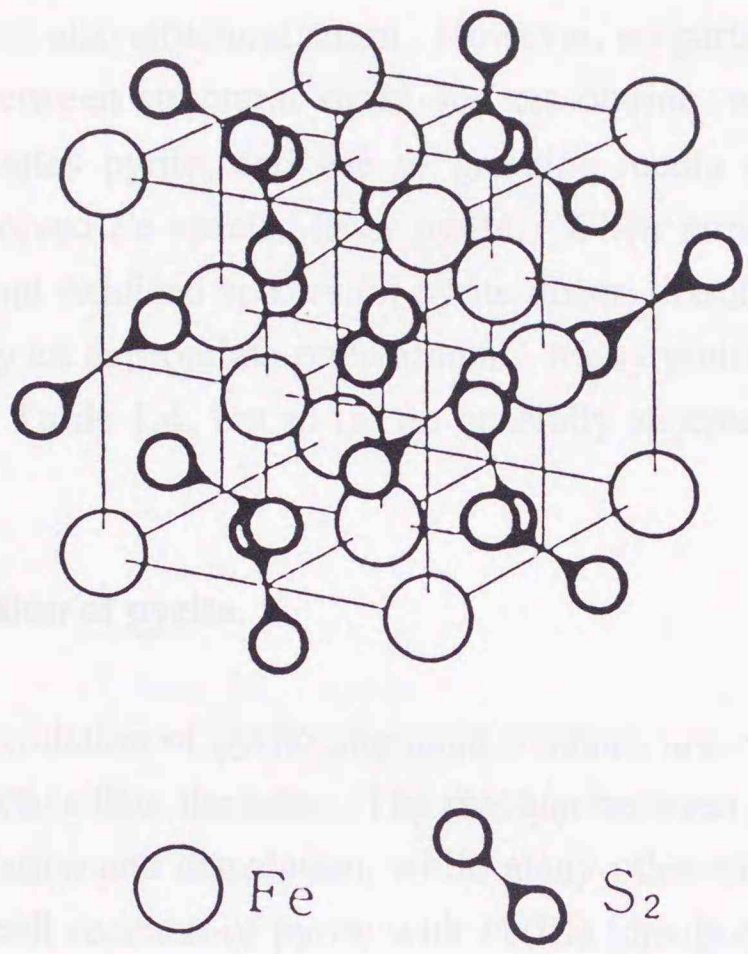

Fig. 1.2 Unit cell in the pyrite crystal (Kato, 1991).

Table 1.3 Electrical, and magnetic properties of pyrite

Properties		Reference
electrical	semiconductor	
	resistance 1.74 (Ωcm)	(Sato, 1984)
	band gap ~0.92 (eV)	(Jarrett, et al., 1968)
magnetic	paramagnitic	
	$\chi = 0.031$ (10^{-6} emu/gm)	(Jarrett, et al., 1968)

To conduct experimental studies of pyrite dissolution, grinding and pretreatment of the pyrite is necessary. Pyrite has a very small solubility product, so that high specific surface area by grinding is favorable. Grinding, however, causes not only increases in specific surface area but also structural strain. However, no particular attention has not been paid to the relation between structural strain and dissolution rate in pyrite. The grinding process also contaminates pyrite, and use of grinding media containing iron affects the measurements of dissolved Fe species from pyrite. When grinding in air, pyrite is easily oxidized by oxygen, and oxidized species on pyrite distort dissolution data. Therefore, they have to be removed by an appropriate pretreatment. Many pretreatment methods have been proposed as shown in **Table 1.4**, but so far no generally accepted pretreatment method has been established.

1.3 Chemical dissolution of pyrite

In the abiotic oxidation of pyrite, the main oxidants are Fe(III) ions and oxygen, the former being more reactive than the latter. The reaction between pyrite and Fe(III) ions (**Fig. 1.1 (b)**) involves oxidation and dissolution, while many other minerals simply dissolve. In geochemistry, the overall reaction of pyrite with Fe(III) ions is conventionally expressed as (Smith and Shumate 1970; Rimstidt and Newcomb, 1993; McKibben and Barnes, 1986; Wiersma and Rimstidt, 1984; Mathews and Robbins, 1972; Garrels and Thompson, 1960; Moses, et al., 1987):

$$FeS_2 + 14\,Fe^{3+} + 8\,H_2O = 15\,Fe^{2+} + 2\,SO_4^{2-} + 16\,H^+ \qquad (1.1)$$

The kinetics of this reaction at ambient temperatures around pH 2 have been extensively studied, as summarized in **Table 1.5**. In these studies, different rate determining variables were investigated by measuring (a) the total dissolved Fe ions and redox potential, *E* (Smith and Shumate 1970; Rimstidt and Newcomb, 1993); (b) Fe(II) ions (McKibben and Barnes, 1986); (c) Fe(III) ions and *E* (Wiersma and Rimstidt, 1984); (d) Fe(III) ions (Mathews and Robbins, 1972); (e) *E* (Garrels and Thompson, 1960); and (f) dissolved S species (Moses, et al., 1987). Only a few papers presented experimental dissolution curves for both Fe and S species measured simultaneously. The stoichiometric dissolution scheme in reaction (1.1) is generally accepted, but it has not been possible to locate reports with stoichiometric dissolution data. Some results have suggested nonstoichiometric dissolution of pyrite on the basis of surface analysis (Buckley and Woods, 1987) or electrochemical measurements (Mycroft et al., 1990). Further, the dissolution data reported by McKibben and Barnes (1986) may also suggest incongruent dissolution, though this was not discussed in the report.

Table 1.4 Pretreatment method of pyrite for dissolution experiments at ambient temperatures

Reference	Method
Garrels, et al. (1960)	Rinsing with 6 mol dm^{-3} H_2SO_4 and distilled water, and drying with acetone.
Smith, et al. (1970)	Washing with warm 2% HCl then with distilled water, and drying under vacuum.
Goldhaber, et al. (1983)	Washing under a nitrogen atmosphere in glove bag with dilute HCl, followed by deoxygenated water, and finally with acetone.
Taylor, et al. (1984b)	Boiling in HCl, rinsing first with distilled water and then with acetone, and drying.
McKibben, et al. (1986)	Ultrasonic cleaning in ethanol for 30 sec and decantation of adhering mineral powder. Rinsing with 1 mol dm^{-3} HNO_3, for 1 min, followed by triply distilled water, then dehydrating in acetone, and finally vacuum-drying.
Moses, et al. (1987)	(1) Rinsing in alternating baths of warm (~50 ℃) 10% HCl and warm acetone, and sterilization with γ-ray irradiation. (2) Rinsing in alternating baths of warm (~50 ℃) 10% HCl and warm acetone, sterilization with UV radiation, then drying under N_2 . (3) Boiling in 6 mol dm^{-3} HCl for 15 min, rinsing twice with 6 mol dm^{-3} HCl, and rinsing at least three times with 50 cm^3 of warm acetone, then drying under N_2.
Sakai, et al. (1987)	Cleaning in 2 mol dm^{-3} HCl and distilled water.
Nicholson, et al. (1988)	Washing repeatedly with deionized water, cleaning ultrasonically for 45 sec, repeated washing with acetone, and vacuum-drying, then rewashing with water, 6 mol dm^{-3} HCl, and finally rinsing with acetone.
Moses, et al. (1991)	Boiling in 6 mol dm^{-3} HCl for 15 min, rinsing twice with 6 mol dm^{-3} HCl, and rinsing at least three times with 50 cm^3 of warm acetone.
Rimstidt, et al. (1993)	Immersing in 1 mol dm^{-3} HCl, washing in distilled water, and then air-drying at 40℃.

Though the results of kinetic studies agree fairly well as shown in **Table 1.5**, the reaction mechanism is still not entirely clear due to the difficulties caused by the properties of pyrite. As described in **Section 1.2**, pyrite crystal is composed of both covalent and ionic bonds, and a kind of semiconductor. Luther (1987) proposed a model of the mechanism based on molecular orbital theory, and Moses, et al. (1987) speculated a consequent of schemes, but none have been experimentally confirmed.

Two different acidic media have been used in the dissolution experiments (**Table 1.5**): hydrochloric acid and sulfuric acid. It is difficult to determine the net amount of dissolved sulfate from pyrite in sulfuric media, though the sulfate media reflects natural environments. Smith and Shumate (1970), and Williamson and Rimstidt (1994) found that the dissolution rate of pyrite is larger in chloride media than in sulfate media. The reason was not fully discussed by Smith and Shumate (1970), but it is considered that the reaction mechanism may be explained by an anionic ligand effect. Oxidation of pyrite by oxygen (reaction (1.2)) is a primary step in the sequence of pyrite weathering.

$$FeS_2 + 7/2\ O_2 + H_2O = Fe^{2+} + 2\ SO_4^{2-} + 2\ H^+ \qquad \text{(mainly chemical reaction)} \quad (1.2)$$

The reaction (1.2) is mainly chemical, and occasionally biological. Singer and Stumn (1970) regarded reaction (1.2) as the rate-determining step. Around pH 2, the kinetics of the chemical reaction (1.2) have been investigated and are summarized in **Table 1.6**. The oxidation rate of pyrite by oxygen is very much slower than that by Fe(III) ions.

1.4 Microbially mediated dissolution of pyrite

Two chemoautotrophic bacteria grow actively in aerobic acid mine drainage: the iron-oxidizing bacteria *Thiobacillus ferrooxidans* and the sulfur-oxidizing bacteria *Thiobacillus thiooxidans* (Brierley, et al., 1973). Microbiological details of the two bacteria are listed in **Table 1.7**. *Thiobacillus thiooxidans* cannot oxidize pyrite without *T. ferrooxidans,* and it is therefore important to establish the interaction mechanism between *T. ferrooxidans* and pyrite. The microbially mediated dissolution of pyrite by *T. ferrooxidans* around pH 2 is conventionally expressed as follows (e. g., Murr, 1980):

$$FeS_2 + 7/2\ O_2 + H_2O = Fe^{2+} + 2\ SO_4^{2-} + 2\ H^+ \qquad \text{(mainly chemical reaction)} \quad (1.2)$$

$$Fe^{2+} + 1/2\ O_2 + 2\ H^+ = Fe^{3+} + H_2O \qquad \text{(biological reaction)} \quad (1.3)$$

$$FeS_2 + 2\ Fe^{3+} = 3\ Fe^{2+} + 2\ S \qquad \text{(chemical reaction)} \quad (1.4)$$

$$FeS_2 + 14\ Fe^{3+} + 8\ H_2O = 15\ Fe^{2+} + 2\ SO_4^{2-} + 16\ H^+ \qquad \text{(chemical reaction)} \quad (1.1)$$

$$2\ S + 3\ O_2 + 2\ H_2O = 4\ H^+ + 2\ SO_4^{2-} \qquad \text{(biological reaction)} \quad (1.5)$$

Table 1.5 Previous works on the oxidation of pyrite with Fe(III) ions at ambient temperatures around pH 2

Reference	pH (acid)	Temperature /℃	[Fe(III)] /mmol dm^{-3}	S_{BET} of pyrite[*1] /m^2g^{-1}	RDV[*2]	Rate/k[*3]
Garrels, el al. (1960)	0~2 (H_2SO_4)	33±2	0.01~1	(75~150 μm)	*E*	$[Fe^{3+}][Fe^{3+}+Fe^{2+}]^{-1}$
Smith, el al. (1970)	2 (HCl/H_2SO_4)	25~50	0.25~250	(105~250 μm)	total Fe, *E*	-
Mathews, el al. (1972)	0~1.5 (H_2SO_4)	30~70	<10	0.66~0.76	Fe(III)	$[Fe^{3+}][Fe^{3+}+Fe^{2+}]^{-1}[H^+]^{0.44}$
Wiersma, el al. (1984)	2 (HCl)	25~50	1	(75~150 μm)	Fe(III), *E*	$[Fe^{3+}]$
McKibben, el al. (1986)	1~2 (HCl)	25~30	$10^{-0.3}$~$10^{-0.55}$	0.0251±0.0013	Fe(II)	$[Fe^{3+}]^{0.58}[H^+]^{-0.50}$
Moses, el al. (1987)	2.27 (HCl)	22~25	$10^{-0.3}$~$10^{-0.55}$	(38~45 μm)	S species	-
Sakai, el al. (1987)	0.5~2.0 (HCl)	30~50	4.6~16.4	(53~74 μm)	Fe(II)	$[Fe^{3+}]^{0.8}[Fe^{2+}]^{-1.4}$
Rimstidt, el al. (1993)	2 (HCl)	25	10^{-2}~$10^{0.5}$	0.047±0.002	total Fe, *E*	$[Fe^{3+}]^{0.62\pm0.10}$
Williamson, el al. (1994)	0.5~3.0 (HCl/H_2SO_4)	25	10^{-1}	0.047±0.002	total Fe, *E*	$[Fe^{3+}]^{0.30}[Fe^{2+}]^{-0.47}[H^+]^{-0.32}$

[*1] specific surface area (or particle size); [*2] rate determining valiable; [*3] k: rate constant.

Table 1.6 Previous works on the oxidation of pyrite with oxygen at ambient temperatures around pH 2

Reference	pH (acid)	Temperature /℃	pO_2 /atm	S_{BET} of pyrite[*1] /m^2g^{-1}	RDV[*2]	Rate/k[3]
Smith, el al. (1970)	2 (HCl/H_2SO_4)	25	(3.7~95 ppm)	(105~250 μm)	Fe(II)	$[O_2]^{0.70}[H^+]^{-0.10}$
Mathews, el al. (1972)	0.7~1.2 (H_2SO_4)	30	0.2~1	0.66~0.76	Fe(II)	$[O_2]^{0.81}$
McKibben, el al. (1986)	1~2 (HCl)	30	0.21~1	0.0251 ± 0.0013	Fe(II)	$[O_2]^{0.49}$

[*1] specific surface area (or particle size); [*2] rate determining valiable; [*3] k: rate constant.

Table 1.7 Microbiological details of *Thiobacillus ferrooxidans* and *Thiobacillus thiooxidans* (Buchanan and Gibbons, 1974)

	T. ferrooxidans	*T. thiooxidans*
Gram stain	negative	negative
shape	short rods	short rods
size	0.5 μm × 1.0 μm	0.5 μm × 1.0~2.0 μm
flagella	monotrichous fragellum	monotrichous fragellum
energy source	Fe(II), reducing S species (strictly autotrophic)	reducing S species (strictly autotrophic)
light	not necessary	not necessary
carbon source	CO_2	CO_2
terminal electron acceptor	O_2	O_2
growth pH (optimum)	1.4~6.0 (2.5~5.8)	0.5~6.0 (2.0~3.5)
growth temperature (optimum)	15~25℃	10~37℃ (28~30℃)

Reaction (1.2) is mainly chemical, but occasionally biological (the "direct contact mechanism" of *T. ferrooxidans*). Below pH 2, Fe(II) ions are only slowly oxidized to Fe(III) ions by oxygen without *T. ferrooxidans*, but with *T. ferrooxidans* the oxidation of Fe(II) ions (reaction (1.3)) occurs at 5~6 orders of magnitude faster than the inorganic reaction rate (Lacey and Lawson, 1970), and quickly regenerates Fe(III) ions in acid solutions. Then, pyrite is directly and chemically oxidized by Fe(III) ions as in reaction (1.4) or (1.1). Pyrite is oxidized and dissolved more rapidly by Fe(III) (reaction (1.4) and (1.1)) than by oxygen (reaction (1.2)). Elemental sulfur, an intermediate product in reaction (1.4), is also oxidized to sulfate by *T. ferrooxidans* (reaction (1.5)). The process (reactions (1.1)~(1.5)) is termed the "indirect contact mechanism" of *T. ferrooxidans* in pyrite dissolution (e. g., Murr, 1980).

Some investigators (Beck and Brown, 1968) did not accept this mechanism, but proposed that the bacteria make direct contact with the pyrite crystals and oxidize them through enzymatic pathways, based on the results that the bacterial population on the pyrite surface is much greater than in solution (Tuovinen and Kelly, 1972). Thus, the "direct contact mechanism" has suggested to cause the microbial oxidation of pyrite. This mechanism is also supported by studies on the oxidation of non-ferrous sulfides such as ZnS and CuS in the presence of *T. ferooxidans* (Silver and Torma, 1974; Duncan and Walden, 1972) where iron is not present in the system. Silverman (1967) attempted to determine which mechanism is more important, and based on the results of O_2 uptake by bacteria and solution analyses, it was concluded that both mechanisms were operating concurrently. Taylor, et al. (1984a;

1984b) suggested that pyrite oxidation is accelerated by a chemical oxidation pathway in anaerobic water-saturated environments (indirect attack), and by a microbially-mediated pathway in well-aerated and unsaturated zone environments (direct attack) using isotopic analyses of ^{34}S (sulfate) and ^{18}O (water). The path of the microbial attack of *Thiobacillus ferrooxidans* on pyrite has remained a controversial issue.

1.5 Remediation and prevention of acidic mine drainage

Studies on cut in the cycles of pyrite weathering as shown in **Fig. 1.1 (a) and (b)** can be divided into two categories, the suppression of chemical reactions of pyrite with Fe(III) ions under anaerobic/aerobic conditions and the inhibition of metabolic reactions of aerobic microorganisms under the aerobic conditions.

Several factors controlling the chemical reaction have been established: (1) pH (**Table 1.5**), (2) surface area of pyrite (**Table 1.5**), (3) concentration of Fe(III) ions (**Table 1.5**), (4) concentration of Fe(II) ions (**Table 1.5**), (5) reduction of Fe(III) to Fe(II) ions (e. g., Blowes, 1994), and (6) formation of secondary iron minerals on pyrite (e. g., Nordstrom, 1982; Jambor, 1994). It is generally accepted that the kinetics of the reaction depends on pH and the concentration of Fe(III) ions.

It has been reported that the Fe(II) ions formed by reactions (1.1) and (1.4) reduce the dissolution rate (Sakai, et al., 1987; Moses and Herman, 1991) in a kind of self-suppressing reaction. Sakai, et al. (1987) added Fe(II) ions to the solution to observe the suppression effect, but the results were inadequate to describe the effect. Further, they changed only Fe(II) ion concentration so the effect of the redox potential was not eliminated. Moses and Herman (1991) did not consider changes in the surface composition of pyrite during oxidation: they discussed the suppression effect based on simple dissolution experiments and did not carry out dissolution experiments by addition of Fe(II) ions. To achieve a better understanding of the overall mechanism of pyrite oxidation with Fe(III) ions it is important to elucidate the effect of Fe(II) ions.

Studies on the adsorption or reduction of toxic ions such as Hg(II), As(III, V), and Cr(VI) ions on pyrite have suggested that pyrite has the potential to remove toxic ions from waste water (Brown, et al., 1979; Brown and Jurinak, 1989; Jean and Bancroft, 1986; Zouboulis, et al., 1993; 1995). The interfacial reactions of Au-complexes/pyrite are related to the geochemistry of concentrating noble metals with pyrite functioning as a reductant (Hyland and Bancroft, 1989; Bancroft, et al., 1990). In mineral processing, a knowledge of the interaction between pyrite and Cu(II) ions, an activator in froth flotation of sulfide, is useful and often indispensable (Voigt, et al., 1994; Perry, et al., 1984). Adsorption chemistry of several cations on pyrite is closely related to the unique physicochemical properties of pyrite

described in **Section 1.2**. Complxation of Fe(III) around pH 2 has not been investigated well systematically, and there are still many factors to consider, such as adsorption, complexation of Fe(III), and others.

Inhibition of growth and respiration in *T. ferooxidans* and *T. thiooxidans* has been studied both microbiologically and biohydrometallurgically (e. g., Walsh and Mitchell, 1975; Wakao, et al., 1983). In bacterial leaching, it is important to develop bacteria with resistance to high concentrations of heavy metal ions. Imai, et al. (1975; 1976) reported that heavy metal ions, such as Cu(II), Zn(II), Ni(II), Co(II), Mn(II), Cd(II), and Cr(III) ions, did not prevent cell growth and the iron-oxidizing activity of *T. ferrooxidans* even at ~10^{-3} mmol dm^{-3}, while U, Mo, and Sn at more than 10^{-3} mol dm^{-3} and Ag^{+} and Hg(II) ions at more than 10^{-5} mol dm^{-3} prevented it.

It is an interesting subject for microbiologists to investigate the resistance to organic compounds and assimilation of them by chemoautotroph (Rittenberg, 1972). Carboxylic acids, amino acids, and keto acids have been tested as inhibitors for *T. ferooxidans* (Dugan, 1975; Tuttle, et al., 1976; 1977; Pronk, et al., 1991), and for *T. thiooxidans* (Iwatsuka, et al., 1960; Butler, et al., 1966; Borichewski, 1967; Lu, et al., 1971). Tuovinen, et al. (1971) also reported that common organic carbon sources at less than 0.5(w/v)%, such as fructose and lactose, inhibited the iron-oxidizing activity and growth of *T. ferrooxidans*. For anionic species, nitrate and chloride were also inhibitory whereas sulfate was not (Tuovinen, et al., 1971). The inhibition by these substances are summarized in **Tables 1.8 and 1.9**.

To achieve the complete inhibition of the activity of *T. ferrooxidans* in acid mine water, sodium lauryl sulfate (SLS) (Imai, et al., 1972; Dugan, et al., 1975; Kleinmann, et al., 1981; Dugan, et al., 1983; Onysko, et al., 1984), alkylbenzene sulfonate (Dugan, 1975; Kleinmann, 1981; Onysko, et al., 1984), sodium benzoate (Dugan, et al., 1983), NaN_3(Iwatsuka, 1960; Arkesteyn, 1979), and N-ethylmaleimide (Arkesteyn, 1979) have been investigated; and to inhibit *T. thiooxidans*, NaN_3 (Adair, 1966) and KCN (Iwatsuka, 1960; Adair, 1966) were examined. Anionic surfactants, especially SLS, are effective inhibitors and have been used practically in mines in the USA (Dugan, 1975; Kleinmann, et al., 1981; Onysko, et al., 1984; Rastrogi, 1996). However, extensive use of detergents is not environmentally acceptable, and the World Health Organization recommends that detergent concentration in flowing water should be below 1.0 ppm. In a view point of protecting environments, more acceptable and practical inhibitors are desired.

Though it has been reported that oxalic acids inhibits cell growth and iron- and sulfur-oxidation in *T. ferrooxidans* (Dugan, 1975; Tuttle, et al., 1976) and *T. thiooxidans* (Iwatsuka and Mori, 1960), the inhibitory effects of humic substances on chemoautotrophic bacteria is not well known.

Recently, in the view point of environmental problems on radioactive wastes, the

Table 1.8 Inhibition of iron-oxidizing activity in *Thiobacillus ferrooxidans*

Inhibitor	Dose /mmol dm^{-3}	Inoculume size	Incubation time	Inhibition / %	Measurement	Reference
Organic acids						
formic acid	10^{-2}	8 mg/5 ml	10 min	100	Fe(II)	Dugan (1975)
	10^{-4}	8 mg/5 ml	10 min	100	O_2 uptake	Pronk, et al. (1991)
acetic acid	10^{-2}	8 mg/5 ml	10 min	75	Fe(II)	Dugan (1975)
oxalic acid	10^{-2}	8 mg/5 ml	10 min	100	Fe(II)	Dugan (1975)
	10^{-2}	0.4 mg(wet)/100 ml	ND	100	Fe(III)	Tuttle, et al. (1976)
fumaric acid	10^{-2}	8 mg/5 ml	10 min	67	Fe(II)	Dugan (1975)
	10^{-2}	0.4 mg(wet)/100 ml	6 days	100	Fe(III)	Tuttle, et al. (1976)
succinic acid	10^{-2}	8 mg/5 ml	10 min	62	Fe(II)	Dugan, et al. (1975)
	10^{-2}	0.4 mg(wet)/100 ml	5 days	100	Fe(III)	Tuttle, et al. (1976)
malic acid	10^{-2}	8 mg/5 ml	10 min	39	Fe(II)	Dugan (1975)
	10^{-2}	0.4 mg(wet)/100 ml	5 days	100	Fe(III)	Tuttle, et al. (1976)
lactic acid	10^{-2}	8 mg/5 ml	10 min	60	Fe(II)	Dugan (1975)
hexanoic acid	10^{-2}	8 mg/5 ml	10 min	90	Fe(III)	Dugan (1975)
	10^{-2}	0.4 mg(wet)/100 ml	10 min	73	Fe(III)	Tuttle, et al. (1977)
oxalacetic acid	10^{-2}	8 mg/5 ml	10 min	60	Fe(III)	Dugan (1975)
	10^{-2}	0.4 mg(wet)/100 ml	10 min	90	Fe(III)	Tuttle, et al. (1977)
propionic acid	10^{-2}	0.4 mg(wet)/100 ml	10 min	60	Fe(III)	Tuttle, et al. (1977)
butyric acid	10^{-2}	0.4 mg(wet)/100 ml	10 min	60	Fe(III)	Tuttle, et al. (1977)
valeric acid	10^{-2}	0.4 mg(wet)/100 ml	10 min	60	Fe(III)	Tuttle, et al. (1977)
aspartic acid	10^{-2}	0.4 mg(wet)/100 ml	10 min	5	Fe(III)	Tuttle, et al. (1977)
benzoic acid	(10 mg/L)	ND	6 weeks	100	Fe(II)	Onysko, et al. (1984)
sorbic acid	(10 mg/L)	ND	6 weeks	100	Fe(II)	Onysko, et al. (1984)
Anionic surfactant						
ABS	(5 mg/L)	5 mg/L	64 h	100	*E*	Dugan (1975)
SLS	(5 mg/L)	5 mg/L	64 h	100	*E*	Dugan (1975)
	(5 mg/L)	ND	6 weeks	100	Fe(II)	Onysko, et al. (1984)
Others						
NaN_3	10^{-5}	ND	3 min	100	O_2 uptake	Arkesteyn (1979)
NEM	10^{-5}	ND	3 min	100	O_2 uptake	Arkesteyn (1979)

ND: not described

Table 1.9 Inhibition of sulfur-oxidizing activity in *Thiobacillus thiooxidans*

Inhibitor	Dose /mol dm^{-3}	Inoculume size	Incubation time	Inhibition / %	Measurement	Reference
Organic acids						
formic acid	10^{-3}~10^{-2}	ND	10 days	100	O_2 uptake	Iwatsuka, et al. (1960)
acetic acid	10^{-3}~10^{-2}	ND	10 days	73.5~100	O_2 uptake	Iwatsuka, et al. (1960)
oxalacetic acid	10^{-5}	0.2 mg protein	20 days	60	Protein	Borichewski (1967)
pyruvic acid	10^{-5}	0.2 mg protein	20 days	16	Protein	Borichewski (1967)
propionic acid	10^{-3}~10^{-2}	ND	10 days	65.2~100	O_2 uptake	Iwatsuka, et al. (1960)
malic acid	10^{-3}~10^{-2}	ND	10 days	0~32.0	O_2 uptake	Iwatsuka, et al. (1960)
maleic acid	10^{-3}~10^{-2}	ND	10 days	0~34.0	O_2 uptake	Iwatsuka, et al. (1960)
oxalic acid	10^{-3}~10^{-2}	ND	10 days	0~15.0	O_2 uptake	Iwatsuka, et al. (1960)
malonic acid	10^{-3}~10^{-2}	ND	10 days	0~50.0	O_2 uptake	Iwatsuka, et al. (1960)
succinic acid	10^{-3}~10^{-2}	ND	10 days	0~81.9	O_2 uptake	Iwatsuka, et al. (1960)
	10^{-3}~10^{-1}	1 ml of 7-day-old culture	12 days	100	Protein	Butler, et al. (1966)
fumaric acid	10^{-3}~10^{-2}	ND	10 days	20~73.2	O_2 uptake	Iwatsuka, et al. (1960)
aspartic acid	10^{-3}~10^{-1}	1 ml of 7-day-old culture	12 days	0	Protein	Butler, et al. (1966)
β-alanine	10^{-2}~10^{-1}	1 ml of 7-day-old culture	12 days	100	Protein	Butler, et al. (1966)
DL-α-alanine	10^{-1}	1 ml of 7-day-old culture	12 days	66	Protein	Butler, et al. (1966)
L-valine	10^{-3}~10^{-2}	ND	33 hours	47~93	$S_2O_3^{2-}$	Lu, et al. (1971)
L-isoleucine	10^{-3}~10^{-2}	ND	33 hours	8~10	$S_2O_3^{2-}$	Lu, et al. (1971)
L-leucine	10^{-3}~10^{-2}	ND	33 hours	16~18	$S_2O_3^{2-}$	Lu, et al. (1971)
L-phenylalanine	10^{-3}~10^{-2}	ND	33 hours	19~22	$S_2O_3^{2-}$	Lu, et al. (1971)
L-methionine	10^{-3}~10^{-2}	ND	33 hours	69~93	$S_2O_3^{2-}$	Lu, et al. (1971)
L-cysteine	10^{-3}~10^{-2}	ND	33 hours	95~98	$S_2O_3^{2-}$	Lu, et al. (1971)
L-tryptophan	10^{-3}	ND	33 hours	2	$S_2O_3^{2-}$	Lu, et al. (1971)
L-tyrosine	10^{-3}	ND	33 hours	11	$S_2O_3^{2-}$	Lu, et al. (1971)
L-arginine	10^{-3}~10^{-2}	ND	33 hours	10~14	$S_2O_3^{2-}$	Lu, et al. (1971)
L-glutamate	10^{-3}~10^{-2}	ND	33 hours	24~28	$S_2O_3^{2-}$	Lu, et al. (1971)
L-histidine	10^{-3}~10^{-2}	ND	33 hours	64~73	$S_2O_3^{2-}$	Lu, et al. (1971)
L-aspartate	10^{-3}~10^{-2}	ND	33 hours	0	$S_2O_3^{2-}$	Lu, et al. (1971)
L-serine	10^{-3}~10^{-2}	ND	33 hours	30~71	$S_2O_3^{2-}$	Lu, et al. (1971)
L-alanine	10^{-3}~10^{-2}	ND	33 hours	15~34	$S_2O_3^{2-}$	Lu, et al. (1971)
L-lysine	10^{-3}~10^{-2}	ND	33 hours	0	$S_2O_3^{2-}$	Lu, et al. (1971)
L-threonine	10^{-3}~10^{-2}	ND	33 hours	0~6	$S_2O_3^{2-}$	Lu, et al. (1971)
L-proline	10^{-3}~10^{-2}	ND	33 hours	0~23	$S_2O_3^{2-}$	Lu, et al. (1971)
L-glutamine	10^{-3}~10^{-2}	ND	33 hours	0	$S_2O_3^{2-}$	Lu, et al. (1971)
L-glycylglycine	10^{-3}~10^{-2}	ND	33 hours	24~30	$S_2O_3^{2-}$	Lu, et al. (1971)
L-asparagine	10^{-3}~10^{-2}	ND	33 hours	18~42	$S_2O_3^{2-}$	Lu, et al. (1971)
Others						
KCN	10^{-5}~10^{-3}	ND	10 days	62~100	O_2 uptake	Iwatsuka, et al. (1960)
	10^{-3}	ND	10 min	100	O_2 uptake	Adair (1966)
NaN_3	10^{-5}~10^{-3}	ND	10 days	83.3~100	O_2 uptake	Iwatsuka, et al. (1960)
	10^{-3}	ND	10 min	100	O_2 uptake	Adair (1966)

ND: not described

interest in interaction of humic substances with metal ions has been rapidly aroused (e. g., Miyajima and Mori, 1996). The effect of humic substances on biogeochemical cycling of Fe(II, III) has also been discussed in field studies (Luther, et al., 1992; 1996). Humic substances are capable of reducing Fe(III) to Fe(II) ions (Skogerboe, et al., 1981), and forming complexes with Fe(III) ions (Wu and Luther, 1995). It is important to study systematically the role of humic substances in the biogeochemical cycles of Fe and S.

1.6 Objectives and outline of the thesis

As described in the previous sections, pyrite is a common sulfide mineral and its weathering causes environmental damage mainly due to the formation of acid mine drainage containing high concentrations of H^+, Fe(III), and sulfate. The oxidation of pyrite is accelerated by the involvement of iron- and sulfur- oxidizing bacteria growing in aerobic environments. It is important to make clear the mechanism of microbial attack to pyrite, and of oxidative dissolution. In biogeochemical point of view, pyrite weathering is also a part of geochemical cycles of Fe and S, and complicate changes in chemical states of sulfur species (from -2 to +6) are especially interested.

The purposes of this study are (a) to clarify the mechanism of microbial attack to pyrite by the iron-oxidizing bacteria *Thiobacillus ferrooxidans*, to establish which mechanism, the "direct" or "indirect" contact mechanism, is predominant, (b) to clarify the mechanism of oxidative dissolution of pyrite by Fe(III) ions, whether the dissolution is congruent or incongruent, and (c) to establish factors suppressing pyrite weathering in order to control strongly acidic drainage. The main oxidant of pyrite in aqueous environments is Fe(III) ions, which precipitates above pH 2.5 and the experimental pH range was confined to around 2, similar to other works on pyrite. The present study was planned carefully to overcome the following experimental difficulties by simplifying systems and by using several analytical methods for one purpose: (1) pyrite is easily oxidized by oxygen, (2) the dissolution rate of pyrite is very slow on a laboratory scale but not on a geochemical one, and (3) microbially mediated reaction is very complicated.

This thesis is composed of eight chapters.

The background and review of previous works on the dissolution of pyrite, and objectives of the study are described in **Chapter 1**, this chapter.

In **Chapter 2**, the microbially mediated dissolution of pyrite by iron-oxidizing bacteria, *Thiobacillus ferrooxidans*, is examined both by solution analysis and surface analysis of pyrite. **Chapter 2** especially discusses the path of the microbial dissolution of pyrite, "direct" or "indirect" based on the experimental results.

In **Chapter 3**, a pretreatment method to obtain a well-defined surface of pyrite is first

established, then oxidative dissolution of pyrite by Fe(III) ions is examined by solution analysis, X-ray photoelectron spectroscopy, and Raman spectroscopy. Stoichiometry of the oxidative dissolution was discussed based on time variations in the amount of released Fe and S species, and on changes in the surface composition.

In **Chapter 4**, the effect of ligands on the oxidizing abilities of Fe(III) ions is investigated to establish means of suppressing the oxidative dissolution of pyrite. Various inorganic and organic acids are surveyed, and the factors controlling their suppression are discussed.

In **Chapter 5**, the effect of cations on the oxidative dissolution of pyrite was investigated, to find other methods of suppressing oxidative dissolution. Eleven different cations including, alkaline, alkaline earth, and transition metal ions, were screened, and the factors controlling suppression effects are discussed.

In **Chapter 6**, inhibitors to iron- and sulfur-oxidizing bacteria were examined taking into account the use of compounds limiting environmental damage. Based on the results in **Chapters 4 and 5**, humic substances and related compounds were selected as inhibitors. The effect of these compounds on cell growth and the substrate-oxidizing ability of bacteria was investigated.

In **Chapter 7,** fulvic, tannic, and oxalic acids were applied to inhibit microbially mediated dissolution of pyrite, building on the results in **Chapters 4, 5 and 6**. The relation between the dissolution behavior of pyrite by bacteria and bacterial growth was investigated, and the functions of these acids are discussed.

Chapter 8 presents the conclusions of the study.

References

Adair, F. W. (1966) Membrane-associated sulfur oxidation by the autotroph *Thiobacillus thiooxidans*. *J. Bacteriol.*, **92**, 899-904.

Arkesteyn, G. J. M. W. (1979) Pyrite oxidation by *Thiobacillus ferrooxidans* with special reference to the sulphur moiety of the mineral. *Antonie van Leeuwenhoek*, **45**, 423-435.

Bancroft, G. M., and Hyland, M. M. (1990) "Spectroscopic studies of adsorption/reduction reactions of aqueous metal complexes on sulphide surfaces." in "*Mineral-Water Interface Geochemistry*" (edited by Hochella, M. F., and White, A. F.), Mineral Society of America, **Chapter 13**, pp. 511-558.

Beck, J. V., and Brown, G. D. (1968) Direct sulfide oxidation in the solubilization of sulfide ores by *Thiobacillus ferrooxidans*. *J. Bacteriol.*, **96**, 1433-1434.

Blowes, D. W., Ptacek, C. J., and Jambor, J. L. (1994) "Remediation and prevention of low-quality drainage from tailings impoundments." in "*Environmental Geochemistry of Sulphide Mine-Wastes*" (edited by Jambor, J. L., and Blowes, D. W.) Vol. 22, Waterloo,

Ontario in Mineralogical Association of Canada. **Chapter 13**, pp. 365-379.

Borichewski, R. M. (1967) Keto acids as growth-limiting factors in autotrophic growth of *Thibacillus thiooxidans*. *J. Bacteriol.*, **93**, 597-599.

Brierley, C. L., and Murr, L. E. (1973) Leaching: use of a thermophilic and chemoautorotrophic microbe. *Science*, **179**, 488-491.

Brown, J. R., Bancroft, G. M., Fyfe, W. S., and MacLean, R. E. N. (1979) Mercury removal from water by iron sulphide minerals. *Environ. Sci. Tech.*, **13**, 1142-1145.

Brown, A. D., and Jurinak, J. J. (1989) Mechanism of pyrite oxidation in aqueous mixtures. *J. Environ. Qual.*, **18**, 545-550.

Buchanan, R. E., and Gibbons, N. E. (eds.) (1974) *Bergry's Manual of Determinative Bacteriology*, 8th Edition Baltimore, Willams & Wilkins Company, pp. 458-461.

Butler, R. G., and Umberit, W. W. (1966) Absorption and utilization of organic matter by the strict autotroph, *Thibacillus thiooxidans*, with special reference to aspartic acid. *J. Bacteriol.*, **91**, 661-666.

Buckley, A. N., and Woods, R. (1987) The surface oxidation of pyrite. *Appl. Sur. Sci.*, **27**, 437-452.

Caruccio, F. T., Geidel, G., and Swell, J. M. (1976) The character of drainage as a function of the occurrence of framboidal pyrite and ground water quality in Eastern Kentucky. *Pap. Symp. Coal Mine Drain Res.*, **6**, 1-16.

Dugan, P. R. (1975) Bacterial ecology of strip mine areas and its relationship to the production of acidic mine drainage. *Ohio J. Sci.*, **75**, 265-279.

Dugan, P. R., and Apel, W. A. (1983) Bacteria and acidic drainage from coal refuse: Inhibition by sodium lauryl sulfate and sodium benzoate. *Appl. Environ. Microbiol.*, **46**, 279-282.

Duncan, D. W., and Walden, C. C. (1972) Microbiological leaching in the presence of ferric iron. *Dev. Ind. Microbiol.*, **13**, 66-75.

Gait, R. I. (1978) The crystal forms of pyrite. *Minreral. Res.*, **9**, 219-229.

Garrels, R. M., and Thompson, M. E. (1960) Oxidation of pyrite by iron sulfate solutions. *Amer. J. Sci.*, **258-A**, 57-67.

Goldhaber, M. B. (1983) Experimental study of metastable sulfur oxidation formation during pyrite oxidation at pH 6-9 and 30℃. *Amer. J. Sci.*, **283-M**, 193-217.

Gould, W. D., Bechard, G., and Lortie, L. (1994) "The nature and role of microorganisms in the tailings environment." in "*Environmental Geochemistry of Sulphide Mine-Wastes*," (edited by Jambor, J. L., and Blowes, D. W.) Vol. 22, Waterloo, Ontario in Mineralogical Association of Canada. **Chapter 7**, pp. 185-199.

Hyland, M. M., and Bancroft, G. M. (1989) An XPS study of gold deposition at low temperatures on sulphide minerals: Reducing agents. *Geochim. Cosmochim. Acta*, **53**, 367-372.

Imai, K., Sugio, T., Yasuhara, T., and Tano, T. (1972) Oxidation of iron by bacteria. *J. Min. Met. Inst. Japan.* **88**, 879-883 (in Japanese).

Imai, K., Sugio, T., Tsuchida, T., and Tano, T. (1975) Effect of heavy metal ions on the growth and iron-oxidizing activity of *Thiobacillus ferooxidans*. *Agr. Biol. Chem.*, **39**, 1349-1354.

Imai, K. (1976) Effect of heavy metal ions on the activity of an iron-oxidizing chemoautotroph. *Proc. Joint MMIJ-AIME Meeting,* Denver, Colo., USA, pp. 321-332.

Imai, K. (1984) *Dokuritsueiyo Saikin (Chemoautotroph bacteria)*, Kagaku Dojin, Kyoto (in Japanese).

Ingledew, W. J. (1982) *Thibacillus ferrooxidans.* The bioenergetics of an acidophilic chemolithotroph. *Biochimica et Biophysica Acta*, **683**, 89-117.

Ishikawa, Y. (1991) *Kuroko (black ore).* Kyoritsu, Tokyo (in Japanese).

Iwatsuka, H., and Mori, T. (1960) Studies of the metabolism of a sulfur-oxidizing bacterium 1. Oxidation of sulfur. *Plant & Cell Physiol.*, **1**, 163-172.

Jambor, J. L. (1994) "Mineralogy of sulphide-rich tailings and their oxidation products." in "*Environmental Geochemistry of Sulphide Mine-Wastes*" (edited by Jambor, J. L. and Blowes, D. W.), Vol. 22, Waterloo, Ontario in Mineralogical Association of Canada, **Chapter 3**, pp. 59-102.

Jarrett, H. S., Cloud, W. H., Bouchard R. J., Bulter, S. R., Frederick, C. G., and Gillson, J. L. (1968) Evidence for itinerant *d*-electron ferromagnetism. *Phys. Rev. Letters*, **21**, 617-620.

Jean, G. E., and Bancroft, G. M. (1986) Heavy metal adsorption by sulphide mineral surfaces. *Geochim. Cosmochim. Acta*, **50**, 1455-1463.

Kato, S. (1991) "X-ray diffraction analysis" Uchidaroukakuho, Tokyo, p.78 (in Japanese).

Kleinmann, R. L. P., Crerar, D. A., and Pacelli, R. R. (1981) Biogeochemistry of acid mine drainage and a method to control acid formation. *Min. Engng.*, **March**, 300-305.

Lacey, D. Y., and Lawson, F. (1970) Kinetics of the liquid-phase oxidation of acid ferrous sulfate by the bacterium *Thiobacillus ferrooxidans*. *Biotech. Bioeng.* **12**, 29-50.

Lu, M. C., Martin, A., and Rittenberg, S. (1971) Inhibition of growth of obligately chemolithophic thiobacilli by amino acids. *Arch. Mikrobiol.*, **79**, 354-366.

Lowson, R. T. (1982) Aqueous oxidation of pyrite by molecular oxygen. *Chemical Reviews*, **82**, 461-497.

Luther III, G. W. (1987) Pyrite oxidation and reduction: Molecular orbital theory considerations. *Geochim. Cosmochim. Acta*, **51,** 3193-3199.

Luther III, G. W., Kostka, J. E., Church, T. M., Sulzberger, B., and Stumm, W. (1992) Seasonal iron cycling in the salt-marsh sedimentary environment: the importance of ligand complexes with Fe(II) and Fe(III) in the dissolution of Fe(III) minerals and pyrite, respectively. *Marine Chemistry*, **40**, 81-103.

Luther III, G. W., Shellenbarger, P. A., and P. L. Brendel, P. L. (1996) Dissolved organic Fe(III) and Fe(II) complexes in salt marsh porewaters. *Geochim. Cosmochim. Acta,* **60**, 951-960.

Mathews, C. T., and Robins, R. G. (1972) The oxidation of iron disulfide by ferric sulphate. *Aust. Chem. Eng.,* **Aug.** , 21-25.

McKibben, M. A., and Barnes, H. L. (1986) Oxidation of pyrite in low temperature acidic solutions: Rate laws and surface textures. *Geochim. Cosmochim. Acta*, **50,** 1509-1520.

Miyajima, T., and Mori, M. (1996) Complexation equilibria of humic substances in aqueous solution (Review). *Bunseki Kagaku*, **45**, 369-399 (in Japanese).

Moses, C. O., Nordstrom, D. K., Herman, J. S., and Mills, A. L. (1987) Aqueous pyrite oxidation by dissolved oxygen and by ferric iron. *Geochim. Cosmochim. Acta*, **51,** 1561-1571.

Moses, C. O., and Herman, J. S. (1991) Pyrite oxidation at circumneutral pH. *Geochim. Cosmochim. Acta*, **55**, 471-482.

Murr, L. E. (1980) Theory and practice of copper sulphide leaching in dumps and in-situ. *Minerals Sci. Engng.*, **12**, 121-189.

Mycroft, J. R., Mcintyre, N. S., Lorimer, J. W., and Hill, I. R. (1990) Detection of sulfur and polysulphides on electrochemically oxidized pyrite surfaces by X-ray photoelectron spectroscopy and Raman spectroscopy. *J. Electroanal. Chem.*, **292,** 139-152.

Nicholson, R. V., Gillham, R. W., and Reardon, E. J. (1988) Pyrite oxidation in carbonate-buffered solutions: 1 Experimental kinetics. *Geochim. Cosmochim. Acta*, **52**, 1077-1085.

Nordstrom, D. K. (1982) "Aqueous pyrite oxidation and the consequent formation of secondary iron minerals." in "*Acid Sulfate Weathering*" (edited by Hossaer, L. R., et al.), **Chapter 3**., *Soil Sci. Soc. Amer.*, pp. 37-63.

Onysko, S. J., Kleinmann, R. L. P., and Erickson, P. M. (1984) Ferrous iron oxidation by *Thiobacillus ferrooxidans*: Inhibition with benzoic acid, sorbic acid, and sodium lauryl sulfate. *Appl. Environ. Microbiol.*, **48**, 229-231.

Ostwald, J., and England, B. M. (1979) The relationship between euhedral and framboidal pyrite in base-metal sulphide ore. *Minreral Mag.*, **43**, 297-300.

Perry, D. L., Tsao, L., and Taylor, J. A. (1984) "Surface studies of the interaction of copper ions with metal sulfide minerals." in "*Proc. Int. Symp. Electrochem. in Mineral and Metal Processing.*" (edited by Rocherdson, P. E., Srinvasan, S., and Woods, R.) The Electrochem. Soc., Pennington, NJ, pp. 169-184.

Pronk, J. T., Meijer, W. M., Hazeu, W., Dijken, J. P., Bos, P., and Keenen, J. G. (1991) Growth of *Thiobacillus ferrooxidans* on formic acid. *Appl. Environ. Microbiol.*, **57**, 2057-2062.

Rastogi, V. (1996) Water quality and reclamation management in mining using bactericides. *Mining Engineering*, **48**, 71-76.

Rittenberg, S. C. (1972) The obligate autotroph --- the demise of a concept. *Antonie Van*

Leeuwenhoek J. Microbiol. Serol. **38**, 457-478.

Rimstidt, J. D., and Newcomb, W. D. (1993) Measurement and analysis of rate data: The rate of ferric iron with pyrite. *Geochim. Cosmochim. Acta*, **57**, 1919-1934.

Sakai, N., Ishizaki, C., Chida, H., and Shimoiizaka, J. (1987) A kinetic study of pyrite oxidation by ferric sulfate. *J. Min. Met. Inst. Japan*, **103**, 395-400 (in Japanese).

Sato, K. (1984) Pyrites from a spectroscopic point of view. *Oyobutsuri*, **53**, 394-401 (in Japanese).

Sato, K. (1985) Pyrite type compounds-with particular reference to optical characterization. *Prog. Crystal Growth and Charat.*, **Vol. 11**, 109-154.

Silver, M., and Torma, A. E. (1974) Oxidation of metal sulphides by *Thiobacillus ferrooxidans* grown on different substances. *Can. J. Microbiol.*, **20**, 141-147.

Silverman, M. P. (1967) Mechanism of bacterial pyrite oxidation. *J. Bacteriol.*, **94**, 1046-1051.

Singer, P. C., and Stumm, W. (1970) Acid mine drainage: The rate-determining step. *Science*, **167**, 1121-1123.

Skogerboe, R. K., and Wilson, S. A. (1981) Reduction of ionic species by fulvic acid. *Anal. Chem.*, **53**, 228-232.

Smith, E. E., and Shumate, K. S. (1970) Sulfide to sulfate reaction mechanism. *Water Pollut. Control Res. Ser. Rept. 14010 FPS 02170, Fed. Water Quality Admin., U. S. Dept. of the Interior*, 1-115.

Taylor, B. E., Wheeler, M. C., and Nordstrom, D. K. (1984a) Isotope composition of sulfate in acid mine drainage as measure of bacterial oxidation. *Nature*, **308**, 538-541.

Taylor, B. E., Wheeler, M. C., and Nordstrom, D. K. (1984b) Stable isotope geochemistry of acid mine drainage: Experimental oxidation of pyrite. *Geochim. Cosmochim. Acta*, **48**, 2669-2678.

Tuttle, J. H., and Dugan, P. R. (1976) Inhibition of growth, iron, and sulfur oxidation in *Thiobacillus ferrooxidans* by simple organic compounds. *Can. J. Microbiol.*, **22**, 719-730.

Tuttle, J. H., Dugan, P. R., and Apel, W. A. (1977) Leakage of cellular material from *Thiobacillus ferrooxidans* in the presence of organic acids. *Appl. Environ. Microbiol.*, **33**, 459-469.

Tuovinen, O. H., Niemela, S. I., and Gyllenberg, H. G. (1971) Effect of mineral nutrients and organic substances on the development of *Thiobacillus ferrooxidans*. *Biothech. Bioengn.* **XIII**, 517-527.

Tuovinen, O. H., and Kelly, D. P. (1972) Biology of *Thiobacillus ferrooxidans* in relation to the microbiological leaching of sulphide ores. *Z. Allg. Mikrobiol.*, **12**, 311-346.

Voigt, S., Szargan, R., and Suoninen, E. (1994) Interaction of copper(II) ions with pyrite and its influence on ethyl xanthate adsorption. *Sur. Inter. Anal.*, **21**, 526-536.

Wakao, N., Mishina, M., Sakurai, Y., and Shiota, H. (1983) Bacterial pyrite oxidation II.

The effect of various organic substances on release of iron from pyrite by *Thiobacillus ferroxidans*. *J. Gen. Appl. Microbiol.*, **29**, 177-186.

Walsh, F., and Mitchell, R. (1975) Mine drainage pollution reduction by inhibition of iron bacteria. *Wat. Res.*, **9**, 525-528.

Williamson, M. A., and Rimstidt, J. D. (1994) The kinetic and electrochemical rate-determining step of aqueous pyrite oxidation. *Geochim. Cosmochim. Acta*, **58**, 5443-5454.

Wiersma, C. L., and Rimstidt, J. D. (1984) Rates of reaction of pyrite and marcasite with ferric iron at pH 2. *Geochim. Cosmochim. Acta*, **48**, 85-92.

Wu, J., and Luther III, G. W. (1995) Complexation of iron (III) by natural organic ligands in Northwest Atlantic Ocean by a competitive ligand equilibration method and a kinetic approach. *Mar. Chem.*, **50**, 159-177.

Zouboulis, A. I., Kydros, K. A., and Matis, K. A. (1993) Arsenic(III) and arsenic(V) removal from solutions by pyrite fines. *Separ. Sci. Technol.*, **28**, 2449-2463.

Zouboulis, A. I., Kydros, K. A., and Matis, K. A. (1995) Removal of hexavalent chromium anions from solutions by pyrite fines. *Wat. Res.*, **29**, 1755-1760.

Chapter 2
Microbially mediated dissolution of pyrite by iron-oxidizing bacteria

Microbially mediated dissolution of pyrite by *T. ferrooxidans* around pH 2, is expressed conventionally as follows (e. g., Murr, 1980):

$$FeS_2 + 7/2\ O_2 + H_2O = Fe^{2+} + 2\ SO_4^{2-} + 2\ H^+ \quad \text{(mainly chemical reaction)} \quad (2.1)$$

$$Fe^{2+} + 1/2\ O_2 + 2\ H^+ = Fe^{3+} + H_2O \quad \text{(biological reaction)} \quad (2.2)$$

$$FeS_2 + 2\ Fe^{3+} = 3\ Fe^{2+} + 2\ S \quad \text{(chemical reaction)} \quad (2.3)$$

$$FeS_2 + 14\ Fe^{3+} + 8\ H_2O = 15\ Fe^{2+} + 2\ SO_4^{2-} + 16\ H^+ \quad \text{(chemical reaction)} \quad (2.4)$$

$$2\ S + 3\ O_2 + 2\ H_2O = 4\ H^+ + 2\ SO_4^{2-} \quad \text{(biological reaction)} \quad (2.5)$$

As described in **Chapter 1**, the mechanism of microbial attack of *Thiobacillus ferrooxidans* to pyrite has long been an object of argument.

In the present chapter, the mechanism of microbially mediated dissolution of pyrite with *T. ferrooxidans,* using instrumental analysis of minerals, such as diffuse reflectance infrared Fourier transformed spectroscopy (DRIFTS), X-ray photoelectron spectroscopy (XPS), and Electron probe X-ray microanalysis (EPMA) in addition to aqueous analysis was investigated.

2.1 Experimental

2.1.1 Pyrite

Pyrite was supplied from the Yanahara mines (Japan). The metal composition in the sample was determined by inductively coupled plasma-atomic emission spectrometry (ICP-AES), after decomposition in a 5:1 mixture of HNO_3 and HF at 150 ℃ for 2 h (Nakamura, 1991), as shown in **Table 2.1**.

Table 2.1 Elemental composition of pyrite from the Yanahara mines (mg g^{-1})

Na	Al	Si	P	S	K	Ca	Mn	Fe	Cu	Zn	As
0.046	1.38	12.0	0.806	523	1.05	1.36	0.055	458	2.10	2.22	<0.075

The pyrite was ground in a vibration ball mill SM-06 (Yokoyama Co. Ltd.) and then sieved to obtain the size fraction between 43~147 μm. The X-ray powder diffraction lines for the sample were measured using NaCl as a standard and they were identical to those of pyrite.

No other diffraction lines were observed with this sample except for a very weak line of SiO_2 (d = 0.338 nm), which did not take part in the dissolution experiments (Sasaki, et al., 1994; Sasaki, 1994). In this chapter, the pretreatment of the sample is not discussed. The specific surface area was determined to be 1.24 m^2g^{-1} by the N_2 adsorption one point BET method with a Quantasorb QS-13 (Yuasa Ionics Co. Ltd., Japan).

2.1.2 Microorganisms and culture

Iron-oxidizing microorganisms, *Thiobacillus ferrooxidans*, were isolated from acid mine drainage in the Toyoha mines (HUTY8906) (Takamori, et al., 1990) and cultivated routinely as follows: the microorganisms are inoculated to a 150 cm^3 of 9K medium (Silverman and Lundgren (1959), i. e. 15 mmol dm^{-3} $(NH_4)_2SO_4$, 2.0 mmol dm^{-3} $MgSO_4 \cdot 7H_2O$, 1.3 mmol dm^{-3} KCl, 5.7 mmol dm^{-3} K_2HPO_4, 0.061 mmol dm^{-3} $Ca(NO_3)_2$, and 160 mmol dm^{-3} $FeSO_4 \cdot 7H_2O$ (energy source)) adjusted to pH 2 with H_2SO_4, in a silico-plugged 500-cm^3 Erlenmeyer flask. The basal solution of 9K (without an energy source) is sterilized by autoclaving at 120 ℃ for 20 min, and glass assemblies are sterilized by heating to 180℃ for 2 h. The flasks are installed in a rotary shaking culture-apparatus TB-16 (Takasaki Kagaku Co. Ltd.) at 30 ℃. Under the conventional shaking condition, dissolved oxygen is saturated in the medium. Iron precipitates like jarosite are often formed during the culture for *T. ferrooxidans*, and they are removed by filtrating the cell suspension through a sterile Whatman No. 41 filter paper. The cells are harvested by centrifugation of the filtrate at 18, 000 × g for 20 min, and resuspended in a sterile H_2SO_4 solution (pH ~2.0) for storage in a refrigerator. Prior to the bacterial dissolution of pyrite, the microorganisms are acclimatized to pyrite in a basal solution of the 9K medium.

2.1.3 Dissolution experiments

The 7.5 g of ground pyrite was put into a silico-plugged 500-cm^3 Erlenmeyer flask containing 150 cm^3 of the basal salt solution in the 9K medium. Then, 5 cm^3 of cell suspension with 1.17 $\times 10^8$ active cells cm^{-3}, *T. ferrooxidans*, were inoculated. A control experiment was also carried out without the microorganisms. All flasks were installed in the rotary shaking culture-apparatus at 30 ℃. Incubation was continued for 11 days. At intervals, pH, redox potential (E), and cell number were measured, and 1 cm^3 of supernatant was pipetted off and filtrated with a 0.20 μm pore membrane filter for solution analysis. Cell numbers were counted microscopically (×600). The Fe(II) and total Fe concentrations were determined by the 1, 10-phenanthroline method, and the sulfate concentration was measured by ionic chromatography (Showa Denko, Shodex IC). The FTIR spectra of the solutions were measured with a FTS-65 (BIO-RAD) by a KRS-5 sandwiching method. After the dissolution experiments, the residue was separated using membrane filters with 0.20 μm pore

size and stored in a N_2 purged desiccator for instrumental analysis.

2.1.4 Instrumental analysis

XPS: The chemical species on the surface of the pyrite were analyzed by XPS (V. G. Scientific, ESCALAB Mk II). The samples were pressed onto copper foil on a holder and introduced into the spectrometer. After evacuating to better than 10^{-5} Pa within 15 min, the sample was transferred into an analyzer chamber of better than 5×10^{-8} Pa and cooled below 150 K, then irradiated with Al Kα X ray (15 kV, 10 mA). The binding energies (E_B) were calibrated with E_B[Au $4f_{7/2}$] = 84.0 eV (full width at half maximum (FWHM) = 1.2 eV). The binding energy of C 1s, E_B[C 1s], corresponding to hydrocarbon caused by contamination in the apparatus was 284.7 $\pm$ 0.1 eV and the contamination caused by cooling was disregarded due to its very small intensity. Data treatment was carried out with a VGS 5250 system. Background was drawn according to the Shirley's method (Shirley, 1972). The obtained spectra were separated into sets of $2p_{3/2}$ and $2p_{1/2}$ using Gaussian-Lorentzian mixed functions with a peak area ratio of approximately 2:1, considering tail parameters (Sherwood, 1990).

Relative sensitivity factors between components 1 and 2, s_1/s_2, are determined according to the following equation:

$$s_1/s_2 = (I_1/I_2)(n_2/n_1), \tag{2.6}$$

where s is the relative sensitivity factor including an escape depth of the electrons, n_2/n_1 the mole ratio of component 2 to component 1, and I the intensity by area in which contributions from X-ray satellite peaks was subtracted by computer calculation. The relative sensitivity factors among S 2p, Fe 2p and K 2p were estimated as shown in **Table 2.2**, by measuring XP-spectra for pure pyrite and analytical grade reagents of $FeSO_4 \cdot 7H_2O$, $FeSO_4(NH_4)_2SO_4 \cdot 6H_2O$, $Fe_2(SO_4)_3(NH_4)_2SO_4 \cdot 24H_2O$, K_2SO_4, $K_2Al_2(SO_4) \cdot 24H_2O$, and $K_4Fe(CN)_6 \cdot 3H_2O$ (Konno, et al., 1991). The XP-spectra for pure pyrite was obtained by measuring the fresh surface of cleaved pyrite in argon.

FTIR: Infrared spectra were obtained by diffuse reflectance infrared Fourier transformed spectroscopy (DRIFTS) (BIO-RAD, FTS-65) with diluted samples in KBr, under the conditions: accumulation, 64 times; resolution, 4 cm^{-1}; detector, TGS; range of wavenumbers, 400~4000 cm^{-1}.

EPMA: The morphology and elemental analysis of pyrite particles were obtained with a X-ray microscopy JXA-8600 Superprobe (JEOL) at 15 kV.

XRD: The secondary minerals formed during oxidation were identified by powdery X-ray diffraction patterns (XRD). The XRD patterns were collected by an X-ray diffractometer 3063 (Rigaku Co. Ltd.) and a monochromator detector under the following conditions: radiation

Cu Kα 35 kV 20 mA; time constant, one second; scanning rate, 0.5 in 2θ deg min^{-1}; chart speed, 40 mm min^{-1}.

Table 2.2 Relative sensitivity factors of S 2p, Fe 2p and K 2p

Compounds	Relative sensitivity factor		
	$s_{S\,2p}/s_{Fe\,2p}$	$s_{S\,2p}/s_{K\,2p}$	$s_{K\,2p}/s_{Fe\,2p}$
FeS_2	$0.14_1 \pm 0.00_2$ [a)]	-	-
$FeSO_4 \cdot 7H_2O$	$0.13_7 \pm 0.00_1$ [a)]	-	-
$FeSO_4(NH_4)_2SO_4 \cdot 6H_2O$	0.14	-	-
$Fe(SO_4)_3(NH_4)_2SO_4 \cdot 24H_2O$	0.14_8	-	-
K_2SO_4	-	$0.39_5 \pm 0.00_4$ [a)]	-
$K_2Al_2(SO_4)_4 \cdot 24H_2O$	-	0.42_5	-
$K_4Fe(CN)_6 \cdot 3H_2O$	-	-	0.33_9
Average	$0.14 \pm 0.00_7$ [a)]	$0.40_5 \pm 0.01_8$ [a)]	

a) 1σ

2.2 Results

2.2.1 Solution analysis

As can be seen in **Fig. 2.1**, the growth curve of *T. ferrooxidans* has a logarithmically growth phase at 5~8 days with a dramatic decrease in pH, whereas the pH of the control experiment was almost constant. **Figure 2.2** shows that Fe(III) and sulfate concentration dramatically increased after 4 days in microbially mediated dissolution of pyrite, in contrast with the control. Changes in *E* were in good agreement with the above results, as shown in **Fig. 2.3**. The FTIR spectra of solution samples after 1~11 day-dissolution were very similar to those of the initial solution, indicating that organic compounds were not present.

2.2.2 Surface analysis

XPS: The S 2p spectra were measured as shown in **Fig. 2.4** and separated into 5 sets (A_S, B_S, C_S, D_S, and E_S) of $2p_{3/2}$ and $2p_{1/2}$, assuming that the difference between $E_B[S\ 2p_{3/2}]$ and $E_B[S\ 2p_{1/2}]$ is 1.2 ± 0.1 eV and that the ratio of the integrated intensities, $I[S\ 2p_{3/2}]/I[S\ 2p_{1/2}]$, is ~2. It was found that four peaks B_S, C_S, D_S, and E_S shifted + 2.1~2.4 eV in E_B, due to the differential charging effect caused by secondary formed and nonconducting compounds on pyrite. Electron binding energies for some related elements and compounds are listed in **Table 2.3**. According to **Table 2.3**, the A_S peaks are correspondent to the original pyrite, and peaks B_S, C_S, D_S, and E_S to pyrite, elemental sulfur, sulfite, and sulfate, respectively. The

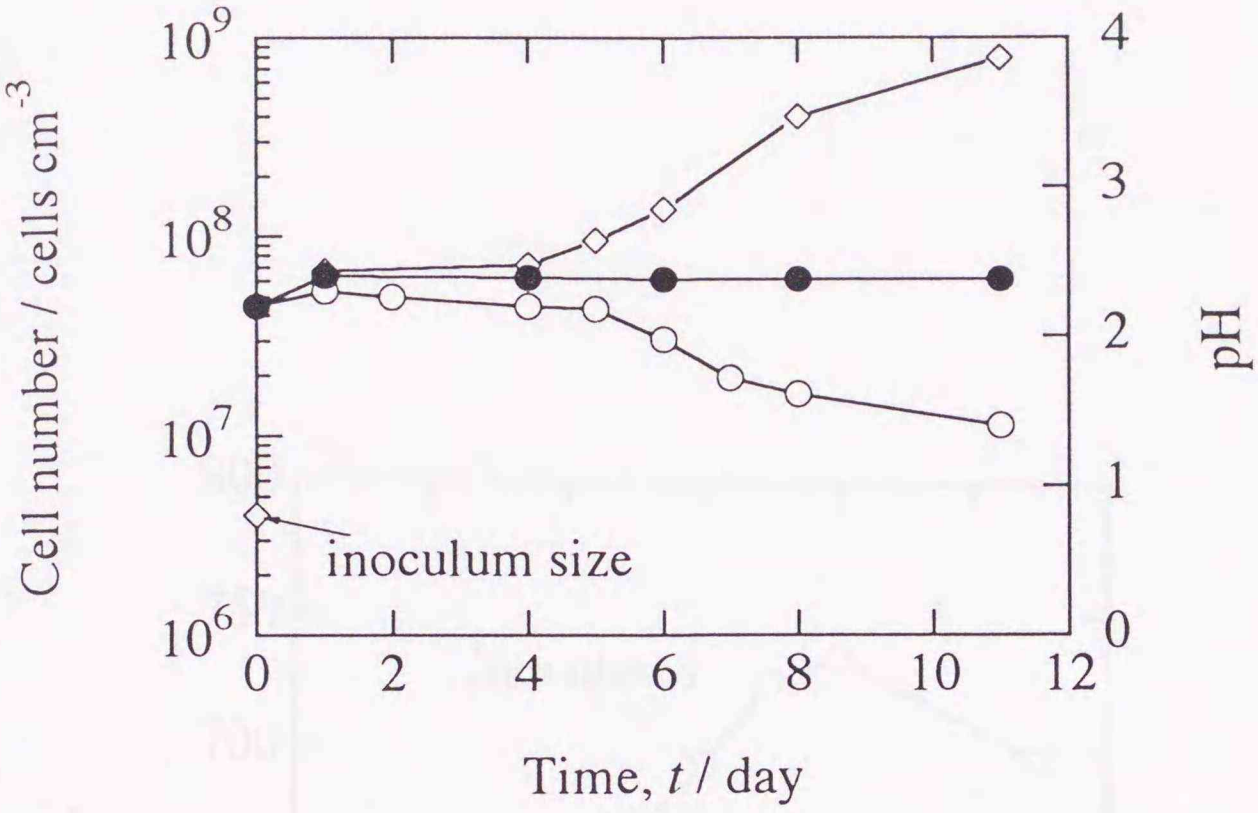

Fig. 2.1 Relationship between cell numbers and pH in microbially mediated dissolution. Symbols: ◇, cell number; ○ & ●, pH. Open and solid symbols indicate results of inoculated and sterilized experiments, respectively.

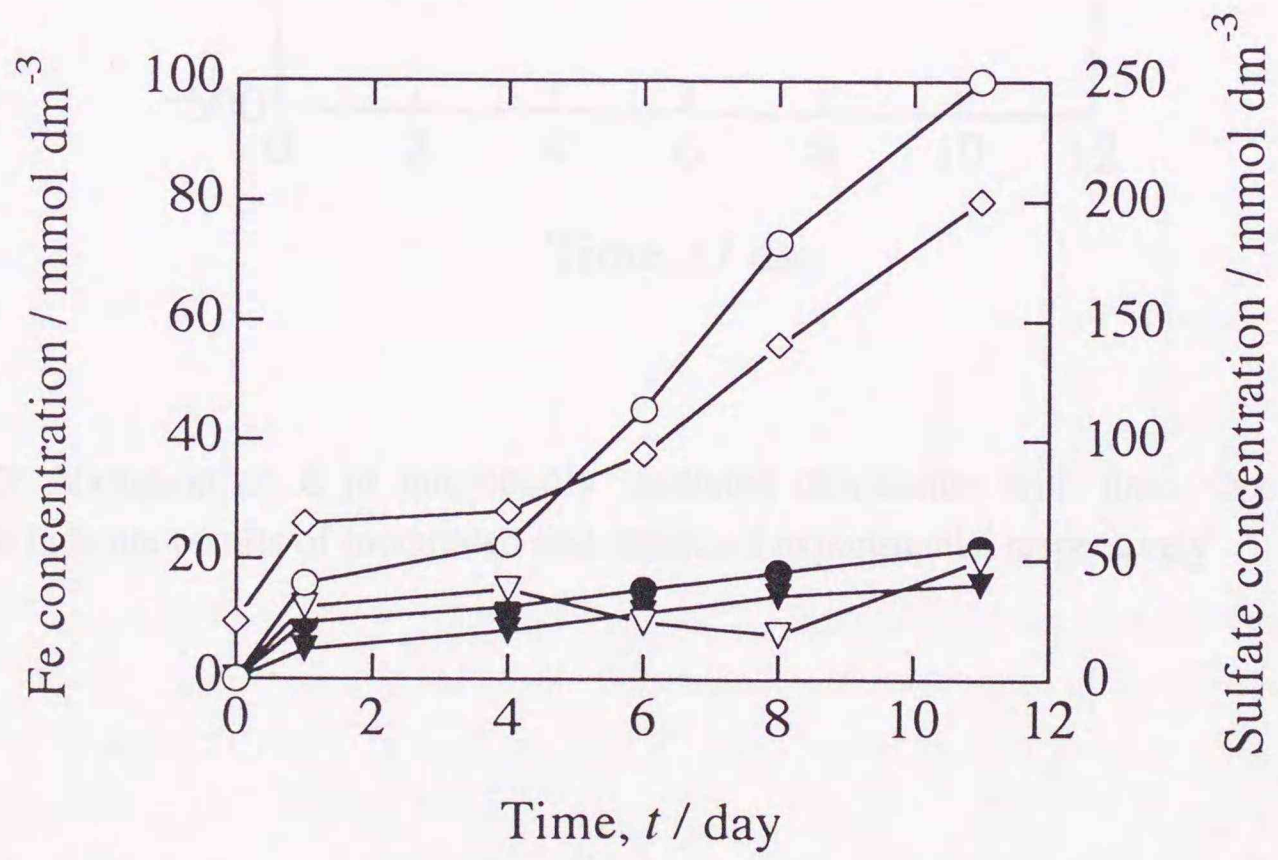

Fig. 2.2 Variation in concentration of total Fe and Fe^{2+} and SO_4^{2-} in microbially mediated dissolution with time. Symbols: ○ & ●, total Fe; ▽ & ▼, Fe^{2+} ; ◇, SO_4^{2-}. Open and solid symbols indicate results of inoculated and sterilized experiments, respectively.

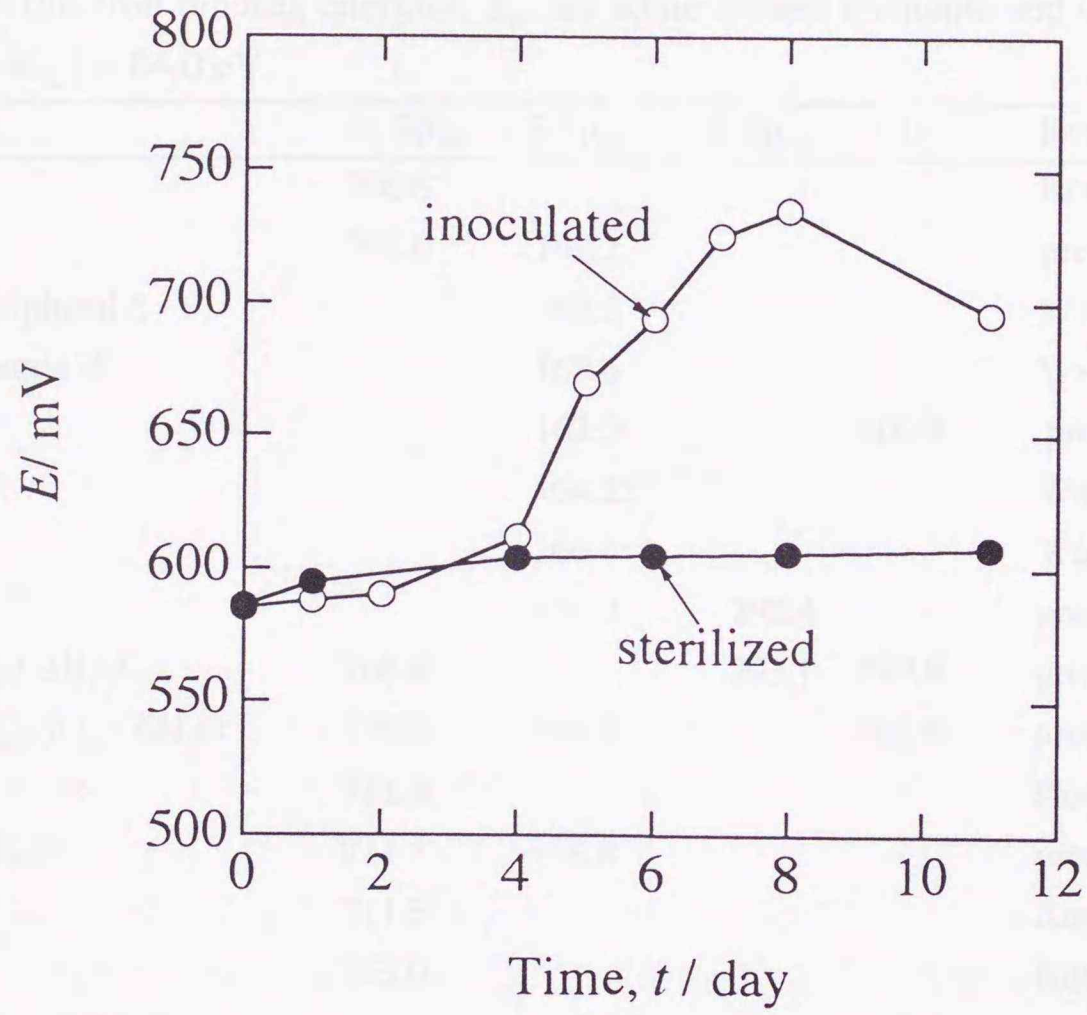

Fig. 2.3 Variation of E in microbially mediated dissolution with time. Open and solid symbols indicate results of inoculated and sterilized experiments, respectively.

FWHM of the separated peaks in S $2p_{3/2}$ was 1.54 eV for pyrite, and 1.60 eV for the others.

In the Fe 2p spectra, there are three apparent peaks (A_{Fe}, B_{Fe}, and C_{Fe}) as shown in **Fig. 2.5**. The FWHM of peak A_{Fe} is the same as one of peak A_S in **Fig. 2.4** , so the A_{Fe} peak corresponds to pyrite. Peaks B_{Fe} and C_{Fe} are assigned to the pyrite and oxidized species (mostly Fe(III) species; Konno and Nagayama, 1980) with the differential charging shift. The difference in E_B[Fe $2p_{3/2}$] between peaks A_{Fe} and B_{Fe} was 2.1~2.4 eV, similar to that in the S 2p spectra.

Table 2.3 Electron binding energies, E_B, for some related elements and compounds corrected by E_B[Au $4f_{7/2}$] = 84.0 eV

Compound	Fe $2p_{3/2}$	S $2p_{3/2}$	K $2p_{3/2}$	N 1s	Remarks
Fe	706.8				Konno, et al., 1980
FeS_2	707.0	162.2			present work
NaS_2O_3 peripheral S		162.5			Wagner, 1990
central S		168.6			Wagner, 1990
l-cysteine		162.9		400.8	present work
S		164.25[a)]			Wagner, 1990
Na_2SO_3		166.6			Wagner, 1990
K_2SO_4		168.0	292.4		present work
$K_4Fe(CN)_6 \cdot 3H_2O$	708.8		293.1	397.9	present work
$FeSO_4(NH_4)_2SO_4 \cdot 6H_2O$	710.8	168.8		401.8	present work
α-Fe_2O_3	711.0				Konno, et al., 1980
$FeSO_4 \cdot 7H_2O$	711.1	168.8			present work
γ-FeOOH	711.3				Konno, et al., 1980
K_2FeO_4	713.0				Konno, et al., 1980
$K_2Al_2(SO_4)_4 \cdot 24H_2O$		168.9	292.9		present work
$Fe_2(SO_4)_3 \cdot nH_2O$	713.3	169.0			present work
$Fe(SO_4)_3(NH_4)_2SO_4 \cdot 24H_2O$	713.5	169.2		402.1	present work

a) E_B at the maximum intensity , not of $2p_{3/2}$.

The relative intensities of $I_{Fe\ 2p}$ and $I_{S\ 2p}$ after biological dissolution are summarized in **Fig. 2.6**. The relative intensities of peaks A_{Fe} and B_{Fe} (corresponding to pyrite-Fe) decreased with time, whereas those of peak C_{Fe} (other Fe species) increased. This was similar to the results of the S 2p spectra (**Fig. 2.6 (b)**).

Figure 2.7 shows spectra changes in the C 1s and K 2p regions. The peak for contamination in the present apparatus was E_B[C 1s] = 284.7 $\pm$ 0.1 eV, as shown in spectrum (a). Peaks shifted + 2.0 eV in E_B after more than 4 days. After 6 days of dissolution, additional peaks were observed around E_B[C 1s] = 288.3 eV, corresponding to cellular carbon

in microorganisms (Castro, et al., 1990). After more than 6 days, these peaks were further additionally observed at E_B[K 2p] ~294 eV and their intensities relatively increased with time to the intensities of the C 1s peaks. **Table 2.4** summarizes E_B-values, based on **Figs. 2.4, 2.5 and 2.7**.

Table 2.4 Electron binding energies, E_B, for pyrite after microbially mediated dissolution. The E_B for surface products were corrected by the pyrite peak positions (A_{Fe} and A_S in **Figs. 2.4 and 2.5**).

Dissolution time /day	E_B/ eV						
	Fe $2p_{3/2}$		S $2p_{3/2}$				K $2p_{3/2}$
	A_{Fe}, B_{Fe}	C_{Fe} [a)]	A_S, B_S	C_S	D_S	E_S	
1	707.0	712.1	162.2	163.8	166.1	-	-
4	707.0	712.6	162.2	163.9	167.0	169.2	-
6	707.0	712.4	162.2	163.7	166.7	168.9	291.9
8	707.0	712.4	162.2	163.9	167.3	169.2	292.2
11	707.0	712.8	162.2	163.8	167.1	169.0	292.2
			Average	163.8_2	166.8_4	169.0_8	292.2
			1σ	0.08	0.47	0.15	0.17

a) Broad peak.

FTIR: The FTIR spectra for pyrite changed with dissolution time as shown in **Fig. 2.8**. In the spectra for unreacted pyrite, the largest band at 1200 cm^{-1} corresponds to the S-O bonding in sulfate. The additional band at 1088 cm^{-1} appeared after one day of dissolution, and a further band at 1005 cm^{-1} appeared after 8 days of dissolution. The two bands increased with time. Three bands at 1200, 1088, and 1005 cm^{-1} are assigned to the vibration modes of S-O bonding in jarosite, $K_3Fe_9(SO_4)_6(OH)_{18}$ (Adler and Kerr, 1965). After 8 days, three bands at 1550, 1650, and 3400 cm^{-1} were also observed, these were assigned to the vibration modes of N-H bonding in polyamide (Riddle and Taft, 1956; Naumann, 1988). This suggests that cellular protein was accumulated on pyrite after 8 days. There were no other organic compounds in the spectra.

EPMA: The morphology of pyrite during biological dissolution is shown in **Fig. 2.9**, in which EPMA was carried out at points (A). It is observed that the surface of pyrite is smooth up to 4 days, similar to unreacted samples, and that it became irregular with increasing dissolution time. In addition to Fe and S the EPMA detected K after more than 6 days of dissolution.

XRD: The XRD patterns of pyrite samples after the biological dissolution were the same as those of unreacted pyrite. Only diffraction lines for pyrite were observed in the samples.

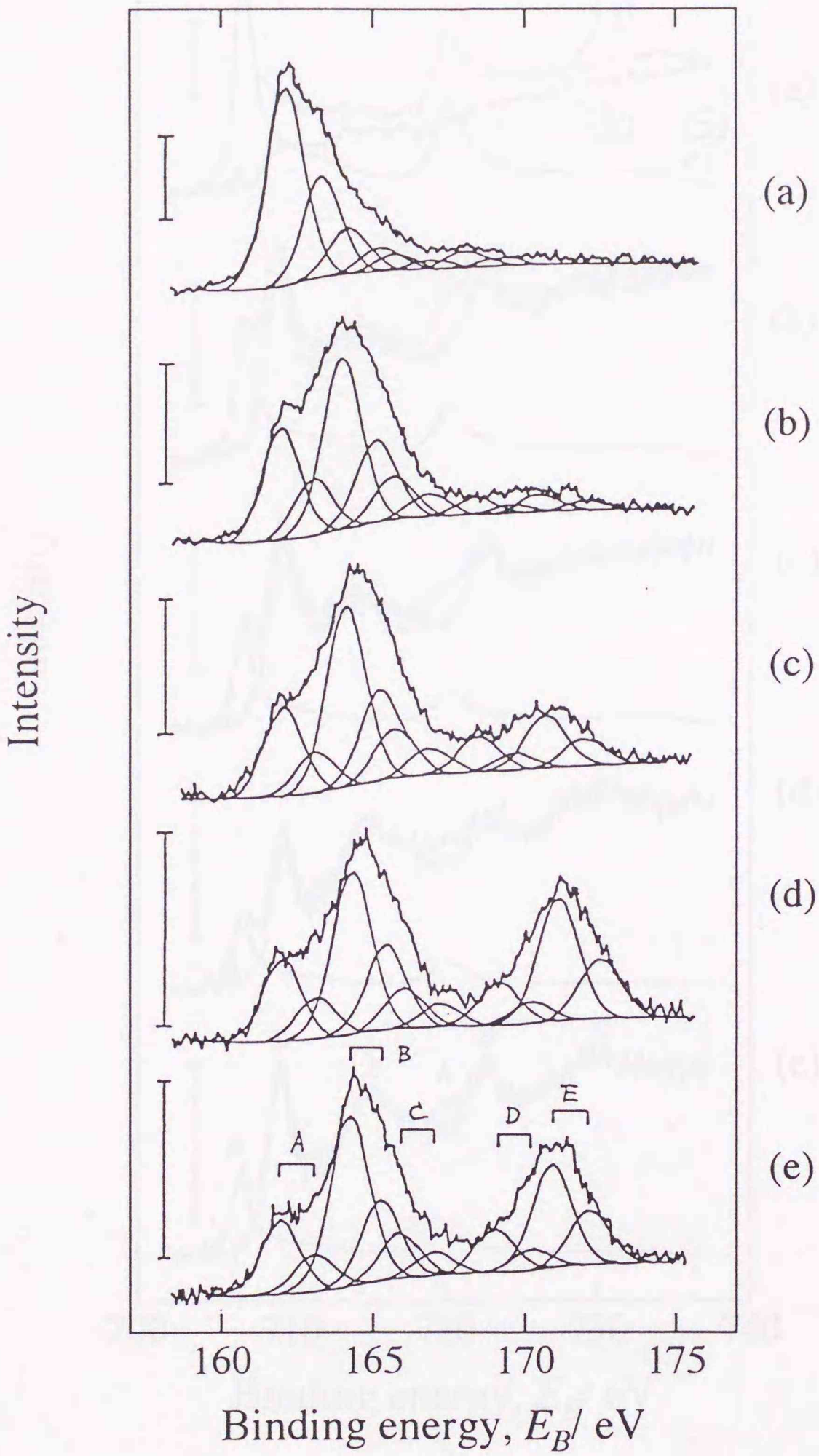

Fig. 2.4 XP-spectra of S 2p for pyrite after microbially mediated dissolution for (a) 1, (b) 4, (c) 6, (d) 8, and (e) 11 days. Vertical bars indicate 500 cps. The spectra were separated into $2p_{3/2}$ and $2p_{1/2}$ sets using Gaussian-Lorentzian mixed functions.

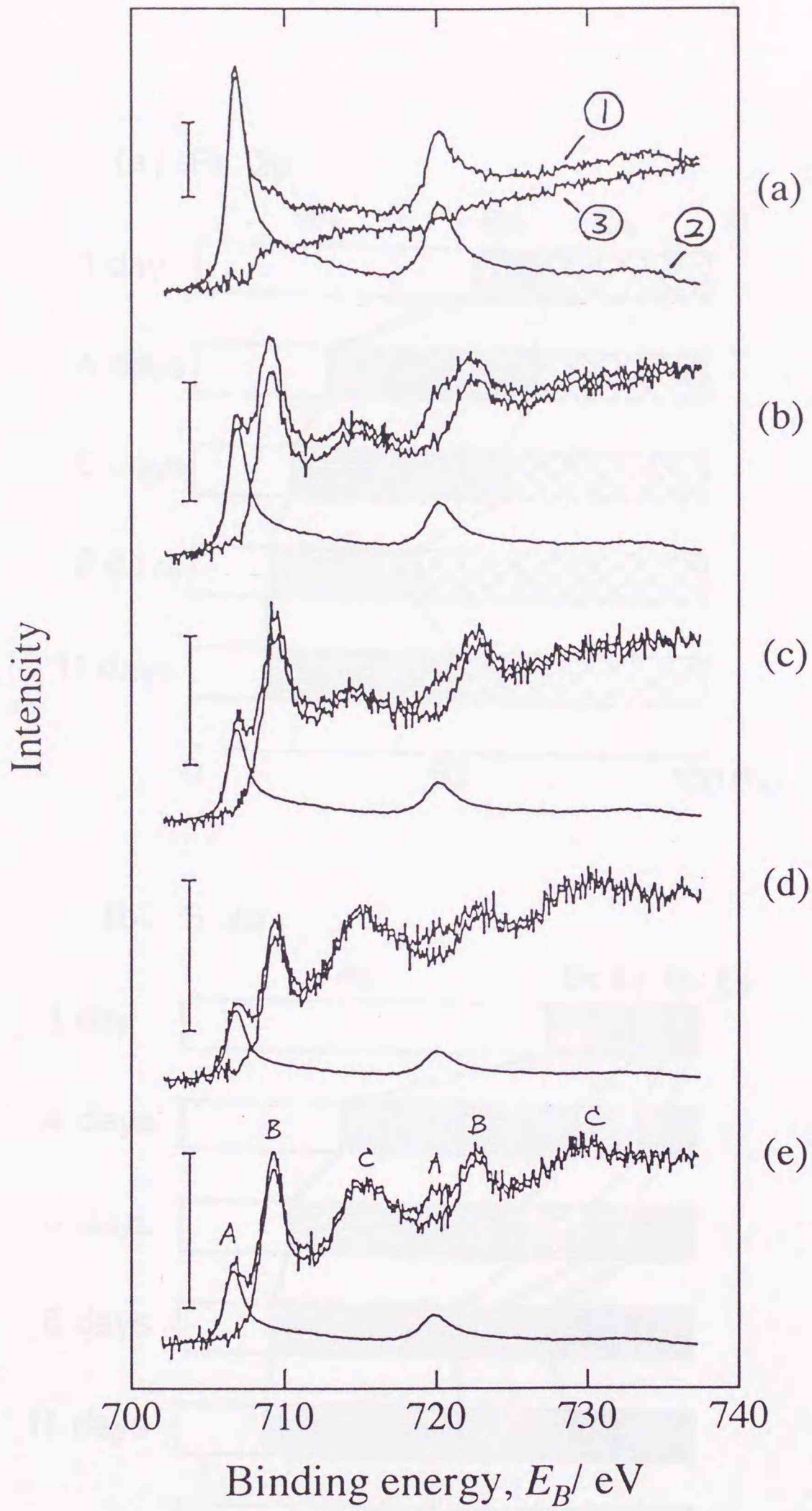

Fig. 2.5 XP-spectra of Fe 2p for pyrite after microbially mediated dissolution for (a) 1, (b) 4, (c) 6, (d) 8, and (e) 11 days. Vertical bars indicate 1 kcps. Symbols: ①, the measured original spectrum; ②, the contribution from unreacted pyrite; ③, the difference between ① and ②.

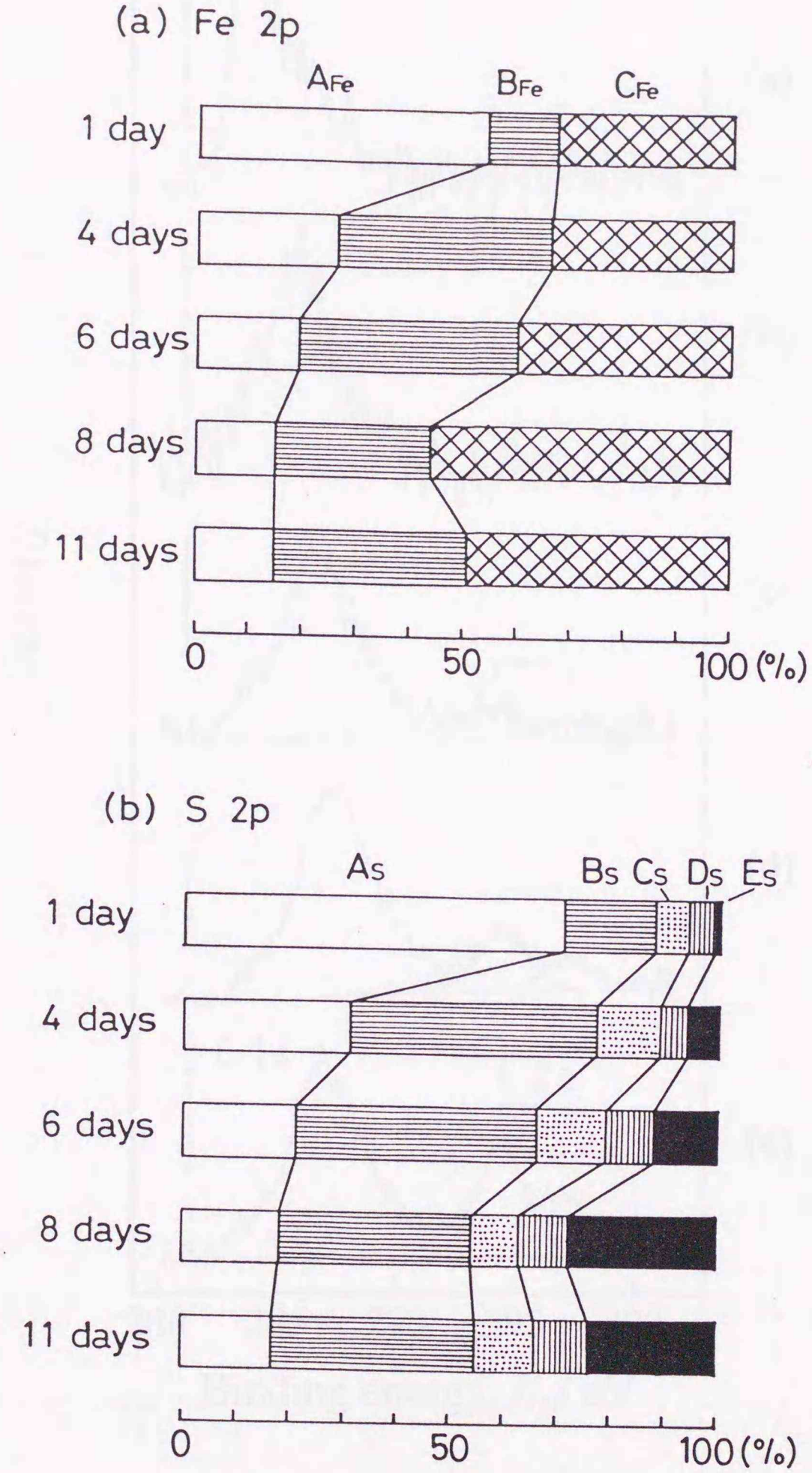

Fig. 2.6 Relative intensities of (a) Fe 2p and (b) S 2p photoelectron peaks for pyrite after microbially mediated dissolution.

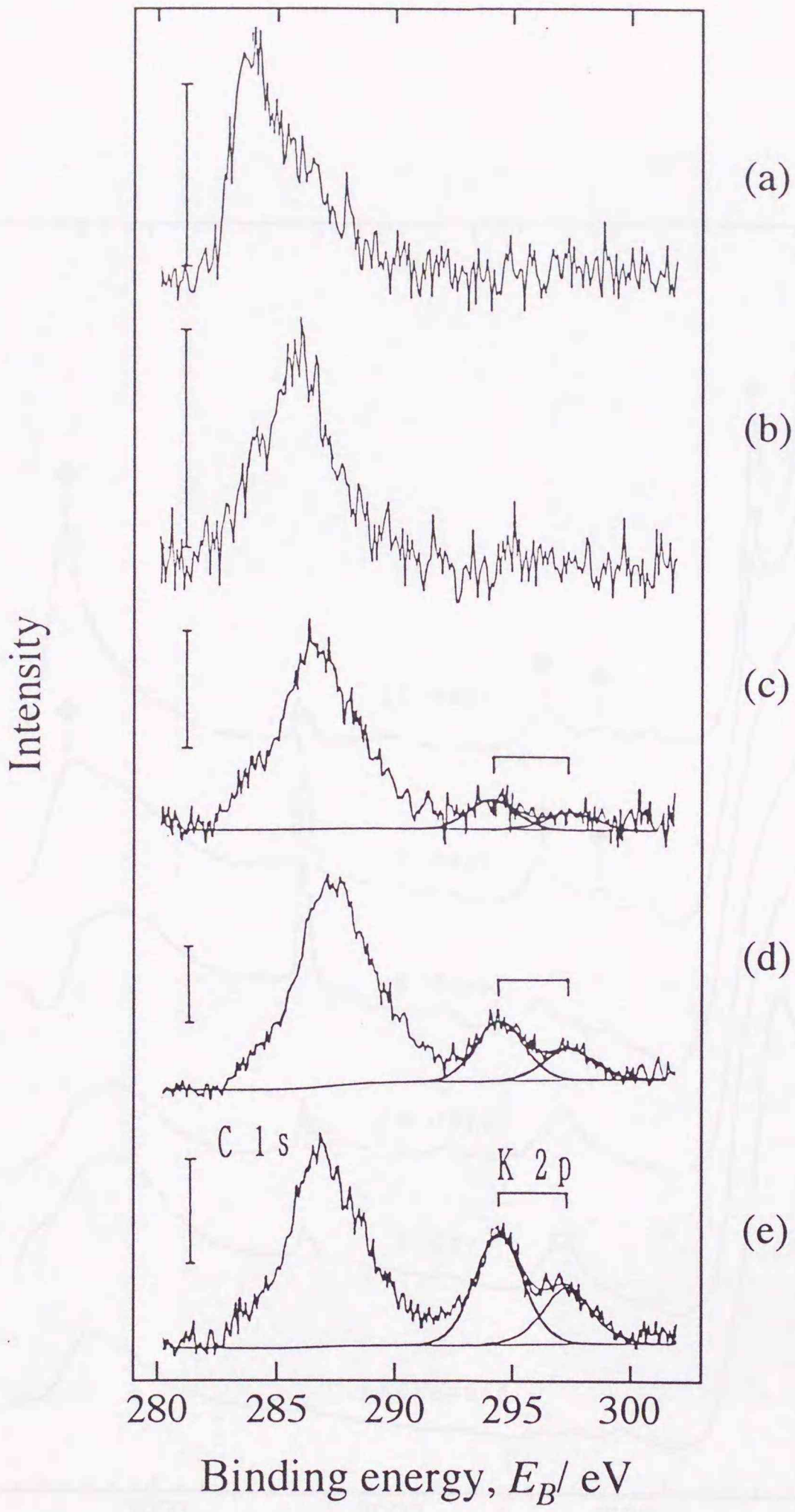

Fig. 2.7 XP-spectra of C 1s and K 2p for pyrite after microbially mediated dissolution for (a) 1, (b) 4, (c) 6, (d) 8 and (e) 11 days. Vertical bars indicate 200 cps. The spectra were separated into the sets of $2p_{3/2}$ and $2p_{1/2}$ using Gaussian-Lorentzian mixed functions.

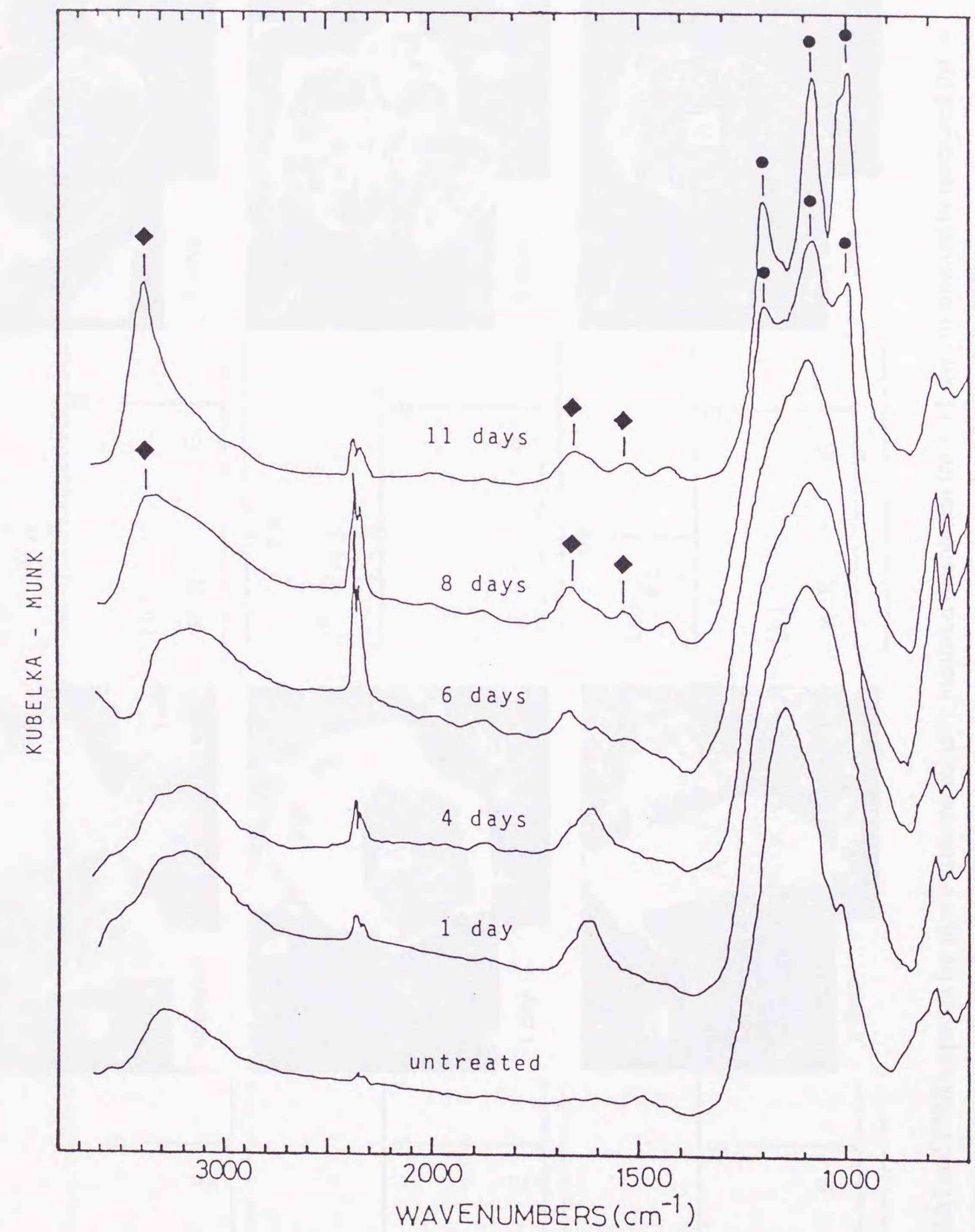

Fig. 2.8 FTIR spectra for pyrite after microbially mediated dissolution for 0-11 days in addition of unreacted pyrite. Symbols: ●, jarosite; ◆, polyamide.

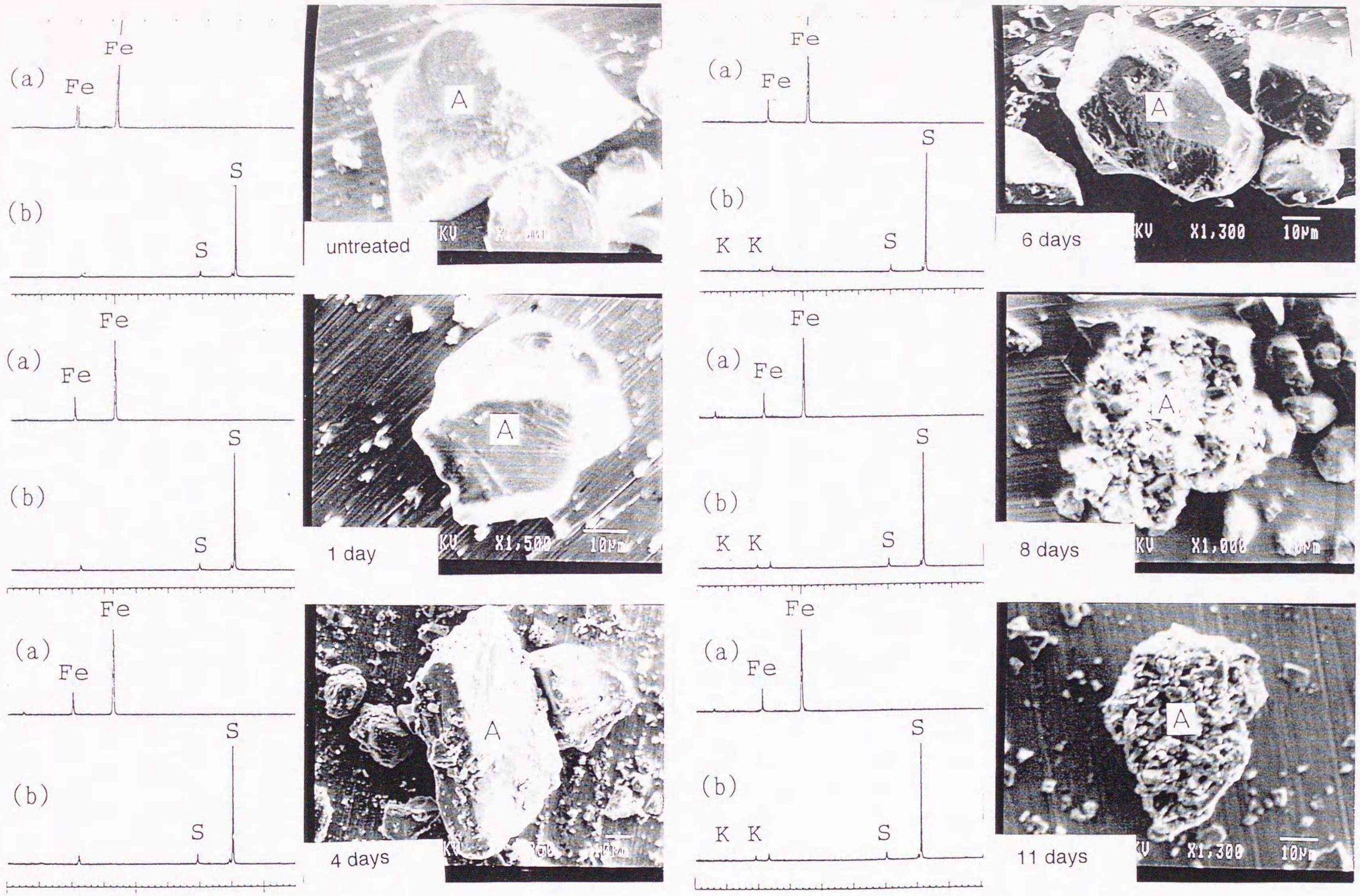

Fig. 2.9 SEM and EPMA-spectra for pyrite after microbially mediated dissolution for 1-11 days in addition to unreacted pyrite. EPMA-spectra were measured at the spots (A) in each photograph, using crystals of (a) LIF and (b) PET.

2.3 Discussion

The microbially mediated dissolution of pyrite is very complicated due to the interaction among mineral, solution, and bacteria. It is important to know the iron-oxidizing activity of microorganisms during the dissolution, and the changes in *E* gives useful information on cell activity.

As shown in **Fig. 2.10**, there is a linear relation between *E* and log([Fe(III)]/[Fe(II)]). This indicates that the *E* in the solution is mainly controlled by the redox system [Fe(III)]/[Fe(II)]. With cell growth, the microorganisms oxidize Fe(II) to Fe(III) ions according to reaction (2.2), leading the increase in *E*. Therefore, *E* may be used to evaluate the iron-oxidizing activity of the bacteria. This was confirmed using voltametry by Brock (1975) and Frenary, et al. (1985). Based on changes in *E* (**Fig. 2.3**), the changes in cell activity in microbially mediated dissolution of pyrite can be divided to three phases: (1) lag (0~4 days), (2) logarithmic (4~8 days), and (3) decelerating (8~11 days).

According to eq (2.6), and using the relative sensitivity factors in **Table 2.2** and XP-intensities in **Figs. 2.4-2.7**, the mole ratios of the surface components to the total iron species (C_{Fe} peaks in **Fig. 2.5**) of surface products formed on pyrite are calculated, as shown with solid lines in **Fig. 2.11**. Here the aqueous species Fe(II), Fe(III), and SO_4^{2-} have been added (broken lines). Changes in both the aqueous and surface phases can be discussed according to the three phases established here.

Until 4 days, pH and *E* were almost unchanged and cell numbers, total Fe, and sulfate in the aqueous phase not very increased (**Figs. 2.1~2.3**). This shows that reactions (2.2) and (2.5) did not yet occur. According to **Fig. 2.11**, $[S]/[Fe_T]$ increased rapidly on the surface. This is reflected in the formation of elemental sulfur on the pyrite by the reaction of pyrite with Fe(III) ions (reaction (2.3)). Only little elemental sulfur was formed, as there were small amounts of Fe(II) ions and sulfate in the aqueous phase. Detection of elemental sulfur is important evidence showing that the microorganisms are indirectly involved in dissolution of pyrite not but directly. The surface incidence of $[SO_4^{2-}]/[Fe_T] < 0.25$ at 0~4 days in **Fig. 2.11** shows that only little insoluble sulfate was formed.

From 4 to 8 days, it was observed (**Figs. 2.1~2.3**) that *E*, cell numbers, total Fe, Fe(III) ions, and sulfate in the aqueous phase increased rapidly, and that pH began to decrease after 5 days. The ratio of $[S]/[Fe_T]$ at the surface was the largest (~0.55) at 4 days and decreased until 8 days (**Fig. 2.11**). This indicates that elemental S and Fe(II) ions were rapidly oxidized by the microorganisms according to reactions (2.2) and (2.5), in concert with active cell-growth. Increased formation of insoluble sulfate is also shown by the increase in $[SO_4^{2-}]/[Fe_T]$ at the surface, from 0.25 to 0.70 (**Fig. 2.11**).

In the last period (8~11 days), aqueous Fe(II) ions and the surface incidence of

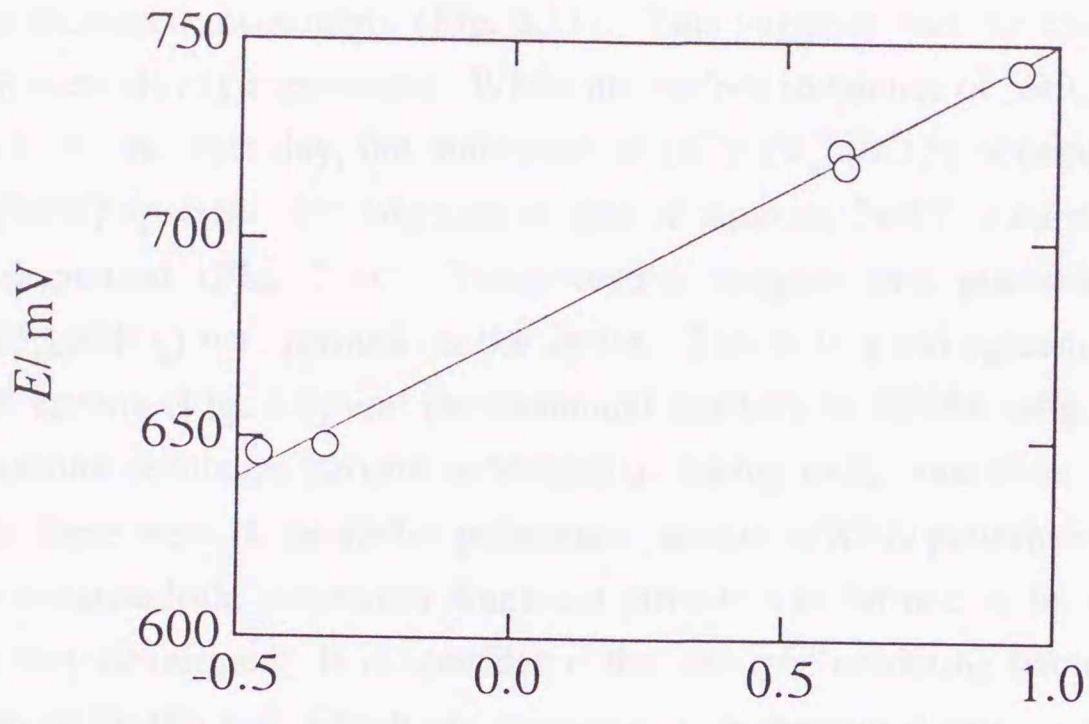

Fig. 2.10 Plots of E against log([Fe(III)]/[Fe(II)]).

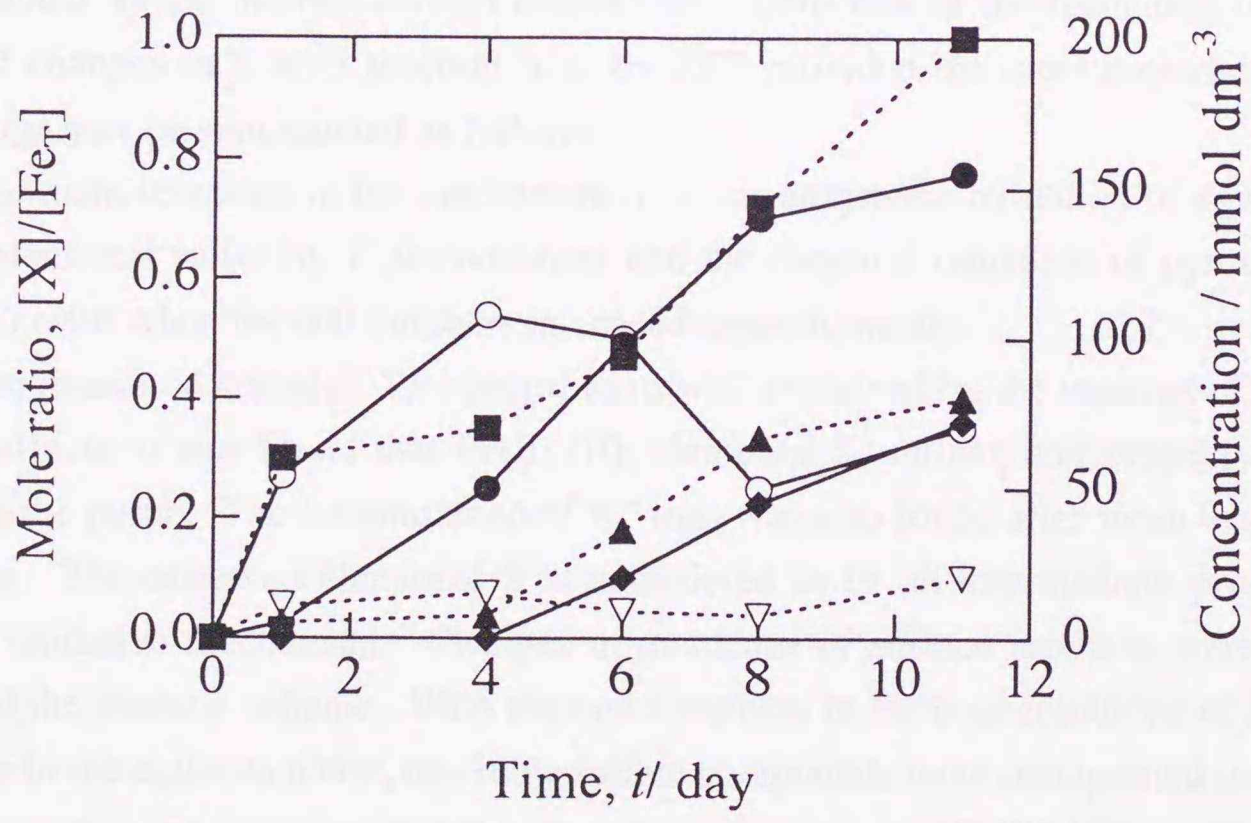

Fig. 2.11 Composition of surface products formed on pyrite and concentration of Fe^{3+}, Fe^{2+}, and SO_4^{2-} in microbially mediated dissolution with time. Solid lines indicate mole ratios [X]/[Fe_T] (left axis). The [Fe_T] means total amount of Fe of the surface products. Symbols on solid lines: ○, X = S; ●, X = SO_4^{2-}; ◆, X = K^+. Broken lines indicate soluble species (right axis). Symbols on broken lines: ▽, Fe^{2+}; ▲, Fe^{3+}; ■, SO_4^{2-}.

[S]/[Fe_T] increased moderately (**Fig. 2.11**). This suggests that the biological reactions (2.2) and (2.5) were slowly suppressed. While the surface incidence of [SO_4^{2-}]/[Fe_T] and [K^+]/[Fe_T] increased. At the 11th day, the mole ratio of [K^+]:[Fe_T]:[SO_4^{2-}] became 1:3:2, where [Fe_T] is mostly Fe(III) species. The increase in rate of aqueous Fe(III) ions slows down (**Fig. 2.11**) and *E* decreased (**Fig. 2.3**). These results suggest that potassium dominant jarosite ($KFe_3(SO_4)_2(OH)_6$) was formed on the pyrite. This is in good agreement with the results of the FTIR spectra (**Fig. 2.8**) and the elemental analysis by EPMA (**Fig. 2.9**). It is considered that potassium dominant jarosite is formed by taking in K^+ ions from the basal 9K medium. However, there were no peaks for potassium jarosite in XRD patterns of the samples. This is possibly because little potassium dominant jarosite was formed or because its crystallization was not very developed. It is considered that the iron-oxidizing bacteria contributed to the formation of Fe(III) ions which are precursor to potassium dominant jarosite (Sasaki, et al., 1995).

2.4 Summary

Microbially mediated dissolution of pyrite with *Thiobacillus ferrooxidans* was carried out and studied with both aqueous solution and mineral surface analysis. The reaction was well explained by the indirect contact mechanism. Detection of the formation of elemental sulfur and changes in S with reaction time by XPS provided the most important evidence. The findings may be summarized as follows.

The main reactions in the mechanism, i. e. the enzymatic oxidation of aqueous Fe(II) ions and elemental sulfur by *T. ferrooxidans* and the chemical oxidation of pyrite by Fe(III) ions, accelerated when the cell numbers increased logarithmically.

The measured complex XP-spectra were well explained by the concept of differential charging effects: it was found that Fe(II, III), elemental S, sulfate, and probably sulfite are formed on the pyrite. The accumulation of K^+ ions was also found after more than 6 days of dissolution. The observed elemental S is considered to be an intermediate product in the indirectly oxidative mechanism. Changes in incidence of surface products were helpful to understand the reaction scheme. With the rapid increase in the concentrations of Fe(III) ions and sulfate in the aqueous phase, insoluble sulfate compounds were precipitated on pyrite.

The redox-potential was dependent on the mole ratio of [Fe(III)]/[Fe(II)] in solutions. The *E* increased in the active phase of the bacteria and decreased in the inactive phase. This indicates that *E* can be a measure of the activity of *T. ferrooxidans* during the reaction. The FTIR and XPS results indicate that the insoluble sulfate compounds formed on the pyrite in the inactive phase may be potassium dominant jarosite.

References

Adler, H. H., and Kerr, P. F. (1956) Variations in infrared spectra, molecular symmetry and site symmetry of sulfate minerals. *Amer. Mineral.*, **50**, 132-147.

Brock, T. D. (1975) Effect of water potential on growth and iron oxidation by *T. ferrooxidans*. *Appl. Microbiol.*, **29**, 495-501.

Castro, V. D., Polzonetti, G., Contini, G., Cozza, C., and Paponetti, B. (1990) XPS study of MnO_2 minerals treated by bioleaching. *Surface and Interface Analysis*, **16**, 571-574.

Frenary, J., Wiertz, J., and Ek, C. (1985) *Microbiol. Eff. Metall. Processes*, Metall. Society, New York, pp.35-50.

Konno, H. and Nagayama, M. (1980) X-ray photoelectron spectra of hexavalent iron. *J. Electron. Spectrosc. Rel. Phen.*, **18**, 341-343.

Konno, H., Sasaki, K., M. Tsunekawa, T. Takamori, and R. Furuichi (1991) X-ray photoelectron spectroscopic analysis of surface products on pyrite formed by bacterial leaching. *Bunseki Kagaku*, **40**, 609 -616 (in Japanese).

Murr, L. E. (1980) Theory and practice of copper sulphide leaching in dumps and in-situ. *Minerals Sci. Engng.*, **12**, 121-189.

Nakamura, Y. (1991) Mineral. *Bunseki*, **8**, 613 (in Japanese).

Naumann, D., Fijala, V., and Labischinski, H. (1988) The differentiation and identification of pathogenic bacteria using FT-IR and multivariate statistical analysis. *Mikrochim. Acta[Wien]*, **1**, 373-377.

Riddle, J. W., and Taft, R. A. (1965) Bacterial identification by infrared spectrophotometry. *J. Bacteriol.*, **72**, 593-603.

Sasaki, K., Konno, H., and Inagaki, M. (1994) Structural strain in pyrite evaluated by X-ray powder diffraction. *J. Mater. Sci.* , **29**, 1666-1669.

Sasaki, K. (1994) Effect of grinding on the rate of oxidation of pyrite by oxygen. *Geochim. Cosmochim. Acta*, **58**, 4649-4655.

Sasaki, K., Tsunekawa, M., and Konno, H. (1995) Characterization of argentojarosite formed from biologically oxidized Fe^{3+} ions. *Can. Mineral.*, **33**, 1311-1319.

Sherwood, P. M. A. (1990) *Practical Surface Analysis, 2nd ed.*, (edited by Seah, M. P. and Briggs, D.), John Wiley & Sons Inc, New York, pp.555-586.

Shirley, D. A. (1972) High resolution X-ray photoemission spectrum of the valence bands of gold. *Phys. Rev.*, **B5**, 4709-4714.

Silverman, M. P., and Lundgren, D. G. (1959) Studies on the chemoautotrophic iron bacterium *Ferrobacillus ferrooxidans*. 1. An improved medium and a harvesting procedure for securing high cell yield. *J. Bacteriol.*, **77**, 642-647.

Takamori, T., Sasaki, K., Tsunekawa, M., and Hirajima, T. (1990) Leaching behavior

and its mechanism in the leaching of a chalcopyrite concentrate by *Thiobacillus ferrooxidans*. *J. Min. Mat. Processs. Inst. Japan*, **106**, 173-179 (in Japanese).

Wagner, C. D. (1990) in Briggs, D. and Seah, M. P. (Eds.), *Practical Surface Analysis* (2nd ed.), **Vol. 1**, John Wiley & Sons, Ltd., New York, pp. 595-634.

Chapter 3
Chemical dissolution of pyrite by Fe(III) ions

In **Chapter 2** it is clear that *Thiobacillus ferrooxidans* are indirectly involved in dissolution of pyrite. This indicates that direct oxidants are Fe(III) ions and oxygen in bacterial oxidation, the former being more reactive than the latter (e. g., McKibben and Barnes, 1986). As described in **Chapter 1**, oxidative reaction of pyrite with Fe(III) ions was expressed as reaction (3.1) in geochemistry (Smith and Shumate 1970; Rimstidt and Newcomb, 1993; McKibben and Barnes, 1986; Wiersma and Rimstidt, 1984; Mathews and Robbins, 1972; Garrels and Thompson, 1960; Moses, et al., 1987), and as reaction (3.2) in biohydrometullurgy (Murr, 1980).

$$FeS_2 + 14\,Fe^{3+} + 8\,H_2O = 15\,Fe^{2+} + 2\,SO_4^{2-} + 16\,H^+ \quad (3.1)$$

$$FeS_2 + 2\,Fe^{3+} = 3\,Fe^{2+} + 2\,S \quad (3.2)$$

To understand better the mechanism of pyrite oxidation with Fe(III) ions, it is important to know whether pyrite dissolves stoichiometrically or nonstoichiometrically (Luther, 1987; Moses et al., 1987). It needs also to make well-defined surface of stoichiometric composition for pyrite, because the pretreatment method of pyrite is not fully established as described in **Chapter 1 (Table 1.4)**.

In the present chapter, pretreated pyrite with the well-defined surface is confirmed by XPS and Raman spectroscopy: Raman spectra provides useful informations to distinct chemical species of sulfur, which was not precisely specified by XPS, such as distinction among sulfide, polysulfide and elemental sulfur. The oxidative dissolution of the pretreated pyrite by Fe(III) ions in chloride solutions is investigated. The stoichiometry is discussed based on the dissolution data for Fe and S species measured simultaneously and the results of XPS and Raman spectroscopy.

3.1 Experimental

3.1.1 Pyrite and its pretreatment

Pyrite was supplied from the Yanahara mines (Japan). The elemental composition and characterization by XRD of this sample was described in **Chapter 2**. Pyrite was ground using a tungsten carbide ball mill P-5 (Fritsch Co. Ltd. Germany). The samples were pretreated to establish a well-defined surface of the stoichiometric composition according to

two previous methods (McKibben and Barnes, 1986; Moses, et al., 1987; 1991).

Method 1: The pyrite was ultrasonically cleaned in ethanol for 30 sec with adhering mineral powder decanted, and then the pyrite was rinsed with 1 mol dm^{-3} HNO_3 for one minute, followed by rinsing three times in distilled water, before dehydrating in acetone, and finally it was vacuum-dried using an aspirator (McKibben and Barnes, 1986).

Method 2: The pyrite was boiled in 6 mol dm^{-3} HCl for 15 min, rinsed twice with 6 mol dm^{-3} HCl, and rinsed at least three times with 50 cm^3 of warm acetone (Moses, et al., 1987; 1991).

After both pretreatments, samples was dried under N_2 and supplied for XPS and Raman spectroscopic measurements.

The specific surface area of the pretreated pyrite was determined by the N_2 gas adsorption BET method on a Quantasorb QS-13 (Yuasa Ionics Co. Ltd.) with a QS-300 cell for low value measurements. Each result was in good agreement with the data obtained by the N_2 gas adsorption 7 points BET method on a Autosorb AS-1 (Yuasa Ionics Co. Ltd.). The average of twelve experiments was 0.40 ± 0.060 ($\pm 1\sigma_n$, $n = 12$) $m^2\ g^{-1}$.

3.1.2 Dissolution experiments

Dissolution experiments were carried out using a batch reactor with an impeller and a G2 glass ball filter for N_2 bubbling. The solution was sufficiently stirred to suspend pyrite particles. All assemblies were made of glass and rinsed with a diluted HNO_3 solution before use to avoid iron contamination. As the oxidant, 0-15 mmol dm^{-3} $FeCl_3 \cdot 6H_2O$ were used. The initial pH was adjusted to 2.0 with super special grade (SSG) HCl. To avoid complications by a two oxidant-system, dissolved oxygen was removed to the extent that the oxidation of pyrite and dissolved Fe(II) ions by dissolved oxygen was insignificant. Prior to each dissolution experiment, 200 cm^3 of each solution was deaerated by bubbling N_2 gas ($\geqq$ 99.999%) for one hour: the dissolved oxygen in the deaereted solution was under 1 ppm. Then, 2.00 g of the just pretreated pyrite powder was added to the solution. The dissolution experiment was carried out for 72 h under N_2 bubbling at room temperature (not controlled). Solution pH was also not controlled, since pH does not affect the dissolution rate in the range between 0 and 2 (Wiersma and Rimstidt, 1984). At appropriate intervals, 1 cm^3 of solution was sampled and filtrated with a 0.20 μm pore membrane filter for solution analysis, and pH and *E* measurements. The total Fe and Fe(II) concentrations were determined by the 1, 10-phenanthroline method and the total S concentration by ICP-AES (SEIKO Co. Ltd., SPS 1200). Dilution of the sampled solution was performed with a 0.01 mol dm^{-3} SSG HCl solution. After the dissolution experiment, the residue was separated by filtration and stored in a N_2 purged desiccator for XPS and Raman spectroscopic analysis. XP-spectra were collected by the described procedure in **Chapter 2**.

3.1.3 Raman spectroscopy

For Raman spectroscopy, excitation was accomplished by a single line 488.0 nm wavelength light from an Ar ion laser. The power of incidence was about 50 mW at the sample point. The Raman scattered light was detected between 600 cm^{-1} and 100 cm^{-1} by a triple type monochromator (JASCO R-800T) equipped with a photomultiplier (Hamamatsu R-464) and a photon counter, and between 1600 cm^{-1} and 600 cm^{-1} by a double type monochromator. The band path of the monochromator was about 8 cm^{-1}. The pyrite sample was diluted to 5 wt% with KBr powder and 0.30 g of the mixture was compressed to form a 10 mmϕ disk. A rotating apparatus was used for the measurement of the disk to avoid heating effects of the laser beam. The laser light was polarized parallel to the plane of incidence and the incidence angle was 80 degree. The Raman scattered light was collected in the incidence plane in the direction normal to the incident laser light.

3.2 Results and discussion

Typical dissolution curves of pyrite in 0.01 mol dm^{-3} HCl containing 15 mmol dm^{-3} Fe(III) ions are shown in **Fig. 3.1**. From the net amount of dissolved iron in **Fig. 3.1**, the average thickness of the pyrite dissolved is calculated to be 6.2 nm. It corresponds to an average of more than 10 lattice layers of pyrite crystal, though uniform dissolution does not take place in acid solutions, actually (McKibben and Barnes, 1986).

The total amount of i species in the solution per unit initial surface area of pyrite at time t is expressed as $x_i(t)$ in mmol m^{-2}, where i indicates S, Fe(II) or Fe(III). Assuming that pyrite is dissolved with Fe(III) ions according to reaction (3.1), the stoichiometry at t, $n(t) = x_S(t)/x_{Fe}(t)$, can be expressed theoretically using $x_{Fe(II)}(t)$ and the initial amount of Fe(III) ions per unit initial surface area of pyrite, $x_{Fe(III)}(0)$, as:

$$\begin{aligned} n_{theo}(t) &= x_S(t) / (x_{Fe(III)}(t) + x_{Fe(II)}(t)) \\ &= 2\, x_{Fe(II)}(t) / (15\, x_{Fe(III)}(0) + x_{Fe(II)}(t)) \end{aligned} \qquad (3.3)$$

In **Fig. 3.2** the theoretical stoichiometric ratio, $n_{theo}(t)$, is compared with the observed stoichiometric ratio, $n_{obs}(t)$, obtained from the experimental data, showing that $n_{theo}(t)$ is larger than $n_{obs}(t)$, and that the difference between $n_{theo}(t)$ and $n_{obs}(t)$ increases with time. This indicates that iron dissolves more easily than sulfur from pyrite. The values of $n_{theo}(t)$ can also be calculated by using $x_S(t)$ or $x_{Fe}(t)$, and though the values are less accurate than with $x_{Fe(II)}(t)$, the results were similar to **Fig. 3.2**.

The XP-spectra for (a) the cleaved pyrite, (b) ground pyrite, (c) the pretreated pyrite by method 1 and (d) the pretreated pyrite by method 2 are shown in **Figs. 3.3** and **3.4**.

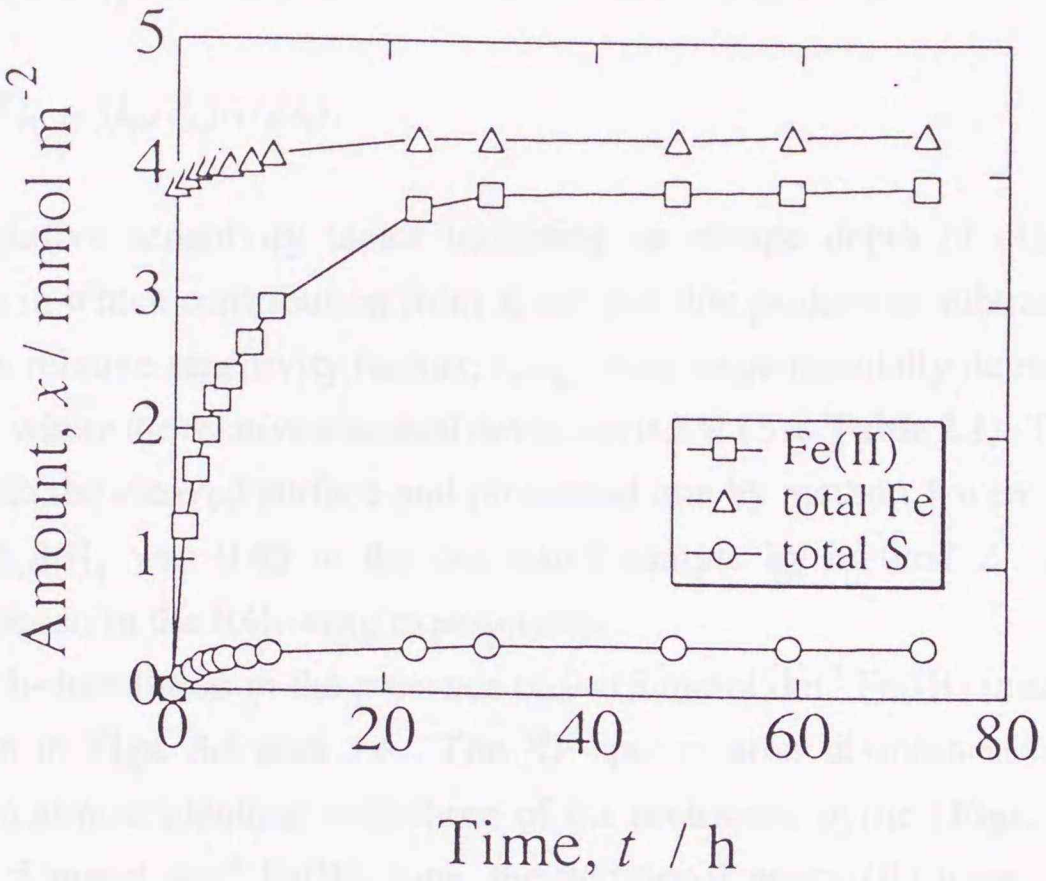

Fig. 3.1 Dissolution curves of pyrite by 15 mmol dm^{-3} Fe(III) ions in a HCl solution at pH 2.0.

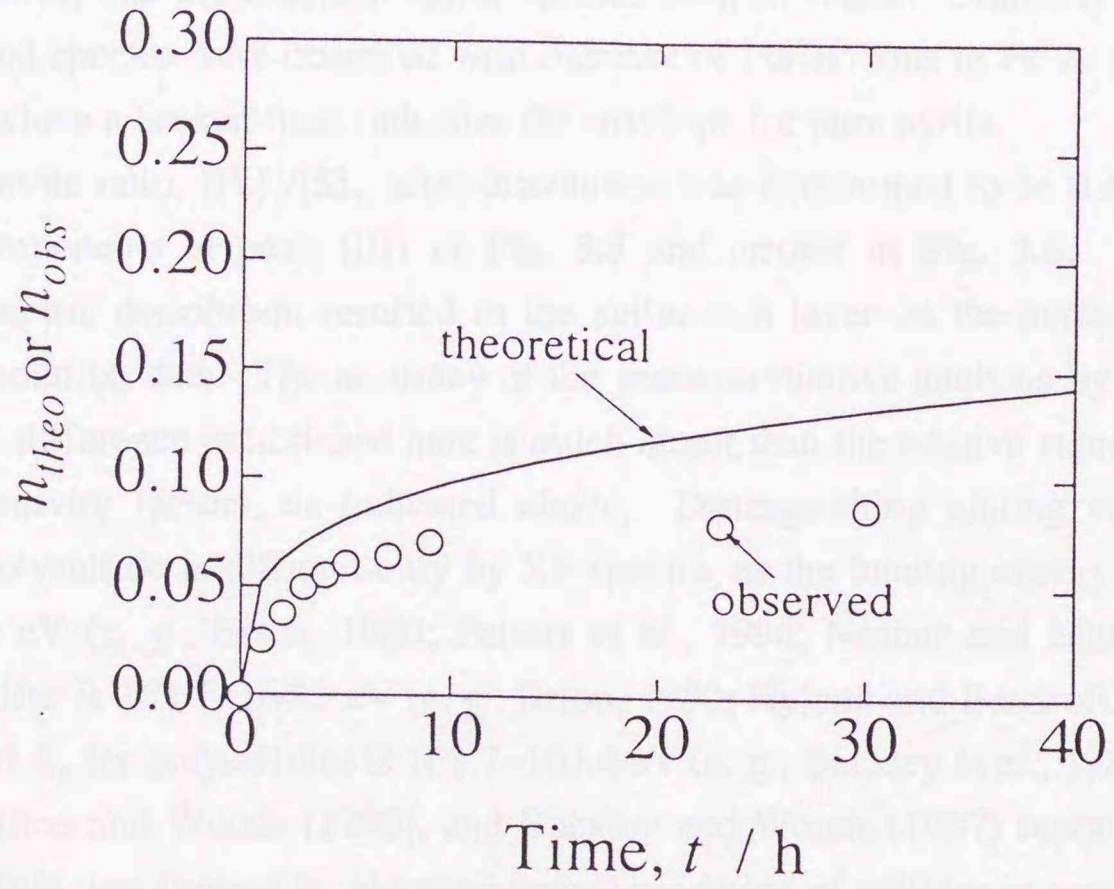

Fig. 3. 2 Theoretical and observed ratios, $n(t) = x_S(t)/x_{Fe}(t)$.

Figures 3.3 and 3.4 indicate that the oxidized species were formed by grinding (a spectrum (b)), and that they were removed by both pretreatments (spectra (c) and (d)). The surface composition, $[Fe]_T/[S]_T$ mole ratios, was calculated according to eq(3.4).

$$[Fe]_T/[S]_T = (I_{Fe}/s_{Fe})/(I_S/s_S), \tag{3.4}$$

where s is a relative sensitivity factor including an escape depth of electrons, and I an intensity by area in which contribution from X-ray satellite peaks was subtracted by computer calculation. The relative sensitivity factors, s_S/s_{Fe}, were experimentally determined to be 0.14 $\pm$ 0.00_7 ($\pm$ 1σ), where the relative standard deviation is 5 % (See **Table 2.1**). The compositions, $[Fe]_T/[S]_T$, of both the cleaved surface and pretreated one by method 1 were determined to be 0.50, while $[Fe]_T/[S]_T$ was 0.45 in the pretreated sample by method 2. Accordingly, the method 1 was chosen in the following experiments.

After 72 h-dissolution in the presence of 0~15 mmol dm^{-3} Fe(III) ions, XP-spectra for pyrite are shown in **Figs. 3.5 and 3.6**. The XP-spectra after dissolution in the absence of Fe(III) ions were almost identical with those of the pretreated pyrite (**Figs. 3.3 and 3.4**). In the presence of 5 mmol dm^{-3} Fe(III) ions, the additional peaks (II) were observed at E_B[S $2p_{3/2}$] ~164.4 eV in **Fig. 3.5**. In the presence of 15 mmol dm^{-3} Fe(III) ions, further additional peaks appeared at E_B[S $2p_{3/2}$] ~166.2 eV: peaks (I), (II), and (III) are correspondent to pyrite, elemental sulfur, and the oxidized sulfur species such as sulfite. Similarly to S 2p spectra, more oxidized species were observed with increase of Fe(III) ions in Fe 2p spectra as shown in **Fig. 3.6**, where a broken lines indicates the envelope for pure pyrite.

The mole ratio, $[Fe]_T/[S]_T$, after dissolution was determined to be 0.34, excluding the oxidized components at peak (III) in **Fig. 3.5** and arrows in **Fig. 3.6**. It indicates that nonstoichiometric dissolution resulted in the sulfur-rich layer on the surface, in agreement with the dissolution data. The accuracy of the semiquantitative analysis by XPS is not very high, but the difference established here is much larger than the relative standard deviation of relative sensitivity factors, as indicated above. Distinguishing among sulfide, elemental sulfur and polysulfide is difficult only by XP-spectra, as the binding energy, E_B, for pyrite is 162.2~163.0 eV (e. g., Brion, 1980; Peisert et al., 1994; Nesbitt and Muir, 1994), E_B for elemental sulfur is 163.7~164.3 eV (e. g., Brion, 1980; Hyland and Bancroft, 1989; Peisert et al., 1994) and E_B for polysulfides is 161.7~163.4 eV (e. g., Buckley et al., 1988) .

Hamilton and Woods (1980), and Buckley and Woods (1987) reported that a metal-deficient sulfide was formed by electrochemical oxidation of sulfides in acidic solutions (pH 4.6), and polysulfide was detected by XPS, mass spectroscopy, and voltammetry. Mycroft, et al. (1990) reported that after anodic oxidation at 700 mV (SCE) in near-neutral aqueous chloride solutions for more than one hour, polysulfide was detected on pyrite by Raman

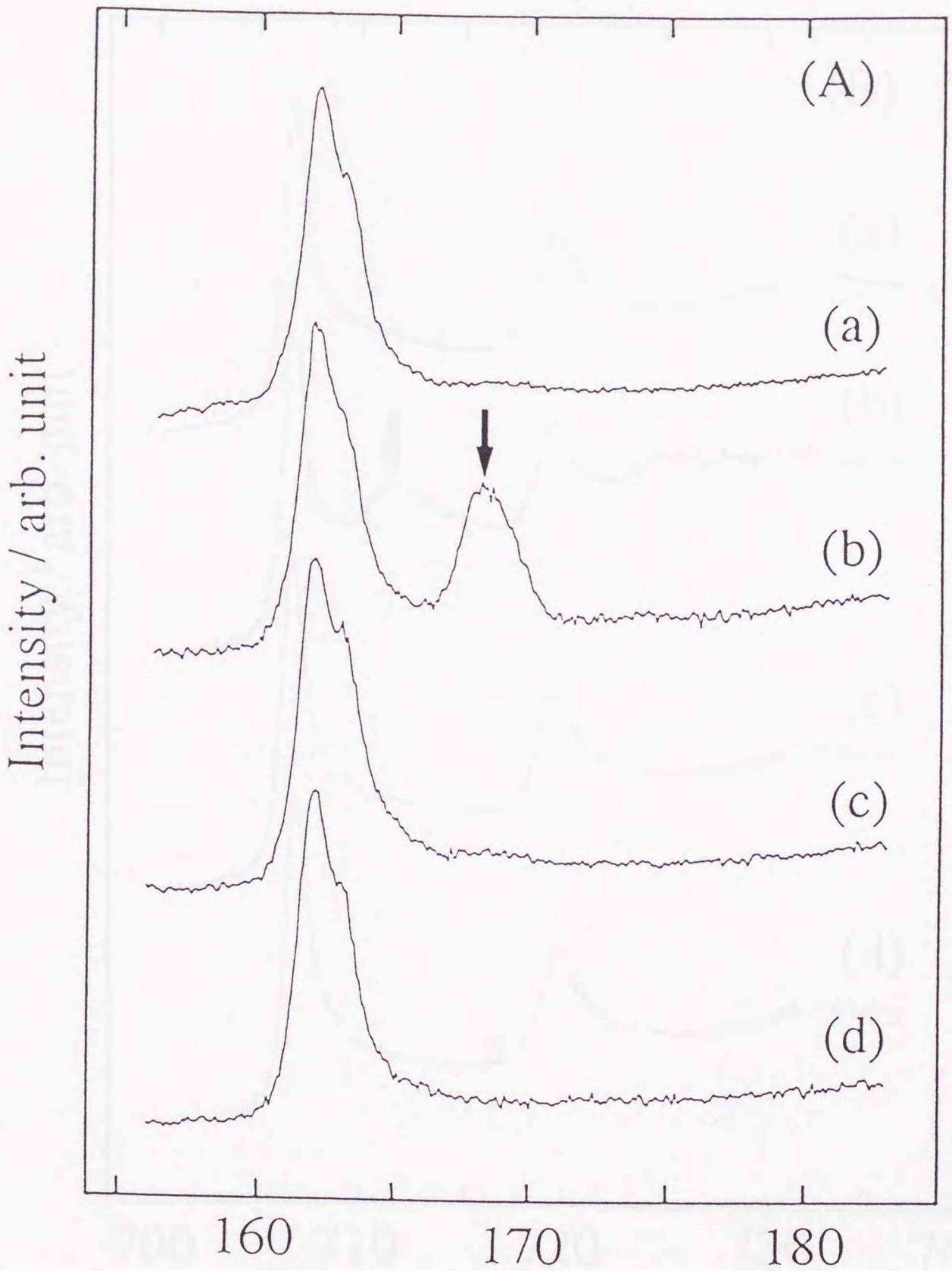

Fig. 3.3 The XP-spectra of S 2p for pyrite. (a) cleaved pyrite, (b) after grinding, (c) pretreated pyrite by method 1, and (d) pretreated pyrite by method 2. An arrow shows the oxidized species.

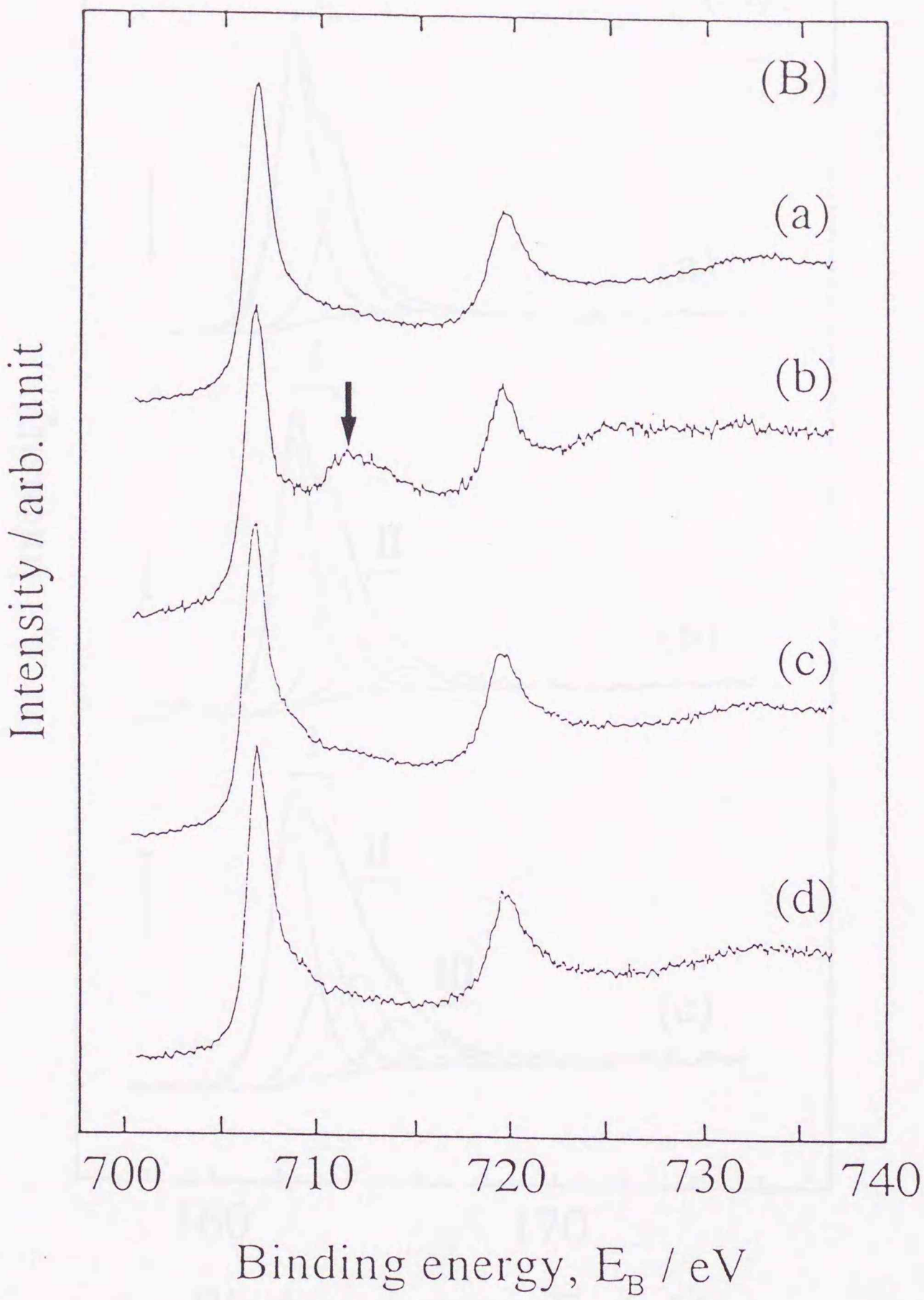

Fig. 3.4 The XP-spectra of Fe 2p for pyrite. (a) cleaved pyrite, (b) after grinding, (c) pretreated pyrite by method 1, and (d) pretreated pyrite by method 2. An arrow shows the oxidized species.

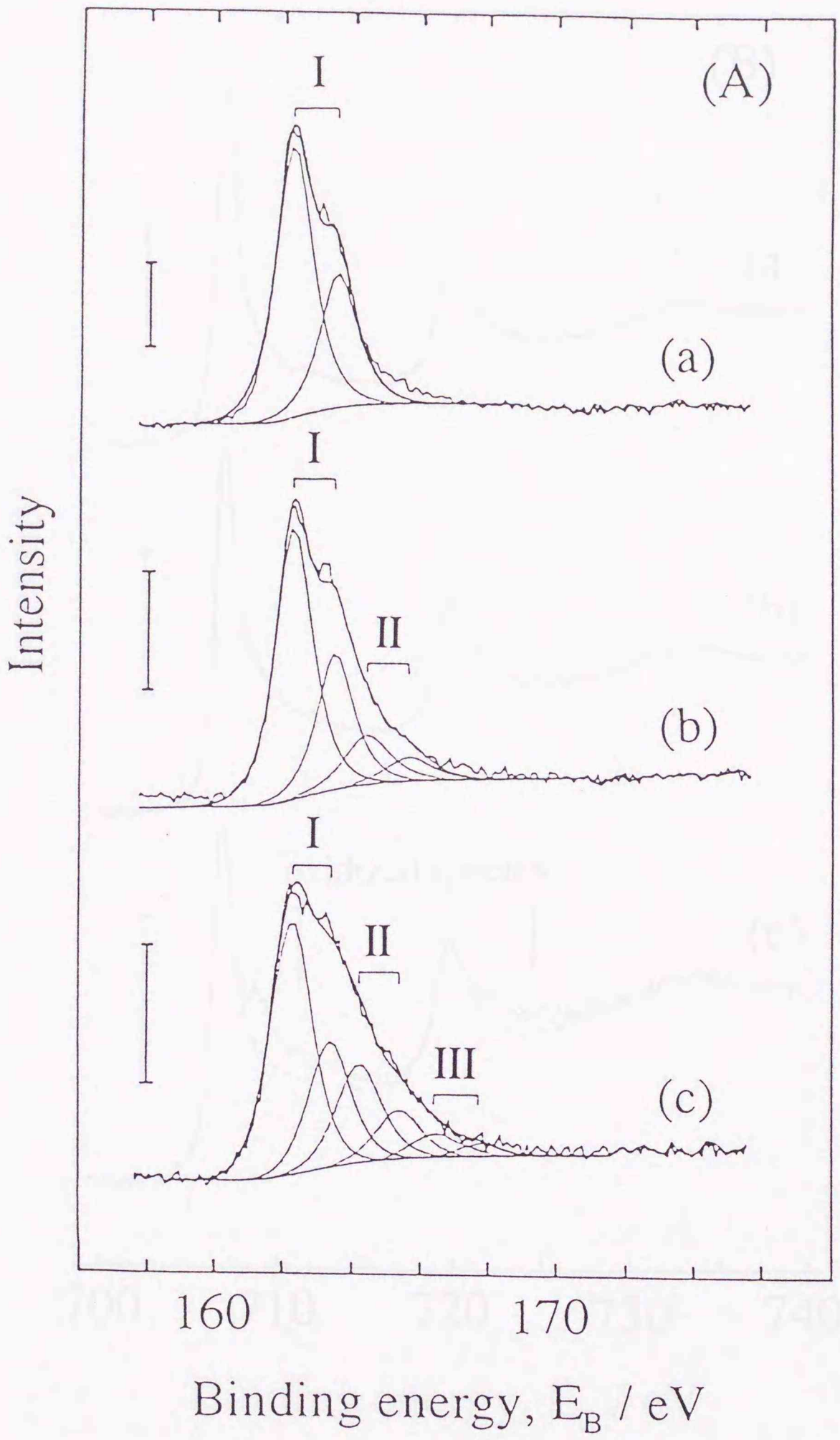

Fig. 3.5 The XP-spectra of S 2p for the pyrite after 72 h-dissolution with (a) [Fe(III)] = 0 mmol dm^{-3}, (b) [Fe(III)] = 5 mmol dm^{-3}, and (c) [Fe(III)] = 15 mmol dm^{-3}. Vertical bars indicate 500 cps.

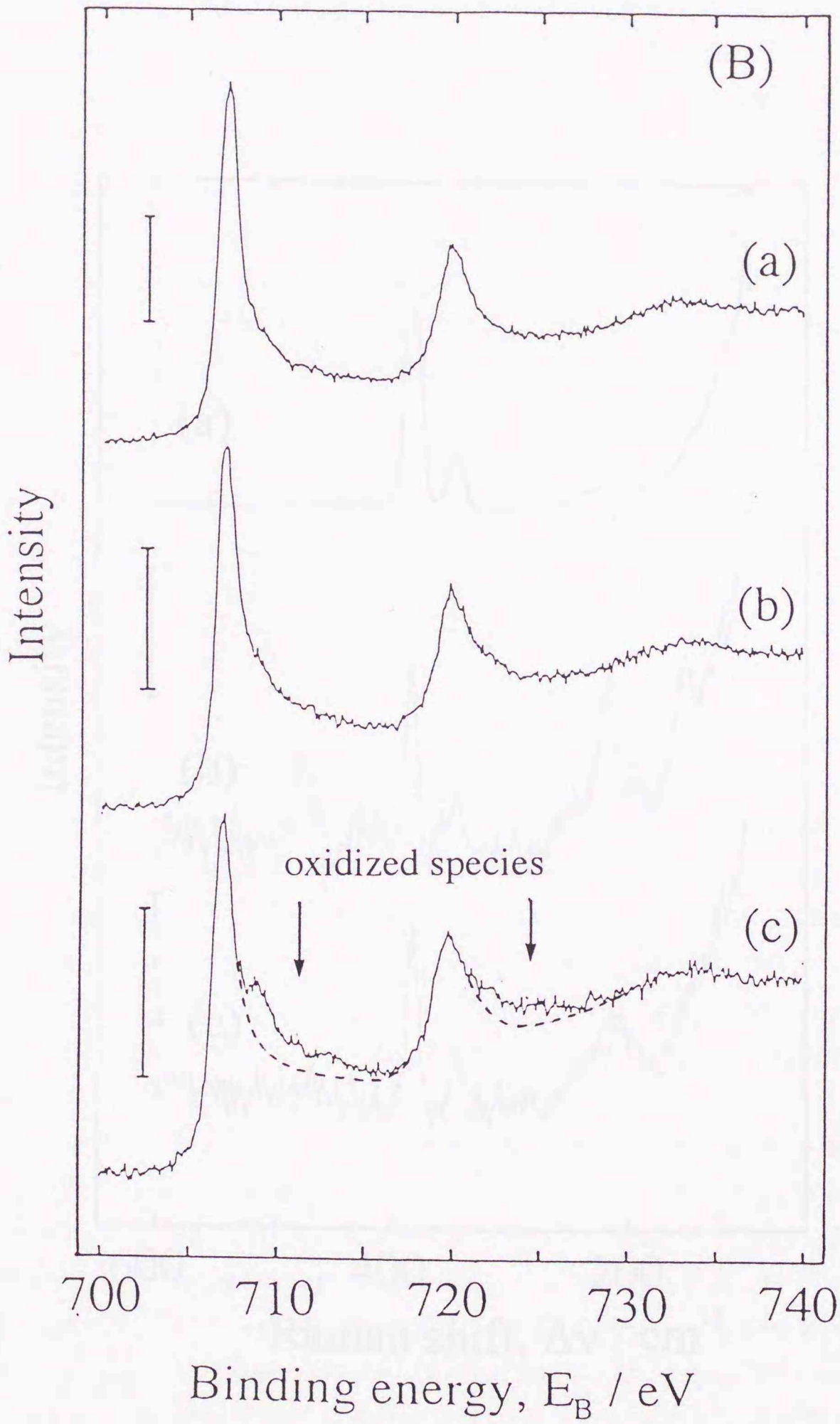

Fig. 3.6 The XP-spectra of Fe 2p for the pyrite after 72 h-dissolution with (a) [Fe(III)] = 0 mmol dm^{-3}, (b) [Fe(III)] = 5 mmol dm^{-3}, and (c) [Fe(III)] = 15 mmol dm^{-3}. Vertical bars indicate 1 kcps.

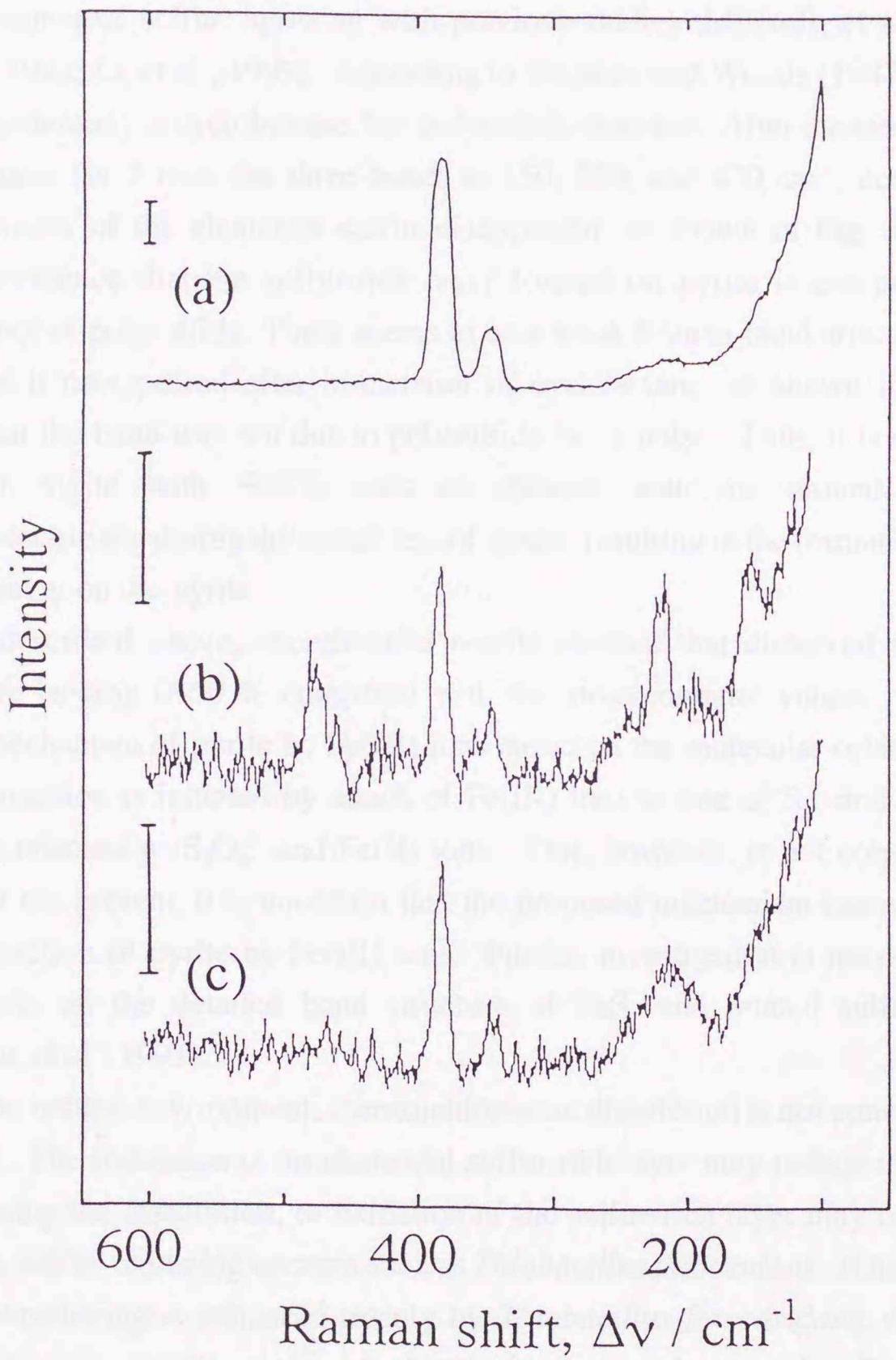

Fig. 3.7 The Raman spectra for pyrite. Vertical bars indicate a scattering light intensity of 1 kcps. (a) pretreated pyrite by method 1, (b) after dissolution by 15 mmol dm^{-3} Fe(III) ions and (c) after immersion of the oxidized pyrite in cyclohexane for 5 min.

spectroscopy. The Raman spectrum was measured to elucidate further the composition of the sulfur-rich layer. As shown in **Fig. 3.7 (a)**, the Raman spectrum of the same sample with (c) in **Figs. 3.3 and 3.4** has two Raman bands: at 353 and 387 cm^{-1}. They are assigned to vibration modes of pyrite. After dissolution with 15 mol dm^{-3} Fe(III) ions, the additional bands at 150, 220, and 470 cm^{-1} were appeared (**Fig. 3.7 (b)**), assigning to S-S vibration modes of elemental sulfur, agreeing with previous studies (Mycroft, et al., 1990; Mernagh and Truda, 1993; Li, et al., 1993). According to Buckley and Woods (1987), elemental sulfur dissolves moderately in cyclohexane, but polysulfide does not. After the sample was immersed in cyclohexane for 5 min, the three bands at 150, 220, and 470 cm^{-1}, corresponding to the vibration modes of the elemental sulfur disappeared, as shown in **Fig. 3.7 (c)**. This is an additional evidence that the sulfur-rich layer formed on pyrite is composed of elemental sulfur and not of polysulfide. There seems to be a weak Raman band around 460 cm^{-1} in **Fig. 3.7 (b)**, but it disappeared after immersion in cyclohexane, as shown in **Fig. 3.7 (c)**. It indicates that the band was not due to polysulfide but a noise. Thus, it is concluded that the reaction of pyrite with Fe(III) ions in chloride solutions around pH 2 proceeds nonstoichiometrically during the initial tens of hours, resulting in the formation of an elemental sulfur-rich layer on the pyrite.

As described above, experimental results showed that dissolved amounts of sulfur species were lacking 0~50 % compared with the stoichiometric values. According to the oxidation mechanism of pyrite by Fe(III) ions based on the molecular orbital theory (Luther, 1987), the reaction is initiated by attack of Fe(III) ions to one of S_2^{2-} and finally one pyrite molecule is released as $S_2O_3^{2-}$ and Fe(II) ions. This, however, is not consistent with above results. For the present, it is uncertain that the proposed mechanism can explain the overall oxidation reaction of pyrite by Fe(III) ions. Further investigation is necessary, considering recent reports on the detailed band structure of FeS_2 and related sulfides (Sato, 1985; Temmerman, et al., 1993).

In the natural environment, nonstoichiometric dissolution is not considered to continue indefinitely. The formation of an elemental sulfur-rich layer may reduce the dissolution rate and finally stop the dissolution, or oxidation of the sulfur-rich layer may occur by processes like those by sulfur-oxidizing bacteria such as *Thiobacillus thiooxidans*. It has been considered that pyrite weathering is enhanced mainly by *Thiobacillus ferrooxidans*, which can oxidize Fe(II) ions in acidic environments. Much attention has not been paid to *T. thiooxidans*, since it mainly oxidizes elemental sulfur to sulfate but rarely does sulfide to sulfate, with no ability to oxidize Fe(II) ions to Fe(III) ions. The present data, however, suggests that *T. thiooxidans* might also play an important role in pyrite weathering in coexistence with *T. ferrooxidans*.

3.3 Summary

The stoichiometry of pyrite dissolution by Fe(III) ions was studied in chloride media around pH 2. Pyrite was found to dissolve nonstoichiometrically during the initial tens of hours and a sulfur-rich layer was formed on the pyrite due to preferential dissolution of iron. The major constituent of the layer was elemental sulfur, identified by X-ray photoelectron spectroscopy (XPS) and Raman spectroscopy.

References

Brion, D. (1980) Etude par spectroscopie de photoelectrons de degradation superficielle de FeS_2, $CuFeS_2$, ZnS et PbS a l'air et dans l'eau. *Appl. Surf. Sci.*, **5**, 133-152.

Buckley, A. N., and Woods, R. (1987) The surface oxidation of pyrite. *Appl. Sur. Sci.*, **27**, 437-452.

Buckley, A. N., Wouterlood, H. J., Cartwright, P. S. and Gillard, R. D. (1988) Core electron binding energies of platinum and rhodium polysulfides. *Inorg. Chim. Acta,* **143**, 77-80.

Garrels, R. M., and Thompson, M. E. (1960) Oxidation of pyrite by iron sulfate solutions. *Amer. J. Sci.*, **258-A**, 57-67.

Hamilton, I. C., and Woods, R. (1980) An investigation of surface oxidation of pyrite and pyrrhotite by linear potential sweep voltammetry. *J. Electroanal. Chem.*, **118**, 327-343.

Hyland, M. M., and Bancroft, G. M. (1989) An XPS study of gold deposition at low temperatures on sulfide minerals: Reducing agents. *Geochim. Cosmochim. Acta*, **53,** 367-372.

Li, J., Zhu, X., and Wadsworth, M. E. (1993) Raman spectroscopy of natural and oxidized metal sulfides. *EPD Congress (eds. Hager J. P.)*, pp.229-244.

Luther, III. G. W. (1987) Pyrite oxidation and reduction: Molecular orbital theory considerations. *Geochim. Cosmochim. Acta*, **51,** 3193-3199.

Mathews, C. T., and Robins, R. G. (1972) The oxidation of iron disulfide by ferric sulphate. *Aust. Chem. Eng.*, **Aug.** , 21-25.

McKibben, M. A., and Barnes, H. L. (1986) Oxidation of pyrite in low temperature acidic solutions: Rate laws and surface textures. *Geochim. Cosmochim. Acta*, **50,** 1509-1520.

Mernagh, T. P., and Trudu, A. G. (1993) A laser Raman microprobe study of some geologically important sulphide minerals. *Chemical Geology*, **103**, 113-127.

Moses, C. O., Nordstrom, D. K., Herman, J. S., and Mills, A. L. (1987) Aqueous pyrite oxidation by dissolved oxygen and by ferric iron. *Geochim. Cosmochim. Acta*, **51,** 1561-1571.

Moses, C. O., and Herman, J. S. (1991) Pyrite oxidation at circummneutral pH. *Geochim. Cosmochim. Acta*, **55**, 471-482.

Murr, L. E. (1980) Theory and practice of copper sulphide leaching in dumps and in-situ. *Minerals Sci. Engng.*, **12**, 121-189.

Mycroft, J. R., Mcintyre, N. S. , Lorimer, J. W., and Hill, I. R. (1990) Detection of sulfur and polysulphides on electrochemically oxidized pyrite surfaces by X-ray photoelectron spectroscopy and Raman spectroscopy. *J. Electroanal. Chem.*, **292,** 139-152.

Nesbitt, H. W., and Muir, I. J. (1994) X-ray photoelectron spectroscopic study of a pristine pyrite surface reacted with water vapour and air. *Geochim. Cosmochim. Acta*, **58,** 4667-4679.

Nicholson, R. V., Gillham, R. W., and Reardon, E. J. (1988) Pyrite oxidation in carbonate-buffered solution: 1. Experimental kinetics. *Geochim. Cosmochim. Acta*, **55**, 1077-1085.

Peisert, H., Chasse, T., Streubel, P., Meisel, A., and Szargan, R. (1994) Relaxation energies in XPS and XAES of solid sulfur compounds. *J. Electron Spectrosc. Relat. Phenom.*, **68**, 321-328.

Rimstidt, J. D., and Newcomb, W. D. (1993) Measurement and analysis of rate data: The rate of ferric iron with pyrite. *Geochim. Cosmochim. Acta*, **57**, 1919-1934.

Sato, K. (1985) Pyrite type compounds - with particular reference to optical characterization. *Proc. Crystal Growth and Charact.*, **11**, pp.109-154.

Smith, E. E., and Shumate, K. S. (1970) Sulfide to sulfate reaction mechanism. *Water Pollut. Control Res. Ser. Rept. 14010 FPS 02170, Fed. Water Quality Admin., U. S. Dept. of the Interior*, pp.1-115.

Temmerman, W. M., Durham, P. J., and Vaughan, D. J. (1993) The electronic structures of the pyrite-type disulfides (MS_2, where M = Mn, Fe, Co, Ni, Cu, Zn) and the bulk properties of pyrite from local density approximation (LDA) band structure calculations. *Phys. Chem. Minerals*, **20**, 248-254.

Wiersma, C. L., and Rimstidt, J. D. (1984) Rates of reaction of pyrite and marcasite with ferric iron at pH 2. *Geochim. Cosmochim. Acta*, **48**, 85-92.

Chapter 4
Effect of anionic species on the reactivity of pyrite with Fe(III) ions

As described in **Chapters 2 and 3**, the most important oxidants to pyrite in natural environments are Fe(III) ions (Singer, et al., 1970). The reaction of pyrite with Fe(III) ions in acid solutions has been conventionally expressed as:

$$FeS_2 + 14\,Fe^{3+} + 8\,H_2O = 15\,Fe^{2+} + 2\,SO_4^{2-} + 16\,H^+. \qquad (4.1)$$

In general, it has been known that the ligands which form complexes with Fe(III) ions affect dissolution of minerals (Luther, et al., 1992; Bondietti, et al., 1993). As shown in **Table 1.5**, sulfate or chloride media was used in laboratory studies on pyrite dissolution. Knowledge of the ligand effect by anionic species is also useful to determine substances suppressing the oxidative dissolution of pyrite. Further, the information of ligands effect in pyrite dissolution may give us a key factor in a better understanding of the redox mechanism and pathway of electron transfer. In the present chapter, the effect of anionic ligands on the oxidative dissolution of pyrite by Fe(III) ions was studied around pH 2.

4.1 Experimental

4.1.1 Pyrite

Pyrite sample and its pretreatment were described in **Chapter 3**.

4.1.2 Dissolution experiments

Dissolution experiments were carried out in the same manner as in **Chapter 3**. Six kinds of anionic ligand were used, and the concentrations were changed systematically with the initial pH adjusted as shown in **Table 4.1**. The reagents were: Nos. 1-10, $FeCl_3 \cdot 6H_2O$ and NaCl in SSG HCl solutions; Nos. 11-14, $Fe(NH_4)(SO_4)_2 \cdot 12H_2O$ and K_2SO_4 in H_2SO_4 solutions; Nos. 15-17, $FeCl_3 \cdot 6H_2O$ and K_2HPO_4 in SSG HCl solutions; and Nos. 18-22, $(COOH)_2 \cdot 2H_2O$ in SSG HCl solutions. The pH was adjusted using NaOH. In the case of CN^- and CDTA, Fe(III)-CDTA and $[Fe(CN)_6]^{3-}$ ions were directly added. With oxalate, dissolution experiments were carried out under light shielding to avoid decomposition of Fe(III)-oxalate complexes. At intervals in each dissolution experiment, 1 cm^3 of supernatant was pipetted off and filtrated with a 0.20 μm pore size membrane filter for solution analysis. The total Fe concentration and Fe(II) ion concentration were determined by the 1, 10-phenanthroline method and the total S concentration by ICP-AES (SEIKO Co. Ltd., SPS

Table 4.1 Details of dissolution experiments

No.	Total concentration / mmol dm^{-3}				pH	
	Cl^-	SO_4^{2-}	PO_4^{3-}	oxalate	initial	final
	$[Fe(III)]_T$ = 5 mmol dm^{-3}					
1	25	-	-	-	2.06	1.92
2	25	-	-	-	2.00	1.91
3	25	-	-	-	2.04	1.91
4	55	-	-	-	2.06	1.92
5	70	-	-	-	2.00	1.91
6	100	-	-	-	2.01	1.92
7	160	-	-	-	2.06	1.92
8	200	-	-	-	2.06	1.92
9	200	-	-	-	2.00	1.91
10	200	-	-	-	2.03	1.91
11	-	13	-	-	2.17	2.06
12	-	60	-	-	2.17	2.06
13	-	100	-	-	2.17	2.06
14	-	196	-	-	2.17	2.06
15	25	-	0.1	-	2.01	1.95
16	25	-	1	-	1.99	1.95
17	25	-	5	-	1.86	1.86
18	25	-	-	0.5	2.03	1.89
19	25	-	-	5	2.08	2.06
20	25	-	-	10	2.01	2.01
21	25	-	-	20	2.02	2.02
22	25	-	-	50	2.00	1.99
23	$[Fe(CN)_6^{3-}]$ = 5 mmol dm^{-3}				2.06	2.15
24	[FeCDTA] = 5 mmol dm^{-3}				1.92	1.90

1200). Dilution of the sampled solution was performed with a 0.01 mol dm^{-3} SSG HCl solution. After the dissolution experiments, the residue was separated by filtration using a 0.20 μm pore size membrane filter and stored in a N_2 purged desiccator for XPS analysis. XPS analysis was also carried out in the same manner as in **Chapter 3**.

4.2 Results

4.2.1 Dissolution behavior

Typical dissolution curves of pyrite by Fe(III) ions in chloride solutions indicate that Fe(II) ions, total Fe and total S increase with dissolution time, as shown in **Fig. 4.1(A, B)**. When there is an initially large amount of sulfate, it is difficult to estimate the sulfur species dissolved from pyrite. In the presence of phosphate, the complex of Fe(III)-phosphate became colloidal, and this interfered with the analysis of total Fe. Therefore, the amount of released Fe(II) was used as a parameter to estimate the pyrite dissolution here.

We assumed that dissolution data within 40 h are interpolated with the following equation:

$$x_{Fe(II)} = a \cdot t^m + b \qquad (4.2)$$

where $x_{Fe(II)}$ is the amount of Fe(II) per unit initial surface area of pyrite, t is the dissolution time, and m, a and b are constants. It is clear that the obtained curves are in good agreement with the experimental data, as shown in the example in **Fig. 4.2**. Relative standard deviations of $x_{Fe(II)}$ were within $\pm$ 6% in all experiments.

The $x_{Fe(II)}$ values at different t were obtained from the simulated dissolution curves, and plotted against chloride ion concentration as shown in **Fig. 4.3 (A)**. The $x_{Fe(II)}$ decreased slightly with increasing amount of chloride ions, and more with sulfate ions (**Fig. 4.3 (B)**).

With phosphate ions, the solution becomes turbid above around 5 mmol dm^{-3} probably due to the formation of colloidal Fe(III)-phosphate polymers. The release of Fe(II) ions was markedly inhibited by small amounts of phosphate, as seen in **Fig. 4.3 (C)**. In experiment No. 17, the membrane filter were increasingly clogged with longer dissolution times. Further, control experiments in the phosphate solution ($[PO_4^{3-}]_T$ = 5 mmol dm^{-3}) without pyrite showed that the amount of Fe(III) ions passing through the 0.2 μm pores of the membrane filter was smaller than the initial concentration and decreased with time as shown in **Fig. 4.4**. Small amounts of oxalate also inhibited the release of Fe(II) ions as shown in **Fig. 4.3 (D)**, but without clogging the membrane filter.

The results shown in **Fig. 4.5** clearly indicate that pyrite is not dissolved by the Fe(III)-CDTA complex. As the Fe(II)-1, 10-phenanthlorine complex is more stable than

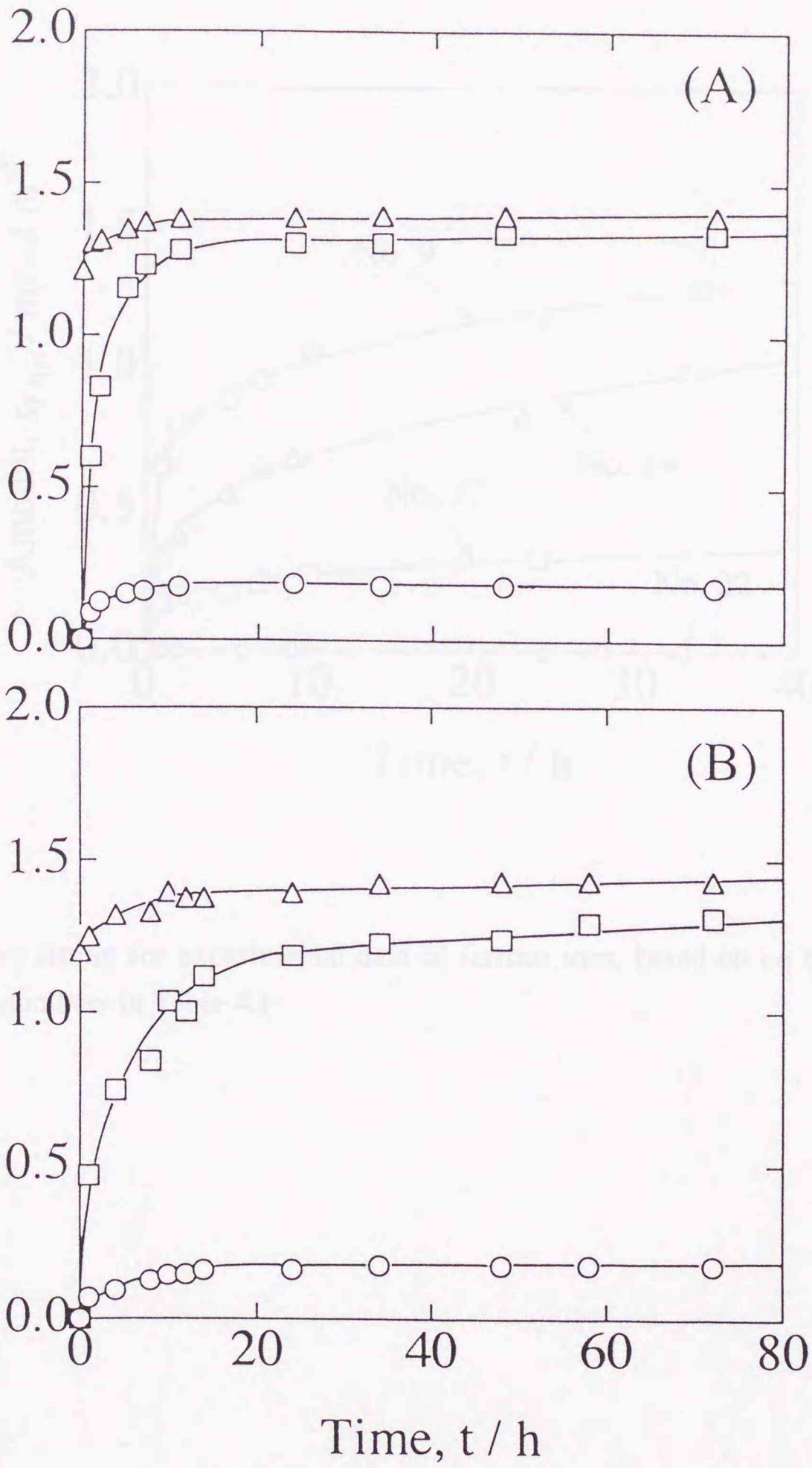

Fig. 4.1 Results of dissolution experiment: (A) No. 3 and (B) No. 7 in Table 4.1. Symbols: □, $x_{Fe(II)}$; △, x_{Fe}; ○, x_{S}.

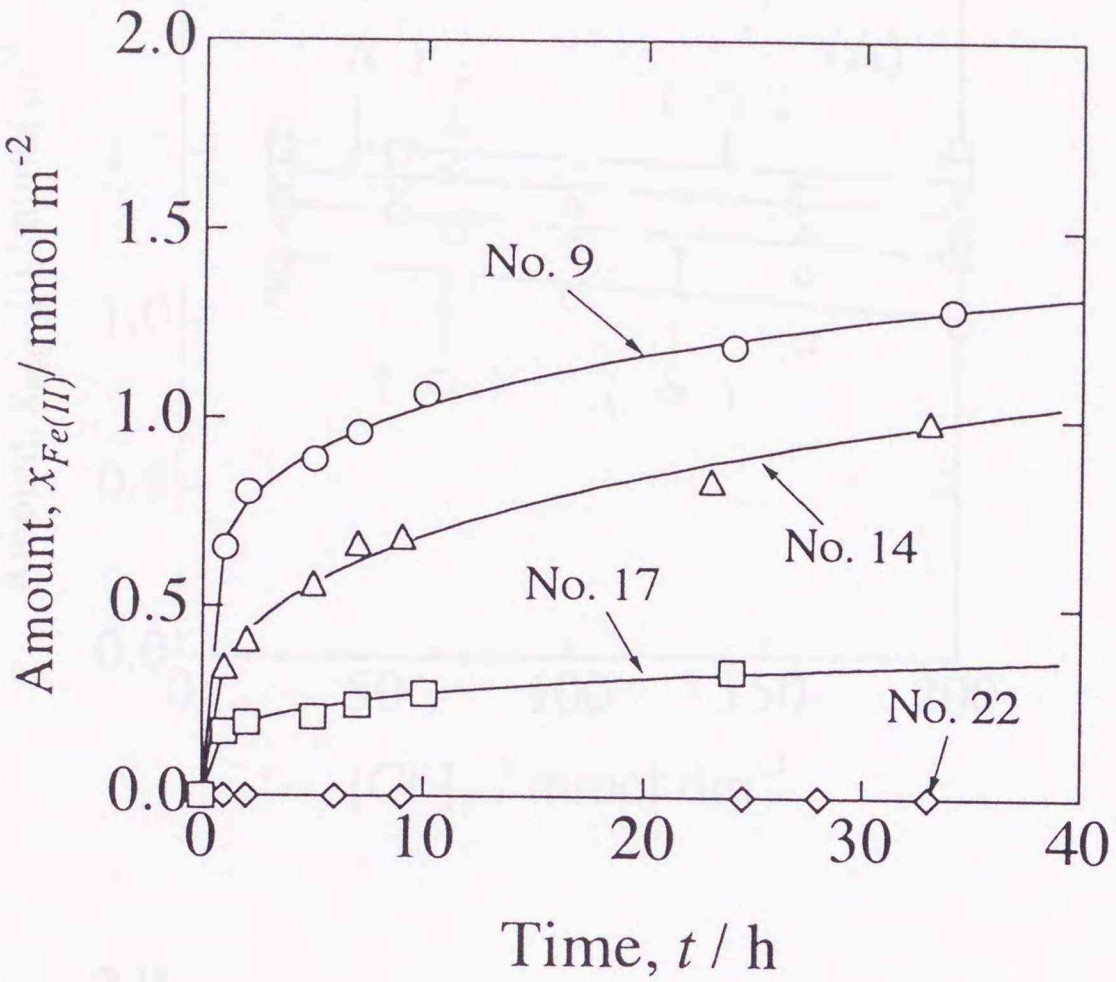

Fig. 4.2 Curve fitting for experimental data of ferrous ions, based on eq (4.2) in the text. Experimental numbers in Table 4.1.

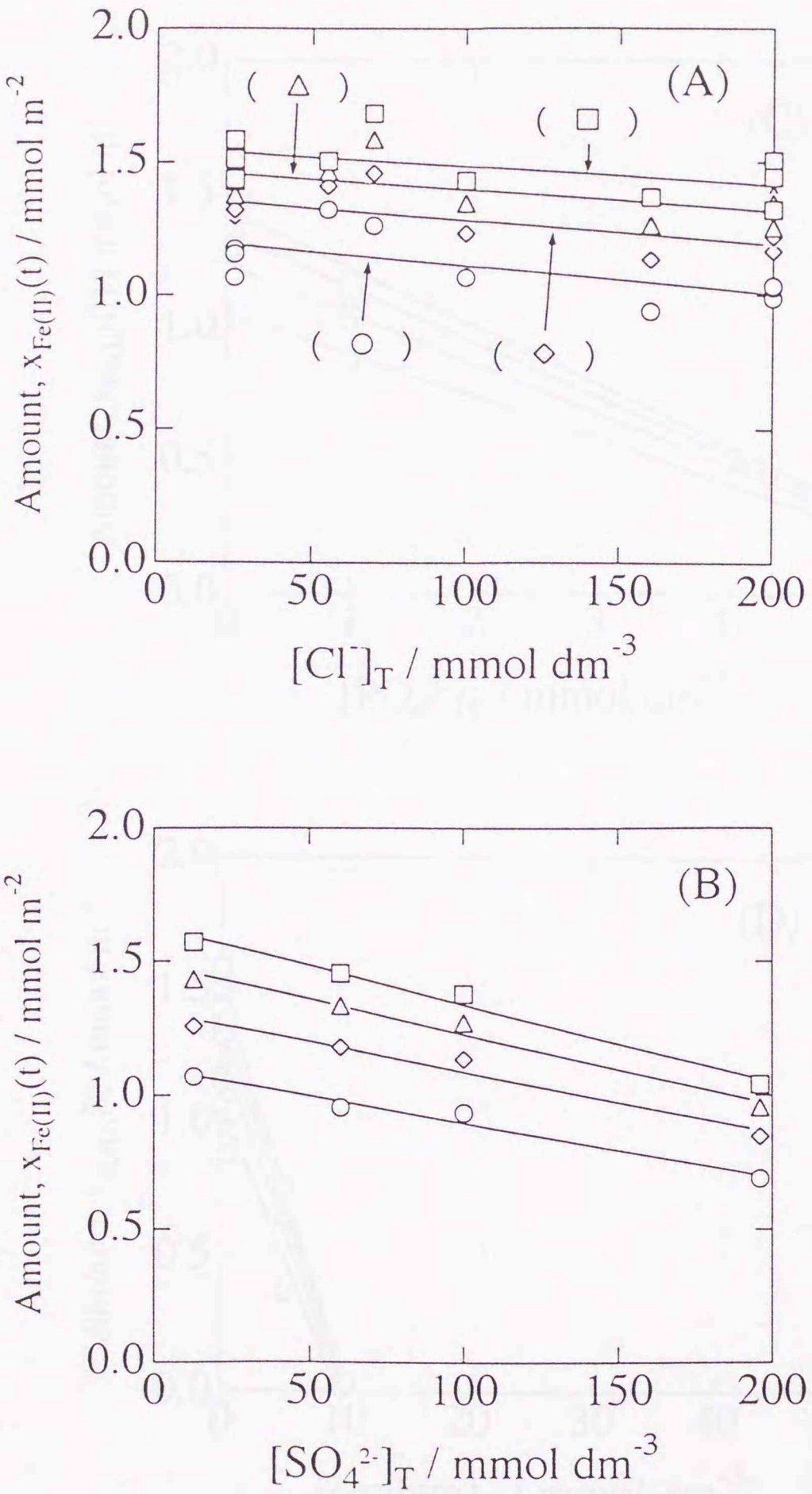

Fig. 4.3 (A)(B) $x_{Fe(II)}(t)$ versus the concentration of total anionic ligands. (A) chloride; and (B) sulfate. Symbols: ○, t = 10 h; ◇, t = 20 h; △, t = 30 h; □, t = 40 h.

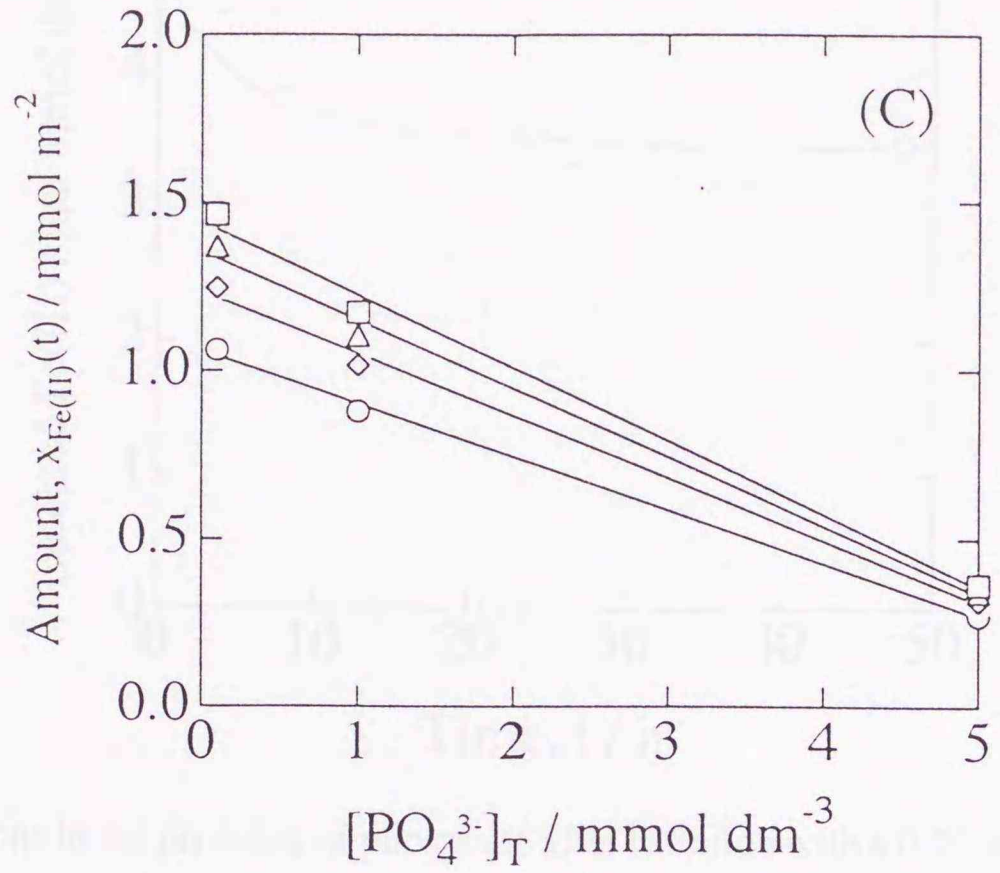

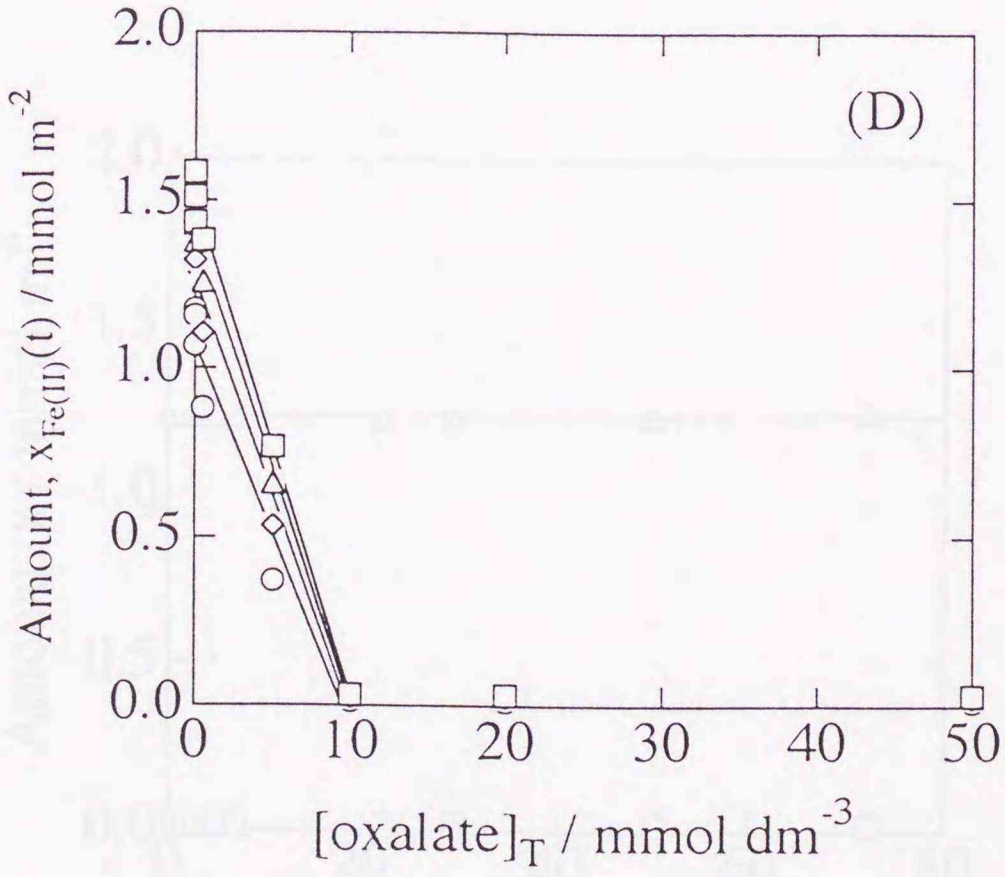

Fig. 4.3 (C)(D) $x_{Fe(II)}(t)$ versus the concentration of total anionic ligands. (C) phosphate; and (D) oxalate. Symbols: ○, t = 10 h; ◇, t = 20 h; △, t = 30 h; □, t = 40 h.

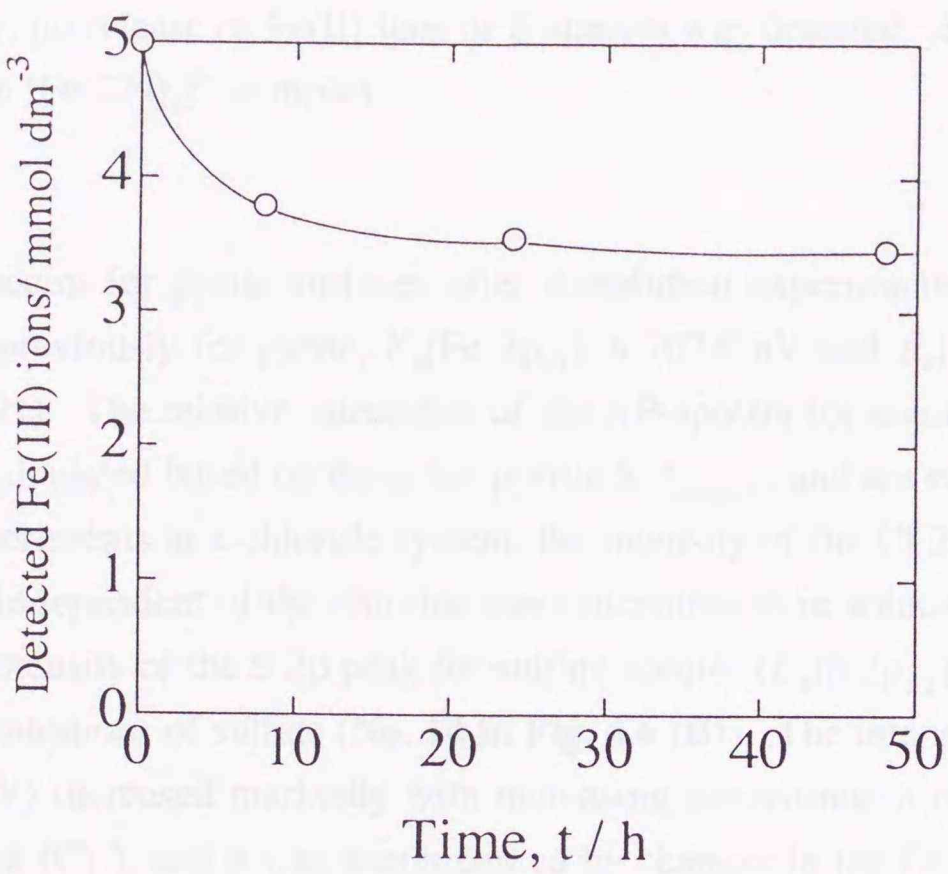

Fig. 4.4 Fe(III) ions in the presence of phosphate after filtration with a 0.20 μm pore-membrane filter. Initial concentrations: $[Fe(III)]_T = [PO_4^{3-}]_T = 5$ mmol dm^{-3}.

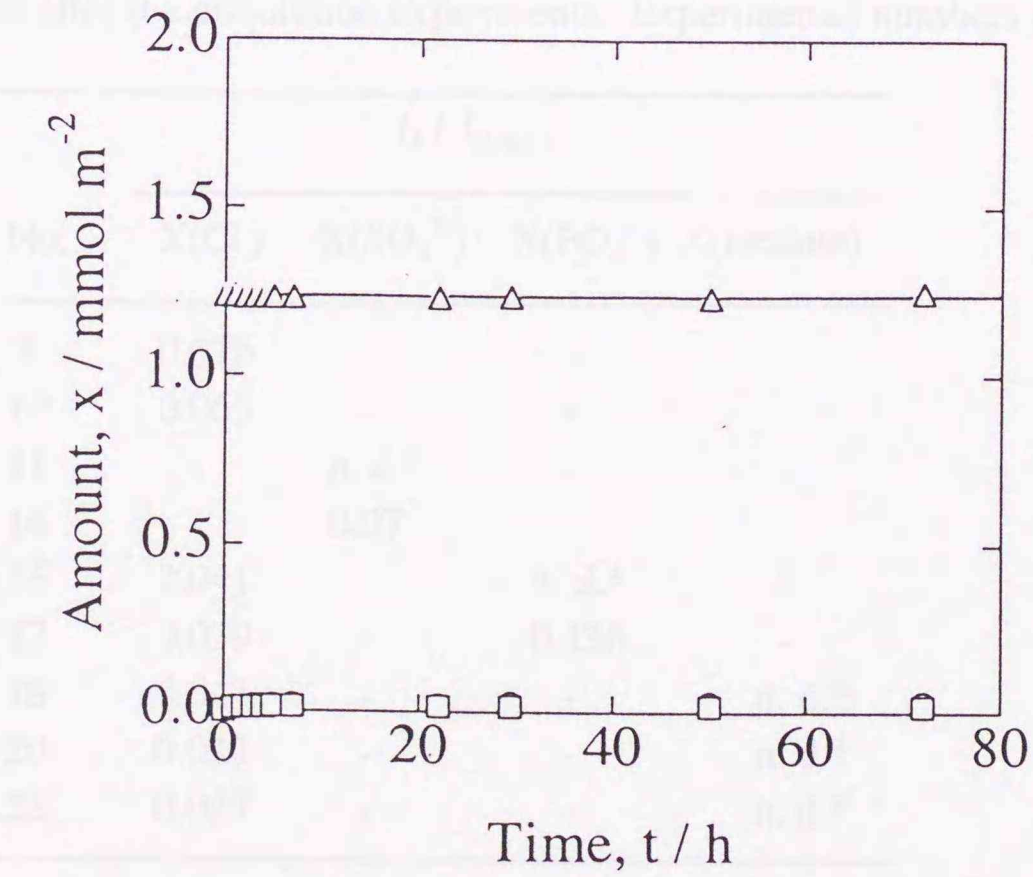

Fig. 4.5 Results of dissolution experiment No. 24 in Table 4.1. Symbols: □, $x_{Fe(II)}$; △, x_{Fe}; ○, x_S.

Fe(II)-CDTA (Basolo, et al., 1967), Fe(II) ions can be determined by the 1, 10-phenanthlorine method. However, no release of Fe(II) ions or S species was detected. Similarly, pyrite was not oxidized by the $[Fe(CN)_6]^{3-}$ complex.

4.2.2 XP-spectra

The XP-spectra for pyrite surfaces after dissolution experiments are shown in **Fig. 4.6**. As reported previously for pyrite, $E_B[Fe\ 2p_{3/2}]$ is 707.0 eV and $E_B[S\ 2p_{3/2}]$ is 162.2 eV (Konno, et al., 1991). The relative intensities of the XP-spectra for anionic species, I_X, after dissolution were calculated based on those for pyritic S, $I_{pyritic\ S}$, and are summarized in **Table 4.2**. After the experiments in a chloride system, the intensity of the Cl 2p peak (E_B[Cl 2p] = 198-199 eV) was independent of the chloride ion concentration in solution (**Fig. 4.6 (A)** and **Table 4.2**). The intensity of the S 2p peak for sulfate species ($E_B[S\ 2p_{3/2}] \sim 168$ eV) was low even at high concentrations of sulfate (**No. 14 in Fig. 4.6 (B)**). The intensity of the P 2p peak (E_B[P 2p] ~ 134 eV) increased markedly with increasing concentration of phosphate species in solution (**Fig. 4.6 (C)**), and it was accompanied by changes in the Fe 2p spectra (**Nos. 15 and 17 in Fig. 4.6 (E)**), small peaks corresponding to oxidized iron species at around 4 eV higher positions than those for pyrite. The C 1s peak for oxalate carbon appears at around E_B = 288.5 eV, but no adsorption of oxalate species on pyrite was observed, even with 50 mmol

Table 4.2 Intensities of XP-spectra for anionic species, I_X, relative to those for pyritic-S, $I_{pyritic\text{-}S}$, on pyrite after the dissolution experiments. Experimental numbers in Table 4.1.

	$I_X / I_{pyritic\ S}$			
No.	$X(Cl^-)$	$X(SO_4^{2-})$	$X(PO_4^{3-})$	X(oxalate)
3	0.075	-	-	-
10	0.065	-	-	-
11	-	n. d.*	-	-
14	-	0.07	-	-
15	0.041	-	n. d.*	-
17	0.039	-	0.136	-
18	0.043	-	-	n. d.*
20	0.033	-	-	n. d.*
22	0.027	-	-	n. d.*

* not detected.

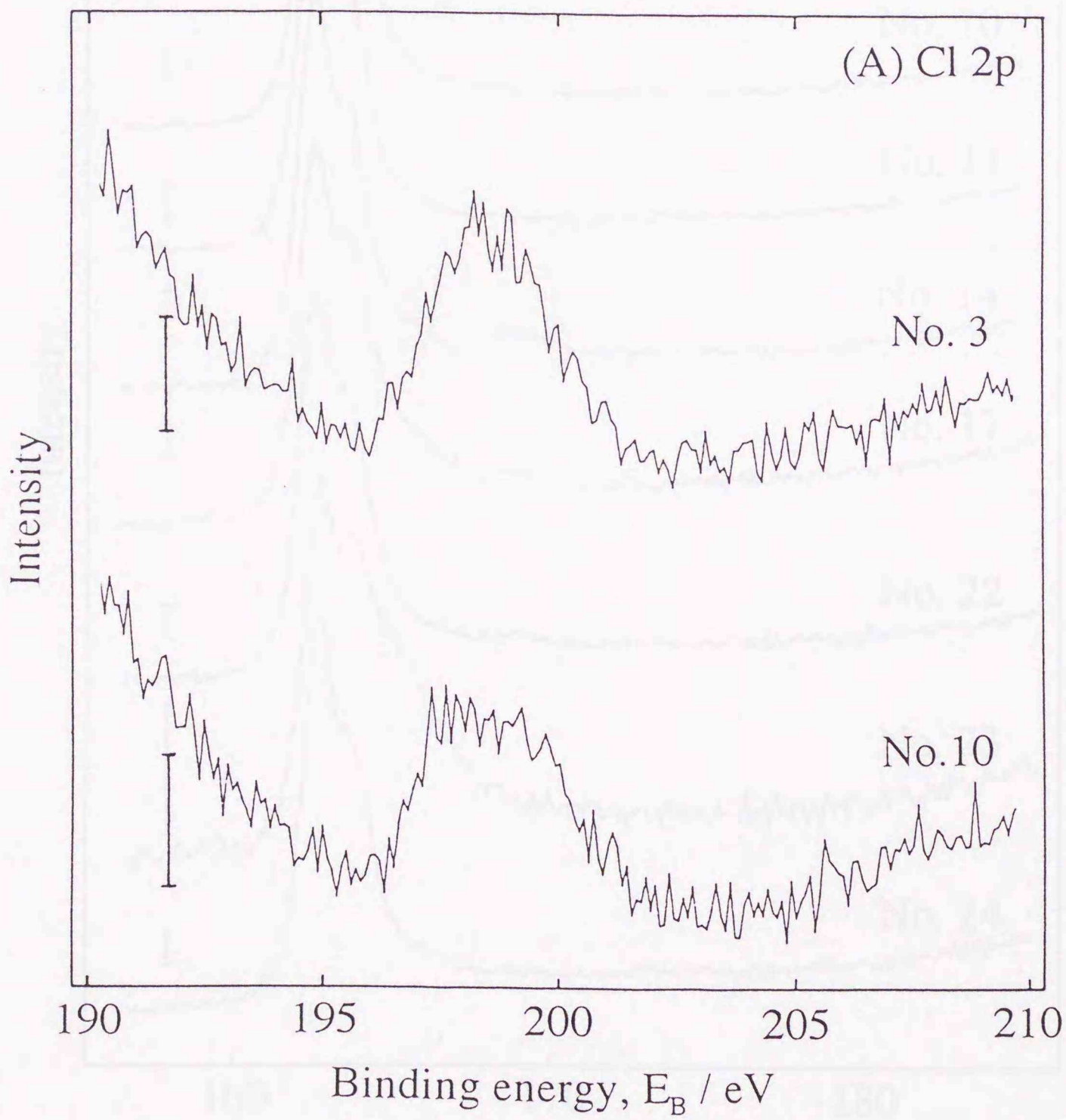

Fig. 4.6 (A) The XP-spectra of Cl 2p for pyrite after dissolution. Vertical bars indicate 100 cps. Experimental numbers are given in Table 4.1.

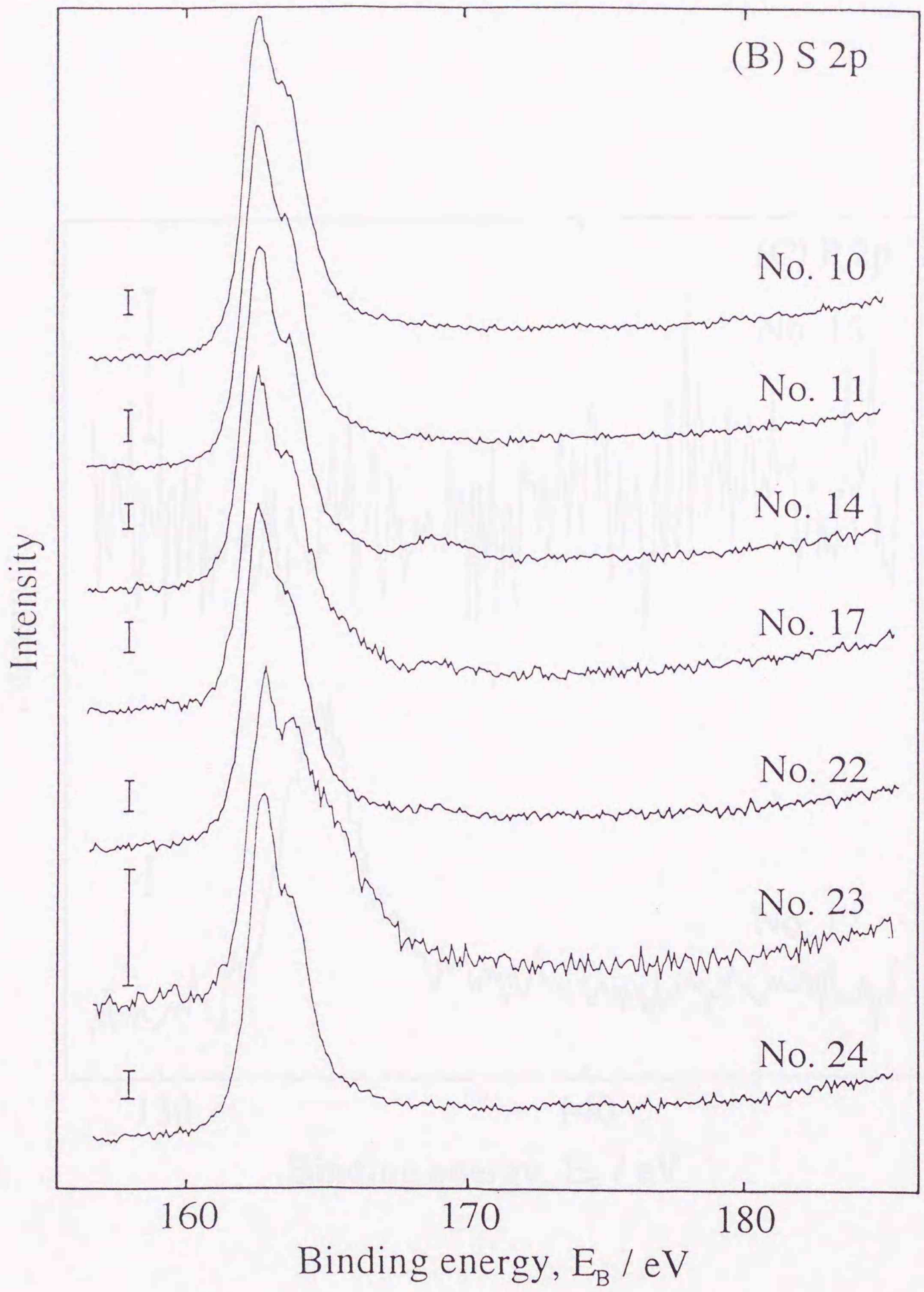

Fig. 4.6 (B) The XP-spectra of S 2p for pyrite after dissolution. Vertical bars indicate 250 cps. Experimental numbers are given in Table 4.1.

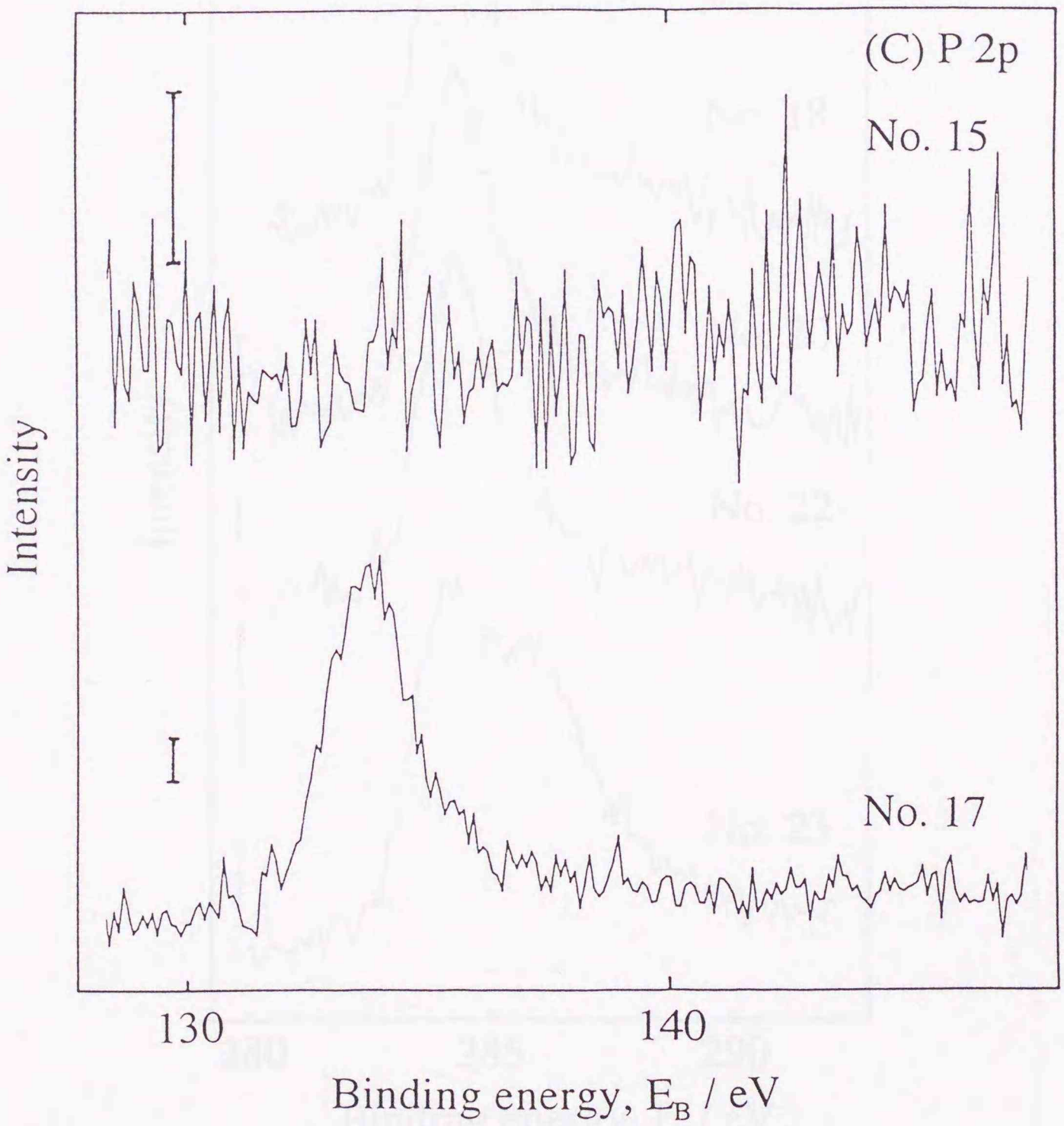

Fig. 4.6 (C) The XP-spectra of P 2p for pyrite after dissolution. Vertical bars indicate 50 cps. Experimental numbers are given in Table 4.1.

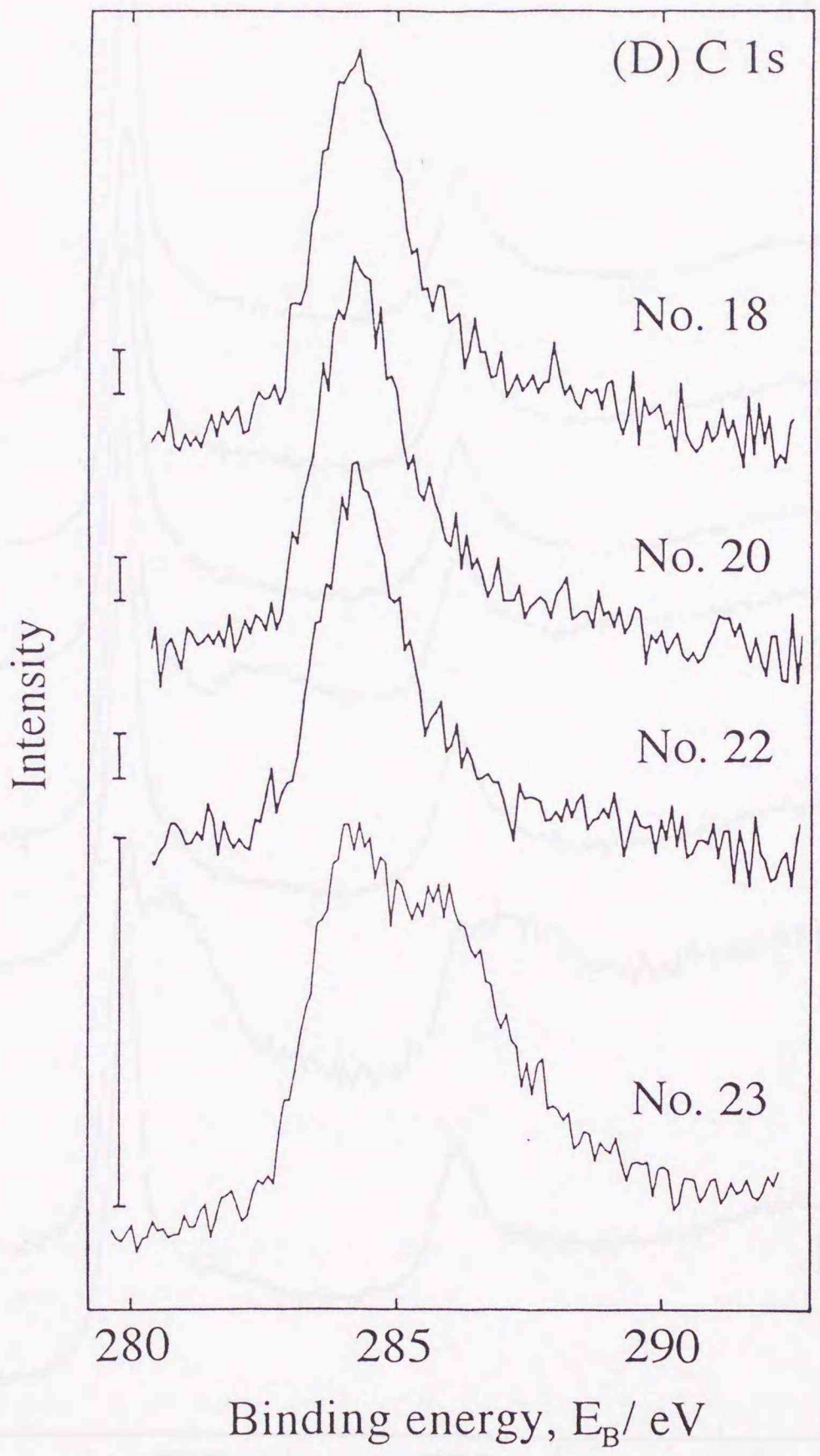

Fig. 4.6 (D) The XP-spectra of C 1s for pyrite after dissolution. Vertical bars indicate 500 cps. Experimental numbers are given in Table 4.1.

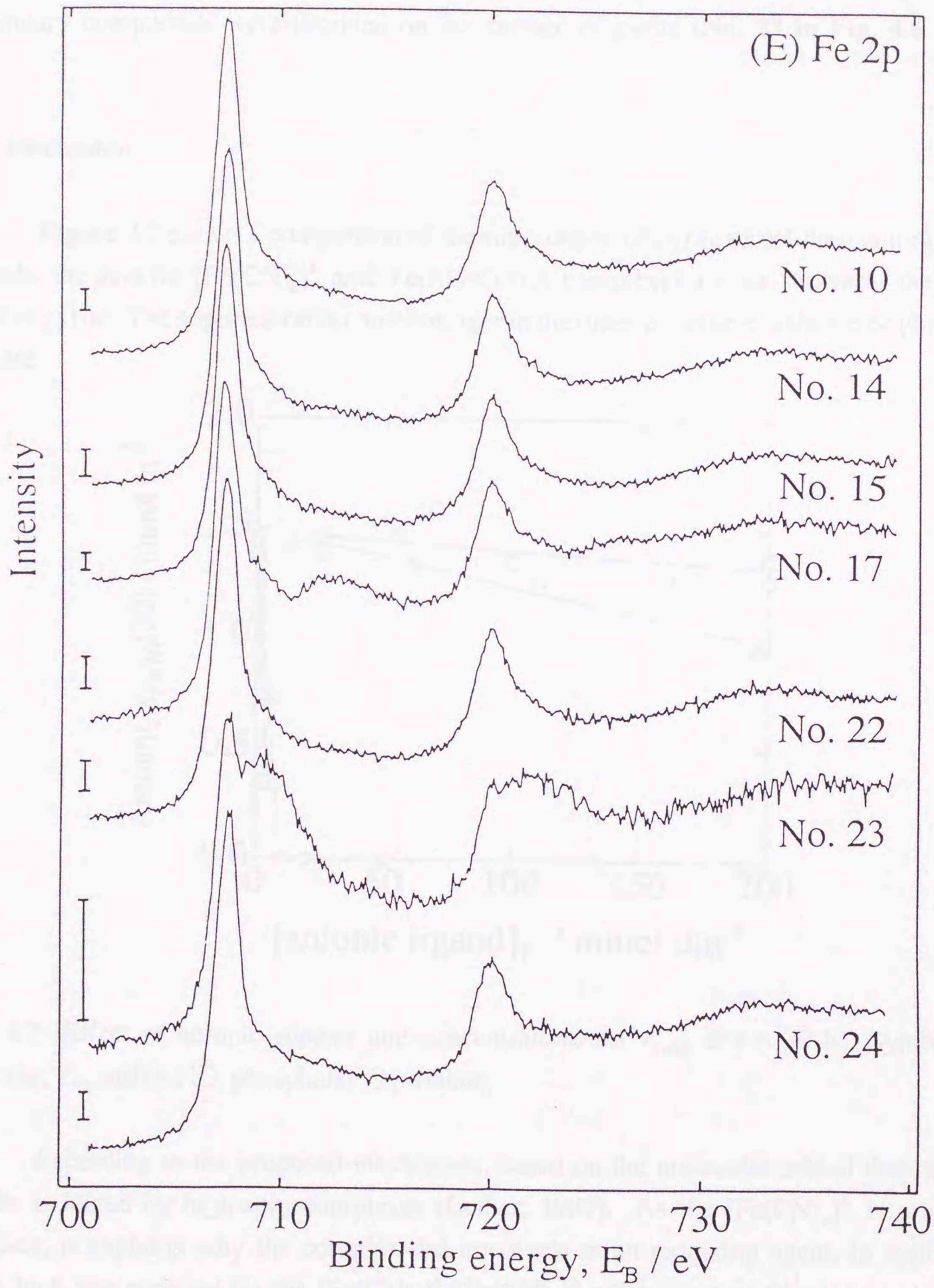

Fig. 4.6 (E) The XP-spectra of Fe 2p for pyrite after dissolution. Vertical bars indicate 500 cps. Experimental numbers are given in Table 4.1.

dm^{-3} oxalate (**No. 22 in Fig. 4.6 (D)**). Similarly, in the case of the Fe(III)-CDTA complex, only pyrite was detected in the XP-spectra (**No. 24 in Fig. 4.6 (B) and (E)**). Addition of $[Fe(CN)_6]^{3-}$ complex resulted in signals corresponding to pyrite which were very weak and secondary compounds were detected on the surface of pyrite (**No. 23 in Fig. 4.6 (B) and (E)**).

4.3 Discussion

Figure 4.7 shows a comparison of the suppression of pyrite dissolution among anionic ligands, the data for $[Fe(CN)_6]^{3-}$ and Fe(III)-CDTA complexes are not shown as they do not oxidize pyrite. The suppression became stronger in the order chloride < sulfate <<< phosphate~ oxalate.

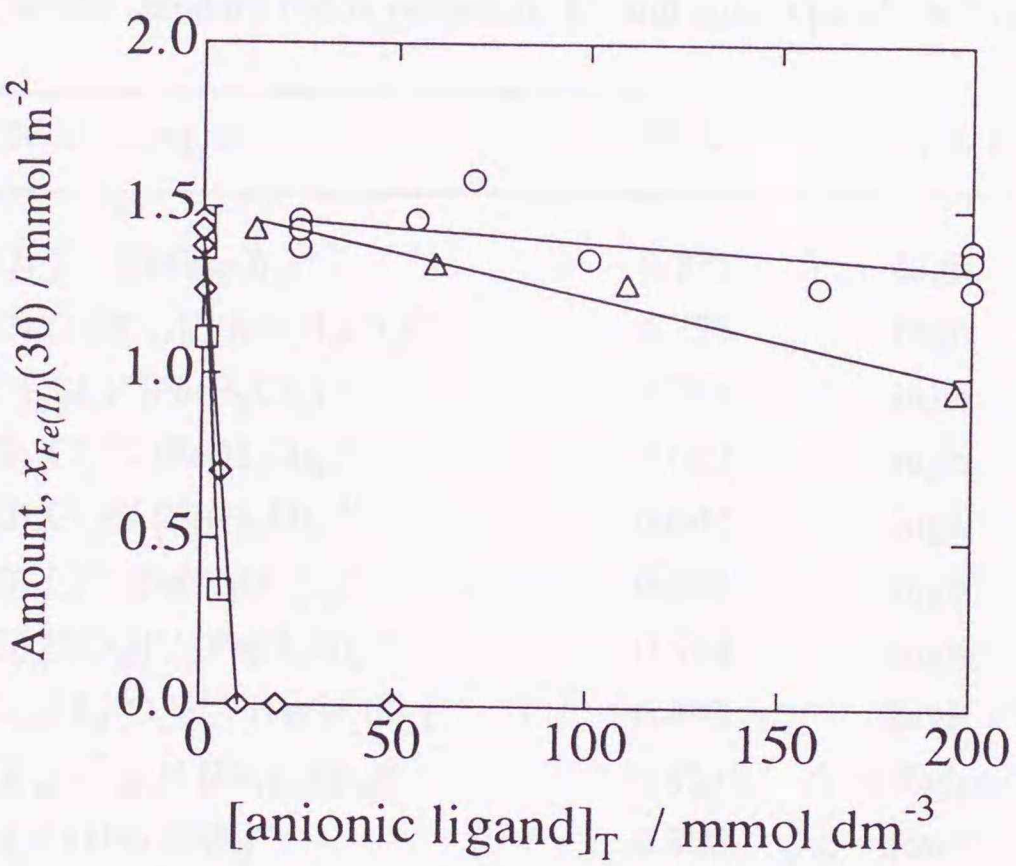

Fig. 4.7 Effect of anionic species and concentrations on $x_{Fe(II)}$ at t = 30 h. Symbols: ○, chloride; △, sulfate; □, phosphate; ◇, oxalate.

According to the proposed mechanism, based on the molecular orbital theory, pyrite can be oxidized by high-spin complexes (Luther, 1987). As the $[Fe(CN)_6]^{3-}$ is a low-spin complex, it explains why the complex did not work as an oxidizing agent, in spite of the fairly high rate constant for the $[Fe(CN)_6]^{3-}/[Fe(CN)_6]^{4-}$ redox reaction (Basolo, et al., 1967). By addition of $[Fe(CN)_6]^{3-}$ complex, secondary compounds were formed and covered a part of the pyrite surface, but this is not considered to be the reason why $[Fe(CN)_6]^{3-}$ ions did not oxidize pyrite as no dissolution was observed early in the experiments. The spin-type explanation

cannot be applied to the Fe(III)-CDTA complex, since this is a high-spin complex and labile (Basolo, et al., 1967; Ueno, 1992). Another mechanism has proposed that the oxidation of pyrite by Fe(III) aquoions is accomplished by the transfer of electrons through coodinated water molecules (Moses, et al., 1987). The results with Fe(III)-CDTA (**Fig. 4.5**) may be explained by a total absence of coodinated water molecules in the complex. It is considered that the stability of the complex species is also an important factor, since it affects the standard redox potential, E^0. Except for "back donating" ligands such as 1, 10-phenanthroline, Fe(III)-complexes are generally more stable than Fe(II)-complexes. Accordingly, the complex formation leads to a lower E^0 as shown in **Table 4.3** , where E^0 values were calculated by using stability constants (Smith, et al., 1972a; 1972b). The ligand effect can be explained based on the order of potential of the oxidant.

Table 4.3 Calculated standard redox potential, E^0, and spin type of Fe(III) complexes.

Redox couple	E^0/ V	Spin type
$[Fe(H_2O)_6]^{3+}$/ $[Fe(H_2O)_6]^{2+}$	0.771	high
$[Fe(H_2O)_5(HPO_4)]^{+}$/ $[Fe(H_2O)_6]^{2+}$	0.725	high
$[Fe(H_2O)_3Cl_3]$/ $[Fe(H_2O)_6]^{2+}$	0.703	high
$[Fe(H_2O)_5Cl]^{2+}$/ $[Fe(H_2O)_6]^{2+}$	0.682	high
$[Fe(H_2O)_4Cl_2]^{+}$/ $[Fe(H_2O)_6]^{2+}$	0.644	high
$[Fe(H_2O)_4L]^{+}$/ $[Fe(H_2O)_2L_2]^{2-}$	0.630	high
$[Fe(H_2O)_5(SO_4)]^{+}$/ $[Fe(H_2O)_6]^{2+}$	0.534	high
$[Fe(H_2O)_5(H_2PO_4)]^{2+}$/ $[Fe(H_2O)_6]^{2+}$	0.493	high
$[Fe(H_2O)_4(SO_4)_2]^{-}$/ $[Fe(H_2O)_6]^{2+}$	0.451	high
$[Fe(CN)_6]^{3-}$/ $[Fe(CN)_6]^{4-}$	0.360	low
$[Fe(H_2O)_5(OH)]^{2+}$/ $[Fe(H_2O)_5(OH)]^{+}$	0.340	high
$[Fe(H_2O)_2L_2]^{-}$/ $[Fe(H_2O)_2L_2]^{2-}$	0.269	high
$[FeY]^{-}$/$[FeY]^{2-}$	0.104	high
$[FeL_3]^{3-}$/ $[Fe(H_2O)_2L_2]^{2-}$	- 0.017	high

H_4Y, cyclohexanediaminetetraacetic acid (CDTA)

H_2L, oxalic acid

Concentration distributions for complexes in the Fe(III)-chloride and Fe(III)-sulfate systems are shown in **Fig. 4.8 (A) and (B)**, calculated at pH 2 as a function of total ligand concentration using reported stability constants (Smith, et al., 1972a; 1972b). The experimental

ranges are shown by broken lines in **Fig. 4.8**. From **Fig. 4.8 (A) and (B)** and **Table 4.3**, it is clear that with increasing concentration of anionic ligands, oxidant species weaker than Fe(III) aquoions increase in the systems. In chloride solutions, the increase in $x_{Fe(II)}(t)$ in the initial ten hours is larger in a smaller $[Cl^-]_T$ solution (**Fig. 4.1**). It indicates that the increase in Fe(III)-chloride complexes leads to slower oxidation. The fractional changes in the Cl^- and SO_4^{2-} coordinated species in the experimental ranges are parallel to the results of dissolution experiments, as shown in **Fig. 4.7** where the suppression by sulfate was stronger than that by chloride.

The dissolution behavior in oxalate systems is also explained by considering E^0 and suppression. At $[oxalate]_T > 10$ mmol dm^{-3}, oxidative dissolution of pyrite did not occur (**Fig. 4.3 (D)**). As shown around $[oxalate]_T = 10$ mmol dm^{-3} in **Fig. 4.8 (D)**, the fractions of the stronger oxidant species, such as $[Fe(H_2O)_6]^{3+}$ and $[Fe(H_2O)_4(C_2O_4)]^+$, decrease steeply and the dominant species become $[Fe(H_2O)_2(C_2O_4)_2]^-$ and $[Fe(C_2O_4)_3]^{3-}$, which are much weaker oxidants than sulfate or chloride complexes (**Table 4.3**). Neither adsorption of oxalate ions nor other compounds on pyrite was observed by XPS even at $[oxalate]_T = 50$ mmol dm^{-3} (**No. 22 in Fig. 4.6 (B), (D) and (E)**) so that adsorption cannot be the reason of suppression. As the $[Fe(H_2O)_2(C_2O_4)_2]^-/[Fe(H_2O)_2(C_2O_4)_2]^{2-}$ couple did not oxidize pyrite, it is reasonable that the weaker oxidant Fe(III)-CDTA complex also did not.

For phosphate systems, the formation of colloidal or polynuclear Fe(III) species plays an important role in the $[PO_4^{3-}]_T > 5$ mmol dm^{-3} range, in addition to the above complexation effects. The results of control experiments, conducted in $[Fe(III)]_T = [PO_4^{3-}]_T = 5$ mmol dm^{-3}, indicate that about 30% of Fe(III) species may be colloid and unable to pass pores of 0.20 μm (**Fig. 4.4**). This suggests that most Fe(III) ions are polymerized and that the fractions of mononuclear species are much lower than the calculated values shown in **Fig. 4.8(C)**. Further, it is evident from the XPS measurements (**No. 17 in Fig. 4.6(C) and (E)**, and **Table 4.2**) that there was deposition of Fe(III)-phosphate compounds and/or adsorption of phosphate ions on the surface of pyrite. This may not be the main factor reducing the dissolution but may be secondary, since they reduce $[Fe(III)]_T$ in solution and block active sites of the surface. Thus, the drastic suppression by phosphate ions is not due to the complex formation alone.

As can be seen in **Fig. 4.1 (A)**, $x_{Fe(II)}(t)$ gradually approaches to $x_{Fe}(t)$ with time and the difference becomes less than a fraction of $[Fe(H_2O)_5(OH)]^{2+}$ complex (**Fig. 4.8(A)**). It implies that $[Fe(H_2O)_5(OH)]^{2+}$ complex functions as an oxidant of pyrite.

The above qualitative discussion can explain the ligand effect on the oxidative dissolution of pyrite by Fe(III) ions. From the discussion on E^0 and **Table 4.3**, it may be assumed that E^0 for SO_4^{2-}/pyrite-S is lower than for $[Fe(H_2O)_5(OH)]^{2+}/[Fe(H_2O)_5(OH)]^+$ but higher than for $[Fe(H_2O)_2(C_2O_4)_2]^-/[Fe(H_2O)_2(C_2O_4)_2]^{2-}$. A further quantitative discussion is deferred, since some stability constants for complex species formation are not reported and also due to the

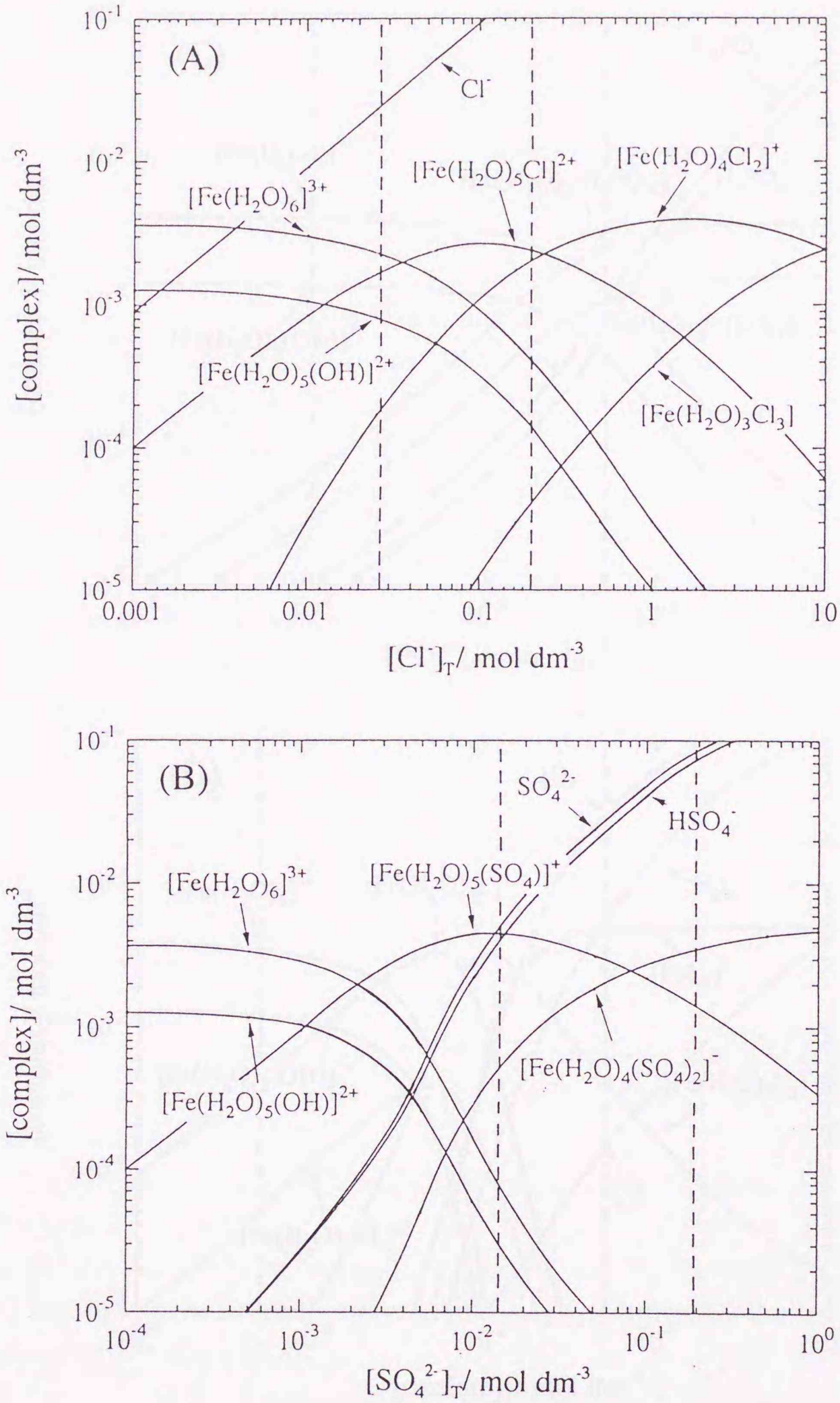

Fig. 4.8 (A)(B) Proportions of Fe(III) complexes and ions calculated from stability constant at $[Fe(III)]_T = 5$ mmol dm^{-3} and pH 2.0. (A) chloride; (B) sulfate.

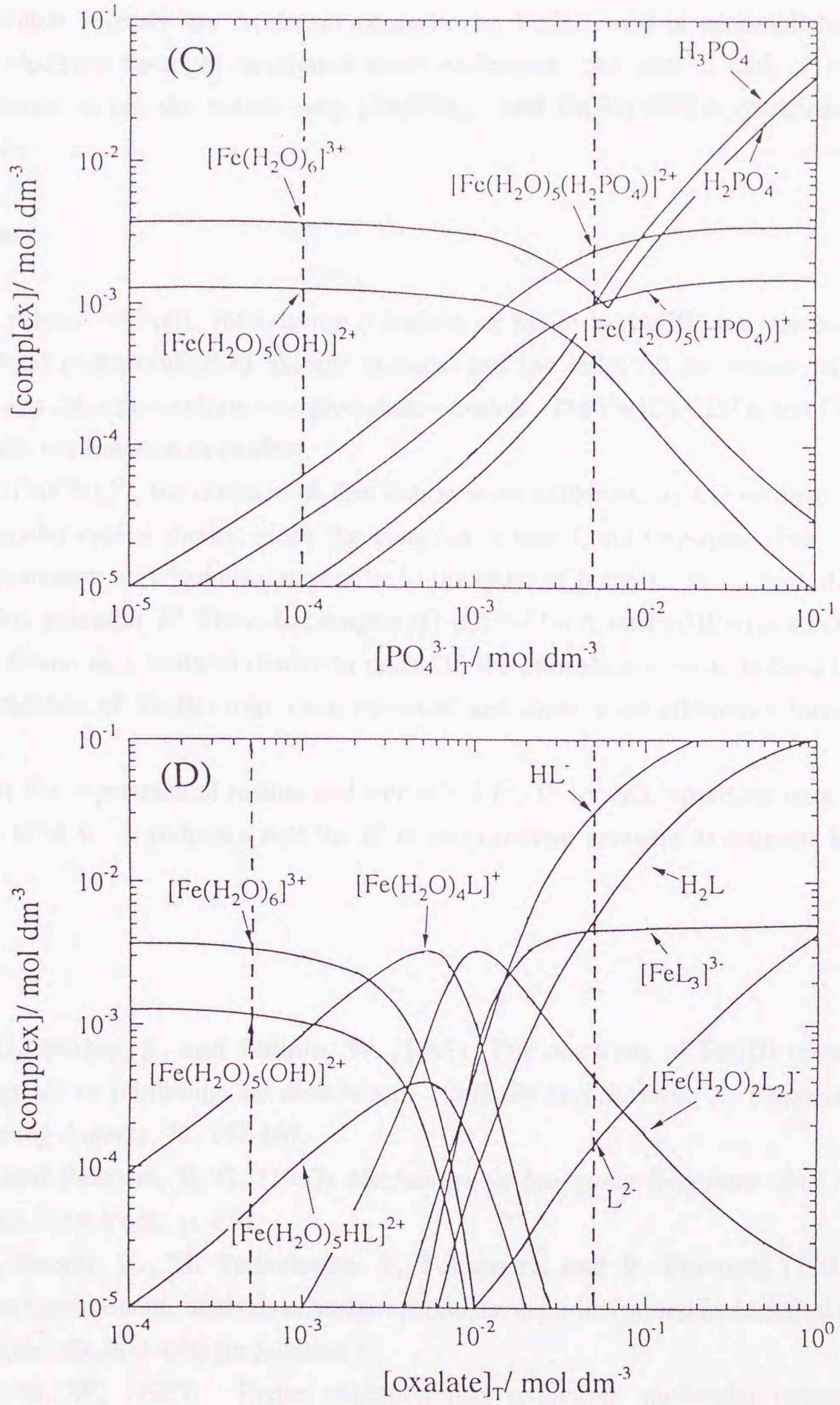

Fig. 4.8 (C)(D) Proportions of Fe(III) complexes and ions calculated from stability constant at $[Fe(III)]_T = 5$ mmol dm^{-3} and pH 2.0. (C) phosphate; (D) oxalate, $H_2L = (COOH)_2$.

differences among reported stability constants. It must be noted here that the present results do not establish whether the oxidation of pyrite by Fe(III) ions is accomplished by the transfer of electrons through coodinated water molecules. At least, a lack of coodinated water molecules is not the reason why $[Fe(CN)_6]^{3-}$ and Fe(III)-CDTA complexes do not oxidize pyrite.

4.4 Summary

The release of Fe(II) ions during oxidation of pyrite by Fe(III) ions decreased with increasing total concentration of anionic species, and the order of the anions suppressing dissolution was chloride < sulfate <<< phosphate~ oxalate. The Fe(III)-CDTA and $[Fe(CN)_6]^{3-}$ complexes did not function as oxidant.

For $[Fe(CN)_6]^{3-}$, the absence of dissolution were explained by the mechanism based on the molecular orbital theory, since the complex is innert and low-spin. For others, the order of suppression was found to be parallel to the order of potential as oxidant, that is, the standard redox-potential, E^0. The redox couples of Fe(III)-CDTA and Fe(III)-oxalate complexes have lower E^0 and they reduced oxidation rates. In the phosphate system, colloid formation and polynucleation of Fe(III) ions were observed and these were additional factors in the suppression.

From the experimental results and calculated E^0, E^0 for SO_4^{2-}/pyrite-S may be in the range 0.27~0.34 V. It indicates that the E^0 is an important measure to estimate the ligand effect.

References

Bondietti, G., Singer, J., and Stumm, W. (1993) The reactivity of Fe(III) (hydr)oxides: effects of ligands in inhibiting the dissolution. *Colloids and Surfaces A: Physicochemical and Engineering Aspects*, **72**, 157-167.

Basolo, F., and Pearson, R. G. (1967) *Mechanism of Inorganic Reactions. 2nd ed.* John Wiley & Sons, New York, p. 454.

Konno, H., Sasaki, K., M. Tsunekawa, T. Takamori, and R. Furuichi (1991) X-ray photoelectron spectroscopic analysis of surface products on pyrite formed by bacterial leaching. *Bunseki Kagaku*, **40**, 609 -616 (in Japanese).

Luther III, G. W. (1987) Pyrite oxidation and reduction: molecular orbital theory considerations. *Geochim. Cosmochim. Acta*, **51**, 3193-3199.

Luther III, G. W., Kostka, J. E., Church, T. M., Sulzberger, B., and Stumm, W. (1992) Seasonal iron cycling in the salt-marsh sedimentary environment: the importance of ligand

complexes with Fe(II) and Fe(III) in the dissolution of Fe(III) minerals and pyrite, respectively. *Marine Chemistry*, **40**, 81-103.

Moses, C. O., Nordstrom, D. K., Herman, J. S., and Mills, A. L. (1987) Aqueous pyrite oxidation by dissolved oxygen and by ferric iron. *Geochim. Cosmochim. Acta*, **51**, 1561-1571.

Smith, R. M., and Martell, A. E. (1972a) *Critical Stability Constants.* **Vol. 3**, Plenum Press, New York, p. 92.

Smith, R. M., and Martell, A. E. (1972b) *ibid*, **Vol. 4**, Plenum Press, New York, p. 7.

Singer, P. C., and W. Stumm, W. (1970) Acidic mine drainage: the rate-determining step. *Science*, **167**, 1121-1123.

Ueno, K. (1992) *Nyumon Kireto Kagaku (Chelate Chemistry, An Introduction)*, Nankodo, Tokyo, p. 149 (in Japanese).

Chapter 5
Effect of metal ions on the reactivity of pyrite with Fe(III) ions

As described in **Chapter 3**, the reaction of pyrite with Fe(III) ions in acid solutions has been conventionally expressed as

$$FeS_2 + 14\,Fe^{3+} + 8\,H_2O = 15\,Fe^{2+} + 2\,SO_4^{2-} + 16\,H^+, \qquad (5.1)$$

however, an additional reaction,

$$FeS_2 + 2\,Fe^{3+} = 3\,Fe^{2+} + 2\,S, \qquad (5.2)$$

is also taking place in parallel with reaction (5.1), resulting in the nonstoichiometric release of Fe ions and sulfate ions to the solution. Further, it has been reported that Fe(II) ions which are formed by the reaction (5.1) reduce the dissolution rate (Sakai, et al., 1987). It is a kind of self-suppressing reaction. This indicates that Fe(II) ions may act to suppress the weathering of pyrite in the geological cycle of Fe and S. For a better understanding of the overall mechanism of pyrite oxidation with Fe(III) ions, it is important to elucidate the effect of Fe(II) ions.

Studies on the adsorption or reduction of toxic ions on pyrite have suggested that pyrite has the potential to remove toxic ions such as Hg(II), As(III, V) and Cd(VI) ions from waste water (Brown, et al., 1979; Jean, et al., 1986; Zouboulis, et al., 1993; 1995). The interfacial reactions of Au-complex/pyrite were related to geochemical aspects in concentrating noble metals with pyrite functioning as a reductant (Hyland, et al., 1989; Bancroft, et al., 1990). In a field of mineral processing, knowledge on the interaction between pyrite and Cu(II) ions, an activator in froth flotation of sulfide, is useful and often indispensable (Voigt, et al., 1994; Perry, et al., 1984). Acid mine waters contain metal cations from other sulfides (Zn(II), Cu(II), and Pb(II) ions). Pyrite has some unique surface properties and further studies on the surface reaction is required.

In this chapter, the effect of metal ions including Fe(II) and Cu(II) ions on the oxidative dissolution of pyrite by Fe(III) ions around pH 2 was investigated by solution and XPS surface analysis.

5.1 Experimental

5.1.1 Pyrite

Pyrite sample and its pretreatment were described in **Chapter 3**.

5.1.2 Dissolution experiments

Dissolution experiments of pyrite were carried out in the same manner as in **Chapters 3 and 4**. If the foreign cations, M^{m+}, with a higher standard redox potential of M^{m+}/M^{n+} (m>n), $E^0_{Mm+/Mn+}$, than 0.771 V(= $E^0_{Fe3+/Fe2+}$), coexist with pyrite in the solution containing Fe(III) ions, M^{m+} ions may function as an oxidant to pyrite similar to Fe(III) ions. Therefore, cations having $E^0 < 0.771$ V were selected in the present work, and the concentrations were systematically set as shown in **Table 5.1**. Reagents used were of analytical grade (AR) and as follows: Nos. 5~31, $FeCl_3 \cdot 6H_2O$; No. 15, KCl; No. 14, NaCl; No. 16, $MgCl_2 \cdot 6H_2O$; Nos. 17~18, $NiCl_2$; Nos. 1 and 19~20, $ZnCl_2 \cdot 2H_2O$; Nos. 2 and 21~22, $CdCl_2 \cdot 2H_2O$; Nos. 23~24, $CaCl_2 \cdot 2H_2O$; Nos. 25~26, $Pb(COOH)_2 \cdot 3H_2O$; Nos. 27~29, $BaCl_2 \cdot 2H_2O$; Nos. 3 and 12~13, $CuCl_2 \cdot 2H_2O$; Nos. 4, 6~7, 9~11, and 31, $FeSO_4 \cdot 7H_2O$. The initial pH of the solution was adjusted to ~2 using SSG HCl and SSG NaOH. After some dissolution experiments, the residues were separated by filtration to measure the XP-spectra as described in **Chapter 2**.

Table 5.1 Details of dissolution experiments and properties of the introduced cations

No.	Foreign cations		HSAB[*1]	pH		E^{0} [*2]	K_{sp} [*2] for sulfate
	M^{n+}	$[M^{n+}]$ /mmol dm^{-3}		initial	final	/ V	/(mol dm^{-3})^2
[Fe(III)] = 0 mmol dm^{-3}							
1	Zn^{2+}	15	MA	2.06	2.06	-0.763 ($Zn^{2+} + 2e^- = Zn$)	
2	Cd^{2+}	15	SA	2.06	2.06	-0.403 ($Cd^{2+} + 2e^- = Cd$)	
3	Cu^{2+}	15	MA	2.06	2.06	+0.538 ($Cu^{2+} + Cl^- + e^- = CuCl$) +0.521 ($Cu^{+} + e^- = Cu$) +0.337 ($Cu^{2+} + 2e^- = Cu$) +0.153 ($Cu^{2+} + e^- = Cu^{+}$)	
4	Fe^{2+}	45	MA	2.00	2.00	+0.771 ($Fe^{3+} + e^- = Fe^{2+}$)	
[Fe(III)] = 1 mmol dm^{-3}							
5	-	-	-	2.10	2.04		
6	Fe^{2+}	3	MA	2.01	2.00		
7	Fe^{2+}	45	MA	2.01	2.00		
[Fe(III)] = 5 mmol dm^{-3}							
8	-	-	-	2.09	1.91		
9	Fe^{2+}	0.5	MA	2.02	1.90		
10	Fe^{2+}	5	MA	2.07	1.97		
11	Fe^{2+}	15	MA	2.11	2.08		
12	Cu^{2+}	5	MA	2.04	1.90		
13	Cu^{2+}	15	MA	2.06	1.93		
14	Na^{+}	75	HA	2.01	1.86		

Table 5.1 (continued)

No.	Foreign cations M^{n+}	$[M^{n+}]$ /mmol dm^{-3}	HSAB*1	pH initial	pH final	E^{0} *2 / V	K_{sp} *2 for sulfate /(mol dm^{-3})^2
[Fe(III)] = 5 mmol dm^{-3}							
15	K^+	75	HA	2.00	1.91		
16	Mg^{2+}	5	HA	2.09	1.91		
17	Ni^{2+}	5	MA	2.02	1.92	-0.250 ($Ni^{2+} + 2e^- = Ni$)	
18	Ni^{2+}	15	MA	2.05	1.93		
19	Zn^{2+}	5	MA	2.00	1.91		
20	Zn^{2+}	15	MA	2.00	1.91		
21	Cd^{2+}	5	SA	2.02	1.87		
22	Cd^{2+}	15	SA	2.02	1.87		
23	Ca^{2+}	5	HA	2.02	1.93	-2.866 ($Ca^{2+} + 2e^- = Ca$)	$10^{-4.62}$
24	Ca^{2+}	15	HA	2.05	1.90		
25	Pb^{2+}	1	MA	1.96	1.85	-0.126 ($Pb^{2+} + 2e^- = Pb$)	$10^{-7.79}$
26	Pb^{2+}	5	MA	2.05	1.91		
27	Ba^{2+}	0.5	HA	2.06	1.91	-2.906 ($Ba^{2+} + 2e^- = Ba$)	$10^{-9.96}$
28	Ba^{2+}	1	HA	2.07	1.92		
29	Ba^{2+}	5	HA	2.08	1.92		
[Fe(III)] = 15 mmol dm^{-3}							
30	-	-	-	1.96	1.73		
31	Fe^{2+}	45	MA	2.08	2.03		

*1 HA: hard acid; MA: moderate acid; SA: soft acid

*2 Refer to Smith and Martell (1976).

5.1.3 XPS measurements

The details of apparatus and procedure were the same as mentioned in **Chapter 2**, except the followings. For measurements of Cu 2p spectra, carbon tape was used in place of copper foil. For the measurements of Ba 3d spectra for pyrite samples and of Fe 2p spectra for $CuFeS_2$ without interference by Auger peaks of Fe 2p and Cu 2p, Mg Kα X ray (15 kV, 10 mA) was used.

The surface composition, n_M/n_S mole ratio (where M means a metal element), was calculated according to eq(2.5) in **Chapter 2**. Correction for the surface contamination layer was not carried out since C 1s peak intensities were always very low and negligible. The relative sensitivity factor between Cu $2p_{3/2}$ and S 2p, $s_{Cu\,2p3/2}/s_{S\,2p}$, was experimentally determined by using the fresh surfaces of chalcopyrite ($CuFeS_2$) cleaved in argon, $CuSO_4 \cdot 5H_2O$ (analytical grade of Kanto Chemicals) and CuSCN (practical grade of Wako Chemicals). The chalcopyrite was natural mineral, supplied from the Sayama mines (Japan) and of purity ~98 %, based on the chemical composition and XRD patterns. The splitting between Cu $2p_{3/2}$ and Cu $2p_{1/2}$ is large enough to take the intensity by area of Cu $2p_{3/2}$ peak independently. Further, oxygen

Auger peaks do not interfere with the Cu $2p_{3/2}$ peak profile. The value of $s_{S\ 2p}/s_{Cu\ 2p3/2}$ was estimated to be 0.11_6 as shown in **Table 5.2**, and nearly equal to the empirical factor (0.128) (Briggs, et al., 1990).

Table 5.2 Relative sensitivity factor between S 2p and Cu $2p_{3/2}$, s_S/s_{Cu}

Compounds	$s_{S\ 2p}/s_{Cu\ 2p3/2}$
$CuSO_4$	0.117
CuSCN	0.116
$CuFeS_2$	0.114
Average	0.116

5.2 Results

As described in **Chapter 3**, there is preferential dissolution of iron species in pyrite, so that both S and Fe species must be considered when examining the dissolution behavior. The dissolved amount of *i* species per unit initial surface area of pyrite at a dissolution time, *t*, is expressed as $\Delta x_i(t)$ in mmol m^{-2}, where *i* indicates total S or Fe(II) ions. Dissolution curves of pyrite by 5 mmol dm^{-3} Fe(III) ions in a HCl solution without foreign cations (**No. 8**) are shown in **Figs. 5.1**.

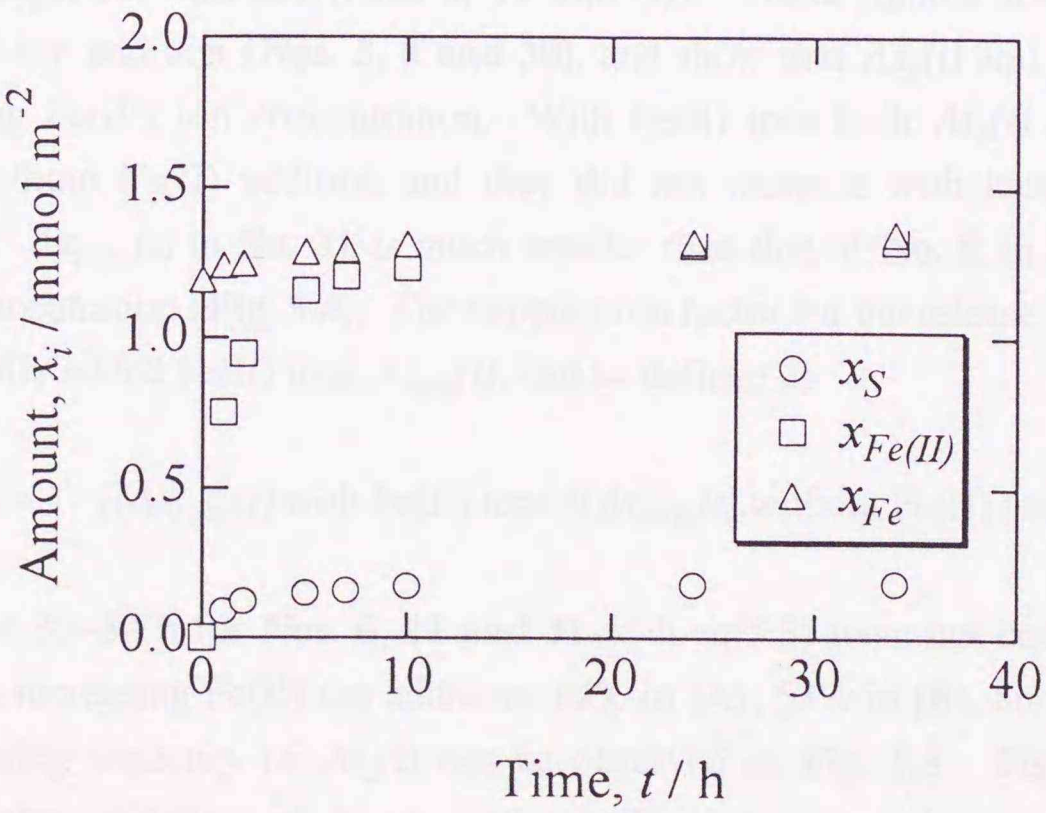

Fig. 5.1 Results of the dissolution experiment No. 8. See Table 5.1 for experiment details.

The $\Delta x_S(t)$ and $\Delta x_{Fe(II)}(t)$ increased with t, but the mole ratio did not agree with the stoichiometry from reaction (5.1). It is evident that the oxidative dissolution of pyrite by Fe(III) ions does not proceed by reaction (5.1) alone. In the present work, the total amounts of S and Fe(II) ions released were used as parameters, but total Fe was not used due to its small change.

5.2.1 Effect of Fe(II) ions

The effects of the initial Fe(II) ion concentration on $\Delta x_S(t)$ and $\Delta x_{Fe(II)}(t)$ are shown in **Fig. 5.2**, where the initial Fe(III) ion concentration was 5 mmol dm^{-3} (**Nos. 8~11**). The $\Delta x_S(t)$ and $\Delta x_{Fe(II)}(t)$ are net amounts of Fe(II) ions and S species dissolved, excluding the initially added amounts. It is clear that both $\Delta x_S(t)$ and $\Delta x_{Fe(II)}(t)$ decreased with increasing Fe(II) ions added. In the early period (< 10 h) there is a decrease in $\Delta x_S(t)$ with increasing Fe(II) ion addition (**Fig. 5.2**), whereas $\Delta x_{Fe(II)}(t)$ changes are not so regular. After dissolution, the pH decreased slightly by Fe(II) ion addition as shown in **Table 5.1.**

As the Fe(II) ions are products of the pyrite oxidation by Fe(III) ions, it is not surprising that the addition of Fe(II) ions to the system reduces the rate of the oxidation. The apparent suppression of the dissolution of pyrite with Fe(III) ions due to Fe(II) ion addition can be explained from an equilibrium point of view, but it does not fully explain the phenomena, as will be detailed in the following.

Dissolution experiments were also conducted at a constant ratio of initial concentration of Fe(II) ions to Fe(III) ions, $[Fe(II)]_0/[Fe(III)]_0$. For the $[Fe(II)]_0/[Fe(III)]_0$ ratio 3 with $[Fe(III)]_0$ of 1 mmol dm^{-3} (**A**), 5 mmol dm^{-3} (**B**), and 15 mmol dm^{-3} (**C**), $\Delta x_S(t)$ and $\Delta x_{Fe(II)}(t)$ are as shown in **Figs. 5.3 and 5.4** (**Nos. 6, 11 and 31**). These figures also show the results without Fe(II) ion addition (**Nos. 5, 8 and 30**), and show that $\Delta x_S(t)$ and $\Delta x_{Fe(II)}(t)$ increased with increasing Fe(III) ion concentration. With Fe(II) ions both $\Delta x_S(t)$ and $\Delta x_{Fe(II)}(t)$ were lower than without Fe(II) addition and they did not increase with increasing Fe(III) ion concentration: $\Delta x_{Fe(II)}(t)$ in **No. 31** is much smaller than that of **No. 8**, in spite of the higher Fe(III) ion concentration (**Fig. 5.4**). The suppression factor for the release of Fe(II) ions from pyrite by initially added Fe(II) ions, $r_{Fe(II)}(t)$, can be defined as

$$r_{Fe(II)}(t) = 1 - \{(\Delta x_{Fe(II)}(t) \text{ with Fe(II) ions})/(\Delta x_{Fe(II)}(t) \text{ without Fe(II) ions})\} \qquad (5.3)$$

The $r_{Fe(II)}$ at t = 33~34 h for **Nos. 6, 11 and 31** with eq(5.3) were not equal each other, but increased with increasing Fe(II) ion addition: 14% in (**A**), 53% in (**B**), and 85% in (**C**). The similar decreasing tendency of $\Delta x_S(t)$ can be observed in **Fig. 5.3**. **Figures 5.3 and 5.4** indicate that the oxidation of pyrite with Fe(III) ions proceeds nonstoichiometrically. Preferential dissolution of Fe species takes place and release of S species is suppressed, and as a result reaction (5.1) does not describe the situation of the present experimental conditions.

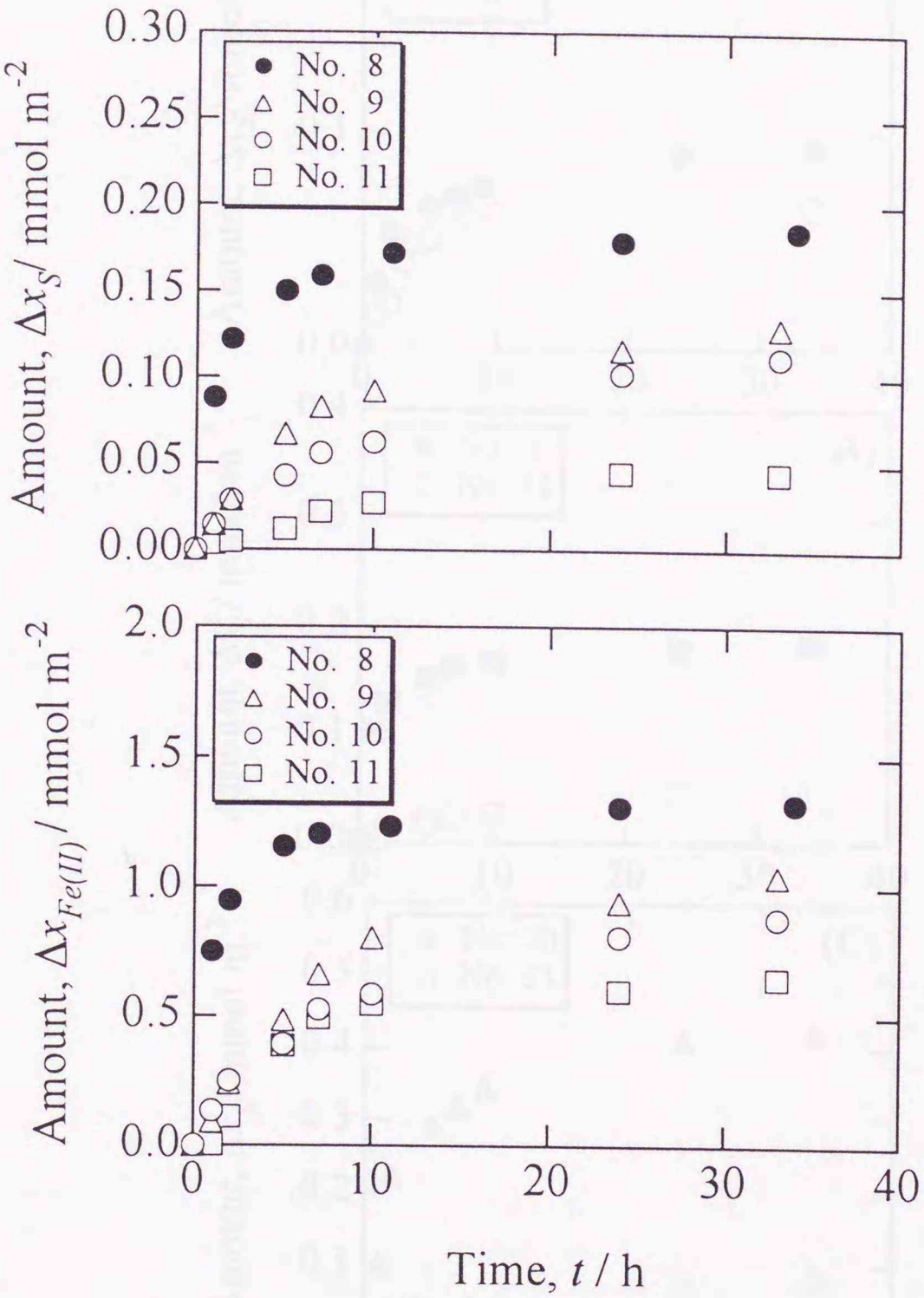

Fig. 5.2 Effect of Fe(II) ions on (a) $\Delta x_S(t)$ and (b) $\Delta x_{Fe(II)}(t)$ at $[Fe(III)]_0 = 5$ mmol dm^{-3}. See Table 5.1 for experiment details.

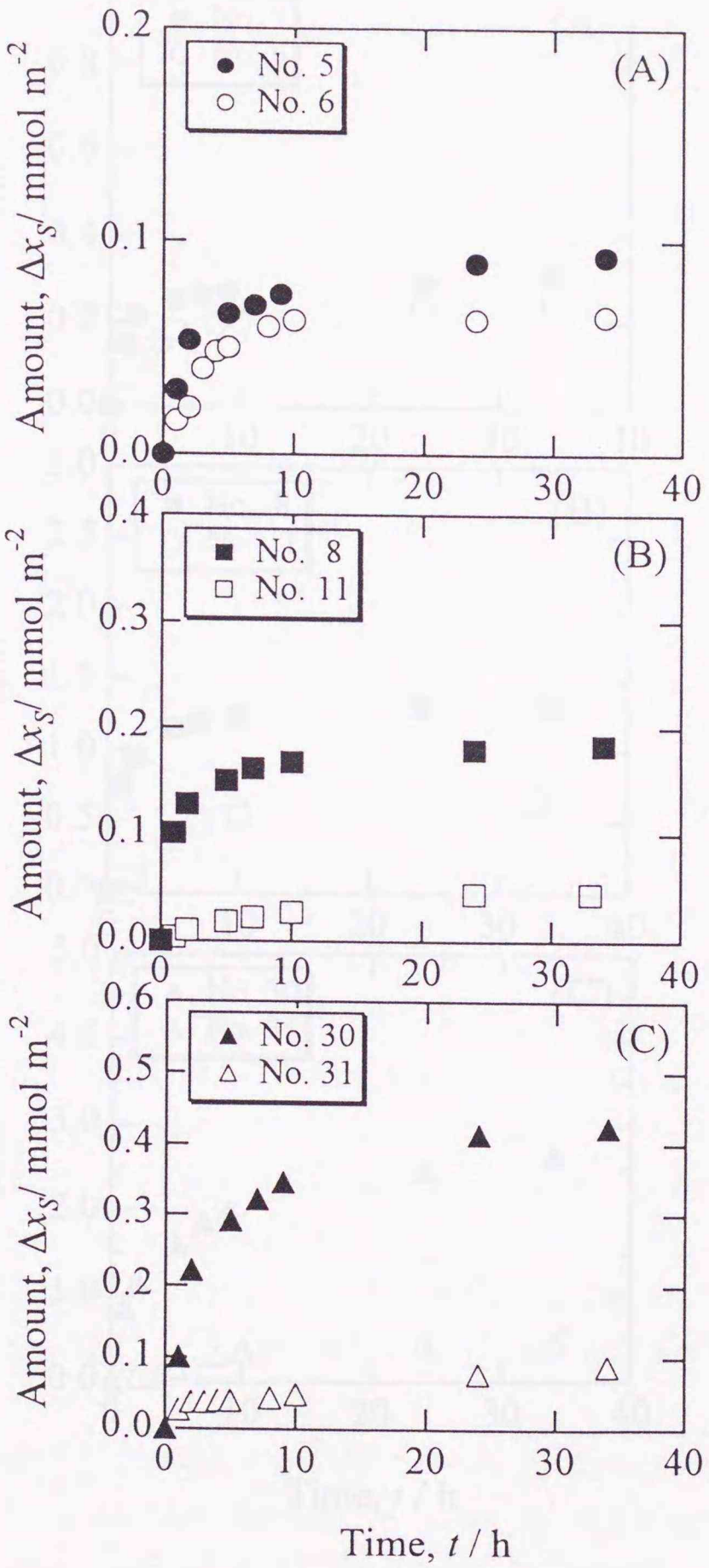

Fig. 5.3 $\Delta x_S(t)$ at $[Fe(II)]_0 / [Fe(III)]_0 = 3$. $[Fe(III)]_0$ = (A) 1, (B) 5, and (C) 15 mmol dm^{-3}. See Table 5.1 for experiment details.

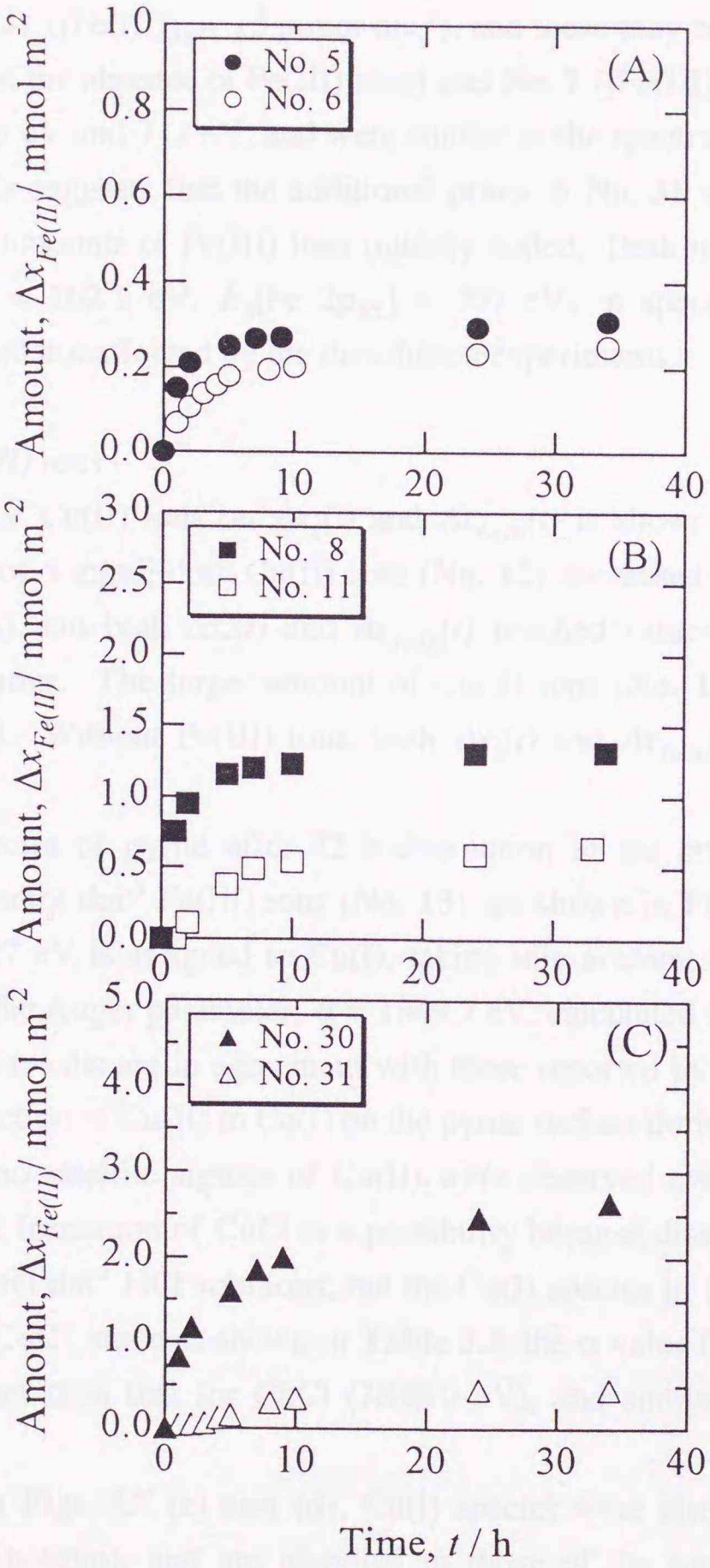

Fig. 5.4 $\Delta x_{Fe(II)}(t)$ at $[Fe(II)]_0 / [Fe(III)]_0 = 3$. $[Fe(III)]_0$ = (A) 1, (B) 5, and (C) 15 mmol dm^{-3}. See Table 5.1 for experiment details.

The XP-spectra for pyrite after 72 h-dissolution in **Nos. 4, 7** and **31** are shown in **Fig. 5.5**. The spectra for pretreated pyrite is also shown and identical to those for pure pyrite. In dissolution experiments **Nos. 4, 7** and **31**, the initial concentration of Fe(II) ions was 45 mmol dm^{-3}. Additional weak peaks around $E_B[S\ 2p_{3/2}]$ = 169 eV and $E_B[Fe\ 2p_{3/2}]$ = 711 eV were observed with **No. 31** ($[Fe(III)]_0$ = 15 mmol dm^{-3}), and these may be attributed to $FeSO_4$. The spectra for **No. 4** (in the absence of Fe(III) ions) and **No. 7** ($[Fe(III)]_0$ = 1 mmol dm^{-3}) showed no peak around 169 eV and 711 eV, and were similar to the spectra for pyrite pretreated prior to dissolution. This suggests that the additional peaks in **No. 31** are due to the oxidation of pyrite by the large amounts of Fe(III) ions initially added. Peak intensities corresponding to pyrite ($E_B[S\ 2p_{3/2}]$ = 162.2 eV, $E_B[Fe\ 2p_{3/2}]$ = 707 eV) in spectra **Nos. 4, 7** and **31** are sufficiently large and not affected by the dissolution experiments.

5.2.2 Effect of Cu(II) ions

The effect of Cu(II) ions on $\Delta x_S(t)$ and $\Delta x_{Fe(II)}(t)$ is shown in **Fig. 5.6 (Nos. 3, and 12-13)**. Addition of 5 mmol dm^{-3} Cu(II) ions (**No. 12**) decreased the initial dissolution rate of pyrite (t < 10 h), but both $\Delta x_S(t)$ and $\Delta x_{Fe(II)}(t)$ reached values similar to those without addition of Cu(II) ions. The larger amount of Cu(II) ions (**No. 13**) clearly decreased both $\Delta x_S(t)$ and $\Delta x_{Fe(II)}(t)$. Without Fe(III) ions, both $\Delta x_S(t)$ and $\Delta x_{Fe(II)}(t)$ remained nearly zero (**No. 3**).

The XP-spectra of pyrite after 72 h-dissolution in the presence of 15 mmol dm^{-3} Cu(II) ions and 5 mmol dm^{-3} Fe(III) ions (**No. 13**) are shown in **Fig. 5.7** (top). The peak at $E_B[Cu\ 2p_{3/2}]$ = 931.7 eV is assigned to Cu(I), taking into account the absence of significant satellite peaks and the Auger parameter, α = 1849.7 eV, calculated from $E_B[Cu\ 2p_{3/2}]$ and the E_K[Cu LMM]. The results are in agreement with those reported by Voigt, et al. (1994). The possibility of a reduction of Cu(II) to Cu(I) on the pyrite surface during the XPS measurements can be ignored as no satellite signals of Cu(II) were observed even at the first scan of the measurements. The formation of CuCl is a possibility because dissolution experiments were carried out in 10^{-2} mol dm^{-3} HCl solutions, but the Cu(I) species in **Figs. 5.7 (c) and (d)** (top) are not assigned to CuCl, since as shown in **Table 5.3**, the α value for Cu(I) species on pyrite is significantly larger than that for CuCl (1848.0 eV), and similar to the Cu(I) species of Cu_2Se.

As shown in **Figs. 5.7 (c) and (d)**, Cu(I) species were also observed on the control experiment **No. 3** (bottom), and are identical to those of the top spectrum (**No. 13**). It suggests that the reduction of Cu(II) to Cu(I) species has no relation to the reaction of pyrite with Fe(III) ions.

The coverage of Cu(I) ions on the pyrite was estimated to be $n_{Cu}/n_S = 0.12_1$ and 0.16_5 for **Nos. 13** and **3** (**Table 5.4**), very similar with and without Fe(III) ions.

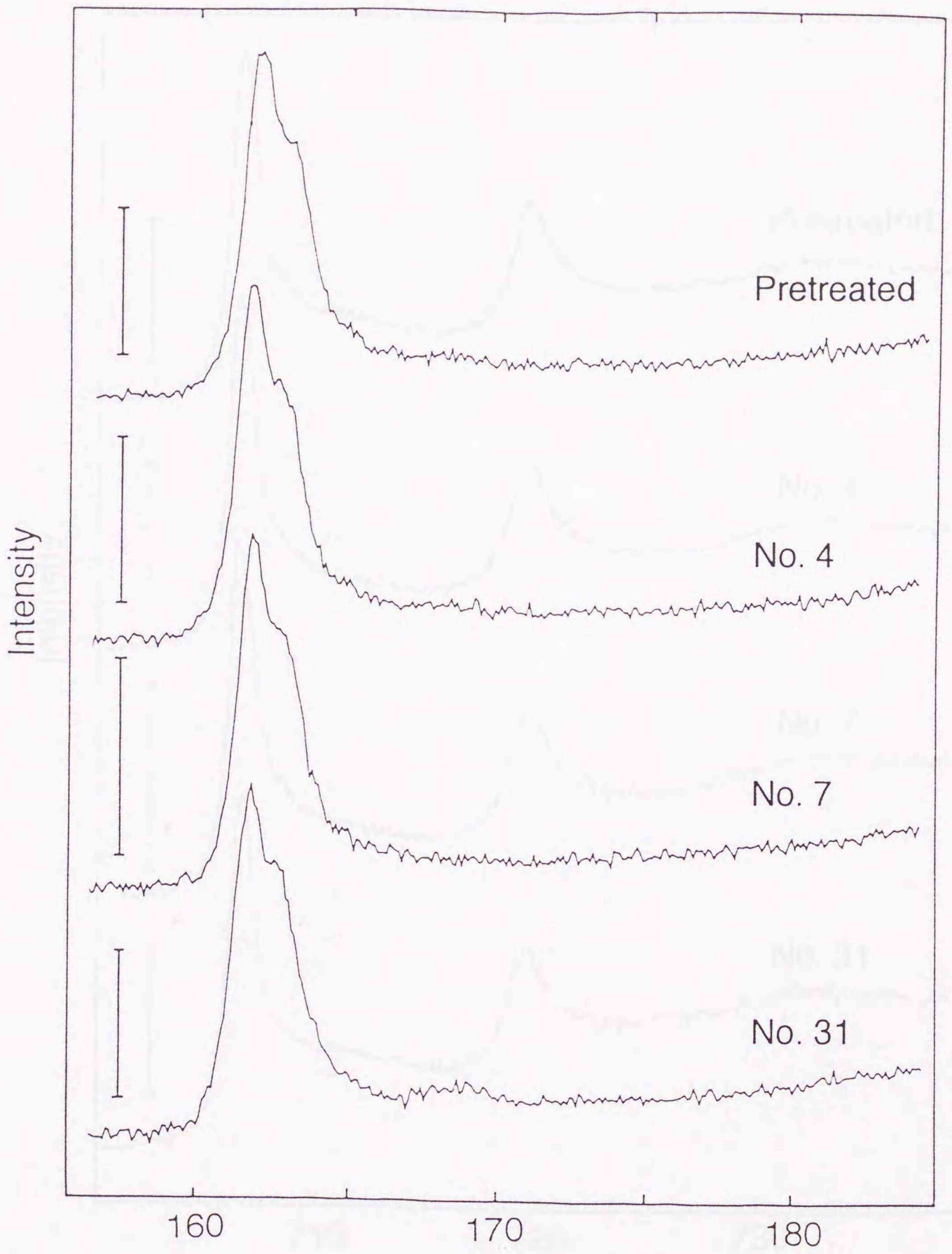

Fig. 5.5 (**A**) XP-spectra of S 2p for pyrite after dissolution experiment Nos. 4, 7, and 31 ($[Fe(II)]_0 = 45$ mmol dm^{-3}). See Table 5.1 for experiment details. Vertical bars: 500 cps.

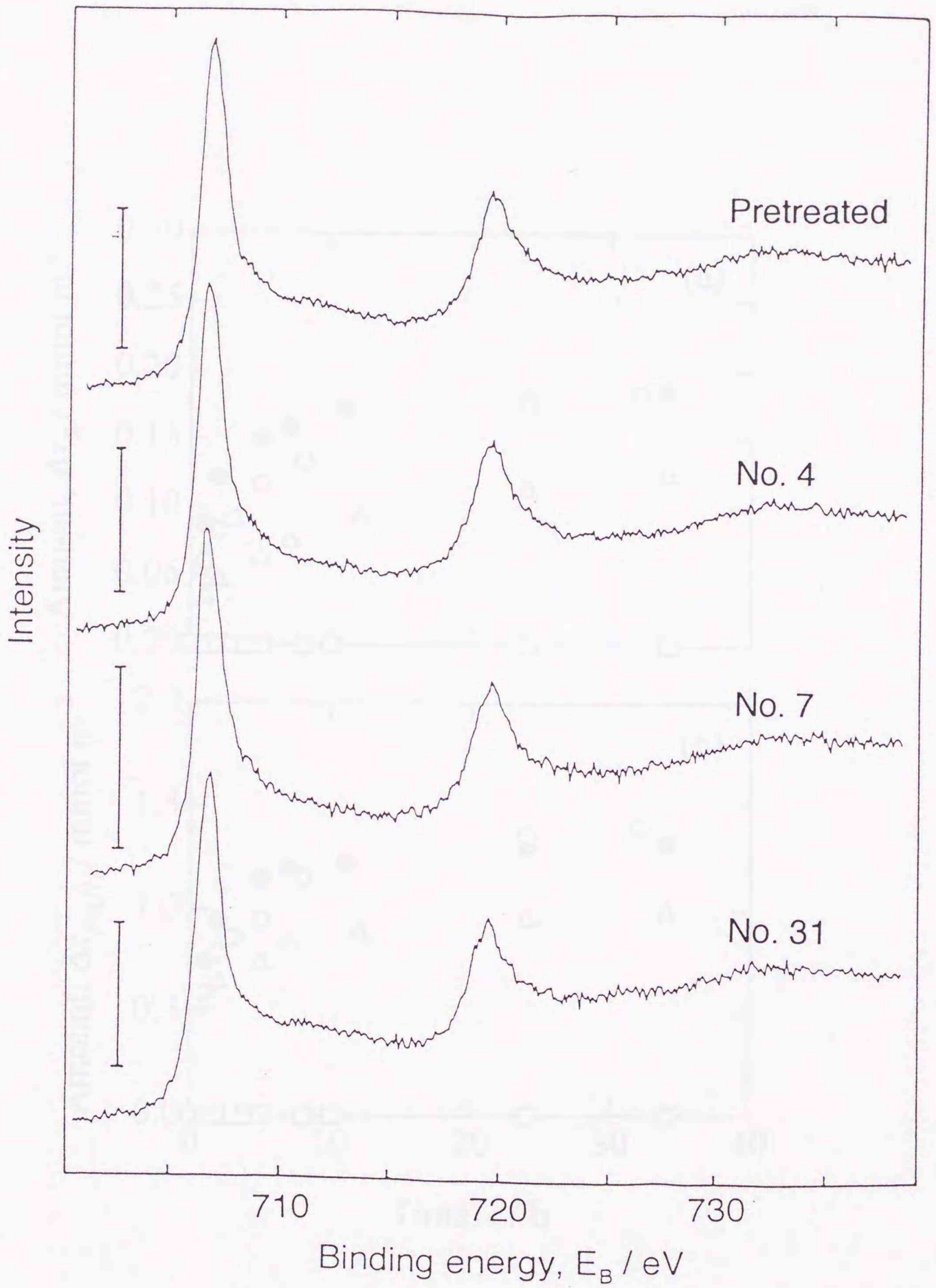

Fig. 5.5 (B) XP-spectra of Fe 2p for pyrite after dissolution experiment Nos. 4, 7, and 31 ($[Fe(II)]_0 = 45$ mmol dm^{-3}). See Table 5.1 for experiment details. Vertical bars: one kcps.

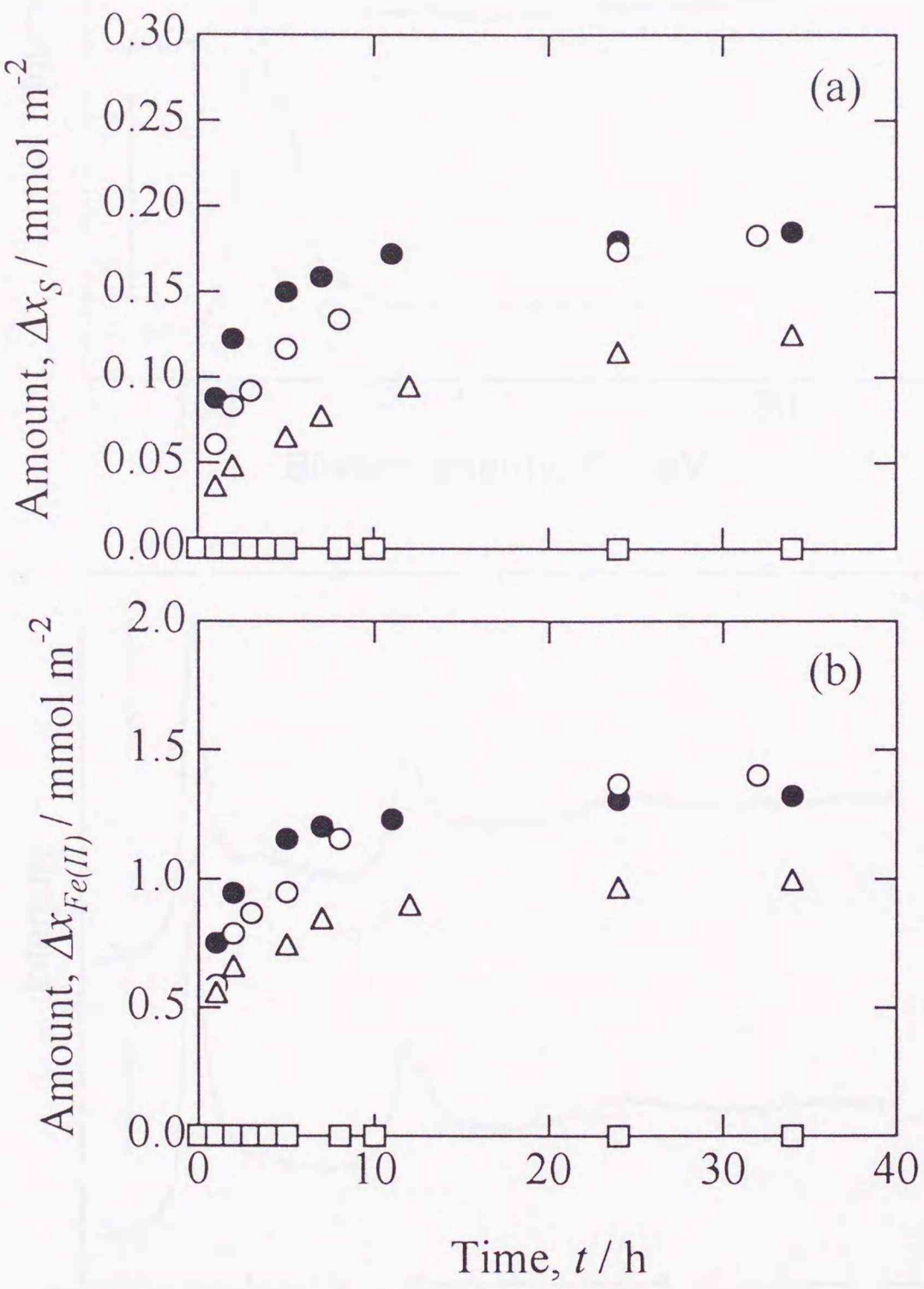

Fig. 5.6 Effect of Cu(II) ions on (a) $\Delta x_S(t)$ and (b) $\Delta x_{Fe(II)}(t)$. Symbols: ●, No. 8; ○, No. 12; △, No. 13; □, No. 3. See Table 5.1 for experimental details.

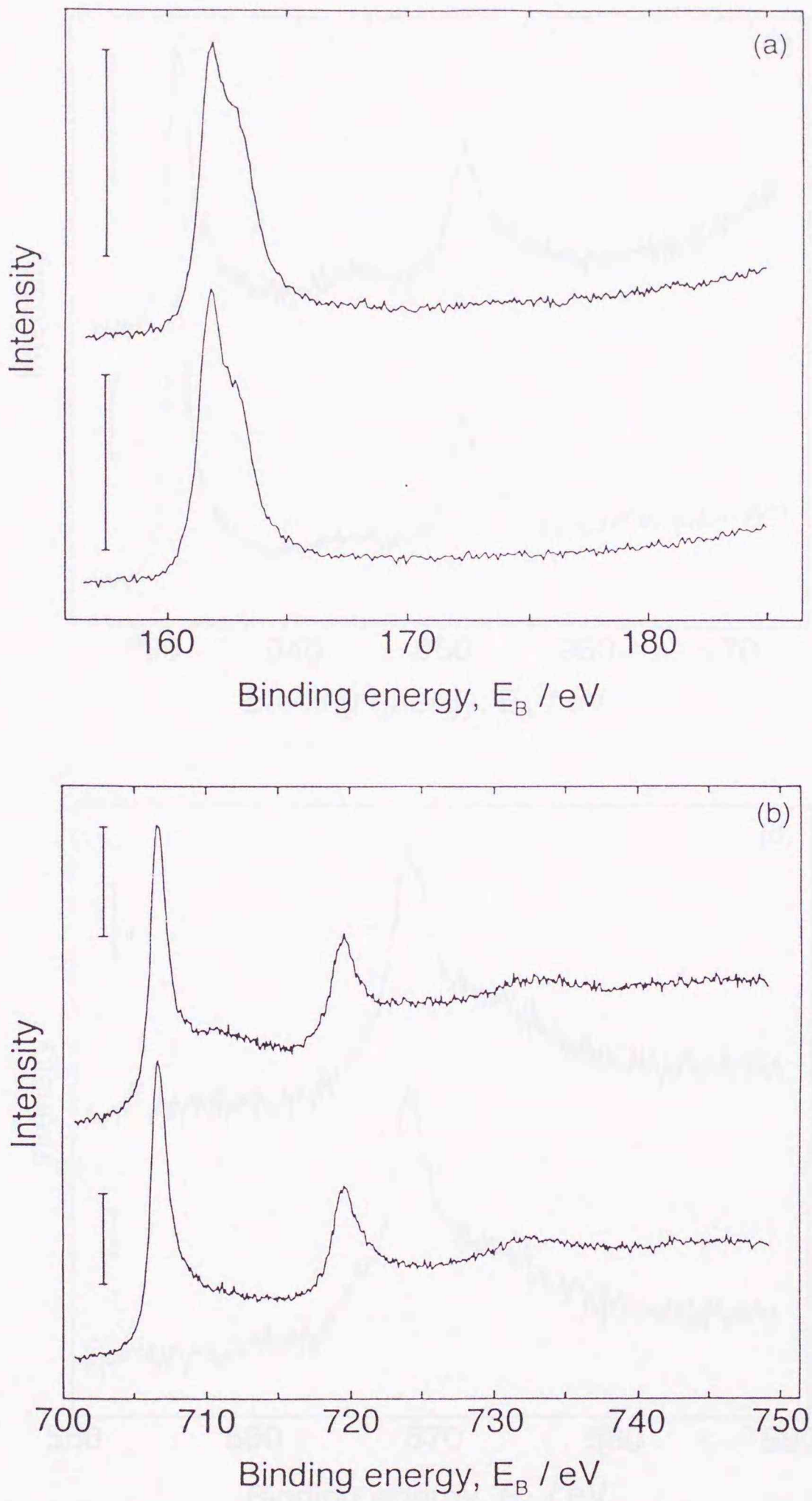

Fig. 5.7 (a) (b) XP-spectra of (a) S 2p, and (b) Fe 2p for pyrite after dissolution Nos. 13 (top) and 3 (bottom). Vertical bars indicate one kcps in (a) and (b). The spectra were obtained by irradiation with Al Kα X-ray (1486.6 eV; 15 kV, 10 mA).

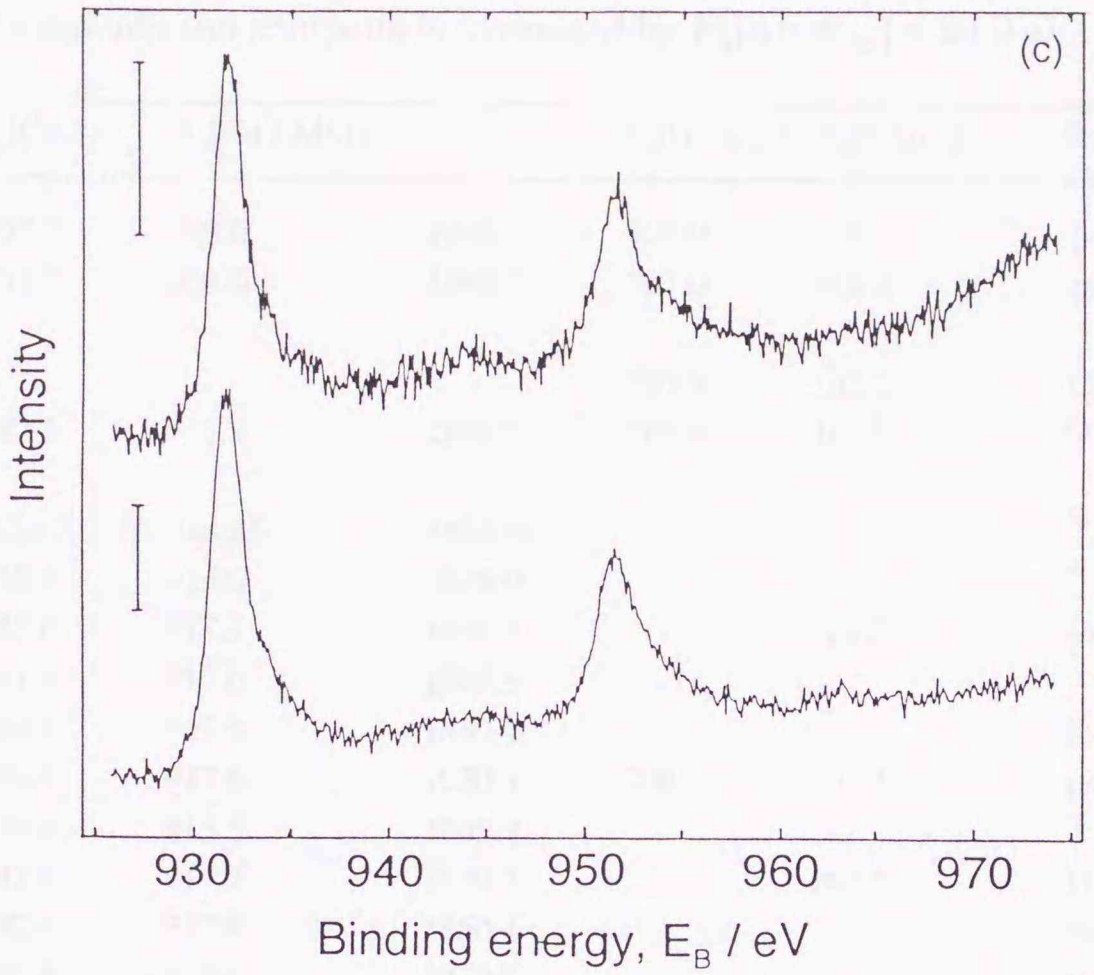

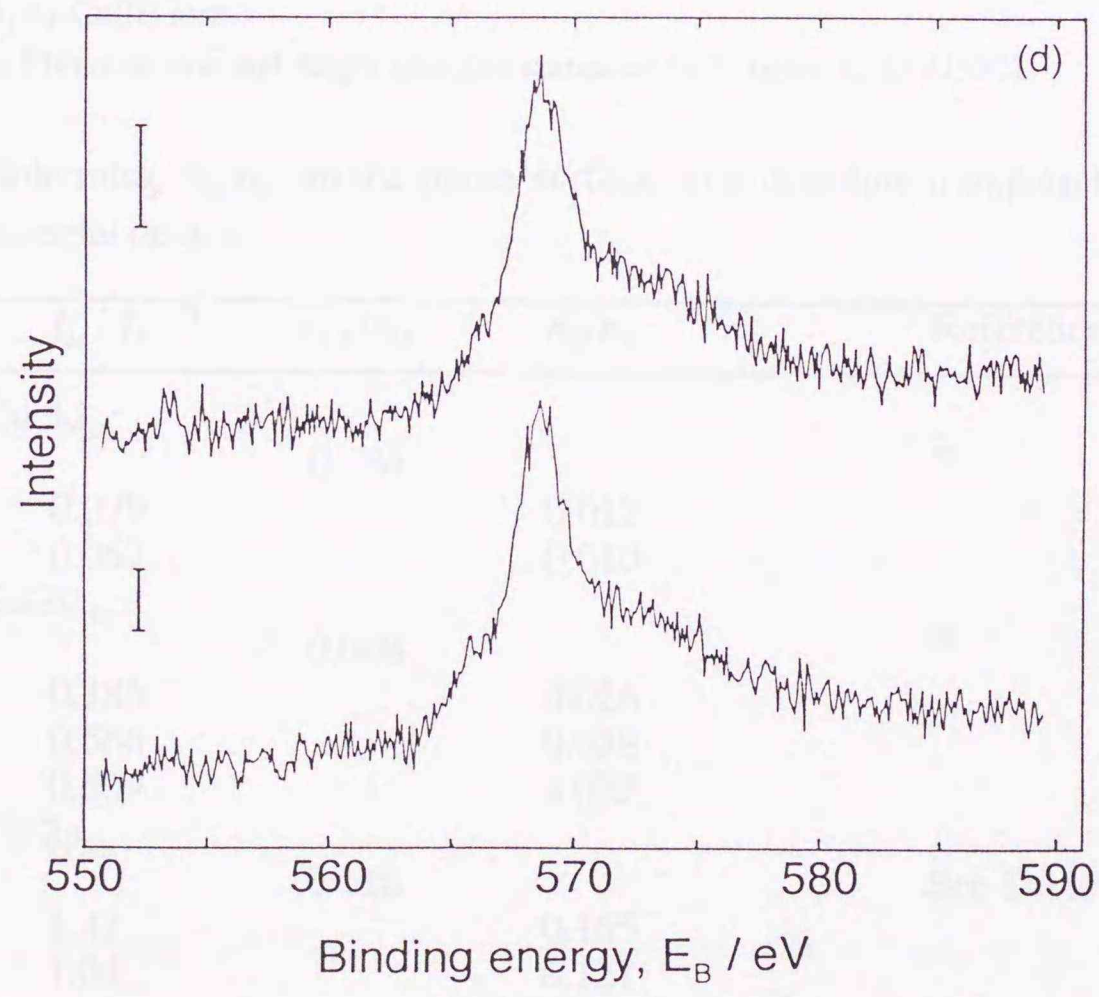

Fig. 5.7 (c) (d) XP-spectra of (c) Cu 2p and (d) Cu LMM for pyrite after dissolution Nos. 13 (top) and 3 (bottom). Vertical bars indicate 500 cps in (c), and 100 cps in (d). The spectra were obtained by irradiation with Al Kα X-ray (1486.6 eV; 15 kV, 10 mA).

Table 5.3 Binding energies, E_B, kinetic energies, E_K, and the auger parameter, α, in eV for some related elements and compounds, corrected by $E_B[\mathrm{Au\ 4f_{7/2}}] = 84.0$ eV

Compounds	E_B[Cu $2p_{3/2}$]	E_K[Cu LMM]	α	E_B[Fe $2p_{3/2}$]	E_B[S $2p_{3/2}$]	References
No. 3	931.7	918.0	1849.7	707.0	162.2	present work
No. 13	931.7	918.0	1849.7	707.0	162.2	present work
FeS_2 [*1]	-	-	-	707.0	162.2	Chapter 2
FeS_2(Cu) [*2]	932.5	917.2	1849.7	707.4	162.6	Voigt, et al., 1994
Cu	932.67	918.65	1851.32	-	-	[*3]
CuCl	932.4	915.6	1848.0	-	-	[*3]
Cu_2S	932.6	917.3	1849.9	-	161.7	Perry, et al., 1984
Cu_2Se	931.9	917.6	1849.5	-	-	[*3]
	932.3	917.8	1850.1	-	-	Romand, et al., 1978
$CuFeS_2$ [*1]	932.3	917.8	1850.3	708.8	161.2	present work
$CuCl_2$	934.4	915.5	1849.9	-	-	[*3]
CuS	932.4	917.9	1850.3	-	162.5	Perry, et al., 1984
	932.6	917.8	1850.4	-	-	Romand, et al., 1978
CuSe	932.4	918.4	1850.8	-	-	Romand, et al., 1978

[*1] with the fresh surface after cleaving in argon

[*2] activated FeS_2 by Cu(II) ions.

[*3] cited from the Photoelectron and Auger Energies compiled by Wagner, C. D. (1990).

Table 5.4 Mole ratio, n_M/n_S, on the pyrite surface after dissolution experiments. See Table 5.1 for experimental details

No.	$I_M / I_{S\,2p}$ [*1]	$s_{S\,2p}/s_M$	n_M/n_S	Reference
M = Cd $3d_{5/2}$				
		0.154		[*2]
2	0.079		0.012	
22	0.067		0.010	
M = Ba $3d_{5/2}$				
		0.068		[*2]
27	0.385		0.026	
28	0.568		0.038	
29	0.509		0.035	
M = Cu $2p_{3/2}$				
		0.116		See Table 5.2
3	1.42		0.165	
13	1.04		0.121	

[*1] contribution from the surface sulfate species were excluded.

[*2] cited from the Photoelectron and Auger Energies compiled by Wagner, C. D. (1990).

5.2.3 Effect of cations other than Fe(II) and Cu(II) ions

The effect of Na^+ and K^+ ions was examined (**Nos. 14~15**) but there was no suppression as shown in **Fig. 5.8**. The scatter in **Fig. 5.8** is due to low concentrations and is not significant for the discussion below. As Fe(II) ions suppress the dissolution of pyrite, several divalent metal ions including Mg(II), Ni(II), Zn(II), and Cd(II) were tested (**Nos. 16~22**). However, they did not suppress the dissolution of pyrite in the presence of Fe(III) ions (**Figs. 5.8~5.11**) even at [Ni(II)], [Zn(II)], or [Cd(II)] = 15 mmol dm^{-3} (**Figs. 5.9~5.11**). In the absence of Fe(III) ions, no dissolution was observed (**Nos. 1~2** in **Figs. 5.10~5.11**), indicating that these three ions cannot dissolve pyrite. Further, the amount of metal ions adsorbed on the pyrite surface was the same with pyrite dissolved and undissolved. For an example with 15 mmol dm^{-3} Cd(II) ion addition (**Nos. 2 and 22**), the mole ratio, n_{Cd}/n_S, on pyrite after dissolution experiments with or without Fe(III) ions was around 0.01 as shown in **Table 5.4**. The values were similar with other ions and concentrations, indicating that there is no interaction with Fe(III) ions in the adsorption of these ions on pyrite.

The effect of Ca(II), Pb(II), and Ba(II) ions (**Nos. 23~29**) which form insoluble or little soluble compounds with sulfate are shown in **Figs. 5.12~5.14**. Here Ca(II) ions did not show any effect, while with Pb(II) and Ba(II) ions $\Delta x_S(t)$ decreased and $\Delta x_{Fe(II)}(t)$ was unaffected. The $\Delta x_S(t)$ decreased with increasing initial concentration of these ions, except at [Ba(II)] $\geqq$ 1 mmol dm^{-3}, where $\Delta x_S(t)$ was unchanged.

The XPS measurements of pyrite after 72 h-dissolution in the presence of Ba(II) ions (**Nos. 27~29**) showed that the mole ratio of Ba(II) to S species excluding sulfate, n_{Ba}/n_S, increased with increasing Ba(II) concentration, but that n_{Ba}/n_S did not increase at [Ba(II)] $\geqq$ 1 mmol dm^{-3}. As shown in **Table 5.4**, the values of n_{Ba}/n_S were larger than those of the other ions that did not show any effect of the dissolution of pyrite, such as Cd(II) ions. It indicates that Ba(II) ions may precipitate as insoluble sulfate but that the amount is very small, since the S 2p peak for sulfate was too low to estimate the intensity accurately. Accordingly, Pb(II) and Ba(II) ions precipitate the sulfate released from pyrite, and do not suppress the pyrite dissolution. There was no effect of Ca(II), maybe due to the solubility of $CaSO_4$ as discussed below.

5.3. Discussion

Several investigators have reported that the dissolution rate is proportional to the concentration ratio of Fe(III) ions to total Fe species in the solution (Garrels, et al., 1960; Mathews, et al., 1972). Garrels, et al. (1960) explained that the rate depends on the frequency of contact of Fe(III) ions on the pyrite surface, and that the surface fraction occupied by Fe(III) ions depends on competition between Fe(III) and Fe(II) ions, with the result that the

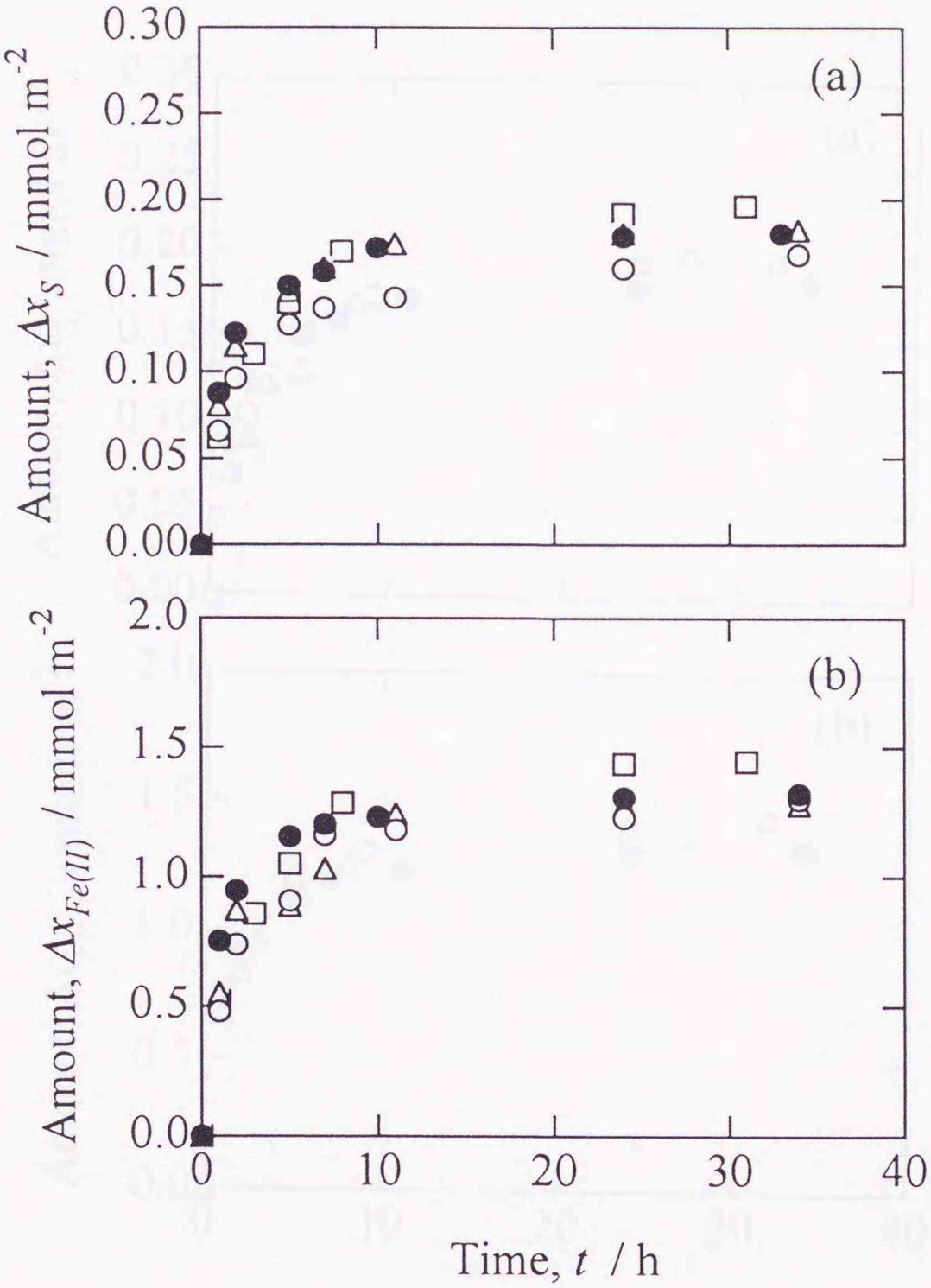

Fig. 5.8 Effect of Na^+, K^+, and Mg(II) ions on (a) $\Delta x_S(t)$ and (b) $\Delta x_{Fe(II)}(t)$. Symbols: ●, No. 8; ○, No. 14; △, No. 15; □, No. 16. See Table 5.1 for experimental details.

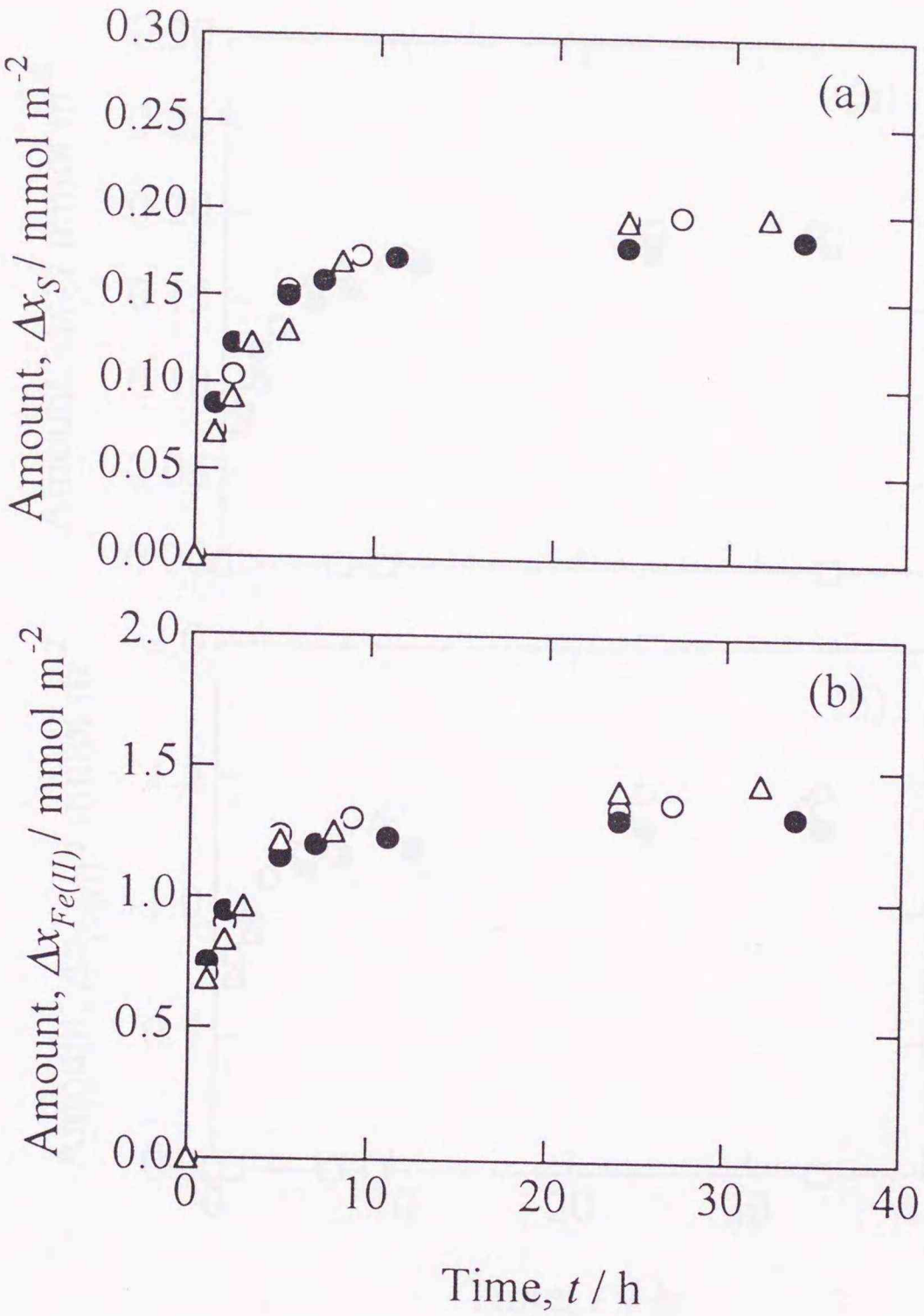

Fig. 5.9 Effect of Ni(II) ions on (a) $\Delta x_S(t)$ and (b) $\Delta x_{Fe(II)}(t)$. Symbols: ●, No. 8; ○, No. 17; △, No. 18. See Table 5.1 for experimental details.

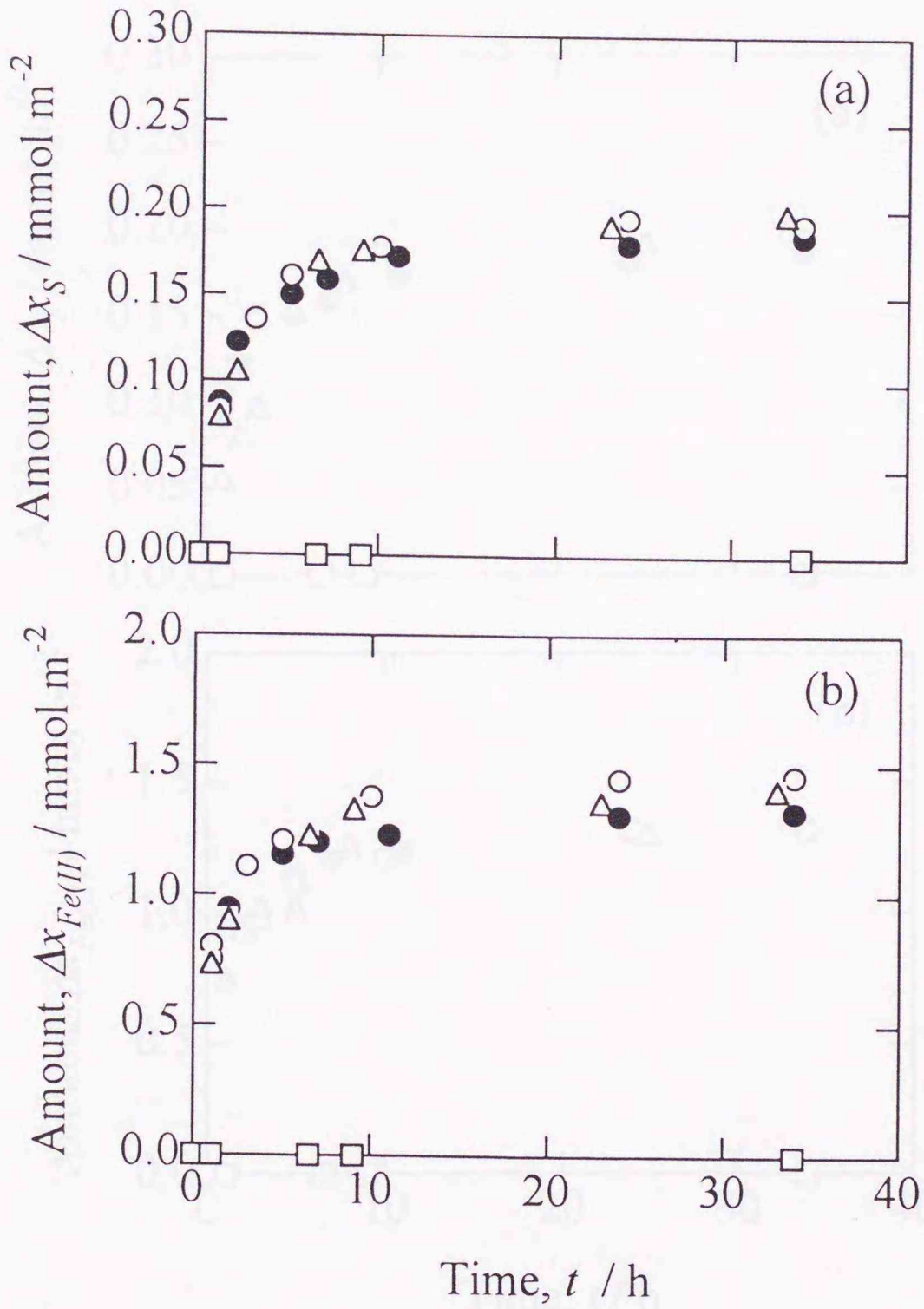

Fig. 5.10 Effect of Zn(II) ions on (a) $\Delta x_S(t)$ and (b) $\Delta x_{Fe(II)}(t)$. Symbols: ●, No. 8; ○, No. 19; △, No. 20; □, No. 1. See Table 5.1 for experimental details.

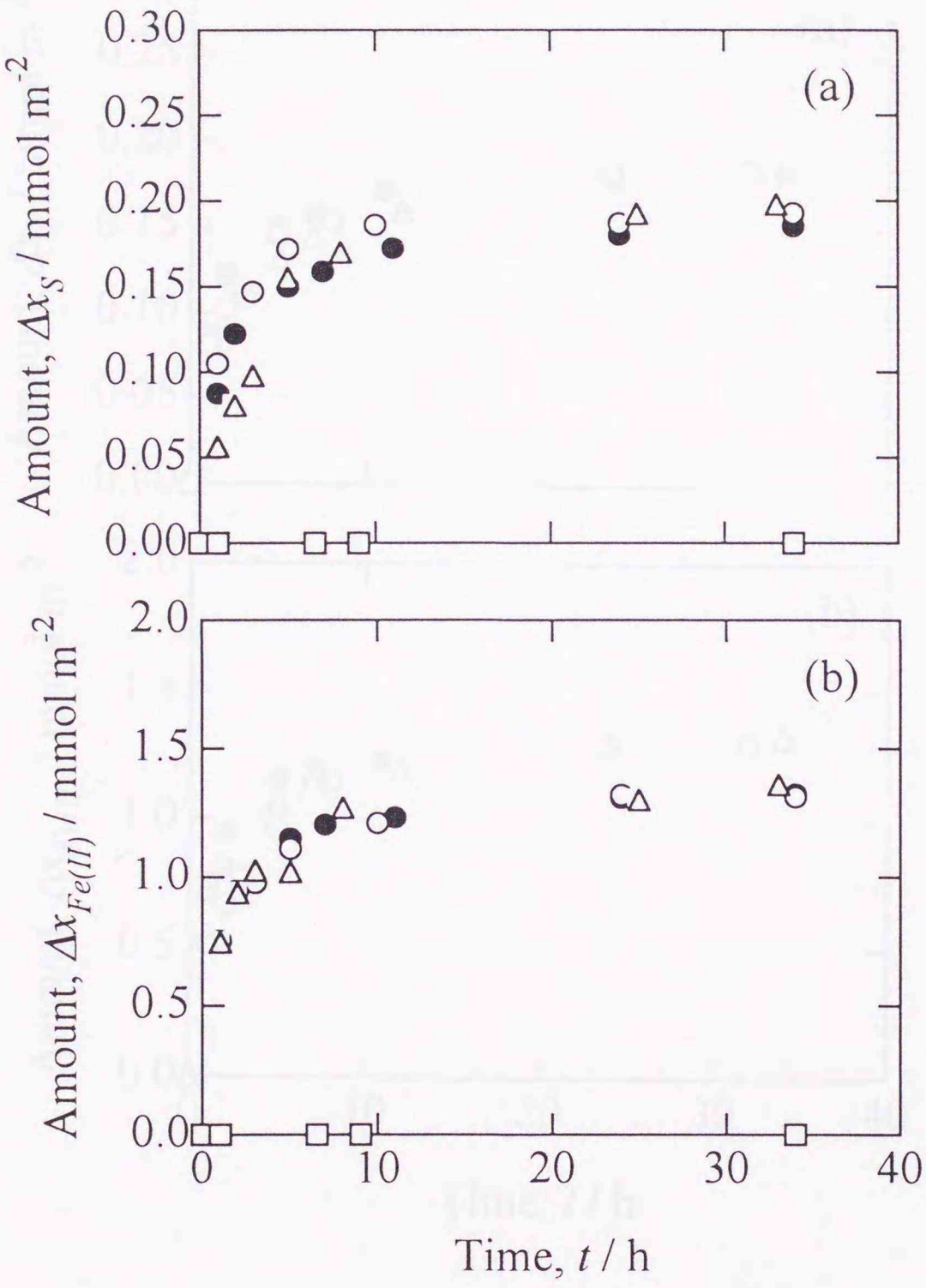

Fig. 5.11 Effect of Cd(II) ions on (a) $\Delta x_S(t)$ and (b) $\Delta x_{Fe(II)}(t)$. Symbols: ●, No. 8; ○, No. 21; △, No. 22; □, No. 2. See Table 5.1 for experimental details.

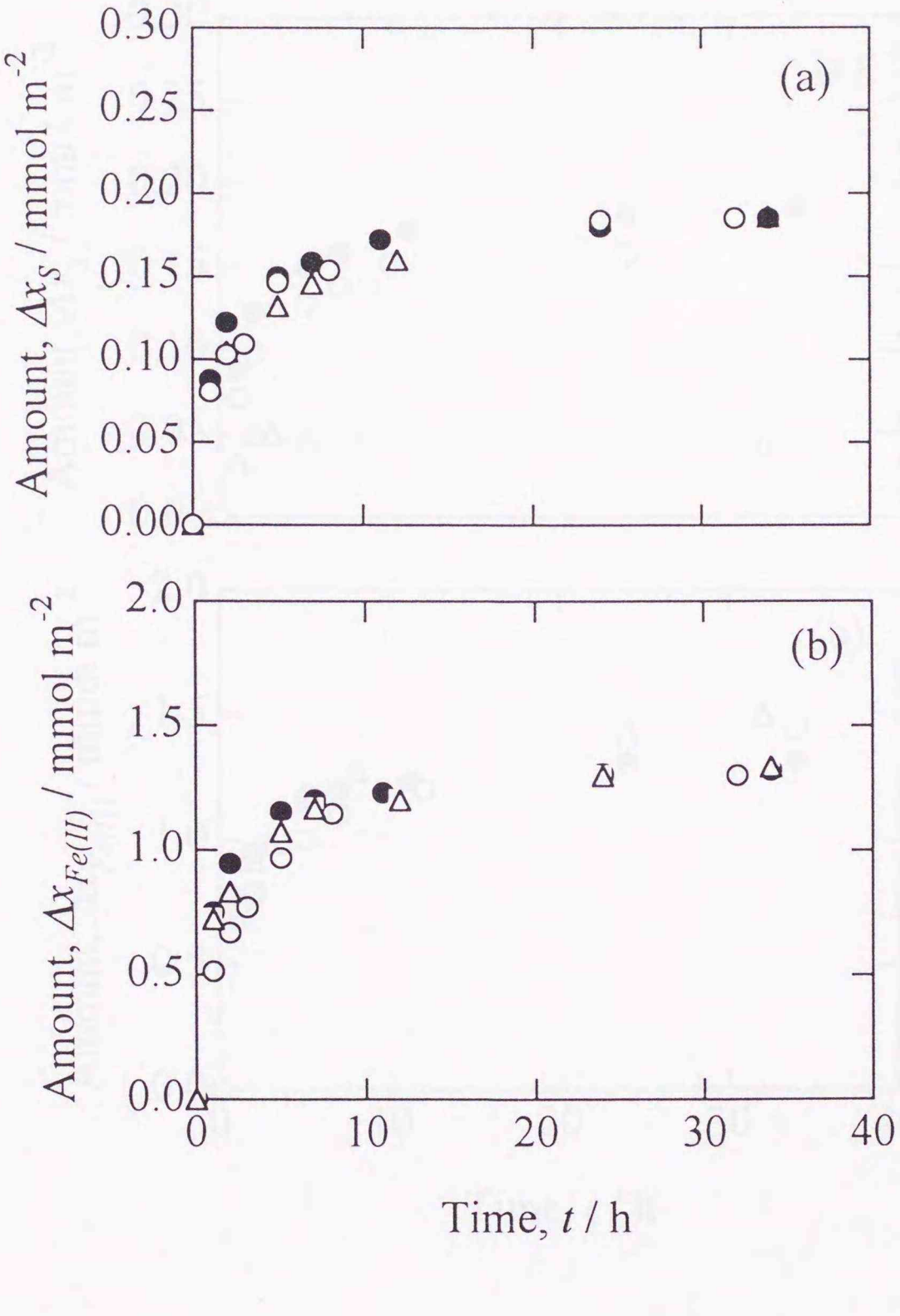

Fig. 5.12 Effect of Ca(II) ions on (a) $\Delta x_S(t)$ and (b) $\Delta x_{Fe(II)}(t)$. Symbols: ●, No. 8; ○, No. 23; △, No. 24. See Table 5.1 for experimental details.

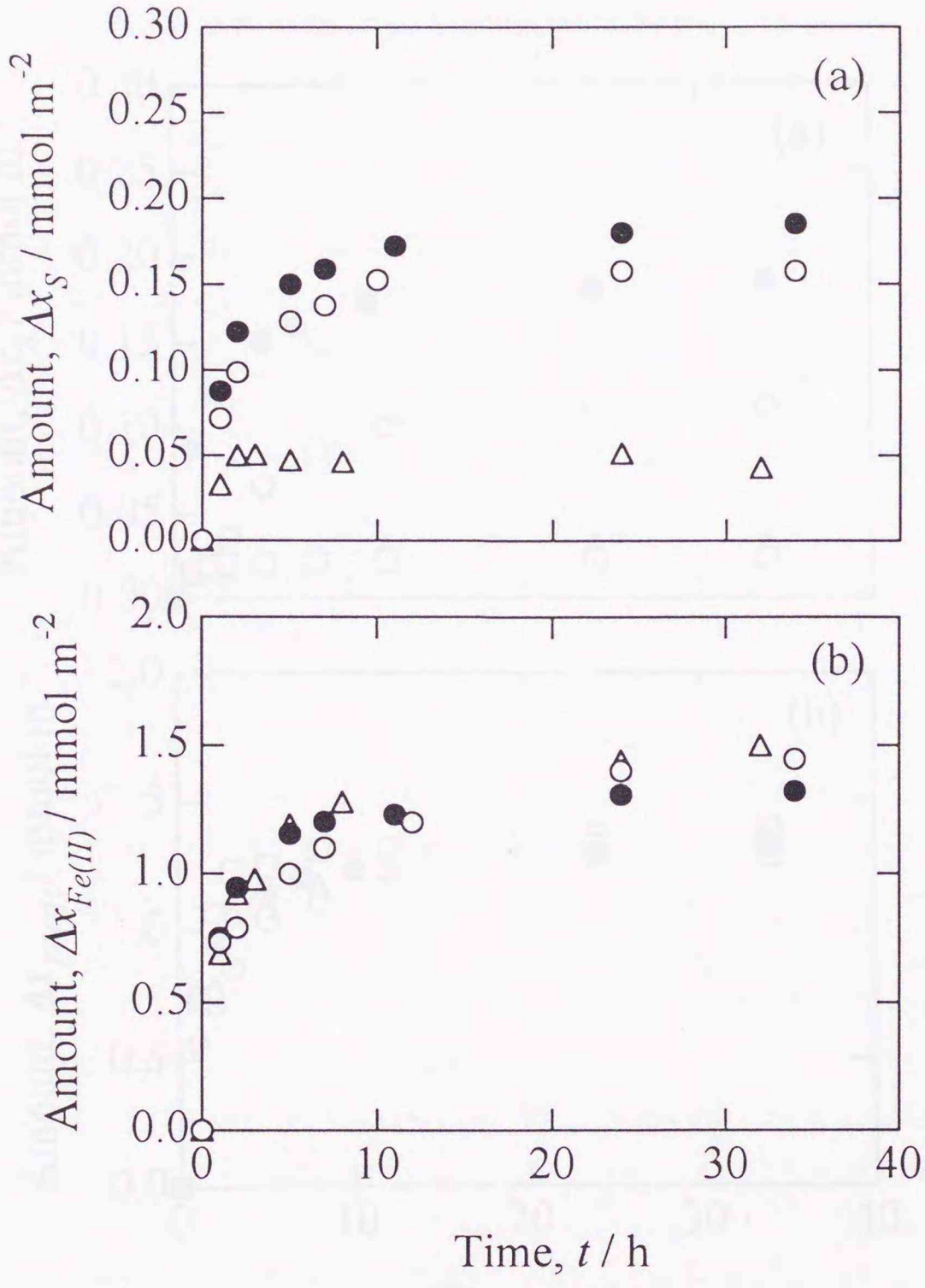

Fig. 5.13 Effect of Pb(II) ions on (a) $\Delta x_S(t)$ and (b) $\Delta x_{Fe(II)}(t)$. Symbols: ●, No. 8; ○, No. 25; △, No. 26. See Table 5.1 for experimental details.

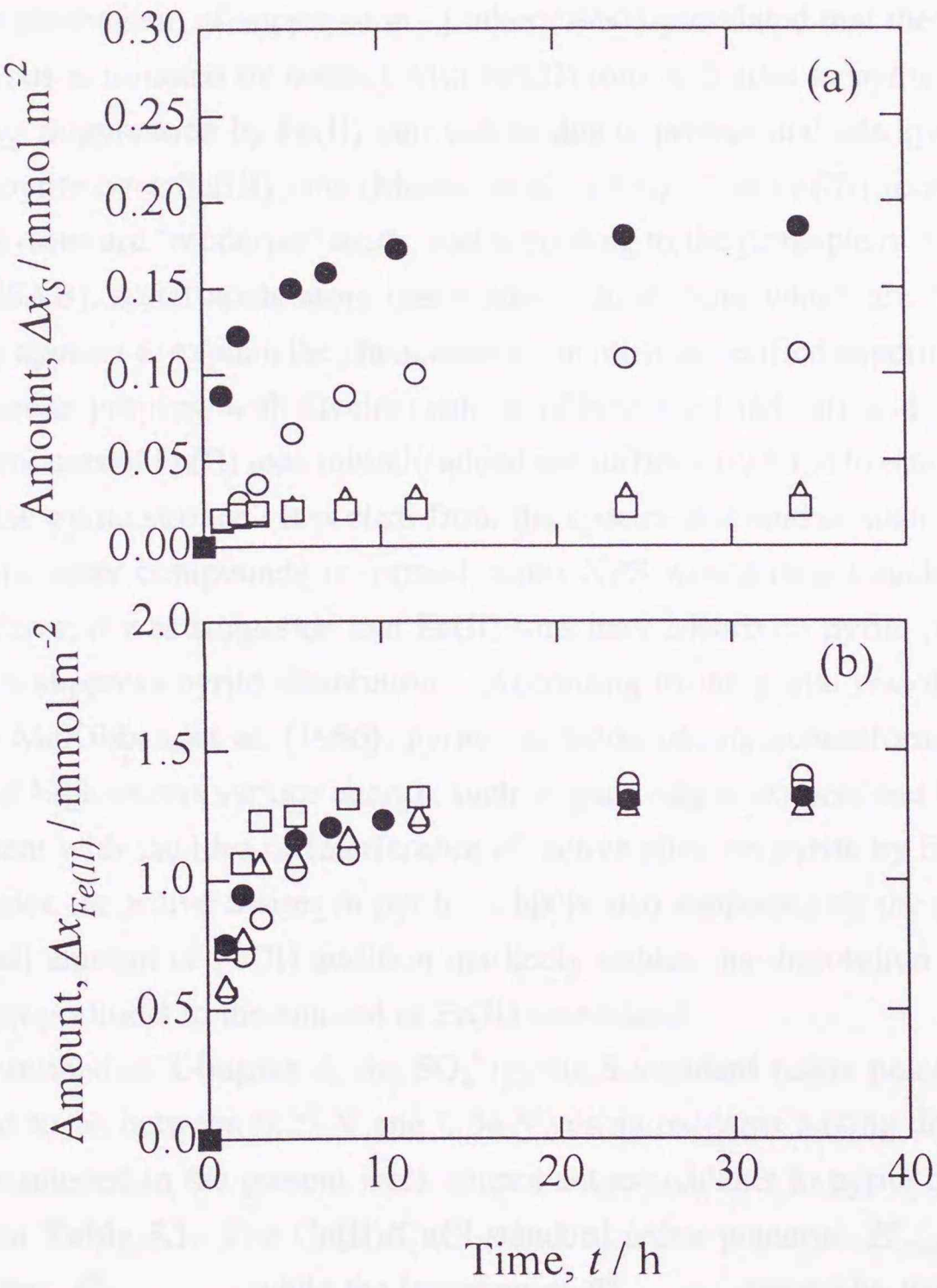

Fig. 5.14 Effect of Ba(II) ions on (a) $\Delta x_S(t)$ and (b) $\Delta x_{Fe(II)}(t)$. Symbols: ●, No. 8; ○, No. 27; △, No. 28; □, No. 29. See Table 5.1 for experimental details.

rate is proportional to the fraction of Fe(III) ions in the total Fe species. Garrels, et al. did not consider preferential adsorption of Fe(II) ions on the pyrite surface, however.

Figure 5.4 shows that the $r_{Fe(II)}(t)$ values are different for the same ratio of $[Fe(II)]_0/[Fe(III)]_0$(14~85%). These experimental results cannot be explained by the equilibrium shift described or the scheme reported by Garrels et al.

Sakai, et al. (1987) reported that initially added Fe(II) ions suppressed the release of Fe(II) ions in pyrite dissolution with Fe(III) ions, but provided no details of sulfur species release or the mechanism of suppression. Luther (1987) postulated that the reaction of pyrite with Fe(III) ions is initiated by contact with Fe(III) ions at S-sites in pyrite by the molecular orbital theory. Suppression by Fe(II) ions can be due to preferential adsorption of Fe(II) ions to S-sites in pyrite over Fe(III) ions (Moses, et al., 1991). The Fe(III) ions are "hard" acids whereas Fe(II) ions are "moderate" acids, and according to the principle of hard and soft acids and bases (HSAB), softer acids more easily adsorb to sulfides which are "soft" bases. The HSAB theory appears to explain the phenomenon but must be verified experimentally. Further, experiments are in progress with divalent cations of both hard and soft acids.

The amounts of Fe(II) ions initially added are sufficiently large to establish a monolayer coverage of the pyrite surface. It is clear from the spectra that neither such adsorbed layer of Fe(II) ions nor other compounds is formed, since XPS would detect such a monolayer on pyrite. As above, it was suggested that Fe(II) ions may adsorb on pyrite preferentially over Fe(III) ions to suppress pyrite dissolution. According to the pyrite dissolution mechanism presented by McKibben, et al. (1986), pyrite oxidation occurs nonuniformly and mainly at special sites of high excess surface energy, such as grain edges, corners and fractures. **Figure 5.5** is consistent with the idea of interference of 'active sites' on pyrite by Fe(II) ions, that is, Fe(II) ions block the active S-sites in pyrite. This is also supported by the results in **Fig. 5.2** that very small amount of Fe(II) addition markedly reduce the dissolution of pyrite and the effect is not proportional to the amount of Fe(II) ions added.

As described in **Chapter 4**, the SO_4^{2-}/pyrite S standard redox potential, $E^0_{SO42-/pyrite\ S}$, was estimated to be between 0.27 V and 0.34 V, using oxidants having different E^0 values. The cations discussed in the present work cannot act as oxidants to pyrite due to their lower E^0 as shown in **Table 5.1**. The Cu(II)/CuCl standard redox potential, $E^0_{Cu(II)/\ CuCl}$, (= + 0.538 V) is higher than $E^0_{SO42-/pyrite\ S}$, while the lowering of $E^0_{Cu(II)/\ CuCl}$ caused by ligand effects is not large as the stability constant of Cu(II)-Cl complex is log K = 0.4 at 25℃ (Smith and Martell, 1976). Therefore, Cu(II) ions should oxidize pyrite, as:

$$FeS_2 + Cu^{2+} + Cl^- + 8\,H_2O = Fe^{2+} + 2SO_4^{2-} + CuCl + 16H^+. \qquad (5.4)$$

However, Cu(II) ions do not oxidize pyrite (**Fig. 5.6 (No. 3)**), and CuCl was not observed by

XPS (**Fig. 5.7** and **Table 5.3**). The K_{sp} of CuCl is 3.2 $\times 10^{-7}$ at 25℃, and CuCl would be detected by XPS, if it is present. This suggests that reaction (5.4) did not occur on the pyrite surface, but that another redox reaction took place between the Cu(II) ions and pyrite.

The Cu(I) species on pyrite (**Fig. 5.7 (c)(d)**) are very similar to Cu(I) species in Cu_2Se (**Table 5.3**). Voigt, et al. (1994) speculated that the surface Cu(I) species are $[Cu^+ S_2^-]$ formed by Cu filling in the Fe sites left vacant by oxidation, as:

$$Cu^{2+}\ (\text{adsorbed}) + S_2^{2-}\ (\text{surface}) = [Cu^+S_2^-](\text{adsorbed}). \qquad (5.5)$$

This implies that pyrite-S reduces the adsorbed Cu(II) to Cu(I). As the coverage of Cu(I) is about 0.17, there would be some change in the S 2p spectra due to the surface S_2^{2-} group. This was not observed, however (**Fig. 5.7 (a)** bottom). This discussion has not specified the source of electron. There is a possibility that free electrons from the bulk pyrite took part, as pyrite is an n-type semiconductor. When the pyrite is dissolved by Fe(III) ions, the number of vacant Fe-sites in FeS_2 must be much larger than without Fe(III) ions, but the Cu(I) coverage was very similar (**Table 5.4**) with and without dissolution of Fe(II) ions from pyrite (**Nos. 3 and 13** in **Fig. 5.6**). The results here are inconsistent with Voigt, et al. (1994) that $[Cu^+S_2^-]$ species easily adsorb on vacant Fe sites. This indicates the possibility, that, preferential to Fe(III) ions, Cu(II) ions adsorbed to active "S-sites" of pyrite not on vacant Fe sites.

As mentioned above, Fe(II) ions suppress pyrite dissolution with Fe(III) ions and it has been apparently explained by Moses, et al. (1991) based on the HSAB theory.

The Na^+, K^+, and Mg(II) ions did not suppress pyrite dissolution. Seemingly, this may also be explained by HSAB theory, since these ions are 'hard' acids and cannot adsorb preferential to Fe(III) ions. However, HSAB theory cannot be applied to the adsorption of Ni(II), Zn(II) and Cd(II) ions: these ions did not suppress the pyrite dissolution in spite of being 'moderate' or 'soft' acids. The present results suggest that the effect of foreign cations on the reactivity of pyrite with Fe(III) ions is not always explained by HSAB theory.

It is clear that Ba(II) or Pb(II) ions do not suppress reactions (5.1) and (5.2), since $\Delta x_{Fe(II)}(t)$ was not affected. From the data without foreign cations (solid circles in **Figs. 5.2, 5.6, and 5.8~5.14**), the concentration of dissolved S species at t ~34 h is calculated to be about 0.72 mmol dm^{-3}. Considering the K_{sp} values (**Table 5.1**) and stability constants of hydroxyl- and chloride-complexes, the concentrations of divalent cations needed to precipitate 99% of the dissolved sulfate are calculated as follows: [Ca(II)] = 6.11 mol dm^{-3}, [Pb(II)] = 4.33 mmol dm^{-3}, and [Ba(II)] = 0.0255 mmol dm^{-3}. Addition of 15 mmol dm^{-3} of Ca(II) ions did not affect $\Delta x_S(t)$ (**Fig. 5.12**). Addition of 5 mmol dm^{-3} of Pb(II) ions decreased $\Delta x_S(t > 10\ h)$ to ~25% (**Fig. 5.13**), and the addition of 1 mmol dm^{-3} Ba(II) ions finally decreased $\Delta x_S(t > 10\ h)$ to ~15% of that without addition (**Fig. 5.14**). These results are parallel to the

values of K_{sp}. Sulfate minerals formed in **Nos. 23~29** possibly correspond to gypsum ($CaSO_4$), anglesite ($PbSO_4$) and barite ($BaSO_4$), which occur as secondary minerals in sulfide-rich tailings (Jambor, 1994). The present results also indicate that sulfate minerals may have been formed in the aqueous phase, not on the surface of the pyrite.

The suppression of pyrite dissolution by Fe(II) ions takes place as Fe(II) ions are preferentially over Fe(III) adsorbed on active sites of pyrite-S. A similar mechanism may work for Cu(II) ions, but there are differences between Cu(II) and Fe(II) ions in the degree of suppression and electron transfer. The addition of very small amounts of Fe(II) ions (0.5 mmol dm^{-3}) markedly reduced $\Delta x_S(t)$ and $\Delta x_{Fe(II)}(t)$, similar to the addition of 15 mmol dm^{-3} Cu(II) ions. The redox reaction involved in the adsorption of Cu(II) ions on pyrite suggests a stronger bonding of Cu species to the pyrite surfaces than simple physical adsorption. So far, we have no explanation why Cu(II) and Fe(II) ions are so highly adsorptive to the pyrite surface. Acid mine water often contains cations from sulfides, so that the present data would be useful when evaluating sulfide ore weathering, but more detailed experimental and theoretical studies are necessary.

5.4 Summary

Suppressing effects of metal cations on pyrite dissolution with Fe(III) ions around pH 2 were investigated.

The Fe(II) ions suppressed dissolution of both Fe and S species from pyrite, that is, inhibited the reactivity of pyrite with Fe(III) ions due to the preferential adsorption over Fe(III) ions to active sites of the pyrite surface. Also Cu(II) ions suppressed the dissolution of both Fe and S species from pyrite, that is, inhibited the reactivity of pyrite with Fe(III) ions. It was interpreted by a mechanism where Cu(II) ions were preferentially adsorbed on active sites of pyrite-S over Fe(III) ions, and reduced to Cu(I) ions stabilized on pyrite-S. Neither Na^+, K^+, Mg(II), Ni(II), Zn(II) nor Cd(II) ions affected the reactivity of pyrite with Fe(III) ions. This suggests that the effects of foreign cations on the reaction cannot be always explained by the HSAB theory. The Ba(II) and Pb(II) ions apparently suppressed dissolution of only S species from pyrite, due to the formation of insoluble sulfates. The Ca(II) ions did not suppress dissolution of S species from pyrite. The order of suppressing of $\Delta x_S(t)$ was Ba(II) > Pb(II) > Ca(II), which is parallel to the values of solubility product, K_{sp}. These results indicate that sulfate minerals are formed in the aqueous phase, not on the surface of pyrite.

References

Bancroft, G. M., and Hyland, M. M. (1990) "Spectroscopic studies of adsorption/reduction reactions of aqueous metal complexes on sulphide surfaces." in *Mineral-Water Interface Geochemistry* (edited by Hochella, M. F., and White, A. F.), *Mineral Society of America*, **Chap.13**, pp. 511-558.

Briggs, D., and Seah, M. P. (Eds.) (1990) *Practical Surface Analysis* (2nd ed.), **Vol. 1**, pp. 635-638, John Wiley & Sons, Ltd., New York.

Brown, J. R., Bancroft, G. M., Fyfe, W. S. and MacLean, R. E. N. (1979) Mercury removal from water by iron sulphide minerals. *Environ. Sci. Tech.*, **13**, 1142-1145.

Garrels, R. M., and Thompson, M. E. (1960) Oxidation of pyrite by iron sulfate solutions. *Amer. J. Sci.*, **258-A**, 57-67.

Hyland, M. M., and Bancroft, G. M. (1989) An XPS study of gold deposition at low temperatures on sulphide minerals: Reducing agents. *Geochim. Cosmochim. Acta*, **53**, 367-372.

Jambor, J. L. (1994) "Mineralogy of sulfide-rich tailings and their oxidation products." in *Environmental Geochemistry of Sulfide Mine-Wastes* (edited by Jambor, J. L., and Blowes, D. W.), Waterloo, Ontario, **Chapter 3**, pp. 59-102.

Jean, G. E., and Bancroft, G. M. (1986) Heavy metal adsorption by sulphide mineral surfaces. *Geochim. Cosmochim. Acta*, **50**, 1455-1463.

Luther, III G. W. (1987) Pyrite oxidation and reduction: Molecular orbital theory considerations. *Geochim. Cosmochim. Acta*, **51,** 3193-3199.

Mathews, C. T., and Robins, R. G. (1972) The oxidation of iron disulfide by ferric sulphate. *Aust. Chem. Eng.*, **Aug.**, 21-25.

McKibben, M. A., and Barnes, H. L. (1986) Oxidation of pyrite in low temperature acidic solutions: Rate laws and surface textures. *Geochim. Cosmochim. Acta*, **50,** 1509-1520.

Moses, C. O., and Herman, J. S. (1991) Pyrite oxidation at circumneutral pH. *Geochim. Cosmochim. Acta*, **55**, 471-482.

Perry, D. L., Tsao, L., and Taylor, J. A. (1984) "Surface studies of the interaction of copper ions with metal sulfide minerals." in *Proc. Int. Symp. Electrochem. in Mineral and Metal Processing* (edited by Rocherdson, P. E., Srinvasan, S., and Woods, R.), The Electrochem. Soc., Pennington, NJ, pp. 169-184.

Romand, R., Roubin, M., and Deloume, J. P. (1978) ESCA studies of some copper and silver selenides. *J. Electron Spectros. Relat. Phenom.*, **Vol. 13**, 229-242.

Sakai, N., Ishizaki, C., Chida, T., and Shimoiizaka, J. (1987) A kinetic study of pyrite oxidation by ferric sulfate. *J. Min. Met. Inst. Soc. Japan,* **103**, 37-42.

Smith, R. M., and Martell, A. E. (1976) *Critical Stability Constants*. **Vol. 4**, Plenum Press, New York, p. 105.

Voigt, S., Szargan, R., and Suoninen, E. (1994) Interaction of copper(II) ions with pyrite and its influence on ethyl xanthate adsorption. *Sur. Inter. Anal.*, **21**, 526-536.

Wagner, C. D. (1990) *Practical Surface Analysis* 2nd ed. (edited by Briggs, D., and Seah, M. P.), **Vol. 1**, John Wiley & Sons, Ltd., New York, pp. 595-634.

Zouboulis, A. I., Kydros, K. A., and Matis, K. A. (1993) Arsenic(III) and arsenic(V) removal from solutions by pyrite fines. *Separ. Sci. Technol.*, **28**, 2449-2463.

Zouboulis, A. I., Kydros, K. A., and Matis, K. A. (1995) Removal of hexavalent chromium anions from solutions by pyrite fines. *Wat. Res.*, **29**, 1755-1760.

Chapter 6
Inhibition of cell growth and iron and sulfur oxidation in *Thiobacillus ferrooxidans* and *Thiobacillus thiooxidans* by natural organic acids

As described in **Chapter 1**, chemoautotrophic iron- and/or sulfur- oxidizing bacteria, *Thiobacillus ferrooxidans* and *Thiobacillus thiooxidans,* often grow actively in mine water and play an important role in pyrite weathering, especially in aerobic environments (Taylor, et al., 1984). The organic inhibition of chemoauthotrophic bacteria of genus *Thiobacillus* has been discussed by several investigators (e. g., Rittenberg, 1972). It was mentioned in **Chapter 4** that oxalic acid prevented the reaction of pyrite with Fe(III) ions. Several investigators reported that oxalic acid are inhibitory to cell growth and substrate oxidizing activity of *T. ferrooxidans* and *T. thiooxidans* as shown in **Tables 1.8 and 1.9**.

In the present chapter, the inhibitory effects of fulvic, tannic and oxalic acids on the cell growth, and iron- and sulfur- oxidation in *T. ferrooxidans* and *T. thiooxidans* are discussed around pH 2. This work has potential utility for selective control of acid production in mine drainage caused by *T. ferrooxidans* and *T. thiooxidans.*

6.1 Experimental

6.1.1 Microorganisms

Iron-oxidizing bacteria, *Thiobacillus ferrooxidans* (HUTY8906), were cultured and harvested as described in **Chapter 2**. Sulfur-oxidizing bacteria, *Thiobacillus thiooxidans*, were supplied by American Type Culture Collection (ATCC 8085), cultivated routinely in a 150 cm^3 of solution containing the basal salt solution of the 9K medium (Silverman and Lundgren, 1959) plus 1.50 g of elemental sulfur as an energy source, adjusted to pH 2.0 with H_2SO_4, in a silico-plugged 500-cm^3 Erlenmeyer flask. Cells were harvested in the same manner as *T. ferrooxidans.* Cell numbers were directly counted by microscopic observation (× 600).

6.1.2 Organic acids

Tannic acid (TA, e.g., $C_6H_2(OH)_3COOC_6H_2(OH)_2COOH$, Koso Chemicals, analytical reagent, AR), fulvic acid (FA), and oxalic acid (OA, $(COOH)_2 \cdot 2H_2O$, Wako Chemicals, AR) were used as inhibitors. Fulvic acid was isolated from the Dando Soil according to International Humic Substances Society (IHSS) method, and provided from the Humic Substances Society of Japan (Watanabe, et al., 1994). The elemental composition of fulvic

acid was 45.57% C, 4.06% H, 1.70% N, 48.09% O, and 0.68% S on ash and water free basis. Functional analysis showed 7.27 meq. COOH, 1.37 meq. phenolic OH, 1.76 meq. alcoholic OH, 5.80 meq. C=O.

6.1.3 Culture tests

The 500-cm^3 brown Erlenmeyer flasks were filled with 150 cm^3 of the 9K medium for the culture of *T. ferrooxidans*, or the 9K basal solution plus 1.50 g of sterilized elemental sulfur for the culture of *T. thiooxidans*, the initial pHs were adjusted to 2.2~2.3 and 0~75.0 mg fulvic, tannic, or oxalic acids was added. The additives are entirely dissolved in the medium. The control culture was set triply without inhibitors. All these flasks were inoculated with 8.00×10^9 cells of *T. ferrooxidans* or *T. thiooxidans*. A sterilized experiment was also performed without microorganisms and inhibitors.

The flasks were installed in a rotary shaking culture-apparatus (Takasaki Kagaku Co. Ltd., TB-16) at 30 ±2 ℃ and incubation was carried out for 14 days, under light shielding to avoid decomposition of carboxylic compounds. At intervals, cell numbers were counted, and 1 cm^3 of surpernatant was pippetted off and filtered with a 0.20 μm pore size membrane filter for solution analysis.

6.1.4 Solution analysis

The solution analysis was carried out as follows. For experiments with *T. ferrooxidans*, the redox potential of the medium (*E*) and the concentration of Fe(II) ions were measured. The Fe(II) ions were determined by the 1, 10-phenanthroline method. The microorganisms oxidize Fe(II) to Fe(III) ions so *E* increases rapidly with the increase in iron-oxidizing activity of *T. ferrooxidans* (**Chapter 2**). In this system, increases in *E* are correlated to iron oxidation and to growth of the microorganism (Dugan and Lundgren, 1964). For experiments with *T. thiooxidans*, the pH and concentrations of dissolved S species were measured. Concentrations of soluble S species were determined by ICP-AES (SEIKO Co. Ltd., SPS 1200). The microorganisms oxidize elemental S to soluble S species and produce H^+ ions during the culture.

6.2 Results

6.2.1 Effect of organic acids on cell growth and iron-oxidizing activity in Thiobacillus ferrooxidans

The effects of fulvic, tannic, and oxalic acids on the cell growth, *E*, and consumption of Fe(II) ions in the culture of *T. ferrooxidans* are shown in **Fig. 6.1**, where the control data without inhibitors are shown with solid circles and are averages of three experiments. The

sterilized data are shown with ×. With 50 ppm of fulvic acid cell growth was suppressed a little and the iron oxidation was delayed about 12 hours. With 500 ppm of fulvic acid there was an extended lag in cell growth and iron oxidation by *T. ferrooxidans* was delayed about 48 hours, cell numbers and *E* recovered after 5 days and were then not inhibited.

Tannic acid prevented cell growth and iron oxidation in *T. ferrooxidans*, in longer periods than fulvic acid. With 500 ppm tannic acid inhibited cell growth completely and inhibited the iron oxidation of 8×10^9 cells of *T. ferrooxidans* for more than 14 days.

Oxalic acid had little effect on the cell growth of *T. ferrooxidans*, *E*, and the oxidation of Fe(II) ions even at 500 ppm (3.97 mmol dm^{-3}), similar to the control experiment. It is considered that there is no lowering of the standard redox potential, E^0, in the presence of 500 ppm oxalic acid, because the concentration of oxalic acid was too small to reduce E^0 by ligand effects (**Chapter 4**).

6.2.2 Effect of organic acids on cell growth and sulfur-oxidizing activity in Thiobacillus thiooxidans

The effects of fulvic, tannic, and oxalic acids on the cell growth, pH, and concentration of dissolved S species in the culture of *T. thiooxidans* are shown in **Fig. 6.2**, where the symbols are the same as those in **Fig. 6.1**. The 50~500 ppm of fulvic acid had a small effect on the cell growth of *T. thiooxidans*, but enhanced the sulfur oxidation.

Tannic acid dramatically inhibited cell growth, pH, and sulfur oxidation in 8.00×10^9 cells of *T. thiooxidans*, in longer periods than fulvic acid, and 500 ppm of tannic acid suppressed them completely for more than 14 days, to the same level as in the sterilized experiments.

Oxalic acid did not affect clearly the cell growth, pH, and sulfur oxidation in *T. thiooxidans* even at 500 ppm.

6.3 Discussion

It is known that carboxylic acids are inhibitory to *T. ferrooxidans* (Tuttle, et al., 1976), and *T. thiooxidans* (Iwastuka and Mori, 1960). Tuttle, et al. (1976) reported that the inhibitory ability of oxalic acid on cell growth and iron oxidation in *T. ferrooxidans* was greater than those of other monocarboxylic acids and α-keto acids, and that 100% of 3.2×10^{10} cells cm^{-3} of *T. ferrooxidans* were inhibited by 10^{-2} mol dm^{-3} of oxalic acid and 10% by 10^{-3} mol dm^{-3} of oxalic acid. Iwatsuka and Mori (1960) used manometric measurements to establish that the inhibition of oxalic acid on cell growth and sulfur oxidation in *T. thiooxidans* was 15% at 10^{-2} mol dm^{-3} and zero at 10^{-3} mol dm^{-3} around pH 3.8 (below pK_2), but cell numbers were not given. In the present work, even 500 ppm of oxalic acid did not show clear inhibition of iron and sulfur oxidation in 5.33×10^7 cells cm^{-3} of *T. ferrooxidans* and *T.*

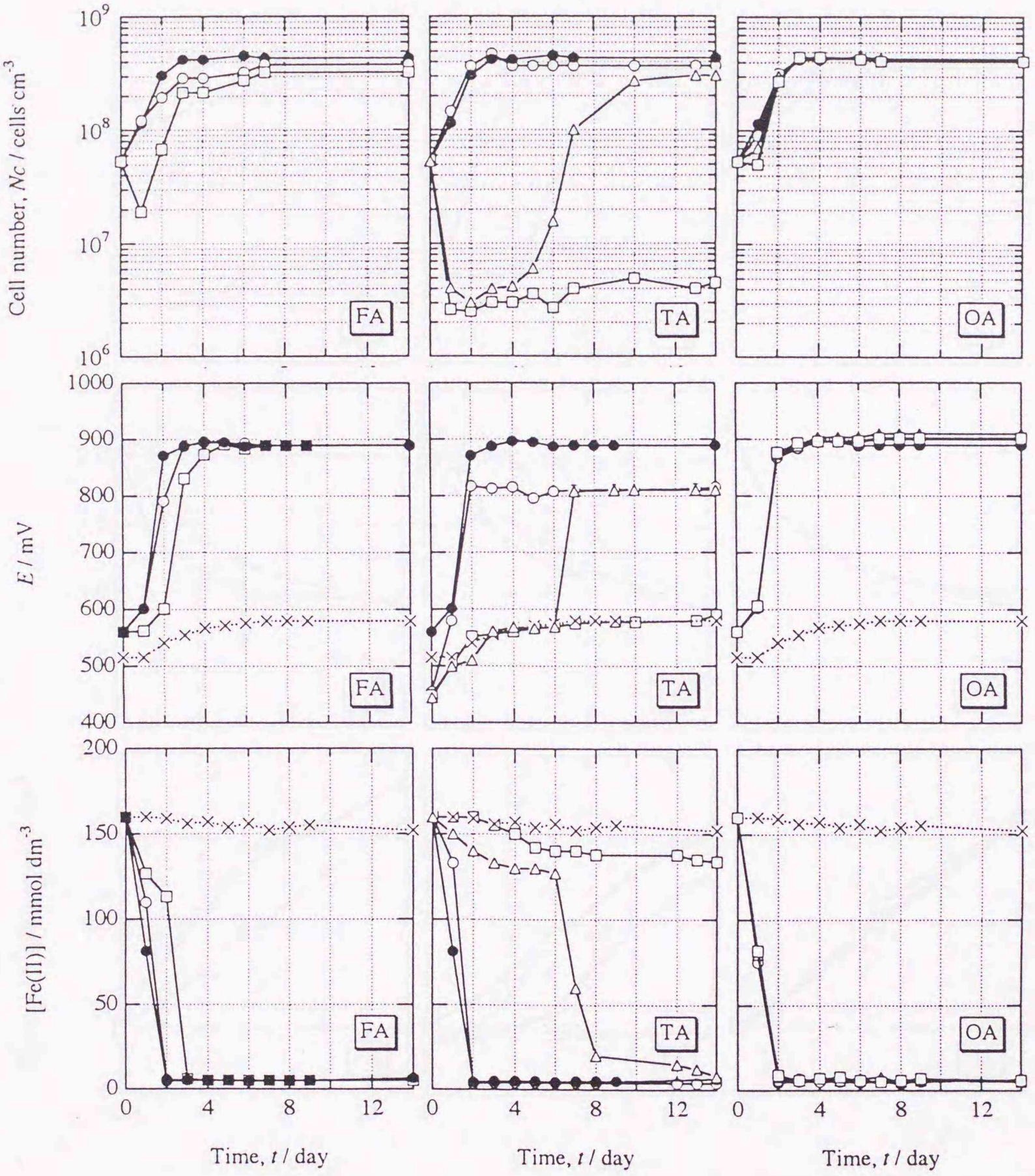

Fig. 6.1 Effect of fulvic acid (FA), tannic acid (TA), and oxalic acid (OA) on the cell growth (top), redox potential, *E*, in the medium (middle), and Fe(II) concentration (bottom) in culture of *T. ferrooxidans*. Symbols: ●, 0 ppm; ○, 50 ppm; △, 150 ppm; □, 500 ppm; ×, sterilized.

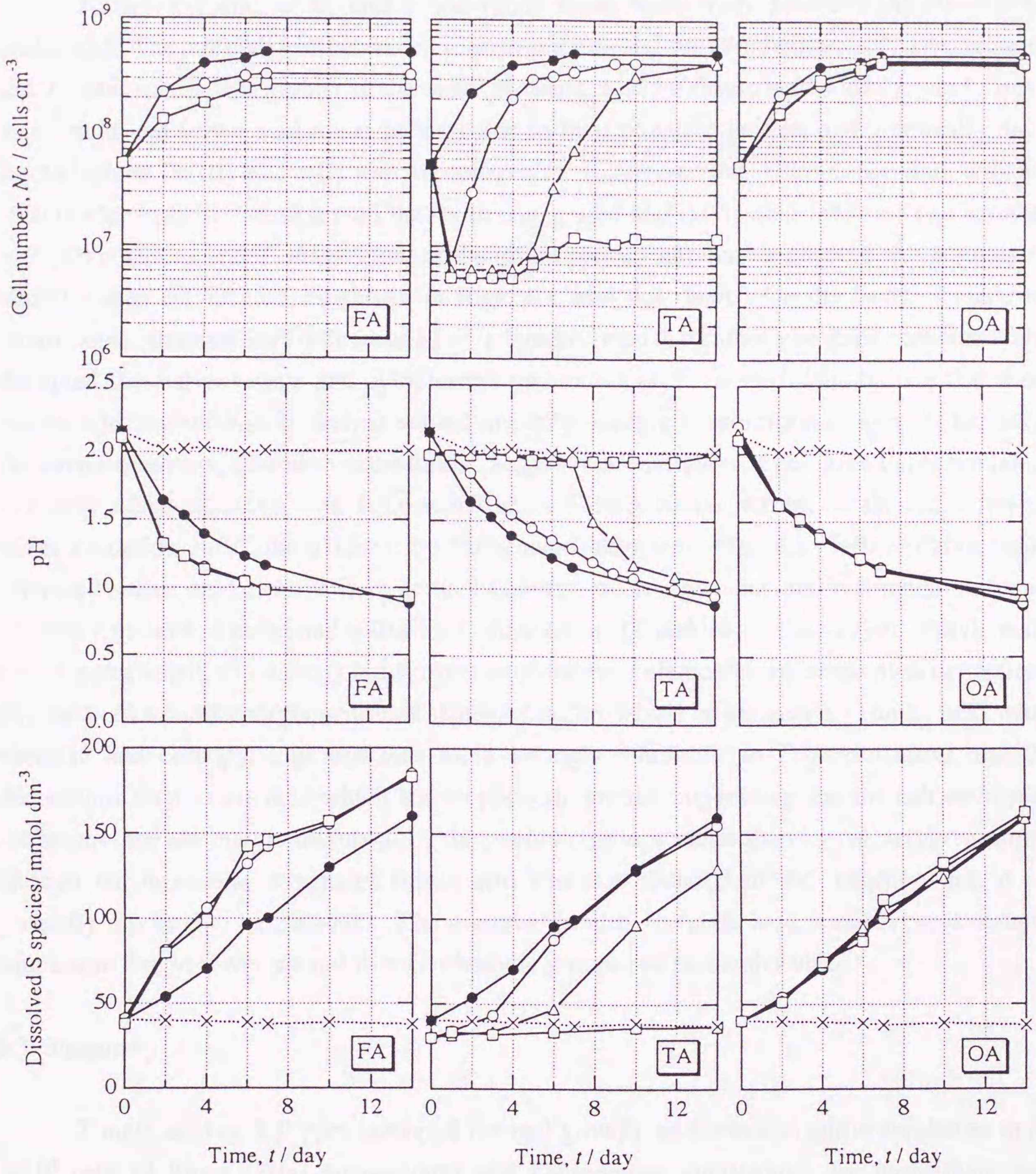

Fig. 6.2 Effect of fulvic acid (FA), tannic acid (TA), and oxalic acid (OA) on the cell growth (top), pH, in the medium (middle), and dissolved S species concentration (bottom) in culture of *T. thiooxidans* Symbols are the same as those given in Fig. 6.1.

thiooxidans, though there was some inhibition of cell growth in *T. ferrooxidans* and *T. thiooxidans* in the earlier periods.

Natural organic acids, tannic and fulvic acids, were more effective inhibitors than oxalic acid. The inhibitory effect on cell growth and iron and sulfur oxidation in *T. ferrooxidans* and *T. thiooxidans* was greater in the order of tannic acid >> fulvic acid > oxalic acid. Both tannic acid and fulvic acid are reductants due to their phenolic groups, and abiotically they would reduce Fe(III) to Fe(II) ions in cultures of *T. ferrooxidans* (Skogerboe and Wilson, 1981). However, it was observed that both tannic acid and fulvic acid inhibited cell growth of *T. ferrooxidans* and *T. thiooxidans* at the initial period, and that tannic acid was a stronger inhibitor than fulvic acid, as shown in **Figs. 6.1 and 6.2 (top)**. On the basis of electron microscopic observations Tuttle, et al. (1977) demonstrated that carboxylic acids nonselectively disrupted the cell envelope and cytoplasmic membrane of *T. ferrooxidans* by reaction with cations which contribute to their structural integrity, leading to inhibition of iron oxidation in the microorganisms. The above results also suggest that inhibition of cell growth is correlated to iron or sulfur oxidation with *T. ferrooxidans* or *T. thiooxidans*, except for the inhibition of sulfur oxidation in *T. thiooxidans* by fulvic acid shown in **Fig. 6.2 (left)**. Fulvic acid enhanced sulfur oxidation. Direct contact between microorganisms and elemental sulfur is necessary to oxidize elemental sulfur by *T. thiooxidans* (Takakuwa, et al., 1979). Fulvic acid acts as a surfactant, and when it is adsorbed on particles of elemental sulfur the pysicochemical affinity between microorganisms and elemental sulfur would be enhanced. Tannic acid with phenolic and carboxylic groups was more strongly inhibitory to *T. ferrooxidans* and *T. thiooxidans* than oxalic acid which has no phenolic groups, suggesting that the cell envelope and membrane are mainly disrupted by the phenolic groups rather than by carboxylic groups. Though the molecular weight of fulvic acid was not obtained in the present work, it is generally reported to be 500~800. The inhibitory ability of fulvic acid is rather weaker than tannic acid due to fewer phenolic and carboxylic groups per molecular unit.

6.3 Summary

Tannic acid at 500 ppm inhibited the cell growth, and iron and sulfur oxidation in 8 $\times 10^9$ cells of *Thiobacillus ferrooxidans* and *Thiobacillus thiooxidans*, for more than two weeks, possibly due to its phenolic group. Fulvic acid inhibited only within the initial two days. Both acids were more effective inhibitors than oxalic acid. The present work indicates that natural organic acids, tannic and fulvic acids, would function both as reductants and ligands to Fe(III) ions and also as inhibitors to *T. ferrooxidans* and *T. thiooxidans* in the environment.

References

Dugan, P. R., and Lundgren, D. G. (1964) Acid production by *Ferrobacillus ferrooxidans* and its relation to water pollution. *Develop. in Industr. Microbiol.* **5,** 250-257.

Iwatsuka, H., and Mori, T. (1960) Studies of the metabolism of a sulfur-oxidizing bacterium 1. Oxidation of sulfur. *Plant & Cell Physiol.*, **1**, 163-172.

Rittenberg, S. C. (1972) The obligate autotroph --- the demise of a concept. *Antonie Van Leeuwenhoek J. Microbiol. Serol.* **38**, 457-478.

Silverman, M. P., and Lundgren, D. G. (1959) Studies on the chemoautotrophic iron bacterium *Ferrobacillus ferrooxidans* II. Manometric studies. *J. Bacteriol.*, **78**, 326-331.

Skogerboe, R. K., and Wilson, S. A. (1981) Reduction of ionic species by fulvic acid. *Anal. Chem.*, **53**, 228-232.

Takakuwa, S., Fujimori, T., and Iwasaki, H. (1979) Some properties of cell-sulfur adhesion in *Thiobacillus thiooxidans*. *J. Gen. Appl. Microbiol.,* **25**, 21-29.

Taylor, B. E., Wheeler, M. C., and Nordstrom, D. K. (1984) Stable isotope geochemistry of acid mine drainage: Experimental oxidation of pyrite. *Geochim. Cosmochim. Acta*, **48**, 2669-2678.

Tuttle, J. H., and Dugan, P. R. (1976) Inhibition of growth, iron, and sulfur oxidation in *Thiobacillus ferrooxidans* by simple organic compounds. *Can. J. Microbiol.*, **22**, 719-730.

Tuttle, J. H., Dugan, P. R., and Apel, W. A. (1977) Leakage of cellular material from *Thiobacillus ferrooxidans* in the presence of organic acids. *Appl. Environ. Microbiol.*, **33**, 459-469.

Watanabe, A., Itoh, K., Arai, S., and Kuwatsuka, S. (1994) Comparison of the composition of humic acid and fulvic acid prepared by the IHSS and NAGOYA method. *Soil Sci. Plant Natr.*, **40(4)**, 601-608.

Chapter 7
Suppression of microbially mediated dissolution of pyrite by originally isolated fulvic acids and related compounds

Pyrite (FeS_2) weathering in mines causes environmental problems. It is well known that chemoautotrophic iron- and sulfur- oxidizing bacteria, *Thiobacillus ferrooxidans* and *Thiobacillus thiooxidans,* often grow actively in mine environments and they play an important role in pyrite weathering, especially in aerobic environments (Singer and Stumn, 1970). The Fe(III) ions are direct oxidants not only in anaerobic environments (McKibben and Barnes, 1986), but also in aerobic environments where iron-oxidizing bacteria are involved mainly according to indirect contact mechanism (**Chapter 2**). Pyrite weathering primarily depends on the reaction between pyrite and Fe(III) ions (**Chapter 3**). However, actual biogeochemical processes in pyrite weathering are more complex, and include many reactions such as adsorption, complexation, oxidation/reduction, precipitation, aggregation, and degradation in addition to dissolution.

According to the previous studies on suppression of pyrite weathering, key factors in suppression can be summarized as: (a) formation of stable Fe(III) complexes (**Chapter 4**), (b) the preferential adsorption of Fe(II) and Cu(II) ions over Fe(III) ions to active sites on the pyrite surface (**Chapter 5**), (c) reduction of Fe(III) to Fe(II) ions (Blowes, 1994), and (d) growth inhibition of *T. ferrooxidans* and *T. thiooxidans* (**Chapter 6**). Further, environmentally acceptable and effective substances are desired to meet the above demands.

Oxidation of pyrite by Fe(III) ions has been reported to be suppressed by oxalic acid (OA) (**Chapter 4**) and humic acids (HA) (Lalvani and Zhang, 1994), because of a lowering of the standard redox potential of Fe(III)/Fe(II), $E^0_{Fe(III)/Fe(II)}$, by complexation. Humic substances (HS) are widely distributed in soil, natural waters, peat, lignites, brown coal, carbonaceous shales, marine and lake deposits, and other ore deposits. Humic substances consist of fulvic acids (FA) and HA (Stevenson, 1985): the former is soluble even at pH 1 whereas the later is insoluble below pH 2, and makes up more than 50% of HS. Similar to HA, FA is capable of complexing and reducing Fe(III) ions (Szilagyi, 1971; Skogerboe and Wilson, 1981), and has more functional groups per molecule unit than HA (e. g., Kuwatsuka, et al., 1992). Further, tannic acids (TA) which are abundant in oak-leaves, are also soluble at very low pH, and has many more carboxylic and phenolic groups per molecule unit than FA. Recently we have found that cell growth and activities in *T. ferrooxidans* and *T. thiooxidans* are inhibited by FA, TA, and OA and that the inhibition is in the order TA>>FA>OA (**Chapter 6**). Effect of HA on the biogeochemical cycling of Fe(II, III) was also discussed in the field studies by Luther, et al (1992; 1996).

The effect of FA and the related organic acids on microbially mediated dissolution of pyrite is an issue in environmental sciences. This chapter presents the effect of FA, TA, and OA, and discusses the potential usefulness for selective control of acid production caused by *T. ferrooxidans* and *T. thiooxidans* in mine drainage.

7.1 Experimental

7.1.1 Organic acids

Fulvic acids were originally purified from Shinshinotsu soil (Japan): The protocol for preparation of fulvic acids (FA) is described in **Appendix 7.1**. The elemental composition of the purified FA sample was 41.26% C, 5.27% H, 0.95% N, 52.16% O, and 0.36% S on ash and water free basis. Full details of the characterization in this sample were described elsewhere (Tanaka, et al., 1996). Related reagents, tannic acids (TA; e. g., $C_6H_2(OH)_3COO$-$C_6H_2(OH)_2COOH$; Koso Chemicals, analytical grade, AR, lot. S3F0614; Wako Chemicals, chemical grade, PR, lot. ESH1058) and oxalic acid (OA; $(COOH)_2 \cdot 2H_2O$, Wako Chemicals, AR) were also used.

7.1.2 Pyrite

Pyrite sample is the same as used in **Chapters 2~5**, ground and sieved to obtain the size fraction between 38-75 μm. Pretreatment of the pyrite was carried out to remove oxidized species on the surface in the manner previously described in **Chapter 3**. The specific surface area after the pretreatment was determined for each experiment by the N_2 adsorption one point BET method with a Quantasorb QS-13 (Yuasa Ionics Co. Ltd.) using a QS-300 cell for small area measurements.

7.1.3 Microorganisms and culture

Iron-oxidizing bacteria, *Thiobacillus ferrooxidans* (HUTY8906), and sulfur-oxidizing bacteria, *Thiobacillus thiooxidans* (ATCC 8085), were cultured and harvested as described in **Chapter 6**.

7.1.4 Reduction of Fe(III) ions by organic acids

Prior to experiments of pyrite oxidation by Fe(III) ions, the reduction rate of Fe(III) to Fe(II) ions by the organic acids was estimated.

Reduction experiments were carried out in a batch reactor with an impeller and G2 glass ball filter for N_2 or air bubbling, at 30 ± 2 ℃ with light shielding to avoid decomposition of organic acids. Dissolved oxygen was below 1 ppm under the N_2 bubbling and saturated under air bubbling. All assemblies were made of glass and rinsed with dilute super special

grade (SSG) HNO_3 solution before use to avoid iron contamination. One mmol dm^{-3} $FeCl_3 \cdot 6H_2O$ solution was prepared with the initial pH adjusted to ~2 by SSG HCl. Tannic acids have no well-defined structure, and two reagents from different suppliers (Koso and Wako) were used. After the desired amounts of TA, FA, or OA were added to 100 cm^3 of solution, the solution was stirred. These organic acids dissolved completely at the concentrations used. At intervals, 1 cm^3 of supernatant was pipetted off and filtered with a 0.20 μm pore size membrane filter for solution analysis. The total Fe and Fe(II) ion concentrations were determined by the 1, 10-phenanthroline method.

7.1.5 Dissolution of pyrite by Fe(III) ions in the presence of organic acids

Prior to microbially mediated dissolution of pyrite, chemical dissolution experiments by Fe(III) ions in the presence of FA, TA, and OA were carried out.

Abiotic dissolution of pyrite by Fe(III) ions in the absence and presence of organic acids was carried out for 72 h in an anaerobic atmosphere using the same apparatus as described in the previous section. Here, 2.00 g of pyrite (0.40 $m^2 g^{-1}$) was added to 200 cm^3 of 1 mmol dm^{-3} $FeCl_3 \cdot 6H_2O$ solution adjusted with HCl to pH ~2 in the presence of 1200 ppm of FA, 120 ppm of TA (Koso), or 252~1260 ppm (2~10 mmol dm^{-3}) of OA. Dissolved Fe(II) ions were determined in the same manner as described in the previous section, and dissolved S species were measured by an ICP-AES SPS 1200 (SEIKO, Co. Ltd.). In the presence of FA, total organic carbon (TOC) was also determined by a carbon analyzer model 1555B (Yuasa Ionics Co. Ltd.). In some experiments, the residue was filtrated after dissolution using a membrane filter with 0.20 μm-pores and the vacuum-dried for XPS (V. G. Scientific, ESCA LAB Mk II) and FTIR analysis. Details of the XPS measurements were described in **Chapter 2**.

7.1.6 Microbially mediated dissolution of pyrite in the presence of organic acids

First, 500-cm^3 brown Erlenmeyer flasks were filled with 200 cm^3 of the 9K basal medium plus 2.00 g of the pretreated pyrite (1.60 $m^2 g^{-1}$) at an initial pH 2.2~2.3. Each medium contains 40~240 mg FA (200~1200 ppm), 2~100 mg TA (Koso; 10~500 ppm), or 25.2~126.0 mg OA (126~630 ppm). The control culture was also set triply without additives. These flasks were put with silico-plugs, and inoculated with 8.00×10^9 cells of *T. ferrooxidans* and 8.00×10^9 cells of *T. thiooxidans*. A sterilized experiment was also performed.

All flasks were installed in a rotary shaking culture-apparatus TB-16 (Takasaki Kagaku, Co. Ltd.) at 30±2 ℃ and incubation was continued for 336 h under light shielding. Conventionally the microorganisms require CO_2 as a carbon source in addition to reduced species of Fe and S as energy sources, but they do not require organic carbon and light (Tuovinen and Kelly, 1972). At intervals, pH, dissolved S species, total Fe, and Fe(II) ions

were measured. Total organic carbon was not determined, due to the involvement of released extracellular substances from the microorganisms in addition to the adsorption of organic substances to pyrite.

After 336 h, the residue was filtrated using a Whatmann filter 41 and vacuum-dried for FTIR analysis and the cell numbers were counted directly in the filtrate. Membrane filters with submicron size pores were not used due to clogging by samples containing high cell densities. For these samples, XPS measurements were abandoned because high densities of organic compounds cause the differential charging effects (**Chapter 2**).

7.1.7 FTIR spectra

Infrared spectra were recorded using a FTIR VALOR III (Jasco, Co. Ltd.) by diffuse reflectance infrared Fourier transformed spectroscopy (DRIFTS) with 5 (w/w) % of sample precipitate in KBr, under the conditions: accumulation, 16 times; resolution, 4 cm^{-1}; detector, TGS; range of wavenumbers, 400~4000 cm^{-1}. A spectrum for the mixture of 2.00 g pretreated pyrite and either 240 mg FA, 100 mg TA, or 126 mg OA was also measured as a reference. The amounts of organic acids are correspondent to the maximum used in microbially mediated dissolution of pyrite.

7.2 Results

7.2.1 Reduction of Fe(III) ions by organic acids

Figure 7.1 shows the relation between the amount of reduced Fe(III) ions for 30 min

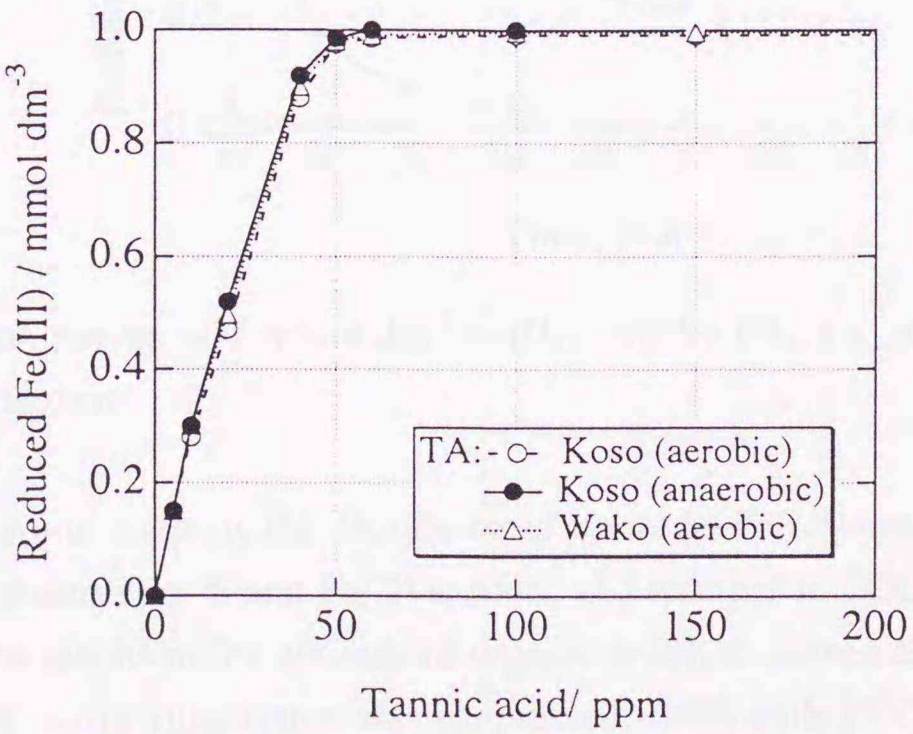

Fig. 7.1 Relation between reduced Fe(III) ions and the amounts of two kinds of TA, Koso (●, ○) and Wako (△) Chemicals. Reduction of Fe(III) was carried out in aerobically (open symbols) and anaerobically (closed ones). Initial Fe(III) ion concentration was 1 mmol dm^{-3}.

and TA concentrations, when the initial concentration of Fe(III) ions was 1 mmol dm^{-3}. Experiments were carried out by two kinds of tannic acids (TA; Koso and Wako) in both aerobic and anaerobic atmospheres. Three curves were almost equal and 60 ppm of TA was required to reduce 1 mmol dm^{-3} Fe(III) ions completely around pH 2. The reducing ability of TA was independent of atmosphere probably due to a very rapid reaction and also independent of reagents. This indicates that the number of functional groups involving reduction per unit amount is almost equal for both reagents (Koso and Wako), therefore the Koso Chemicals TA was used in the following experiments.

Figure 7.2 shows reduction curves of 1 mmol dm^{-3} Fe(III) ions at pH ~2 in an anaerobic atmosphere by FA, TA, and OA. The 60 ppm of TA reduced Fe(III) ions immediately, but OA did not reduce Fe(III) ions even at 1200 ppm (~9.52 mmol dm^{-3}) after 72 h. Fulvic acids reduced Fe(III) ions rapidly with increasing concentration but the reaction was slower than TA. At least 45 h and 1200 ppm of FA were required to reduce 1 mmol dm^{-3} Fe(III) ions completely.

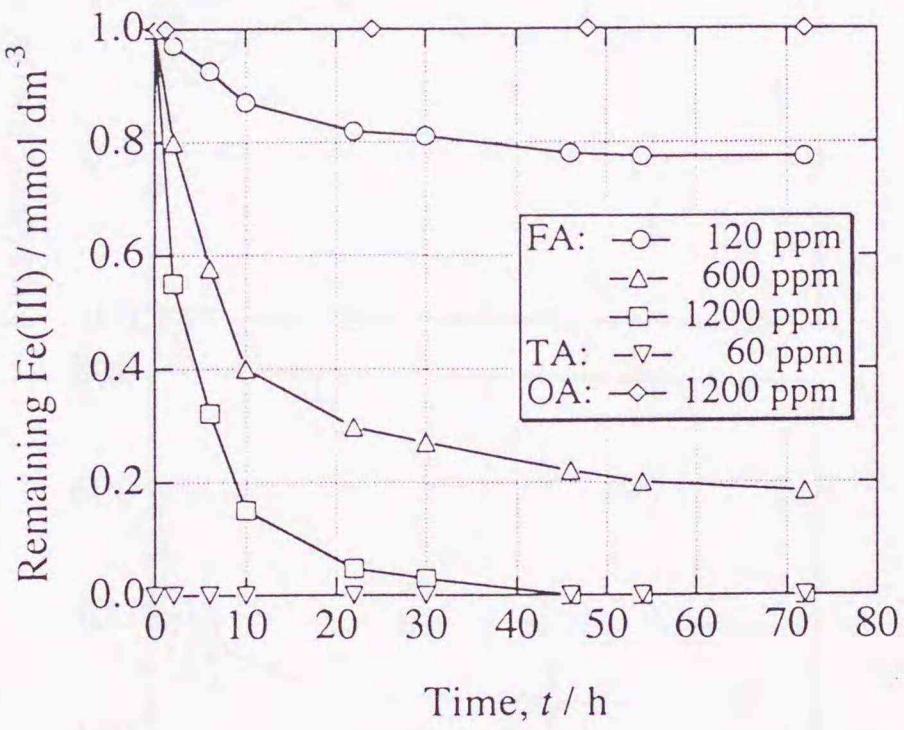

Fig. 7.2 Reduction curves of 1 mmol dm^{-3} Fe(III) ions by FA, TA, and OA around pH 2 in an anaerobic atmosphere.

7.2.2 Effect of organic acids on the dissolution of pyrite by Fe(III) ions

Dissolution curves of S and Fe(II) species, and changes in TOC are shown in **Fig. 7.3**. Compared with the results in the absence of organic acids, dissolved S species data at 72 h in **Fig. 7.3** shows that pyrite dissolution was suppressed ~16% with 1200 ppm of FA and ~50% with 120 ppm of TA. In the presence of 252~1260 ppm (2~10 mmol dm^{-3}) of OA, dissolution of S and Fe(II) was completely suppressed.

In the presence of FA and TA, only a part of the dissolved Fe(II) ions are derived

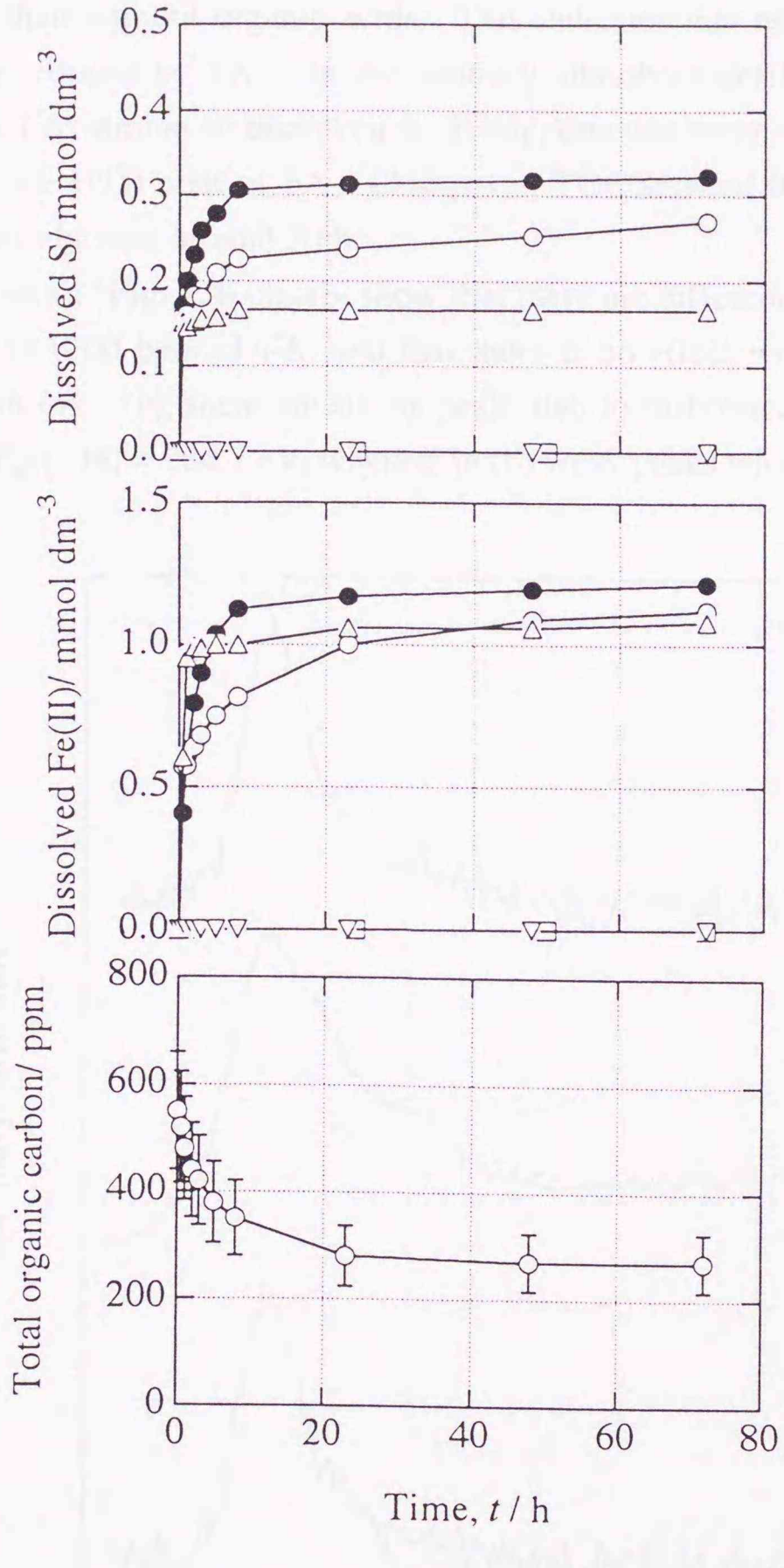

Fig. 7.3 Changes in dissolved S species, dissolved Fe(II) ions, and total organic carbon (TOC) during the dissolution of pyrite by 1 mmol dm^{-3} of Fe(III) ions with and without organic acids. Symbols: ●, no organic acids (control); ○, FA 1200 ppm;△, TA 120 ppm; □, OA 252 ppm; ▽, OA 1260 ppm. Vertical bars indicate the standard deviation of three TOC measurements.

from pyrite, because the added Fe(III) ions are reduced to Fe(II) ions by FA and TA. With 120 ppm of TA, dissolved Fe(II) ions immediately reached 1.0 mmol dm^{-3}. Within 4 h dissolved Fe(II) were larger with TA than without organic acids, while dissolved S were smaller with TA than without organic acids. This indicates that most of the added Fe(III) ions were rapidly reduced by TA. On the contrary, dissolved Fe(II) ions increased slowly with 1200 ppm of FA, similar to dissolved S. It suggests that most of the added Fe(III) ions were not reduced by 1200 ppm of FA. Changes in TOC showed that adsorption of FA to pyrite attained a steady state around 50 h.

The XP-spectra (**Fig. 7.4**) clearly show that there are differences in C 1s spectra, with (b) and without (a) 1200 ppm of FA, and that there is no effect with 1260 ppm (10 mmol dm^{-3}) of OA (c): in (a) ~ (c), there are strong peaks due to carbonaceous contamination with the main peak at E_B[C 1s] = 284.7 eV, whereas in (b) weak peaks which can be assigned to

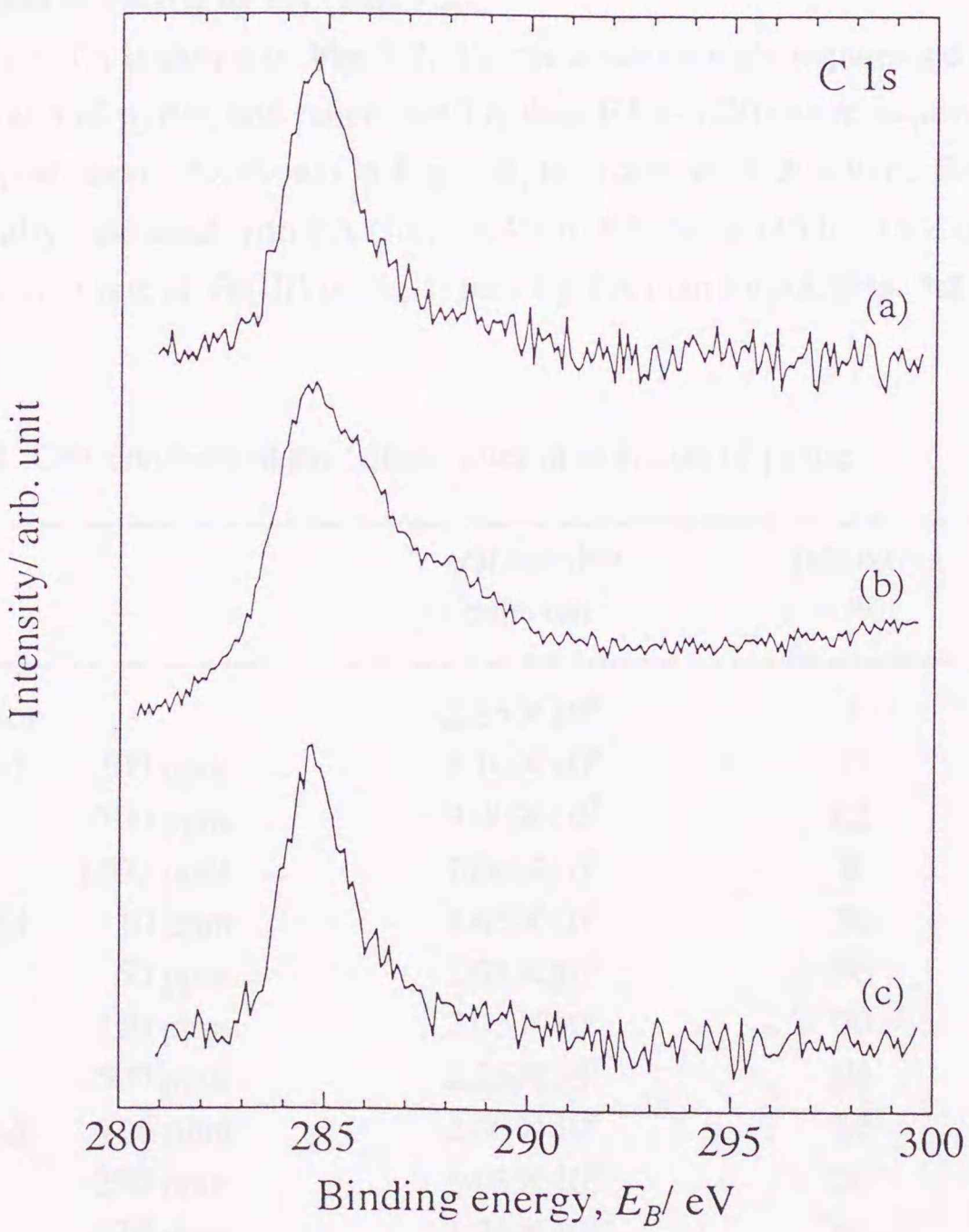

Fig. 7.4 XP-spectra of C 1s for pyrite after dissolution in the absence of organic acids (a), and in the presence of 1200 ppm of FA (b) and 1260 ppm of OA (c).

carboxylic groups, are observed around E_B[C 1s] = 288 eV. It indicates that FA adsorbed on the pyrite surface, and that OA did not, even at 1260 ppm. In the FTIR spectra of pyrite after dissolution, however, no peaks corresponding to adsorbed FA were observed, probably due to the low concentration on the surface.

7.2.3 Microbially mediated dissolution behavior of pyrite

Figure 7.5 shows the effects of FA on the dissolution of S and Fe species, and also pH changes in microbially mediated dissolution of pyrite. Dissolution of S species were suppressed ~50% by 200 ppm of FA at 336 h. The suppression was enhanced by increases in FA, but above 600 ppm no further suppression was observed. Dissolution of Fe species were suppressed 78 % by 200 ppm of FA at 336 h, and the suppression was higher than for the S species. As shown in **Fig. 7.6**, most of the dissolved Fe species were Fe(III) ions, though the fraction of Fe(II) ions increased a little (from 3.4% to 20 % at 336 h) with FA concentration due to the reduction of Fe(III) by FA (**Fig. 7.2**).

The effect of TA is shown in **Fig. 7.7**. Tannic acids strongly suppressed the microbially mediated dissolution of pyrite, and much less TA than FA (~1/20) were required to obtain the same level of suppression. As shown in **Fig. 7.8**, the fraction of dissolved Fe(II) to the total Fe ions dramatically increased with TA (from 3.4% to 84.2% at 336 h). One of the reasons is much larger reduction rate of Fe(III) to Fe(II) ions by TA than by FA (**Fig. 7.2**).

Table 7.1 Cell numbers in the filtrate after dissolution of pyrite

inhibitor		cell number / cells cm^{-3}	inhibition /%
no inhibitor		2.35×10^{8}	0
fulvic acid	200 ppm	1.10×10^{8}	53
(FA)	600 ppm	9.00×10^{7}	62
	1200 ppm	7.00×10^{7}	70
tannic acid	10 ppm	1.65×10^{8}	30
(TA)	50 ppm	1.03×10^{8}	56
	150 ppm	7.05×10^{7}	70
	500 ppm	2.35×10^{7}	94
oxalic acid	126 ppm	2.00×10^{8}	15
(OA)	252 ppm	1.03×10^{8}	56
	630 ppm	3.25×10^{7}	86

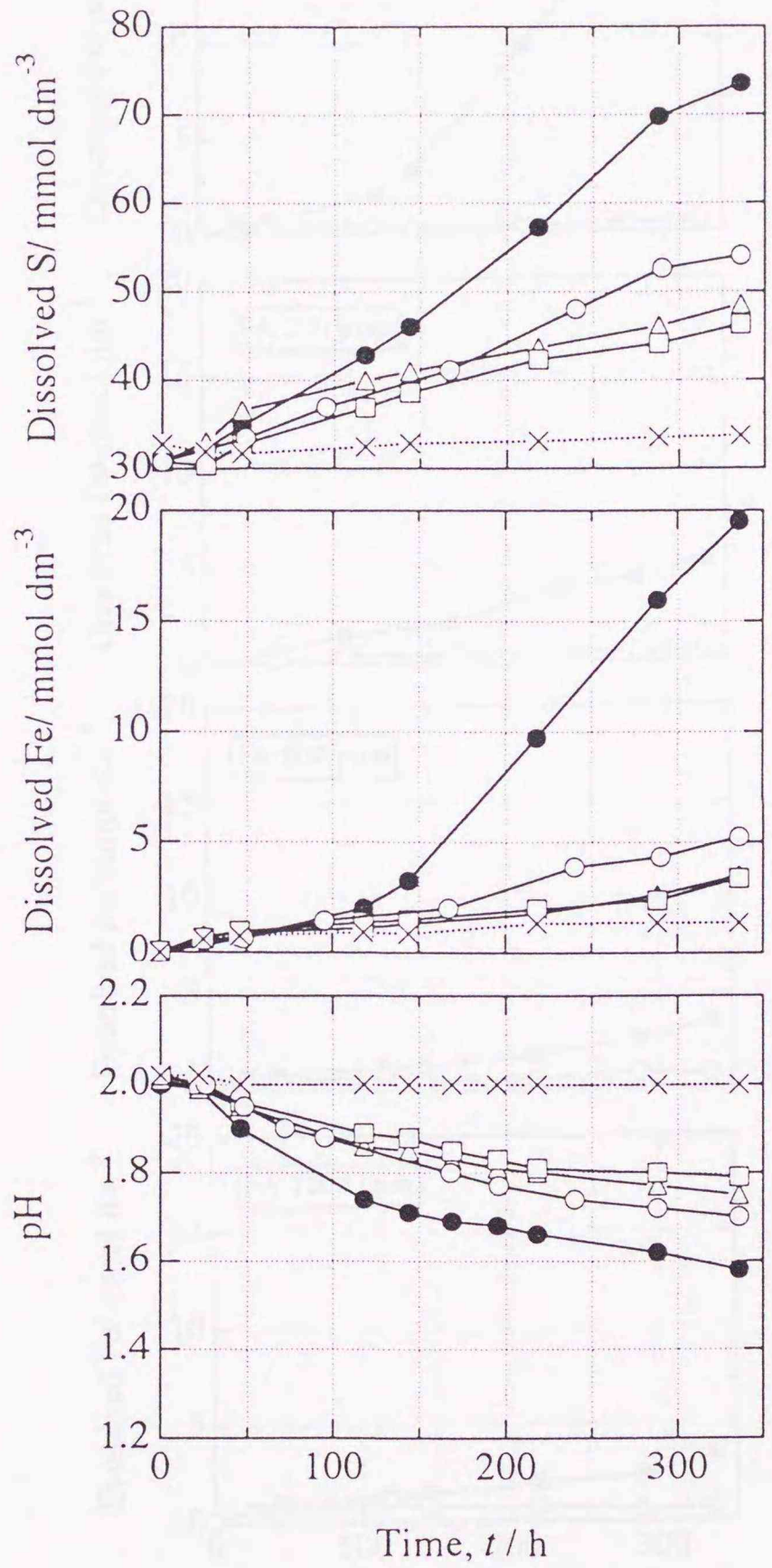

Fig. 7.5 Effect of FA on microbially mediated dissolution of pyrite. Symbols: ●, no inhibitor; ○, FA 200 ppm;△, FA 600 ppm; □, FA 1200 ppm; ×, sterilized.

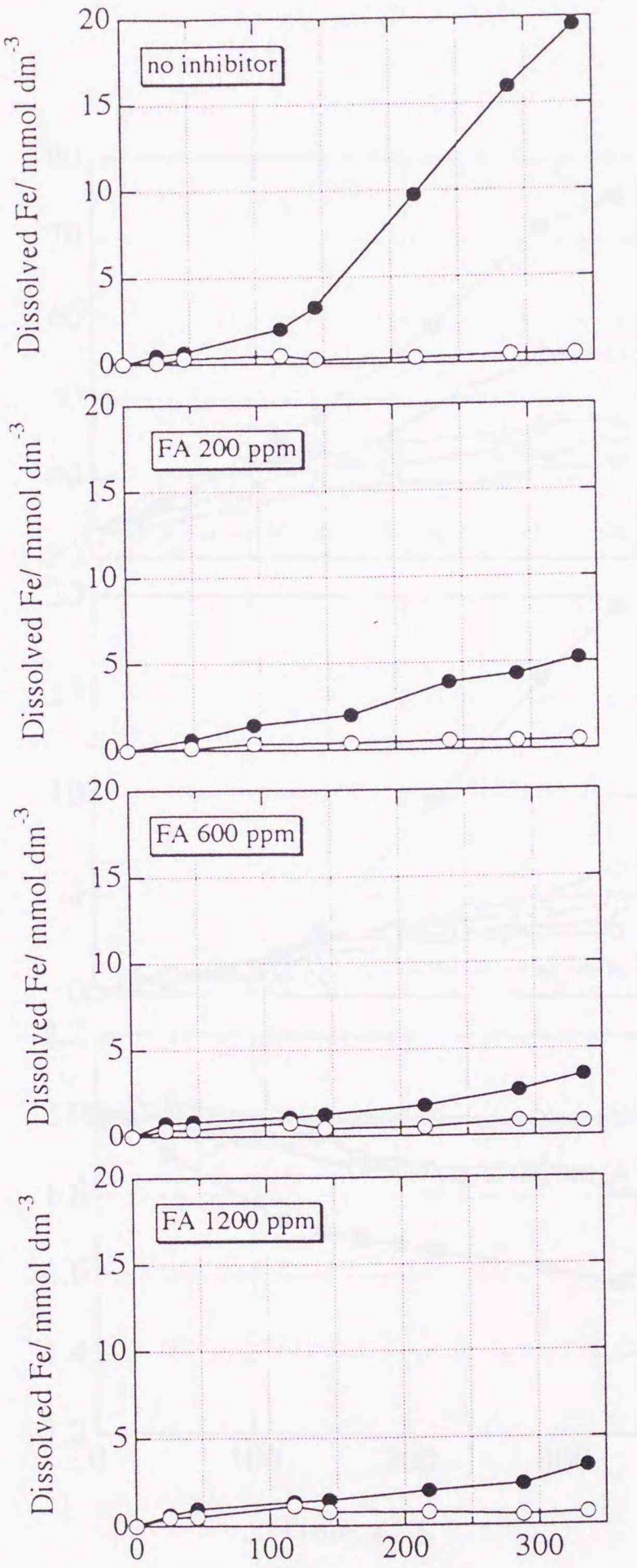

Fig. 7.6 Dissolution curves for total Fe (solid circles) and Fe(II) (open circles) ions in the presence of FA.

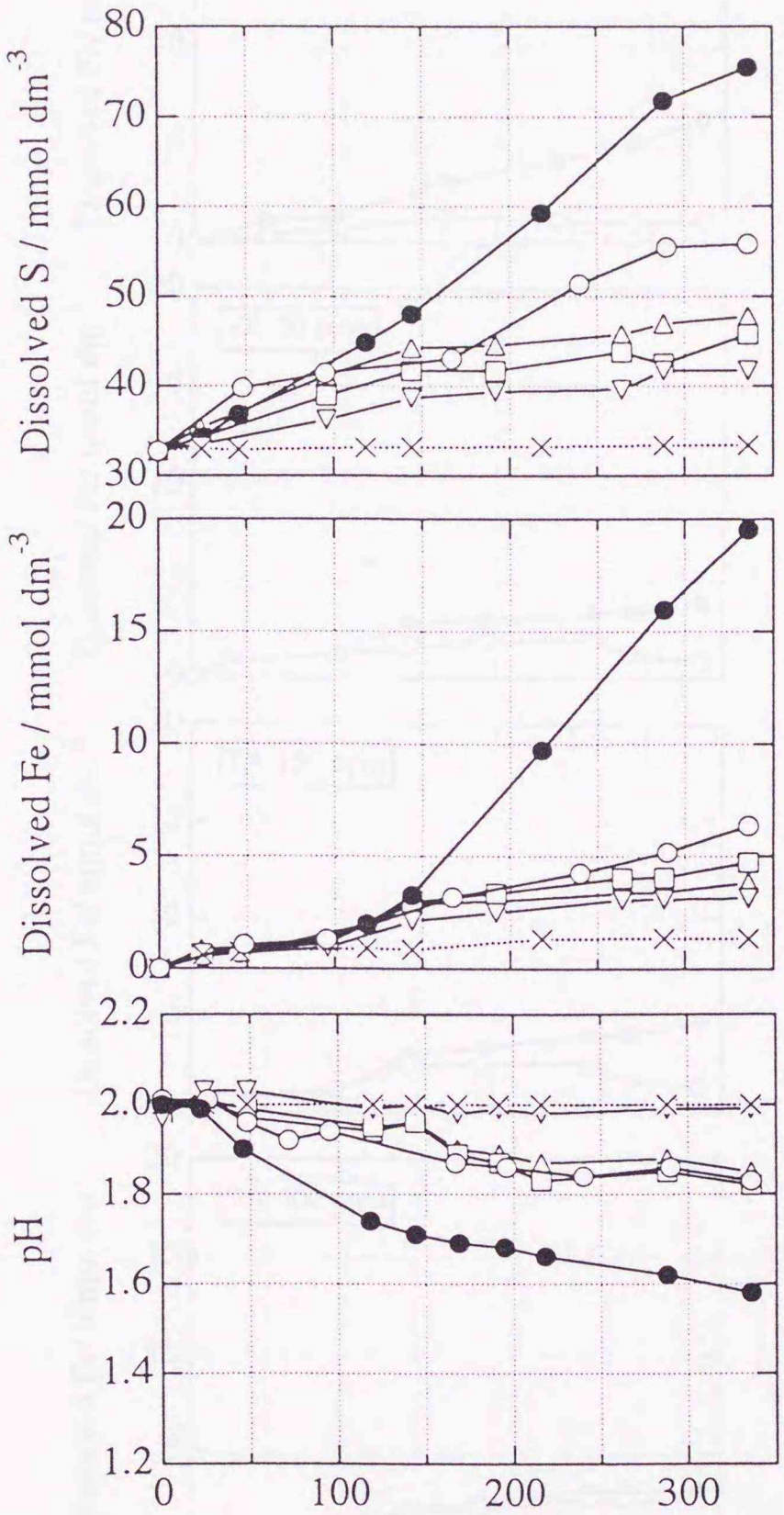

Fig. 7.7 Effect of TA on microbially mediated dissolution of pyrite. Symbols: ●, no inhibitor; ○, TA 10 ppm; △, TA 50 ppm; □, TA 150 ppm; ▽, TA 500 ppm; ×, sterilized.

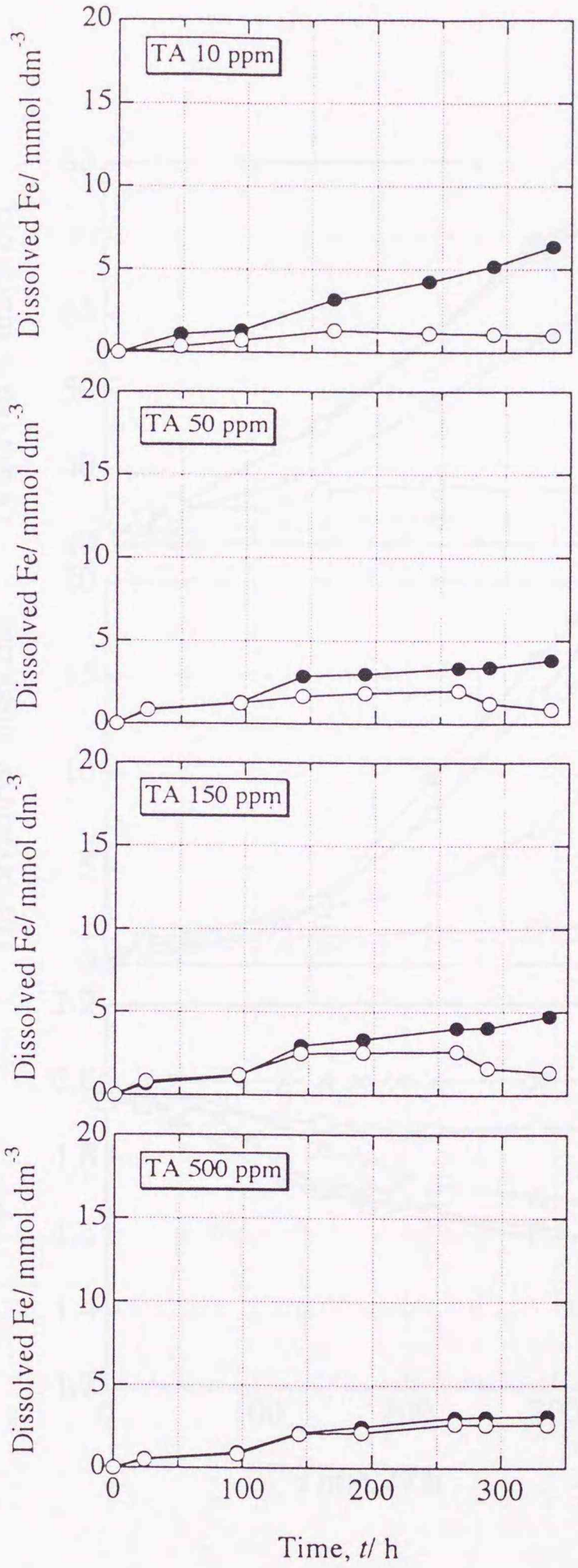

Fig. 7.8 Dissolution curves for total Fe (solid circles) and Fe(II) (open circles) ions in the presence of TA.

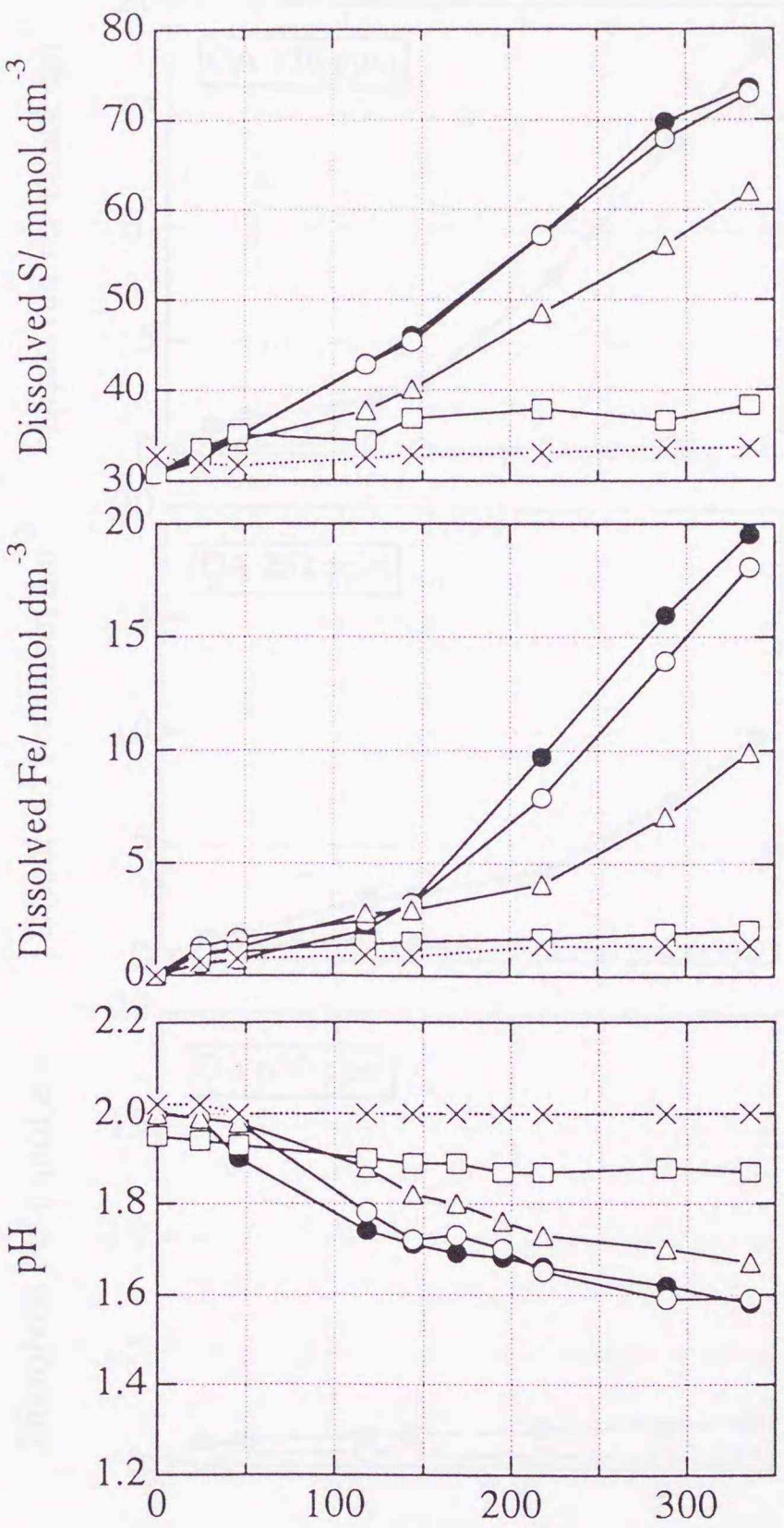

Fig. 7.9 Effect of OA on microbially mediated dissolution of pyrite. Symbols: ●, no inhibitor; ○, OA 126 ppm; △, OA 252 ppm; □, OA 630 ppm; ×, sterilized.

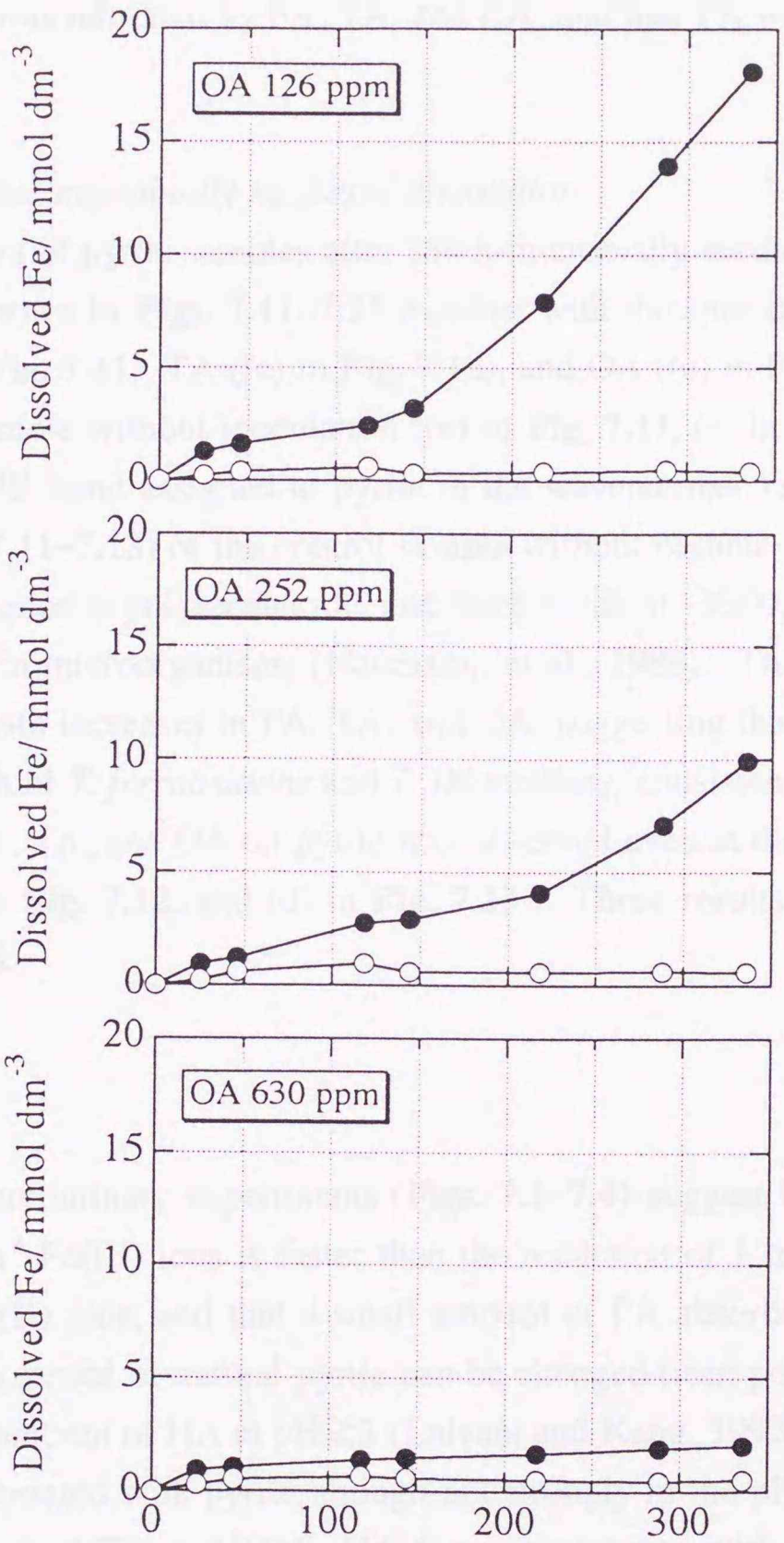

Fig. 7.10 Dissolution curves for total Fe (solid circles) and Fe(II) (open circles) ions in the presence of OA.

Figure 7.9 shows the effects of OA. With 126 ppm (1 mmol dm^{-3}) of OA there is no effect, but there is strong suppression with increasing OA. As shown in **Fig. 7.10**, dissolved Fe species were almost Fe(III) ions independent of OA concentration.

The cell numbers in the filtrate after each experiment is summarized in **Table 7.1**. It shows that cell growth was inhibited by FA, TA, and OA, and that TA was the most effective inhibitor.

7.2.4 FTIR of pyrite after microbially mediated dissolution

The FTIR spectra of pyrite samples after 336 h-microbially mediated dissolution with FA, TA, and OA are shown in **Figs. 7.11~7.13** together with the spectra for the mixtures of pyrite with FA ((d) in **Fig. 7.11**), TA ((e) in **Fig. 7.12**), and OA ((e) in **Fig. 7.13**). As shown in the spectra of the sample without inoculation ((e) in **Fig. 7.11**, (f) in **Fig. 7.12**, and (f) in **Fig. 7.13**), there is no IR band assigned to pyrite in the wavenumber range measured. The spectrum ((a) in **Figs. 7.11~7.13**) of the control sample without organic acid has one band at 1040 cm^{-1} which is assigned to polysaccharide, and three bands at ~3300, 1630 and 1400 cm^{-1} assigned to polyamide in microorganisms (Naumann, et al., 1988). The intensities of these four bands decreased with increases in FA, TA, and OA, suggesting that these organic acids inhibited the cell growth of *T. ferrooxidans* and *T. thiooxidans,* consistent with **Table 7.1**.

No adsorbed FA, TA, and OA on pyrite was observed even at the maximum amounts ((c) in **Fig. 7.11**, (d) in **Fig. 7.12**, and (d) in **Fig. 7.13**). These results are similar to those without microorganisms.

7.3 Discussion

The results of preliminary experiments (**Figs. 7.1~7.4**) suggest that the oxidation of pyrite with 1 mmol dm^{-3} Fe(III) ions is faster than the reduction of 1 mmol dm^{-3} Fe(III) by 1200 ppm of FA to Fe(II) ions, and that a small amount of FA absorbed on pyrite. It was reported that the zeta potential of natural pyrite can be changed from positive to negative by the addition of a small amount of HA at pH$\geqq$3 (Lalvani and Kang, 1992). It is reasonable to consider that FA is associated with pyrite, though not strongly in the pH range investigated. As reported by Lalvani and Zhang (1994), HA forms complexes with Fe(III) ions through carboxylic groups, similar to OA. A relatively low degree of suppression of released S species by FA (**Fig. 7.3**) may be due to the complexation with Fe(III) ions in addition to the adsorption to pyrite. Overall, the reduction of Fe(III) ions by FA does not contribute much to suppress the pyrite dissolution. In the presence of 120 ppm of TA, the reaction of Fe(III) with pyrite is competitive to the reduction of Fe(III) to Fe(II) ions by TA, leading to a 50 % suppression of released S from pyrite (**Fig. 7.3**). Tannic acids do not function as a ligand to

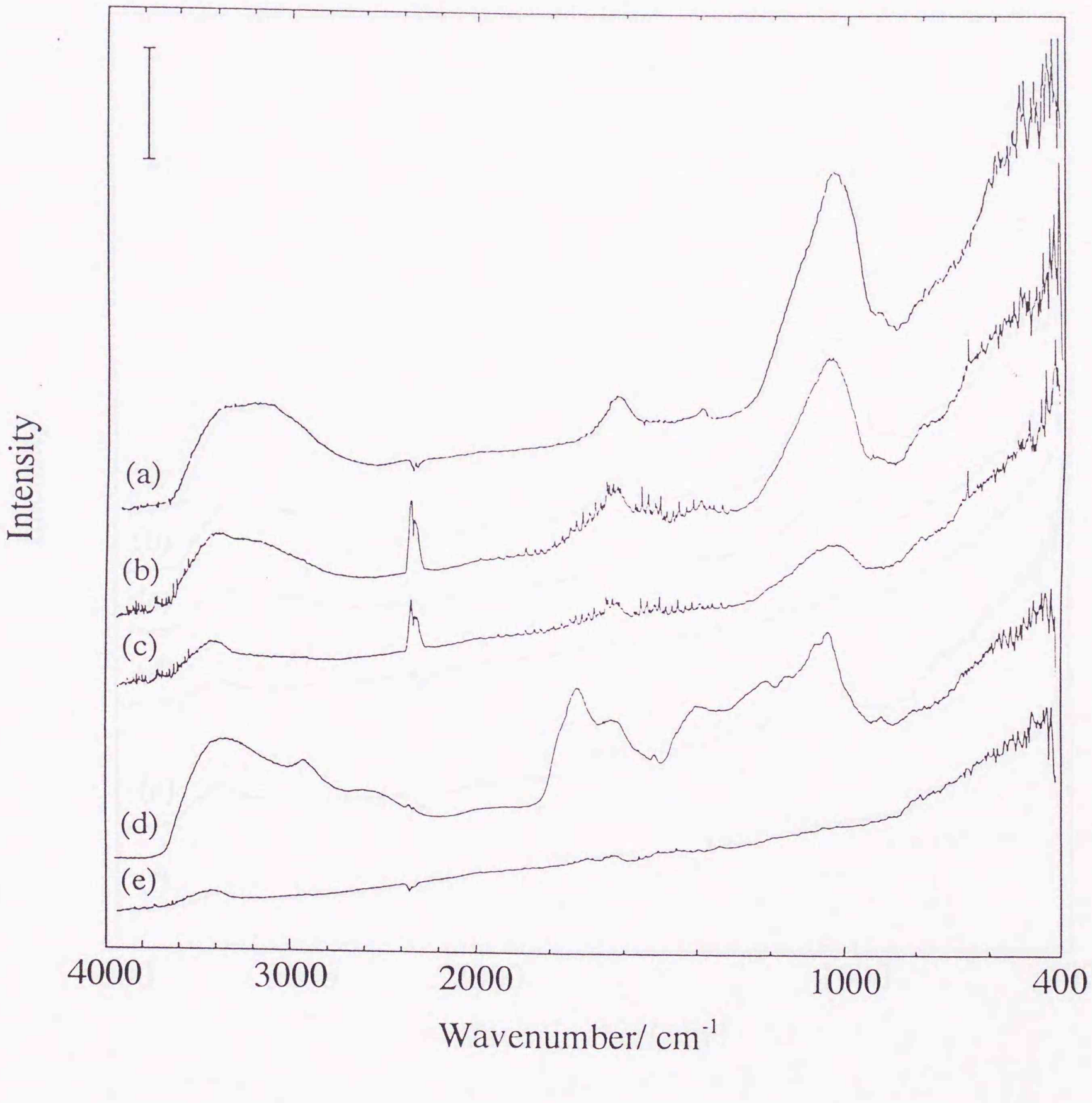

Fig. 7.11 FTIR spectra for pyrite after 336 h-dissolution with (a) no organic acids, (b) FA 600 ppm, (c) FA 1200 ppm, and (e) sterilized, and also for (d) FA isolated from Shinshinotsu soil. A vertical bar indicates one Kubelka-Munk unit for spectra (a)~(c) and (e), and 1/4 Kubelka-Munk unit for spectrum (d).

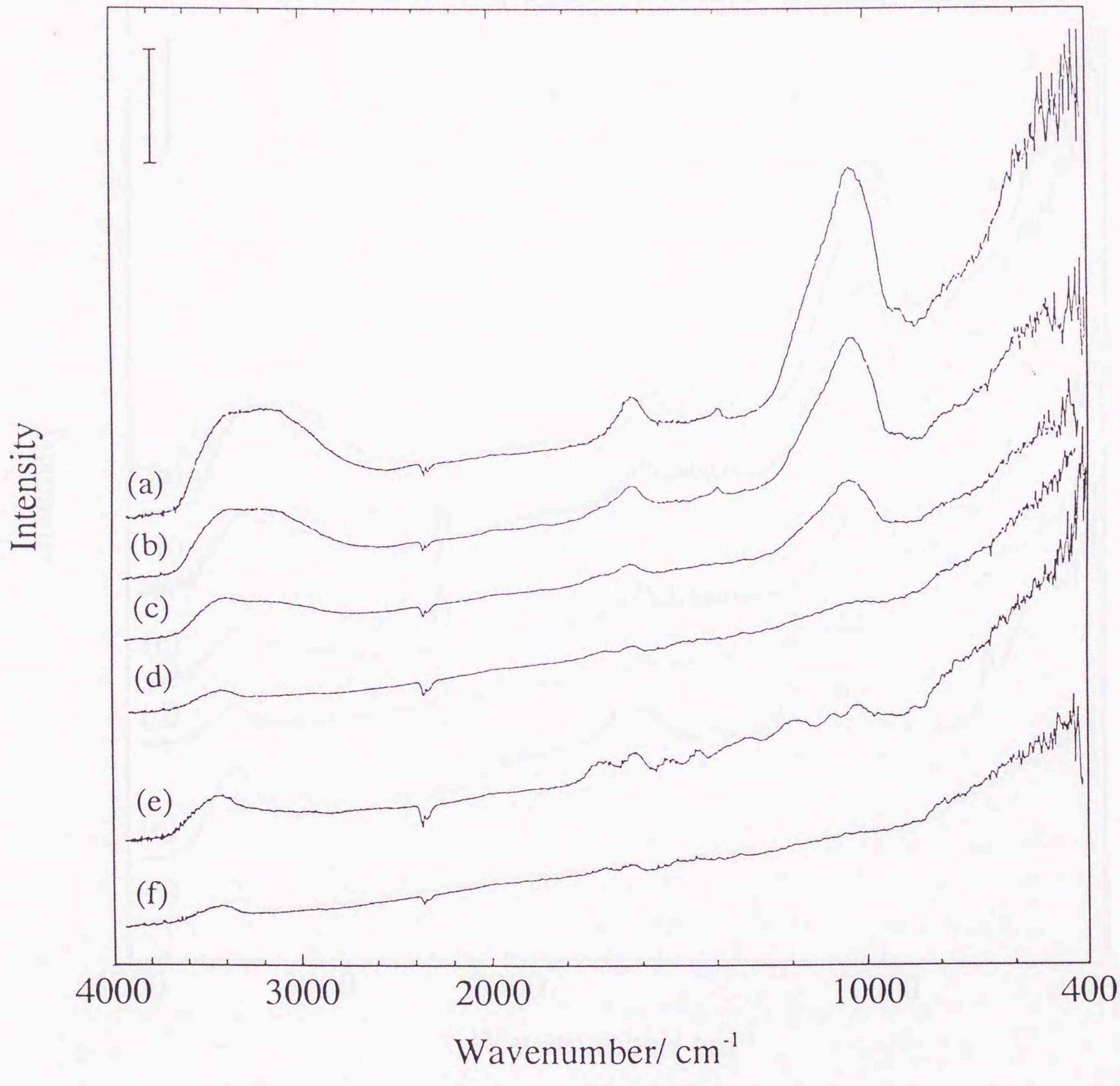

Fig. 7.12 FTIR spectra for pyrite after 336 h-dissolution with (a) no organic acids, (b) TA 50 ppm, (c) TA 150 ppm, (d) TA 500 ppm, and (f) sterilized, and for (e) TA. A vertical bar indicates one Kubelka-Munk unit.

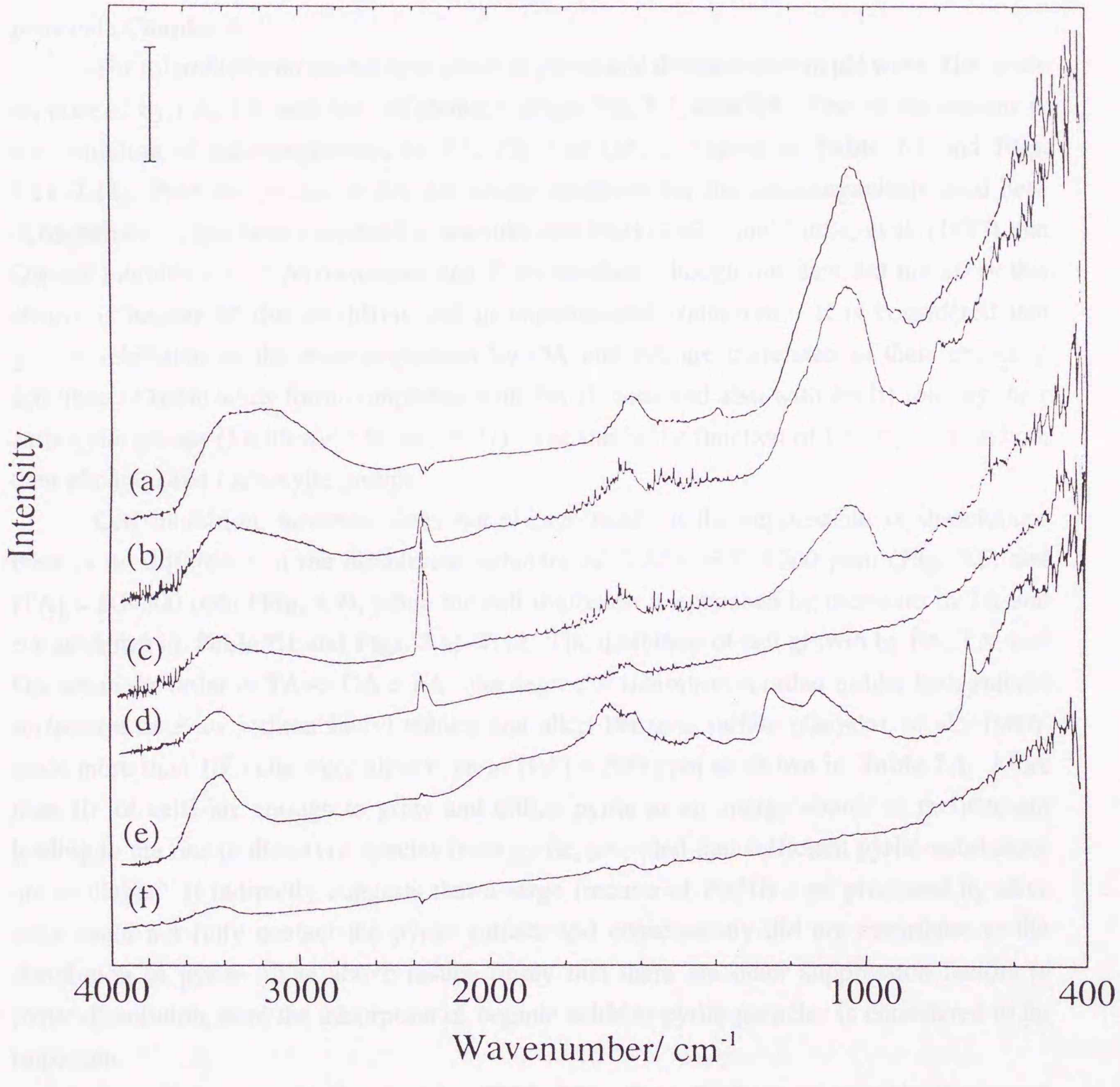

Fig. 7.13 FTIR spectra for pyrite after 336 h-dissolution with (a) no organic acids, (b) OA 126 ppm, (c) OA 252 ppm, (d) OA 630 ppm, and (f) sterilized, and for (e) OA. A vertical bar indicates one Kubelka-Munk unit for spectra (a)~(d) and (f), and 1/4 Kubelka-Munk unit for spectrum (e).

Fe(III) ions because they are strong reductants. In the presence of 252~1260 ppm (2~10 mmol dm^{-3}) of OA, most of Fe(III) ions are in the forms of $[FeL_3]^{3-}$ and $[Fe(H_2O)_2L_2]^-$ according to calculation using stability constants, where H_2L is oxalic acid, $(COOH)_2$. These Fe(III)-complexes were unable to oxidize pyrite due to a lowering of the standard redox potential (**Chapter 4**).

The microbially mediated dissolution of pyrite and the decreases in pH were effectively suppressed by FA, TA, and OA, as shown in **Figs. 7.5, 7.7, and 7.9**. One of the reasons is the inhibition of microorganisms by FA, TA, and OA, as shown in **Table 7.1** and **Figs. 7.11~7.13**. Phenolic groups of TA are strong inhibitors for the microorganisms used here (**Chapter 6**). It has been reported by Iwatsuka and Mori (1960), and Tuttle, et al. (1977) that OA are inhibitory to *T. ferrooxidans* and *T. thiooxidans*, though our data did not show this clearly (**Chapter 6**) due to differences in experimental conditions. It is considered that growth inhibition of the microorganisms by OA and FA are correlated to their chelating activities. Oxalic acids form complexes with Fe(III) ions and also with Fe(II) ions by their carboxylic groups (Smith and Martell, 1977). The inhibitive function of FA depends on both their phenolic and carboxylic groups.

Cell inhibition, however, does not always result in the suppression of dissolution: there is no difference in the dissolution behavior of [FA] = 600~1200 ppm (**Fig. 7.5**) and [TA] = 50~500 ppm (**Fig. 7.7**), while the cell inhibition is enhanced by increases in TA and FA as shown in **Table 7.1** and **Figs. 7.11~7.12**. The inhibition of cell growth by FA, TA, and OA are in the order of TA>> OA > FA: the degree of inhibition is rather milder than anionic surfactants such as sodium lauryl sulfate and alkyl benzene sulfate (Onysko, et al., 1984), since more than 10^7 cells were alive even at [TA] = 500 ppm as shown in **Table 7.1**. More than 10^7 of cells are enough to grow and utilize pyrite as an energy source in the medium leading to the rise in dissolved species from pyrite, provided that sufficient pyrite-substances are available. It indirectly suggests that a large fraction of Fe(III) ions produced by alive cells could not fully contact the pyrite surface and consequently did not contribute to the dissolution of pyrite. The above results imply that there are other suppression factors in pyrite dissolution, here the adsorption of organic acids to pyrite particles is considered to be important.

Though it was not observed by FTIR (**Figs. 7.11~7.13**), it is possible that small amounts of organic acids were adsorbed to pyrite as confirmed by XPS in the preliminary experiments (**Fig. 7.4**). Previously we reported that Fe(II) and Cu(II) ions preferentially adsorbed to active sites of pyrite, leading to the suppression of pyrite dissolution (**Chapter 5**). It has been also reported by Seelinger, et al. (1995) and Pettenkofer, et al. (1991) that there is site-specific interaction for an electron transfer at the (100) plane of pyrite crystal. Accordingly, the high surface coverage need not to suppress the pyrite dissolution.

In biotic system, reduction of Fe(III) ions was negligible in FA and OA systems (**Figs. 7.6 and 7.10**), but was observable for larger concentrations of TA (**Fig. 7.8**). In the presence of 630 ppm of OA (5 mmol dm^{-3}) (**Fig. 7.10 (bottom)**), 1.67 mmol dm^{-3} of Fe(III) ions were finally formed. Most Fe(III) ions are complexed with OA and are unable to oxidize pyrite. Dissolved Fe species were suppressed more strongly than S species in the presence of organic acids, even if it is considered that there is scattering in the determination of S by ICP-AES, possibly due to complexation and polymerization in the presence of the organic acids.

Consequently, it was concluded that the suppression of pyrite dissolution by FA occurred mainly due to cell inhibition and adsorption to the active sites of pyrite surfaces, the contribution of the reduction and complexation of Fe(III) ions were small, while reduction was also important in the presence of TA and complexation important with OA.

7.4 Summary

Microbially mediated dissolution of pyrite showed an effective suppression of a release of S and Fe species and decreases in pH in the presence of more than 10 ppm of TA, and 200 ppm of FA, and 250 ppm of OA. Reduction of Fe(III) ions by FA was not so important to suppress the pyrite dissolution in biotic systems similar to the ones in abiotic. Preliminary experiments without bacteria suggested that adsorption and complexation are important to suppress release of S species from pyrite by FA. In biotic systems, it was suggested that the suppression by FA occurred mainly due to inhibition of microorganisms and adsorption to the active sites of pyrite surfaces in addition to reduction and complexation of Fe(III) ions. The reduction was also important in the presence of TA and complexation important with OA, however.

Accordingly, humic substances are useful for remediation in mine environments. It leads us to suggest that afforestation should be promoted, and that it is also effective to scatter the withered oak-leaves where afforestation is impossible. Humic substances easily form complexes with Cu(II) ions in the environment (e. g., Fukushima, et al. 1991). In the advanced stage, it may enable recovery for valuable metals such as Cu in mine drainage.

References

Blowes, D. W., Ptacek, C. J., and Jambor, J. L. (1994) "Remediation and prevention of low-quality drainage from tailings impoundments." in "*Environmental Geochemistry of Sulphide Mine-Wastes*" (edited by Jambor, J. L., and Blowes, D. W.) Vol. 22, Waterloo, Ontario in Mineralogical Association of Canada. **Chapter 13**, pp. 365-379.

Fukushima, M., Tanaka, S., and Taga, M. (1991) Stability of copper-humic acid complexes in acidified solution. *J. Chem. Soc. Japan.*, **No. 5**, 556-558.

Iwatsuka, H. and Mori, T. (1960) Studies of the metabolism of a sulfur-oxidizing bacterium 1. Oxidation of sulfur. *Plant & Cell Physiol.*, **1**, 163-172.

Kuwatsuka, S., Watanabe, A., Itoh, K., and Arai, S. (1992) Comparison of two method of preparation of humic acid and fulvic acids, IHSS method and NAGOYA method. *Soil Sci. Plant Natr.*, **38(1)**, 23-30.

Lalvani, S. B. and Kang, J. (1992) Coal flotation in the presence of humic acids. *Fuel Sci. Technol. Int'l.*, **10**, 1291-1312.

Lalvani, S. B. and Zhang, G. (1994) Mitigation of pyrite dissolution due to humic acids addition. *Fuel Sci. Technol. Int'l.*, **12**, 963-982.

Luther III, G. W., Kostka, J. E., Church, T. M., Sulzberger, B. and Stumm, W. (1992) Seasonal iron cycling in the salt-marsh sedimentary environment: The importance of ligand complexes with Fe(II) and Fe(III) in the dissolution of Fe(III) minerals and pyrite, respectively. *Marine Chemistry*, **40**, 81-103.

Luther III, G. W., Shellenbarger, P. A., and P. L. Brendel, P. L. (1996) Dissolved organic Fe(III) and Fe(II) complexes in salt marsh porewaters. *Geochim. Cosmochim. Acta,* **60**, 951-960.

McKibben M. A. and Barnes H. L. (1986) Oxidation of pyrite in low temperature acidic solutions: Rate laws and surface textures. *Geochim. Cosmochim. Acta*, **50,** 1509-1520.

Naumann, D., Fijala, V., and Labischinski, H. (1988) The differentiation and identification of pathogenic bacteria using FT-IR and multivariate statistic analysis. *Mikrochim. Acta[Wien]*, **1**, 373-377.

Onysko, S. J., Kleinmann, R. L. P., and Erickson, P. M. (1984) Ferrous iron oxidation by *Thiobacillus ferrooxidans*: Inhibition with benzoic acid, sorbic acid, and sodium lauryl sulfate. *Appl. Environ. Microbiol.*, **48**, 229-231.

Pettenkofer, C., Jaegermann, W., and Bronold, M. (1991) Site specific surface interaction of electron donors and acceptors on FeS_2(100) cleavage planes. *Ber. Bunsenges. Phys. Chem.*, **95**, 560-565.

Seelinger, W., Troughton, G. L., Alonso-Vante, N., and Tributsch, H. (1995) Evidence for site-specific interaction of redox species at the FeS_2/electrolyte interface. *J. Electrochem. Soc.*, **142**, L166-L167.

Singer, P. C. and Stumn, W. (1970) Acid mine drainage: The rate-determining step. *Science*, **167**, 1121-1123.

Skogerboe, R. K., and Wilson, S. A. (1981) Reduction of ionic species by fulvic acid. *Anal. Chem.*, **53**, 228-232.

Smith, R. M., and Martell, A. E. (1977) *Critical Stability Constants.* **Vol. 3**, Plenum Press,

New York, pp. 93-94.

Stevenson, F. J. (1985) "Geochemistry of Soil Humic Substances" in "Humic Substances in Soil, Sediments, and Water" (edited by Aiken, G. R., McKnight, D. M., Wershaw, R. L., and MacCarthy, P.), John Wiley & Sons, Inc.

Szilagyi, M. (1971) Reduction of Fe(III) ion by humic acid preparations. *Soil Science*, **111**, 233-235.

Tanaka, S., Fukushima, M., Sasaki, K., Nakayasu, K., Oba, K., Nakamura, H., and Hasebe, K. (1996) Comparative investigation on copper(II)-binding abilities of humic and fulvic acid extracted from Shinshinotsu peaty soil. submitted to *Anal. Sci.*

Tuttle, J. H., Dugan, P. R., and Apel, W. A. (1977) Leakage of cellular material from *Thiobacillus ferrooxidans* in the presence of organic acids. *Appl. Environ. Microbiol.*, **33**, 459-469.

Tuovinen, O. H., and Kelly, D. P. (1972) Biology of *Thiobacillus ferrooxidans* in relation to the microbiological leaching of sulphide ores. *Z. Allg. Mikrobiol.*, **12**, 311-346.

Appendix 7.1: Purification of fulvic acids

Fulvic acids (FA) were purified from Shinshinotsu peat soil (Hokkaido, Japan), according to the modified International Humic Substances Society (IHSS) method. First 1.0 $\times$ 10^3 g of Shinshinotsu peat soil was leached in 4 $\times$ 10^3 cm^3 of 0.5 mol dm^{-3} NaOH, and kept shaking at room temperature for 72 h. After centrifugation at 1000 $\times$ g for 10 min, the supernatant was filtrated using a Buchner funnel with Toyo filter No. 5A, and then the elution was acidified to pH 1 with SSG HCl and kept for 24 h at room temperature to precipitate the humic acids (HA) fraction.

After the sample was centrifuged at 1000 $\times$ g for 10 min, the precipitate was introduced into the other path (dialysis) to purify the HA fraction and the supernatant was evaporated at 35 ℃ till a volume of 30 cm^3 to purify the FA fraction. During concentration of the FA fraction, NaCl was also deposited and separated by centrifugation at 1000 $\times$ g for 10 min to remove.

The concentrated samples were mounted onto a 5 cm diameter and 35 cm long (total volume, V_t = 687 cm^3) column containing XAD-2 resin (Amberlite), previously conditioned with ~2060 cm^3 (3 $\times$ V_t) of 0.1 mol dm^{-3} SSG HCl. The adsorbed FA on the XAD-2 resin, show as brown bands. They were washed with distilled water and then eluted from the resin using the (1 + 1) mixture of 0.1 mol dm^{-3} NaOH and ethanol as an eluent. The "center cut" elution technique enabled the collection of a highly concentrated central part excluding polysaccharides, sugar, organic acids with low molecular weight, and substances other than

inorganic salts. The "center cut" eluate was evaporated at 35 ℃ to concentrate to ~30 cm^3 to remove ethanol.

The concentrated samples were finally desalted by gel filtration using Sephadex G-10 resin (Pharmacia), 5 cm diameter and 35 cm long (V_t = 687 cm^3), after neutralization with a small amount of SSG HCl to avoid damaging the column.

The eluate of the FA fraction, containing a large amount of Na^+ ions, was directly introduced into the cation-exchange resin, IR-120 (Amberlite), the mixture was thoroughly shaken, the Na^+ ion-adsorbed resin was removed by filtration using a Buchner funnel, and then eluate of the FA fraction was again washed with the fresh resin. The washing was repeated five times to attain complete protonation of the eluate of the FA fraction. The protonated samples were evaporated at 35 ℃ for freeze drying.

Chapter 8
Conclusions

Pyrite (FeS_2) dissolution is important in several biogeochemical processes including formation of acid mine drainage. Understanding the mechanisms of dissolution can help in the selection of methods to abate this environmental problem. Chemoautotrophic iron- and sulfur- oxidizing bacteria, *Thiobacillus ferrooxidans* and *Thiobacillus thiooxidans,* are acidophilic and aerobic species, often grow actively in mine water and play an important role in pyrite weathering. The purposes of the present work were (a) experimentally to clarify the mechanism of microbial attack on pyrite by the iron-oxidizing bacteria, *Thiobacillus ferrooxidans,* (b) to determine the mechanism of oxidative dissolution of pyrite by Fe(III) ions, and (c) to elucidate factors suppressing microbially mediated weathering of pyrite to establish control systems for strongly acidic drainage.

The first chapter provided a brief background of previous works concerned with this endeavor and established the objectives of the research.

In **Chapter 2**, microbially mediated dissolution of pyrite with *Thiobacillus ferrooxidans* was carried out, and investigated with both solution and mineral surface analysis, XPS, FTIR, and XMA. It was found that elemental sulfur, an intermediate in the "indirect contact mechanism" of pyrite dissolution, was formed on the surface of pyrite during oxidation by the bacteria. It was further shown that the mole ratio of elemental sulfur to total Fe on the surface, $[S]/[Fe_T]$ was closely dependent on the activity of the bacteria. These results indicate that the microbial attack on pyrite by *Thiobacillus ferrooxidans* proceeds mainly by the "indirect contact mechanism" not but by the "direct contact mechanism." The redox potential was dependent on the [Fe(III)]/[Fe(II)] mole ratio in the solution, and this presented a measure of the activity of the iron-oxidizing bacteria, *Thiobacillus ferrooxidans*. The results in this chapter show that a key reaction for the oxidative dissolution of pyrite is the oxidation of pyrite by Fe(III) ions both in aerobic and anaerobic environments.

Chapter 3 first established the pretreatment method to obtain a well-defined pyrite surface, essential to obtain reliable dissolution data, and validated the method by XPS and Raman spectroscopy. The stoichiometry of pyrite dissolution by Fe(III) ions was studied in chloride media around pH 2. Pyrite was found to dissolve nonstoichiometrically during the initial tens of hours, and a sulfur-rich layer was formed on the pyrite due to preferential dissolution of iron. The major constituent of the surface layer was elemental sulfur, identified by XPS and Raman spectroscopy.

In **Chapter 4**, the reactivity of pyrite with Fe(III) ions in solutions at pH around 2, containing anionic species, was evaluated by a determination of released Fe(II) ions and by

XPS surface analysis of the pyrite. The release of Fe(II) ions decreased with increasing concentration of total anionic species, and the suppression of pyrite dissolution was in the order chloride < sulfate <<< phosphate~ oxalate. The Fe(III)-CDTA and $[Fe(CN)_6]^{3-}$ complexes did not function as oxidants. For $[Fe(CN)_6]^{3-}$, the results were explained by a mechanism based on the molecular orbital theory, since the complex is an inert and low-spin type. For the others, the order of suppression was found to parallel the order of the potential as oxidant, the standard redox-potential, E^0. The redox couples of Fe(III)-CDTA and Fe(III)-oxalate complexes have lower E^0 and this is considered to be the reason for the absence of oxidation. In the phosphate system, colloid formation and polynucleation of Fe(III) ions were observed and these were additional factors in the suppression. The experimental results and the calculated E^0 indicate that E^0 for SO_4^{2-}/pyrite-S may be around 0.3 V. This means that E^0 is an important measure to estimate ligand effects. Further, the dissolution data in the Fe(III)-oxalate system revealed that electron transfer from pyrite to Fe(III) species is not always accomplished through a ligand water molecule.

In **Chapter 5**, the effects of cations including alkaline, alkaline earth, and transition metal ions on the pyrite dissolution with Fe(III) ions near pH 2 were studied by solution analysis and XPS. The results showed that Na^+, K^+, Ca(II), Mg(II), Ni(II), Zn(II), and Cd(II) ions had no effect, whereas Pb(II), and Ba(II) ions precipitated sulfate ions released from the pyrite; Fe(II) and Cu(II) ions suppressed the release of Fe and S species from the pyrite. Pyrite is a soft base by HSAB theory, but soft and moderate acids such as Cd(II), Ni(II), and Zn(II) did not adsorb significantly, leading to an absence of suppression. At the same time the moderate acids, Fe(II) and Cu(II) ions, lead to the suppression. This suggests that the effect of other cations on pyrite dissolution with Fe(III) ions is not always explained by HSAB theory. After dissolution in the presence of Cu(II) ions, Cu(I) species, very similar to the Cu(I) in Cu_2Se, were formed on the pyrite. It was presumed that at active sites of pyrite-S Fe(II) and Cu(II) ions were adsorbed preferentially over Fe(III) ions, and that Cu(II) ions were reduced to Cu(I) species becoming stabilized on the pyrite, leading to the suppression of pyrite dissolution.

In **Chapter 6**, the inhibition of the cell growth, and iron and sulfur oxidation in *Thiobacillus ferrooxidans* and *Thiobacilus thiooxidans* by fulvic and tannic acids were studied around pH 2, and compared with that of oxalic acid. These inhibitors were selected by taking into account the use of compounds limiting environmental damage, and the selection was based on the results in Chapters 4 and 5 (humic and related compounds can also be reductants and/or complexing agents to Fe(III) ions and may adsorb on the pyrite surface). Tannic acid at 500 ppm inhibited the cell growth, and iron and sulfur oxidation in 8×10^9 cells of *Thiobacillus ferrooxidans* and *Thiobacillus thiooxidans* for more than two weeks, possibly due to its phenolic group, while fulvic acid inhibited them only for the initial two

days. Both were more effective inhibitors than oxalic acid.

By considering the results in Chapters 4~6, the originally isolated fulvic acids were applied to the suppression of microbially mediated dissolution of pyrite by *Thiobacillus ferrooxidans* and *Thiobacillus thiooxidans*, and compared with tannic and oxalic acids in **Chapter 7**. The mechanism of suppression was studied using XPS, FTIR, and solution analysis. Preliminary experiments showed that the reaction rate of Fe(III) with pyrite was faster than the rate of Fe(III) to Fe(II) reduction by fulvic acids, and that fulvic acids adsorbed to the pyrite surface and suppressed dissolution of pyrite moderately. Release of S and Fe species and decreases in pH in microbially mediated dissolution of pyrite were effectively suppressed in the presence of more than 10 ppm of tannic acids, 200 ppm of fulvic acids, and 250 ppm of oxalic acids. The suppression was considered to be due to inhibition of microorganisms by organic acids and their adsorption to the active sites of pyrite surfaces in addition to reduction and complexation of Fe(III) ions by them. The results indicate that humic substances could be useful for remediation and prevention of damage caused by acidic mine drainage.

List of publications

1. H. Konno, K. Sasaki, M. Tsunekawa, T. Takamori, and R. Furuichi: "X-ray photoelectron spectroscopic analysis of surface products on pyrite formed by bacterial leaching." *Bunseki Kagaku*, **40**, 609 -616 (1991) (in Japanese).

2. K. Sasaki, M. Tsunekawa, H. Konno, T. Hirajima, and T. Takamori: "Leaching behavior and surface characterization of pyrite in bacterial leaching with *Thiobacillus ferrooxidans*." *Shigen-to-Sozai (J. Min. Mat. Proc. Inst. Japan)*, **109**, 29-35 (1993) (in Japanese).

3. K. Sasaki, H. Konno, and M. Inagaki: "Structural strain in pyrite evaluated by X-ray powder diffraction." *J. Mater. Sci.* , **29**, 1666-1669 (1994).

4. K. Sasaki, M. Tsunekawa, K. Hasebe, and H. Konno: "Effect of anionic species on the oxidative dissolution of pyrite in acid solutions." *Proc. Intl. Sym. Trace Analysis '94*, Sapporo, pp. 291-294 (1994).

5. K. Sasaki, M. Tsunekawa, and H. Konno: "Nonstoichiometry in the oxidative dissolution of pyrite in acid solutions." *Bunseki Kagaku*, **43**, 911-917 (1994) (in Japanese).

6. K. Sasaki: "Effect of grinding on the rate of oxidation of pyrite by oxygen." *Geochim. Cosmochim. Acta*, **58**, 4649-4655 (1994).

7. K. Sasaki, M. Tsunekawa, K. Hasebe, and H. Konno: " Effect of anionic ligands on the reactivity of pyrite with Fe(III) ions in acid solutions." *Colloids and Surfaces A: Physicochemical and Engineering Aspects*, **101**, 39-49 (1995).

8. K. Sasaki, M. Tsunekawa, T. Ohtsuka, and H. Konno: "Confirmation of sulfur-rich layer formed on pyrite after dissolution by Fe(III) ions." *Geochim. Cosmochim. Acta* , **59**, 3155-3158 (1995).

9. K. Sasaki, M. Tsunekawa, and H. Konno: "Characterization of argentojarosite formed from biologically oxidized Fe(III) ions." *Can. Mineral.*, **33**, 1311-1318 (1995).

10. K. Sasaki, M. Tsunekawa, and H. Konno: "Effect of Fe(II) ions on pyrite oxidation with Fe(III) ions near pH 2." *Shigen-to-Sozai (J. Min. Mat. Proc. Inst. Japan)*, **112**, 48-53 (1996).

11. K. Sasaki, M. Tsunekawa, and H. Konno: "Effect of cations on pyrite oxidation with Fe(III) ions near pH 2." *Shigen-to-Sozai (J. Min. Mat. Proc. Inst. Japan)*, **112**, 231-237 (1996).

12. K. Sasaki, M. Tsunekawa, S. Tanaka, and H. Konno: "Suppression of microbially mediated dissolution of pyrite by originally isolated fulvic acid and the related compounds." *Colloids and Surfaces A: Physicochemical and Engineering Aspects*., **119**, 241-253 (1996).

13. K. Sasaki and M. Tsunekawa: "Evaluation of tannic and fulvic acids as inhibitors of cell growth and iron and sulfur oxidation in *Thiobacillus ferrooxidans* and *Thiobacillus thiooxidans*." *Shigen-to-Sozai (J. Min. Mat. Proc. Inst. Japan)*, **112**, 929-933 (1996).

14. Tanaka, S., Fukushima, M., Sasaki, K., Nakayasu, K., Oba, K., Nakamura, H., and Hasebe, K. (1996) Comparative investigation on copper(II)-binding abilities of humic and fulvic acid extracted from Shinshinotsu peaty soil. *submitted to Anal. Sci.*

Acknowledgments

This work was carried out mainly in the Laboratory of Mineral Processing, Faculty of Engineering, Hokkaido University.

I wish to express my sincere appreciation to the following people: Prof. Masami Tsunekawa, who served as the chief examiner of my dissertation, and Profs. Iwao Nakajima, Hiroshi Ohashi, Tatsuo Shimizu as co-examiners: Assoc. Prof. Hidetaka Konno from the Graduate School of Engineering, Hokkaido University, who collaborated with me and provided constructive advice through discussion: this dissertation couldn't be realized without his continual encouragement: Assoc. Prof. Shunitzu Tanaka from the Graduate School of Environmental Earth Science, Hokkaido University, who collaborated for the preparation of fulvic acids and discussed on the interaction of humic substances, minerals and microorganisms: Prof. Kiyoshi Hasebe from the Graduate School of Environmental Earth Science, Hokkaido University, who also continued encouraging me: Prof. Michio Inagaki from the Graduate School of Engineering, Hokkaido University, who helped me through discussion on the physicochemical properties of pyrite: Prof. Kazue Tazaki from the Faculty of Science, Kanazawa University, who also encouraged me in completion of this dissertation: Prof. Emeritus of Hokkaido University Takakatsu Takamori, who implanted in my mind with an interest in biohydrometallurgy: Assoc. Prof. Toshiaki Ohtsuka from Nagoya Institute of Technology, who helped to measure Raman spectra: Mr. Keiichi Tomita from Hokkaido Industrial Research Institute, who allowed me to use ICP-AES.

I am grateful also to the late Prof. Emeritus of Hokkaido University Tomihito Kambara and Dr. Masao Sugawara, who is now Assoc. Prof. of the University of Tokyo, for their discipline of fundamental science during undergraduate student in the Department of Chemistry, Hokkaido University.

Finally, I would like to thank heartily my father and the deceased mother.

KEIKO SASAKI

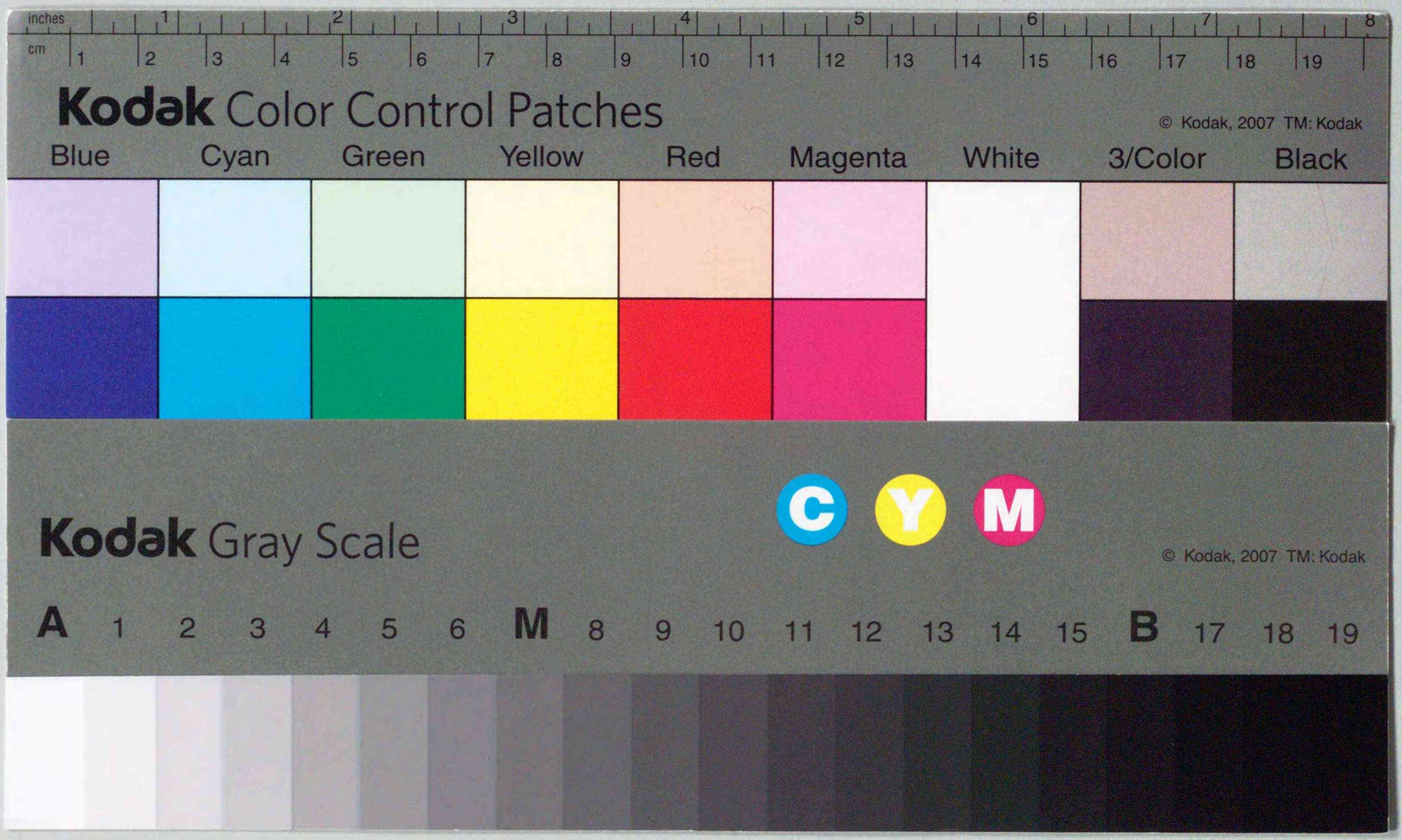
inches
cm
Kodak Color Control Patches
© Kodak, 2007 TM: Kodak
Blue
Cyan
Green
Yellow
Red
Magenta
White
3/Color
Black
Kodak Gray Scale
C
Y
M
© Kodak, 2007 TM: Kodak
A 1 2 3 4 5 6 M 8 9 10 11 12 13 14 15 B 17 18 19